PAGUIGAN, NOEMI D., Ph.D. Investigating the Diversity of Secondary Metabolites from Filamentous Fungi. (2017)
Directed by Dr. Nicholas H. Oberlies. 205 pp.

Natural products continue to be a fertile source of leads for drug discovery, as a large extent of the world's biodiversity has been untapped for their chemical diversity and biological activity. With the continuing need for new drug leads due to the increasing emergence of drug-resistant pathogens and diseases, this dissertation focused on three key strategies in drug discovery including: use of structure-activity relationship studies starting with a known bioactive pharmacophore; exploration of understudied ecological groups for new chemistry; and development of dereplication strategies.

Fungal secondary metabolites are known to possess privileged pharmacophores that can be ideal starting points for semi-synthetic (or synthetic) approaches to explore structure-activity relationship and produce new therapeutic candidates. In this work we examined the effect of fluorine substitution as a strategy to expand the therapeutically-relevant chemical space of isolated fungal secondary metabolites. The chemical space of the isolated and synthesized fungal secondary metabolites were characterized by principal component analysis to correlate the observed bioactivities.

Undoubtedly, fungi have an excellent track record in providing chemical entities that can be developed into life-saving therapeutics. Freshwater ascomycetes, an ecologically distinct group of fungi, offer a unique opportunity to discover new chemical diversity, as they are underexplored in comparison to other niches. Chemical investigations of freshwater fungal isolates presented in this dissertation led to the

isolation and identification of new secondary metabolites. These studies highlighted the untapped potential of this group of organisms.

One of the major challenges of working with natural products is the re-isolation of known compounds. Thus, to circumvent this issue and increase the efficiency of the discovery of new leads, a dereplication methodology using a complementary suite of hyphenated techniques, specifically ultra-performance liquid chromatography-photodiode array-high resolution tandem mass spectrometry for targeted screening of compounds was developed. In conjunction to this, the identified hits were expanded upon by screening for potential analogues using mass defect filtering.

INVESTIGATING THE DIVERSITY OF SECONDARY METABOLITES FROM FILAMENTOUS FUNGI

by

Noemi D. Paguigan

A Dissertation Submitted to
the Faculty of The Graduate School at
The University of North Carolina at Greensboro
in Partial Fulfillment
of the Requirements for the Degree
Doctor of Philosophy

Greensboro
2017

Approved by

_____
Committee Chair

APPROVAL PAGE

This dissertation written by Noemi D. Paguigan has been approved by the following committee of the Faculty of The Graduate School at the University of North Carolina at Greensboro

Committee Chair _____

Committee Members _____

_____

_____

_____
Date of Acceptance by Committee

_____
Date of Final Oral Examination

TABLE OF CONTENTS

Page

LIST OF TABLES

Page

LIST OF FIGURES

Page

CHAPTER I

INTRODUCTION

Nature's molecular archive has long been a reliable source of structural and functional inspiration in the development of therapeutic drugs to treat human diseases.[1-3] It is the single most valuable source of drugs, as over half of the small-molecule approved drugs presently constitute of natural products or have a structure derived from, or a mimic of, a natural product.[1] Natural products has made significant impacts, particularly in the areas of cancer therapies and antibiotics.[4-6] However, in the past decades a majority of pharmaceutical companies has deemphasized reliance on drug discovery efforts in natural products in favor of synthetic combinatorial high-throughput screening methods. The main reason frequently cited for this shift is the decrease in the productivity in terms of the discovery of novel structures in natural products.[6]

This shift, unfortunately, has not met the expected surge in productivity in terms of new leads to fill the demand in the drug discovery pipeline. Rather, it led to a decline in the number of new approved chemical entities as drugs.[7] This may be of little surprise, as Nature has always been an important source for lead compounds suitable for drug development. The dominance of natural product derivatives that are developed as drugs owes largely to their immense chemical structural diversity and biological relevance.[8] The potency of natural products may be explained in an evolutionary point of view,

wherein these secondary metabolites were produced as biologically active chemicals providing adaptive value to the producing organism.[9] Bioactive natural product scaffolds have been well recognized as privileged structures, as they provide ideal starting points for drug discovery. Biologically relevant natural products are also known for their structural complexity, and thus, optimization of their structure to improve inherent drug-like properties is often difficult. Structural diversification is usually accomplished by semi-synthetic approaches to explore structure-activity relationships and produce new drug candidates.

With the continuing need for novel structures as antibiotics and chemotherapeutics, natural products remain relevant to the future of drug discovery. Addressing the demand for unique structural diversity, this dissertation has focused on: use of structure-activity relationship studies starting with a known bioactive pharmacophore from filamentous fungi (Chapter II); exploration of understudied ecological groups for new chemistry with emphasis on freshwater ascomycetes (Chapters III and IV); and implementation of dereplication strategies (Chapter V).

Fungi are non-photosynthetic microorganisms that play an important ecological role as agents of biodegradation and biodeterioration.[10] Fungi have been known to have a high biodiversity, second to insects, that is six times greater than the recognized species of terrestial plants.[10-12] According to current estimates, about 1.5 million[12] of fungal species exists on Earth but only about 135,000[13] of these have been described taxonomically. From these described species, only a fraction have been studied for their

chemistry.[14] To date, there are only about 25,000 fungal secondary metabolites reported, and only for a third of these, the bioactivity have been assigned.[14] Therefore, fungi represent a nearly limitless source for new natural products that can be used as therapeutics leads for drug development.

Fungi are known to biosynthesize a wide array of secondary metabolites with various biological activities. A few species of fungi produce mycotoxins, compounds that are known to be toxic, which can cause a variety of negative effects on plants, animals, and humans.[15] On the other hand, fungi also produce numerous important pharmaceuticals that have tremendous impact on human health (Figure 1).

Historically, natural products from fungi have been one of the most successful sources of drugs that have had broad therapeutic use. The discovery of penicillin from *Penicillium notatum* by Alexander Fleming in 1929,[3,16] which saved millions of lives, paved the way for the discovery of more antibiotics[17] from other fungal sources. Cyclosporin is a natural cyclic polypeptide antifungal-antibiotic isolated from *Tolypocladium inflatum*.[18] Its discovery was important as it is medicinally useful in suppressing immune responses when transplants are grafted.[19] Another significant class of fungal-derived drugs are the statins, also known as hydroxymethylglutaryl-CoA (HMG-CoA) reductase inhibitors, used to lower blood cholesterol levels. Currently, at least three statins are in clinical use including lovastatin and mevastatin, fungal secondary metabolites mainly produced by *Aspergillus terreus* and *Monascus ruber*, and *P. citrinum*, respectively, and simvastatin a semi-synthetic derivative of lovastatin.[20-22]

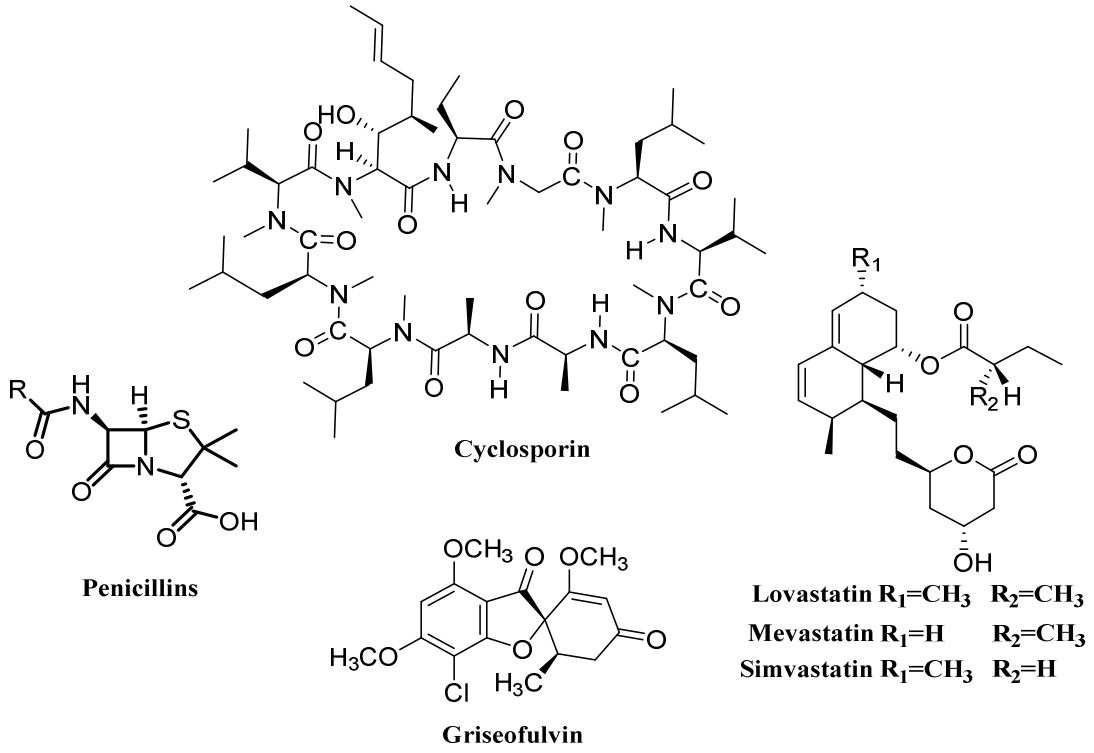

Figure 1. Fungal-Derived Drugs That Have Had a Great Impact on Public Health.

Another remarkable fungal-derived natural product is griseofulvin. Griseofulvin was first isolated and identified from *P. griseofulvum* in 1939.[24] It was developed and approved as an antifungal drug against superficial skin infections in both humans and animals in 1959.[25] Recently, griseofulvin is being considered for cancer treatment due to its antimitotic and antiproliferative activities against various types of cancer cells.[26-29] Recent studies suggest that griseofulvin in combination with nocodazole, an antineoplastic agent, hinders tumor production in both *in vitro* and *in vivo* assays by induction of apoptosis and G_2/M cell cycle arrest.[26] Additionally, griseofulvin has been found to inhibit centrosomal clustering, making tumor cells with supernumerary

centrosomes to undergo multipolar mitoses, thereby leading to cell apoptosis.[27,30] Griseofulvin has a mode of action that is still not well understood, but disruption of the microtubule assembly by tubulin binding in both fungal and mammalian cells has been proposed.[25,28,31]

Chapter II centers on the isolation and characterization of griseofulvin and six related analogues (one new to literature) from a culture of *Xylaria cubensis* (accessioned as MSX48662). The isolation of these fungal metabolites presented an opportunity to evaluate the anticancer and antifungal potential of these compounds. Additionally, this allowed us to investigate the influence of semi-synthetic strategies-fluorination specifically, in expanding the medicinally-relevant chemical space of the isolated fungal metabolites.

One of the important steps in the discovery of new bioactive natural products is the careful selection of the source to investigate. A majority of earlier drug discovery studies performed on fungi involve organisms collected from terrestrial habitats. However, as rediscovery of previously identified metabolites has become increasingly frequent, other habitats have been explored to expand chemical diversity beyond the terrestrial microorganisms. Several approaches have been used in the search for new chemistry with potential bioactivity, and one of these includes an ecology-based rationale.[32-34] It is hypothesized that fungi thrive in competitive or unique ecosystems because they have evolved to produce secondary metabolites that provide them with selective advantage over other competing organisms.[35,36] It is therefore predicted that

fungi from different habitats would produce a diverse and unique collection of secondary metabolites different from their terrestrial counterparts.

Freshwater ascomycetes are an ecological group that is relatively unexplored in terms of its mycology and chemistry. These species belong to the phylum Ascomycota, which is the largest and most phylogenetically diverse group of organisms in the Kingdom Fungi.[37] Freshwater ascomycetes are a taxonomically different group comprising of species of fungi that have part or their whole life cycle in freshwater environments, including lentic (lakes, ponds, and swamps) and lotic habitats (rivers, streams, creeks, and brooks).[38-41] These fungi mostly occur on submerged woody and herbaceous debris, serving as organic matter decomposers.[42]

Studies on freshwater ascomycetes have only been initiated recently, and these organisms still remain poorly known. To date, there are about 675 described species from freshwater habitats.[43] This reported number has increased from a meager 300 species described worldwide from an initial comprehensive review by Shearer.[39] Despite the recent efforts for intensive fungal collections in the past two decades, knowledge on the chemistry of freshwater ascomycetes is still lagging.

To help bridge this knowledge gap, our group is focused on the investigation of fungi collected systematically from different freshwater sources across North Carolina, USA. North Carolina has a unique geographical location, where it is divided into four distinct areas including ranges of the Appalachian Mountains in the western part of the state, Piedmont plateau, Atlantic coastal plain, and the outer banks in the east. With this variety in the geographical features of North Carolina, we hypothesize that the freshwater

ascomycetes from this area have high fungal species diversity. Additionally, these freshwater ascomycetes may have unique adaptations for survival prompting the need for the production of chemically diverse compounds that could potentially be used as new therapeutic leads.

Chapters III and IV are devoted to the isolation and characterization of secondary metabolites from organic extracts of two freshwater ascomycetes (accessioned as G416 and G730) collected from two different regions in North Carolina. Investigation of G416 (recently identified as *Lindgomyces madisonensis* Raja & Oberlies) collected from a submerged wood from Big Beaver Island creek in Madison, North Carolina, led to the isolation of seven acetophenone derivatives (five new to literature and two newly reported as natural products; Chapter III). These fungal secondary metabolites were evaluated for their antimicrobial activity against a panel of pathogenic bacteria and fungi. Chapter IV presents the isolation and identification of three new prenylated xanthenes as well as two known compounds from an organic extract of G730. The fungal strain G730 was isolated from submerged wood collected from a freshwater lake in Hanging Rock State Park, North Carolina. Phylogenetic analysis on a fungal isolate of G730, tentatively identified as Leotiomycetes sp., indicated that the strain may represent a new genus and/or species. Chapter IV also details the characterization of the antivirulence potential of the three new prenylated xanthenes against methicillin resistant *Staphylococcus aureus*.

One of the key driving forces for natural products drug discovery efforts is the identification of new chemical structures that can be used as new drug leads. Therefore,

quick recognition of previously known compounds, referred to as dereplication, in fungal fermentation extracts play a prominent role in drug discovery screening programs. Efficient implementation of dereplication strategies aims to reduce timelines for the "hit-to-lead" process, as well as maximize available financial resources.

An efficient dereplication procedure involves analytical methods that are reliable, robust, rapid, and sensitive to be able to characterize natural products as pure compounds, and even more so in complex mixtures.[44] Chapter V demonstrates the use of an ultraperformance liquid chromatography-photodiode array-high resolution tandem mass spectrometry (UPLC-PDA-HRMS-MS/MS)-based dereplication system to perform targeted screening of secondary metabolites produced by fungi. The application of this UPLC-PDA-HRMS-MS/MS dereplication method has facilitated rapid confirmation of known fungal secondary metabolites at the level of crude extracts. Moreover, in Chapter V, mass defect filtering, a post-acquisition data analysis technique, is presented as an additional approach for the targeted screening of secondary metabolites in fungal extracts. The merger of UPLC-PDA-HRMS-MS/MS dereplication with mass defect filtering permits additional profiling for structurally related components in the sample based on their mass defects. Mass defect filtering therefore allowed characterization for a wider range of secondary metabolites produced by fungal cultures.

CHAPTER II

CHEMOSELECTIVE FLUORINATION AND CHEMOINFORMATIC ANALYSIS OF GRISEOFULVIN: NATURAL VS FLUORINATED FUNGAL METABOLITE

This chapter is intended for publication to *Bioorganic and Medicinal Chemistry* (2017) and is presented in that style. Coauthors include Mohammed Al-Huniti, Huzefa A. Raja, Austin Czarnecki, Joanna E. Burdette, Mariana González-Medina, José L. Medina-Franco, Stephen J. Polyak, Cedric J. Pearce, Mitchell P. Croatt, Nicholas H. Oberlies.

Griseofulvin is a fungal metabolite and antifungal drug used for the treatment of dermatophytosis in both humans and animals. Recently, griseofulvin and its analogues have attracted renewed attention due to reports of their potential anticancer effects. In this study griseofulvin (**1**) and related analogues (**2**-**6**, with **4** being new to literature) were isolated from *Xylaria cubensis* and screened for activity against a panel of cancer cell lines (MDA-MB-435, MDA-MB-231, OVCAR3, and Huh7.5.1) and for antifungal activity against *Microsporum gypseum*. In addition, six fluorinated analogues (**7**-**12**) were synthesized to examine the effects of fluorine incorporation on the bioactivities of this structural class. A comparison of the chemical space occupied by the natural and fluorinated analogues was carried out by using principal component analysis, documenting that the isolated and fluorinated analogues occupy complementary regions of chemical space. However, the most active compounds, including two fluorinated derivatives, were centered around the chemical space that was occupied by the parent

compound, griseofulvin, suggesting that modifications must preserve certain attributes of this privileged pharmacophore to conserve its activity.

Introduction

Bioactive secondary metabolites have had a long history in medicine, as they provide privileged scaffolds for drug discovery.[45-48] As testament to this, from 1981 to 2014 over half of the new small molecule drugs approved by the U.S. FDA were natural products or natural product-derived/natural product-inspired.[1,49] The success of natural products as source of therapeutic agents is driven by their biochemical specificity and high chemical diversity, occupying distinct regions of chemical space that coincide with clinically relevant areas.[46,50]

Fungi are one of the most species-rich organisms, second only to insects, offering a vast resource for discovery of new drug leads. Our recent collaborative efforts underscore the structural complexity and diversity of fungal metabolites.[50-52] As promising compounds are identified, these structural features are of particular relevance, as they can be used to stimulate semi-synthetic[53,54] approaches to explore structure-activity relationships and produce new drug candidates.

The natural product griseofulvin (**1**, Figure 2), (2*S*,6'*R*)-7-chloro-2',4,6-trimethoxy-6'-methyl-3H-spiro[benzofuran-2,1'-cyclohexan]-2'-ene-3,4'-dione, is a potent antifungal drug orally administered for the treatment of dermatophytosis (i.e., fungal infection of the skin) in both humans and animals.[55-58] Since its isolation and discovery from a filamentous fungus in 1939,[24] most research has focused on the identification of griseofulvin analogues, either from nature or synthetically, but to date, only the original

compound (**1**) has been developed into a marketable antifungal drug, first approved in 1959.[56] Recently, there has been a renewed interest in **1** due to its antimitotic and antiproliferative activities against various types of cancer cells.[26,27,29,30,59] Griseofulvin has a mode of action that is still not well understood, but disruption of the microtubule dynamics in both fungal and mammalian cells has been proposed.[25,56,60] Thus, aside from being an antifungal drug, it may also be a clinically-viable candidate for cancer chemotherapy.[25,31,59-62] Due to these reasons, it was decided that griseofulvin was worth further investigation.

The introduction of fluorine into a bioactive compound has been shown to impart a range of effects, often altering physicochemical profiles by modulating acid/base properties, electronegativity, lipophilicity, and metabolic stability.[63,64] Focusing on these unique properties, fluorine has been exploited in the design and optimization of biologically active molecules.[63,65,66] With our interest in late stage fluorination of secondary metabolites,[53] we envisioned the ability to prepare various fluorinated griseofulvin derivatives. We further rationalized that **1**, already proven to be a successful therapeutic, was a good candidate to investigate the influence of fluorine substitution as a strategy to expand the medicinally-relevant chemical space of fungal metabolites.

An isolate of the filamentous fungus *Xylaria cubensis* (strain MSX48662) was found to be a prolific producer of **1**, biosynthesizing over 100 mg per a single rice-based fermentation culture grown in a 2.8 L Fernbach flask,[67] and thus, it was used for resupply purposes. Hence, the fungal extract was subjected to further studies and afforded six

compounds, including **1** and structurally related analogues, four of which were known (**2**, **3**, **5**, and **6**) and one of which (**4**) was new to the literature. Seven additional analogues (**7**, **8a/8b**, **9-12**, all fluorinated) were produced using **1**, **3** and **4** as starting materials. All 12 compounds were evaluated for cytotoxicity against cancer cell lines, including human melanoma cancer cells (MDA-MB-435), human breast cancer cells (MDA-MB-231), human ovarian cancer cells (OVCAR3), and human hepatoma (Huh7.5.1) cells[68]. Moreover, the antifungal potency of **1-12** against *Microsporum gypseum* was assessed in a disk diffusion assay. Characterization of the chemical space of the isolated and synthesized analogues was also carried out by principal component analysis to correlate structural modifications with the observed bioactivities.

Results and Discussion

Isolation of griseofulvin (1) and related analogues (2-6). Organic extracts ($CHCl_3$/CH_3OH) from the rice-based fermentation cultures of MSX48662 were partitioned with organic solvents, subjected to flash chromatography, and were purified using preparative HPLC to yield griseofulvin (**1**) and five structurally related analogues (**2-6**), with **4** being new to literature. The structures of compounds **1**-**3** and **5**-**6** were established by analysis of HRESIMS and NMR data, all of which compared favorably to the literature (See the Supporting Information for spectral data).[69,70]

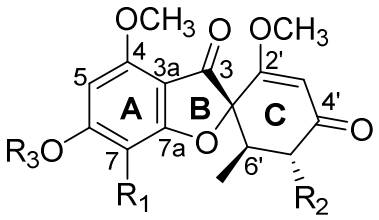

	R_1	R_2	R_3
1	Cl	H	CH_3
2	Cl	OH	CH_3
3	H	H	CH_3
4	H	OH	CH_3
5	H	H	H
6	Cl	H	H

Figure 2. Structures of Griseofulvin (1) and Related Analogues (2-6) Isolated from *Xylaria cubensis*.

Compound **4** was isolated as a white solid. The NMR and HRESIMS data (m/z 335.1119 $[M+H]^+$) both indicated a molecular formula of $C_{17}H_{18}O_7$, corresponding to a difference of an additional OH (16 Da) relative to **3**. The ^{1}H NMR spectrum of **4** (Table 7 and Figures 9-11) showed similarities to **3**, including signals for a 1,2,3,5-tetrasubstituted aromatic ring, as evidenced by the meta-coupled aromatic proton signals at δ_H 6.06 and δ_H 6.22 ($^3J_{HH}$ = 1.1 Hz), an isolated olefinic proton, three methoxy groups, as well as a methyl group. However, it was also clear from these data that the diastereotopic methylene proton α-H-5´ in **3** was replaced with a hydroxy moiety in **4**, thus shifting β-H-5´ to the more downfield region of the spectrum (δ_H 4.71). The large coupling constant ($^3J_{HH}$ = 12.1 Hz) observed between H-5´ and H-6´ placed both protons in trans-diaxial positions, imparting 5´-OH and 6´-CH_3 in equatorial positions, analogous to that of **2**. Based on these observations, the configuration at C-5´ was established as *R*. A comparison of the observed specific rotation value ($[\alpha]_D^{27}$ +343) of **4** with those for **1** ($[\alpha]_D^{27}$ +340), **2** ($[\alpha]_D^{27}$+306) and **3** ($[\alpha]_D^{27}$ +386) revealed that the configurations at C-2 (*S*) and C-6´ (*R*) of these compounds were identical. Thus, the structure of compound **4**

was established as shown (Figure 2) and identified as (2*S*,5´*R*,6´*R*)- 7-dechloro-5´-hydroxygriseofulvin.

Semi-synthesis and structure elucidation of fluorinated analogues. There are a few reports on the fluorination of griseofulvin and its analogues.[71,72] For example, monofluorinated and difluorinated griseofulvin analogues have been prepared by Taub and co-workers in 1963 and Barton and co-workers in 1972 by electrophilic fluorination of griseofulvin using either perchloryl fluoride ($FClO_3$)[73,74] or fluoroxytrifluoromethane (CF_3OF),[75] two of the earliest electrophilic fluorine reagents. These harsh conditions resulted in the formation of several mono- and difluorinated products, including reaction of the enol-ether and some *gem*-difluoro derivatives. In this study, our goal was to chemoselectively fluorinate ring A of griseofulvin without affecting the other functional groups, especially the enol-ether motif. Thus, Selectfluor, was used as the electrophilic fluorination reagent, since it is known to be milder and typically more chemoselective than other fluorination reagents.[76-78] Indeed, this strategy yielded only ring A fluorinated-derivatives; each substrate gave two mono-fluorinated compounds, with fluorination at either C-5 or C-7, which allowed us to probe the chemical space of these analogues.

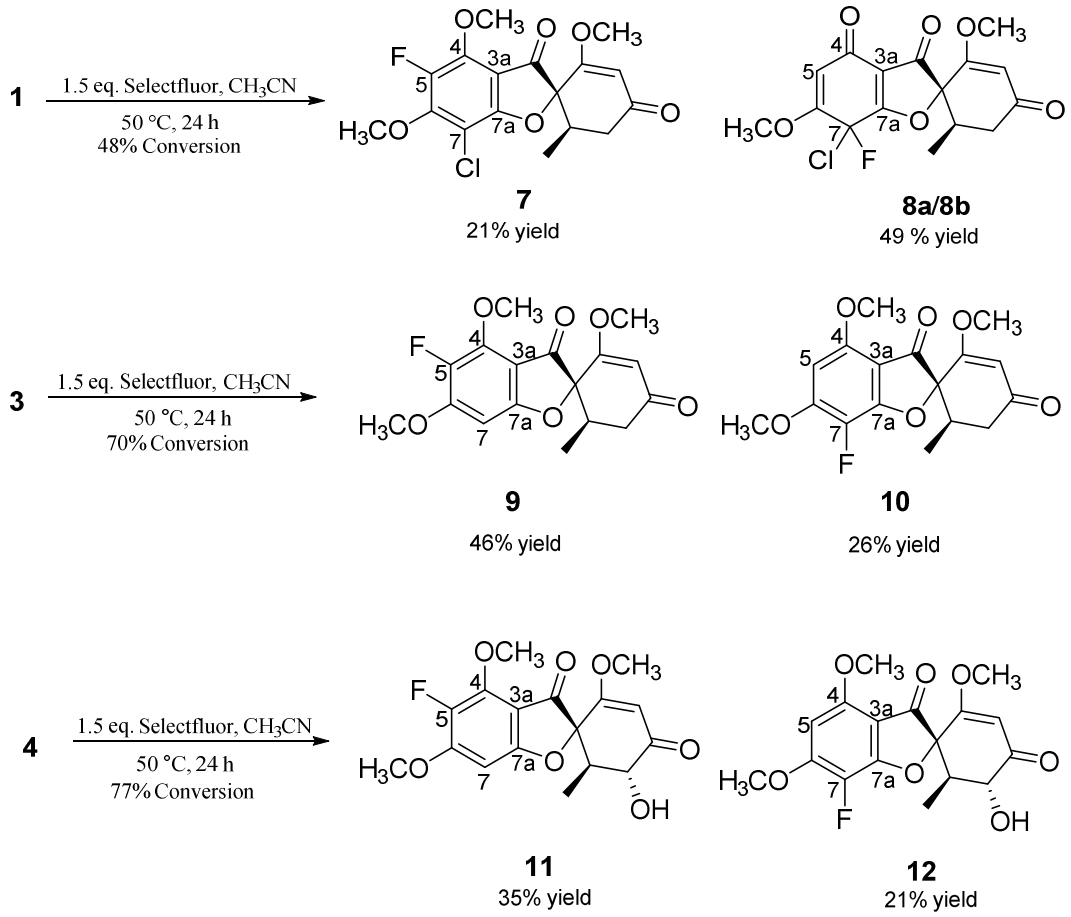

Figure 3. Semi-Synthesis of Fluorinated Compounds 7-12 with Selectfluor. The percent yields shown were calculated based on recovered starting material.

Seven fluorinated products (**7**, **8a/8b**, **9**-**12**) were obtained from Selectfluor reactions with compounds **1**, **3**, and **4** (Figure 3). Addition of a solution of **1** (dissolved in CH_3CN) to a CH_3CN solution of Selectfluor afforded one minor compound (**7**) and an inseparable diastereoisomeric mixture of **8a/8b** with a ratio of 2:1, as revealed by interpretation of the ^{1}H NMR data (Figure 19). The HRMS data for **7** indicated the incorporation of one fluorine atom with a molecular formula of $C_{17}H_{16}ClFO_6$. A comparison of the ^{1}H NMR data (Table 10, Figure 14) of **7** with **1** suggested the

attachment of a fluorine atom into ring A, as evidenced by the absence of the aromatic H-5 signal. In addition, the methoxy groups at C-4 and C-6 resonated as doublets due to through-space coupling[79] with a coupling constant of J_{HF} = 3.1 Hz for both. Their chemical shifts were slightly downfield ($\Delta\delta$ 0.14-0.22, Figure 15) due to their proximity to the F atom at C-5. ^{19}F-^{13}C HMQC data (Figure 16) showed a correlation between the fluorine atom and C-5, which resonated as a doublet at δ_C 142.9 with a large coupling constant of 244.3 Hz typical of a $^1J_{CF}$ bond in an aromatic ring,[80] further supporting the position of fluorine. Additionally, the doublet signals observed for C-4 ($^2J_{CF}$ = 9.0 Hz) and C-6 ($^2J_{CF}$ = 12.1 Hz) corroborate the attachment of fluorine at C-5. Altogether, these data identify **7** as 5-fluorogriseofulvin, which was previously reported by Barton and co-workers by the treatment of griseofulvin with fluoroxytrifluoromethane.[72]

The NMR and HRESIMS data (m/z 357.0543 $[M+H]^+$) for compounds **8a/8b** supported a molecular formula of $C_{16}H_{14}ClFO_6$. Following the interpretation of edited-HSQC (Figure 20) and HMBC (Figure 21) experiments, the ^{13}C and ^{1}H NMR data (Table 11) were assignable to 16 carbon atoms consisting of two methoxy groups, one methyl, three methine (two sp^2 and one sp^3), one methylene, and nine non-protonated carbons (three carbonyls, four olefinic with three of them oxygenated, and two fully substituted carbons). Comparison of the NMR data between **1** and **8a**/**8b** indicated that rings B and C of both compounds were identical. However, modifications were made in ring A of **8a**/**8b**, as the NMR data indicated oxidation at C-4 to a ketone due to the absence of a methoxy group and the presence of an extra carbonyl carbon (δ_C 176.9). The doublet signal observed for H-5 ($^3J_{HF}$ = 1.8 Hz) and the doublet signal observed for ^{19}F ($^3J_{HF}$ =

1.8 Hz) indicated the addition of fluorine to ring A (Figure 22). The doublet signal ($^1J_{CF}$ ~243 Hz) observed for C-7, along with an HMQC correlation between ^{19}F and C-7 (δ_C ~94), suggested the attachment of fluorine to C-7 (Figure 23). The assignment of fluorine being at C-7 was further supported by the doublet splitting patterns observed for C-6 ($^2J_{CF}$ = 19.1 Hz) and C-7a ($^2J_{CF}$ = 21.0 Hz). Thus, the structures of the diastereoisomers were assigned as shown in Figure 3. We have previously observed similar reactivity with Selectfluor reactions,[53] as have others with Selectfluor[81] and other related reagents[82-88].

The reaction of Selectfluor with **3** afforded two mono-fluorinated structural isomers **9 (**major) and **10** (minor), both with a molecular formula of $C_{17}H_{17}FO_6$ based on HRESIMS data. Comparison of the ^1H NMR data of **9** (Table 12) and **10** (Table 13) with those of **3** indicated the loss of one aromatic proton signal attributed to H-5 and H-7, respectively. In compound **9**, the C-4 methoxy resonance appeared more deshielded compared with the corresponding signal in **3** ($\Delta\delta$ 0.3), and showed a doublet splitting pattern due to a through space coupling with the fluorine at C-5 (Figure 24-25). Unlike its chloro-analogue (**7**), this coupling was observed for the methoxy group at C-4 only, which suggested that, in the preferred conformer, the methoxy group at C6 in **9** is rotated away from the fluorine. Alternatively, compound **7** prefers to adopt a conformation where the methoxy group at C-6 is in close proximity to the fluorine due to the steric effect imposed by the chlorine atom.[89,90] On the other hand, the methoxy groups in compound **10** showed no through-space coupling with the fluorine.

^1H NMR data for compound **9** also showed a doublet at δ 6.37 ($^3J_{HF}$ = 6.3 Hz), which was assigned to H-7 due to long-range coupling with fluorine (Figure 24-25). The

correlation detected between the fluorine and C-5 (δ_C 139.6, doublet, $^1J_{CF}$ = 237.5 Hz) in the ^{19}F-^{13}C-HMQC data (Figure 26) suggested the connection of fluorine to position 5. The attachment of fluorine at C-5 was further corroborated by the small doublet splitting observed for C-4 ($^2J_{CF}$ = 8.8 Hz) and C-6 ($^2J_{CF}$ = 11.3 Hz), establishing the structure of **9** as 5-fluoro-7-dechlorogriseofulvin. The structure of **10** was established in an analogous manner and was identified as 7-fluoro-7-dechlorogriseofulvin (Table 13; Figure 29-33), which was previously reported by Taub and co-workers.[71]

As was the case for **3**, reaction of compound **4** with Selectfluor yielded two mono-fluorinated structural isomers, **11** and **12**. The HRESIMS data served to verify the number of incorporated fluorine atoms in the compounds, while the NMR data was analyzed in the same manner as **9** (Table 14-15; Figure 34-43). This exercise established the structures of **11** and **12** as the 5′-OH analogues of compounds **9** and **10**, respectively.

Biological evaluation. Griseofulvin (**1**) and all 11 analogues (**2-12**) were evaluated for their cytotoxic activity against three different cancer cell lines, specifically MDA-MB-435, MDA-MB-231, and OVCAR3 (Table 1 and Table 16).

Table 1. Cytotoxicity Results for the Active Compounds.[a]

Compound	IC_{50} MDA-MB-435[c]	MDA-MB-231[d]	OVCAR3[e]
1	6.4 µM	*inactive*	48.5 µM
10	22.0 µM	*inactive*	*inactive*
Vinblastine[b]	0.5 nM	8.8 nM	1.8 nM

[a]A compound was indicated as *inactive* if no activity was observed at 50 µM. Compounds 2-9 and 11-12 were inactive (see Table 16).
[b]Positive control; [c]Human melanoma cancer cells; [d]Human breast cancer cells
[e]Human ovarian cancer cells

Compounds **1** and **10** had moderate cytotoxicity, with IC_{50} values ranging from approximately 6 to 50 µM. As a complementary dataset, we also tested **1**-**12** for cytotoxicity in human hepatoma Huh7.5.1 cells; the data were in agreement (refer to Figure 44 and Table 18). These results were in accordance with earlier studies,[25,91] demonstrating that structural modifications in the 2´ position retain or increase the cytotoxicity of the analogues, while alterations at any other position do not retain the cytotoxicity of **1**, as was the case for all the analogues tested in this study.

All compounds (**1**-**12**) were also tested in an antifungal assay against *Microsporum gypseum*, a dermatophyte that causes tinea capitis, tinea corpus, and other fungal infections of the skin.[92,93] As shown in Tables 2 and 17, compound **10** retained the activity of **1**, while **7** showed a slight decrease in activity. Compound **10** has previously been reported to retain the activity of **1** against the plant pathogen *Botrytis alii*,[71] but its activity against dermatophytes, particularly *M. gypseum*, has not been reported. The antifungal activity of **7** has not been reported previously.

Table 2. Antifungal Results Against *Microsporum gypseum* for the Active Compounds.[a]

Compound	Zone of Inhibition (mm)[a] 25 µg/disk
1[b]	35 ± 1
7	23 ± 1
10	34 ± 1

[a]Mean diameter of inhibition zones expressed as the mean of four replicates ± standard deviation. Results for the Other Compounds in this Study are Shown in Table S15.
[b]Positive control

Principal component analysis. The introduction of fluorine into molecules often results in significant changes in their molecular properties and biological activities.[66,94] The small atomic size, very high electronegativity, and low polarizability of the fluorine atom are just a few of the characteristics that can have important consequences in a lead optimization program, particularly one focused on modifying privileged scaffolds. To compare the distribution in chemical space between the natural analogues (**1**-**6**) versus the fluorinated analogues (**7**-**12**), principal component analysis (PCA) was performed. Eleven molecular properties that describe the electron distribution, molecular surface, and solubility of the compounds were used in an attempt to emphasize the variation given by the addition of a fluorine, with the goal of finding a pattern in the data set. The first two principal components (PC1, PC2) retrieved 68% of the covariance, whereas the first three principal components (PC1 – PC3) retrieved 87% of the covariance. Interestingly, two electronic descriptors, namely electron affinity (EA (eV)) and electrotopological state (Estate), had the highest contribution to PC1, while QPlogS, a descriptor related to the

solubility of the compounds, had the highest contribution to PC2. The dipole moment of the molecule, an electronic descriptor, had the highest contribution to PC3. These results further emphasized that the addition of a fluorine atom changed mostly the electronic distribution within the molecules, as reflected in the clear separation in the PCA of the fluorinated vs. non-fluorinated analogues of griseofulvin (Figure 4).

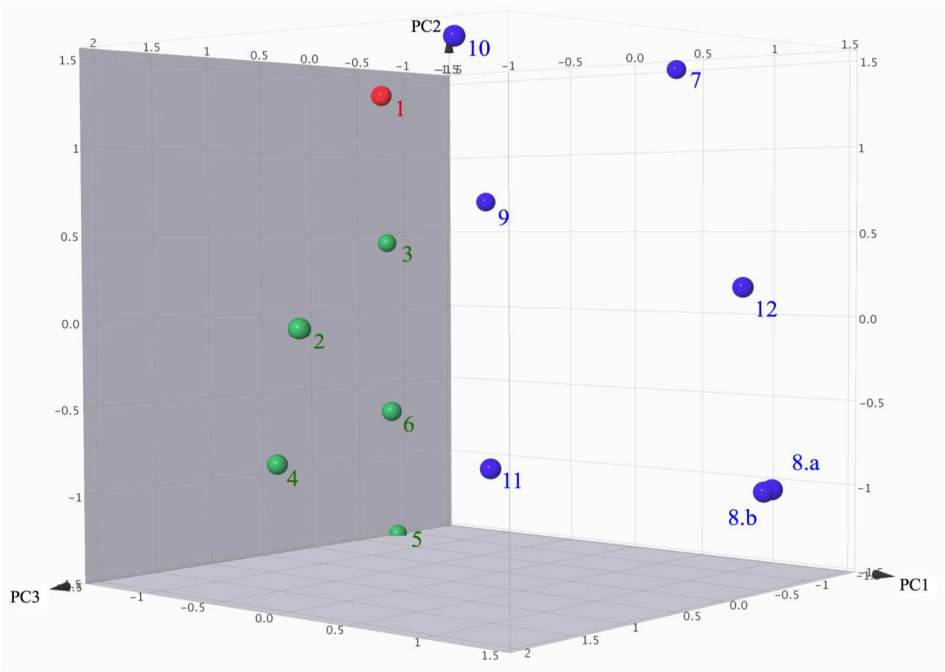

Figure 4. Visual Representation of the Chemical Space of Griseofulvin (1, Red), Structurally Related Fungal Analogues (2-6, Green) and Fluorinated Semisynthetic Derivatives (7-12, Blue). This 3D plot was generated with the principal component analysis of 11 descriptors. The first three principal components recovered 87% of the covariance. The electron affinity (EA (eV)) and electrotopological state (Estate) had the highest contribution to the first principal component, while the predicted aqueous solubility (QPlogS) had the highest contribution to the second principal component. Lastly, dipole moment had the highest contribution to the third principal component.

The 3D representation of the chemical space of **1**-**12** revealed several interesting features (Figure 4). For example, the 3D plot showed that the fungal metabolites clustered together, occupying a distinct region in the chemical space different from the fluorinated analogues, further illustrating that fluorine incorporation modified the molecular properties of the analogues. Additionally, fluorinated analogues **7**, **9**, and **10** were closer to griseofulvin in chemical space, suggesting that these analogues had similar electron distribution, solubility, and surface characteristics, which could indicate that these compounds had similar bioactivities. Similar results were observed on the 2D plot with PC1 and PC2 (Figure 45). The correlation between similarity in chemical space and similarity in bioassay results held true for **7** and **10** but not for **9**. For **7**, this observation can be rationalized given that the van der Waals radius of a fluorine atom (1.47 Å) is only slightly larger than that of hydrogen (1.20 Å). For compound **7**, the replacement of the hydrogen atom with a fluorine atom at C-5 did not impart a large change in molecular volume or the overall structure of the compound, thus retaining the antifungal activity. The highly electronegative nature and the geometric size of chlorine at C-7 of ring A is an important feature of **1** in order to retain its biological effect. The properties of the chlorine atom, particularly at the C-7 position (ortho relative to the C-6 methoxy group), may also impart steric constraints and/or electrostatic effects that may be necessary for optimum molecular recognition between the compound and an active site/receptor. Compound **9** lacks the chlorine atom at the C-7 position, and this may explain why no biological activity was observed for this compound. A fluorine atom at C-7, instead of chlorine, as was the case in compound **10**, may induce a similar electronic effect on the

compound. The difference in electronegativity between the fluorine and carbon creates a large dipole moment in this bond, contributing to the overall electronic nature of the molecule, and this could lead to specific interactions with an active site/receptor. Although **10** retains the antifungal activity and cytotoxicity of **1**, a decrease in potency was observed, which may be explained by a decrease in the steric bulk in **10** at C-7 due to a difference in van der Waals radius between a fluorine atom (1.47 Å) and chlorine (1.75 Å). The differences in activity observed for **7** and **10** against *M. gypseum* and the cancer cell lines could indicate a difference in the mode of action of **1** toward fungal and mammalian cells, which is still a subject of some debate.[25,56,95]

A 2D plot of predicted aqueous solubility (QPlogS) and electron affinity (eV) similarly illustrated the variance in the distribution of the analogues across the chemical space (Figure 5). The addition of an electrophilic fluorine to the griseofulvin analogues increased the electron affinity of the compounds, and this was manifested in chemical space as separating the fluorinated analogues from the natural secondary metabolites. Compound **7**, which is the C-5 fluorinated derivative of **1**, shared similar molecular properties in chemical space as **1**, but compared to the natural fungal analogues, **7** had a higher electron affinity. Moreover, Figures 4 and 5 illustrate that analogues **8a**/**8b**, which lost the aromaticity at ring A, were in a different region of chemical space, far from the rest of the analogues. Overall, it was observed that in **8a/8b** the addition of a fluorine to ring A significantly altered the properties of these compounds compared to griseofulvin (**1**). These changes could explain in part why **8a/8b** were inactive. Overall, the addition

of fluorine or a hydroxy group to the A or C rings improved the predicted solubility (Figure 5).

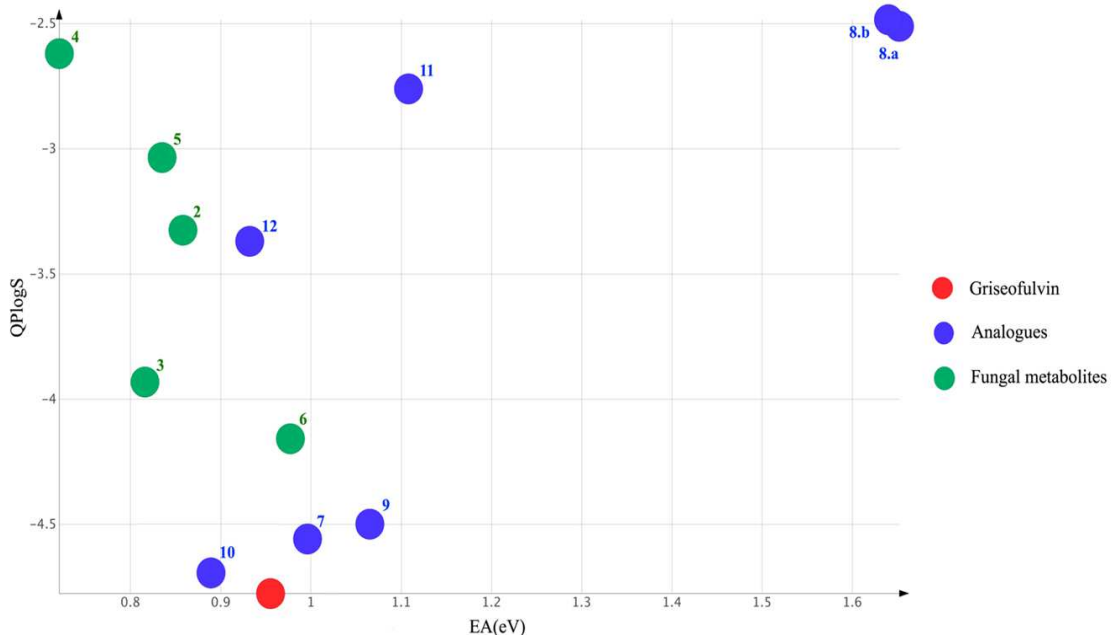

Figure 5. A 2D Visual Representation of the Chemical Space of Griseofulvin (1, Red), Structurally Related Fungal Analogues (2-6, Green) and Fluorinated Semisynthetic Derivatives (7-12, Blue). The 2D representation was generated using two descriptors, predicted aqueous solubility (QPlogS; y-axis) and electron affinity [EA(Ev); x-axis]. The substructures found on the derivatives and natural products but not on griseofulvin's structure are depicted in red.

Conclusion

In summary, griseofulvin (**1**) and five analogues (**2-6**), with **4** being new to the literature, were isolated from *X. cubensis*. Additionally, a series of fluorinated analogues (**7-12**) were synthesized, each requiring only a single step from the isolated natural products using Selectfluor. The chemoselective nature of Selectfluor allowed for direct, site-specific mutation of the natural products without the use of protecting groups or

other redox-modifications. Of the synthesized analogues, **8a**/**8b**, **9**, **11**, **12** are reported for the first time. All compounds were tested against the dermatophyte *M. gypseum* and in cytotoxicity assays against human melanoma cancer cells (MDA-MB-435), human breast cancer cells (MDA-MB-231), human ovarian cancer cells (OVCAR3), and human hepatoma cells (Huh7.5.1). Of the analogues, **10** retained the activity of **1** against *M. gypseum*, while **7** displayed less potency. Only compound **10** exhibited cytotoxic activity, but was less active compared to **1** against the MDA-MB-231 cells. To visualize the differences in the molecular and physicochemical properties generated by the addition of a single fluorine atom to the fungal secondary metabolites, PCA was used based on descriptors related to the electron distribution, solubility and molecular surface of the compounds. These descriptors captured the variation in the molecular properties and demonstrated that fluorinated analogues occupy a different region of chemical space than the fungal secondary metabolites. In addition, it was observed that the compounds **7** and **10** were close to griseofulvin in the chemical space, results that were consistent with the bioassay testing. Taken together, these results demonstrate the value of cheminformatics analyses to study structure-properties relationships and anticipate if a compound could be active based on similarity to a known active compound.

Experimental Section

General experimental procedures. All solvents and chemicals were purchased from standard suppliers and were used without any further purification. The NMR data were collected using either a JEOL ECS-400 spectrometer (JEOL USA, Inc.) operating at 400 MHz for ^{1}H and 100 MHz for ^{13}C, and equipped with JEOL normal geometry

broadband Royal probe; or a JEOL ECA-500 spectrometer (JEOL USA, Inc.) operating at 500 MHz for ^{1}H and 125 MHz for ^{13}C; or an Agilent 700 MHz NMR spectrometer (Agilent Technologies, Inc., Santa Clara, CA, USA) operating at 700 MHz for ^{1}H and 175 MHz for ^{13}C, and equipped with a cryoprobe. NMR chemical shift values were referenced to residual solvent signals for $CDCl_3$ (δ_H/δ_C 7.26/77.2). Data for ^{1}H NMR are reported as follows: chemical shift (δ ppm), multiplicity (s = singlet, d = doublet, t = triplet, q = quartet, sept = septet, m = multiplet), coupling constant (Hz), and integration; whereas ^{13}C NMR analyses were reported in terms of chemical shift. HRESIMS data were obtained using a Thermo QExactive Plus mass spectrometer (ThermoFisher, San Jose, CA, USA) with an electrospray ionization source coupled with a Waters Acquity ultraperformance liquid chromatography (UPLC) system (Waters Corp.). The UPLC separation was performed using an Acquity BEH C_{18} column (50 mm x 2.1 mm i.d., 1.7 µm) equilibrated at 40 °C and a flow rate set at 0.3 mL/min. The mobile phase consisted of a linear CH_3CN/H_2O (acidified with 0.1% HCOOH) gradient starting at 15% CH_3CN to 100% CH_3CN over 8 min. The mobile phase was held for another 1.5 min at 100% CH_3CN before going back to the starting conditions. The HPLC separations were performed using Varian ProStar HPLC system connected to a ProStar 335 photodiode array detector (PDA) with UV detection set at 210 nm and 254 nm. Preparative reversed phase HPLC purification of samples was performed on a Phenomenex Gemini-NX C_{18} (5 µm; 250 × 21.2 mm) column using a 21 mL/min flow rate of the mobile phase consisting of a mixture of CH_3CN and H_2O (with 0.1% HCOOH). Flash column chromatography was carried out with a Teledyne ISCO

Combiflash Rf connected to an ELSD and PDA detectors with UV detection set at 200-400 nm. Optical rotation data were acquired on a Rudolph Research Autopol III polarimeter (Rudolph Research Analytical, Flanders, NJ, USA). The UV data were acquired using a Varian Cary 100 Bio UV−Vis spectrophotometer (Varian Inc., Walnut Creek, CA, USA). The optical density (OD) at 600 nm was acquired using Thermo Scientific™ Genesys™ 20.

Fungal strain identification. Fungal strain MSX48662 was isolated from cedar wood collected in Little Rock, Arkansas and was identified using morphological and molecular methods[96] as described in detail previously.[67] Based on morphological characterization and molecular phylogenetic analysis, strain MSX48662 was identified as *Xylaria cubensis* (Sordariomycetes, Ascomycota). The sequence data for the strain utilized in the study was deposited in GenBank under accession number KX229783.

Fermentation, extraction, and isolation of natural products (1-6). The fermentation of fungal strain MSX48662 was performed using procedures described previously with slight modifications. [97-99] Briefly, a fresh culture of the fungus was grown on a malt extract slant. Subsequently, a small agar plug with mycelium was inoculated in a liquid medium consisting of 2% soy peptone, 2% dextrose, and 1% yeast extract (YESD media). This was followed by incubation for approximately 7 days at room temperature (22 ℃) with shaking. The seed culture was used to inoculate a Fernbach flask (2.8 L) containing rice (150 g) and H_2O (300 mL) and grown at rt for a period of 20 days.

The solid fermentation culture was extracted by addition of 1:1 $CH_3OH/CHCl_3$ (500 mL), followed by agitation for 16 h, and filtered. To the filtrate, 900 mL of $CHCl_3$

and 1500 mL of H_2O were added, and stirred for 30 min. The biphasic solution was partitioned, and the organic phase was collected and dried *in vacuo.* The resulting dried extract was further partitioned between CH_3OH/CH_3CN (1:1, 300 mL) and hexanes (300 mL) to obtain fractions weighing 2 g and 4 g, respectively. The CH_3OH/CH_3CN soluble partition was then adsorbed on Celite 545, and subjected to silica flash chromatography on a 24 g RediSep Rf Gold Si-gel column, eluting with use of a gradient solvent system of hexane/$CHCl_3$/CH_3OH at a flow rate of 35 mL/min over 71 column volumes for a duration of 68 min to give 100 fractions each containing 25 mL. The resulting fractions were then pooled according to their ELSD and UV profiles, which resulted to 16 subfractions.

Fraction 6 (230 mg) was subjected to preparative reversed-phase HPLC eluting with a linear gradient from 30% to 50% CH_3CN in H_2O (0.1% HCOOH) over 30 min to afford compound **1** (92 mg, t_R = 20.0 min), **2** (1.0 mg, t_R = 15.5 min), **3** (64 mg, t_R = 16.5 min), and **4** (15 mg, 12.5 min). Fraction 7 (115 mg) was purified using the same preparative HPLC conditions yielding more of compounds **2** (11 mg, t_R = 15.5 min) and **4** (17 mg, t_R = 12.5 min). Fraction 9 (250 mg) was similarly chromatographed but using a linear gradient from 20% to 40% CH_3CN in H_2O (0.1% HCOOH) over 15 min followed by an increase in the gradient to 80% CH_3CN to afford compounds **5** (1.9 mg, t_R = 17.0 min) and **6** (2.7 mg, t_R = 21.5 min).

Griseofulvin ((2*S*,6'*R*)-7-chloro-2',4,6-trimethoxy-6'-methyl-3H-spiro[benzofuran-2,1'-cyclohexan]-2'-ene-3,4'-dione; **1**): White solid; $[\alpha]_D^{27}$ +340 (*c* 0.1, $CHCl_3$); UV (MeOH) λ_{max} (log ε) 236 (4.4), 291 (4.4), 331 (3.7) nm; ^{1}H NMR (400 MHz, $CDCl_3$) δ =

0.96 (d, *J* = 6.8 Hz, 3H), 2.42 (dd, *J* = 16.8 Hz, 4.6 Hz, 1H), 2.84 (m, 1H), 3.03 (dd, *J* = 16.8 Hz, 13.4 Hz, 1H), 3.61 (s, 3H), 3.98 (s, 3H), 4.03 (s, 3H), 5.53 (s, 1H), 6.13 (s, 1H); ^{13}C NMR (100 MHz, $CDCl_3$) δ = 14.4, 36.5, 40.1, 56.5, 56.8, 57.1, 89.5, 90.9, 97.3, 105.0, 105.2, 157.9, 164.7, 169.6, 170.9, 192.6, 197.2 (See Table 4 and Figure 6); HRESIMS m/z 353.0781 $[M+H]^+$ (calc'd for $C_{17}H_{18}ClO_6$, 353.0786).

5'-Hydroxygriseofulvin ((2*S*,5'*R*,6'*R*)-7-chloro-5'-hydroxy-2',4,6-trimethoxy-6'-methyl-3H-spiro[benzofuran-2,1'-cyclohexan]-2'-ene-3,4'-dione; **2**): White solid; $[\alpha]_D^{27}$ +306 (*c* 0.05, MeOH); UV (MeOH) λ_{max} (log ε) 236 (4.2), 291 (4.2), 331 (3.6) nm; ^{1}H NMR (700 MHz, $CDCl_3$) δ = 1.11 (d, *J* = 6.7 Hz, 3H), 2.64 (dq, *J* = 12.2 Hz, 6.7 Hz, 1H), 3.65 (s, 3H), 3.99 (s, 3H), 4.04 (s, 3H), 4.68 (d, *J* = 12.2 Hz, 1H), 5.61 (s, 1H), 6.14 (s, 1H); ^{13}C NMR (175 MHz, $CDCl_3$) δ = 11.1, 43.6, 56.6, 57.1, 57.2, 71.5, 89.7, 91.2, 97.4, 101.8, 105.2, 158.0, 165.0, 169.8, 171.5, 192.6, 197.5 (See Table 5 and Figure 7); HRESIMS m/z 369.0738 $[M+H]^+$ (calc'd for $C_{17}H_{18}ClO_7$, 369.0736).

7-Dechlorogriseofulvin ((2*S*,6'*R*)-2',4,6-trimethoxy-6'-methyl-3H-spiro[benzofuran-2,1'-cyclohexan]-2'-ene-3,4'-dione; **3**): White solid; $[\alpha]_D^{27}$ +386 (*c* 0.1, MeOH); UV (MeOH) λ_{max} (log ε) 239 (4.4), 287 (4.4), 321 (3.8) nm; ^{1}H NMR (400 MHz, $CDCl_3$) δ = 0.94 (d, *J* = 6.6 Hz, 3H), 2.39 (dd, *J* = 16.8 Hz, 4.7 Hz, 1H), 2.74 (m, 1H), 3.03 (dd, *J* = 16.8 Hz, 13.4 Hz, 1H), 3.61 (s, 3H), 3.89 (s, 3H), 3.90 (s, 3H), 5.53 (s, 1H), 6.03 (d, *J* = 1.9 Hz, 1H), 6.23 (d, *J* = 1.9 Hz, 1H); ^{13}C NMR (100 MHz, $CDCl_3$) δ = 14.4, 36.7, 40.2, 56.2, 56.2, 56.8, 88.6, 90.0, 93.5, 104.4, 104.9, 159.2, 170.5, 171.5, 176.2, 192.7, 197.6 (Table 6 and Figure 8); HRESIMS m/z 319.1175 $[M+H]^+$ (calc'd for $C_{17}H_{19}O_6$, 319.1176).

7-Dechloro-5'-hydroxygriseofulvin ((2*S*,5'*R*,6'*R*)-5'-hydroxy-2',4,6-trimethoxy-6'-methyl-3H-spiro[benzofuran-2,1'-cyclohexan]-2'-ene-3,4'-dione; **4**): White solid; $[\alpha]_D^{27}$ +343 (*c* 0.1, MeOH); UV (solvent) λ_{max} (log ε) 230 (4.4), 288 (4.4), 321 (3.7) nm; ^{1}H NMR (400 MHz, $CDCl_3$) δ = 1.11 (d, *J* = 6.6 Hz, 3H), 2.55 (dq, *J* = 12.1 Hz, 6.6 Hz, 1H), 3.66 (s, 3H), 3.91 (s, 3H), 3.92 (s, 3H), 4.71 (d, *J* = 12.1 Hz, 1H), 5.61 (s, 1H), 6.06 (d, *J* = 1.1 Hz, 1H), 6.22 (d, *J* = 1.1 Hz, 1H); ^{13}C NMR (100 MHz, $CDCl_3$) δ = 11.2, 43.9, 56.3, 56.3, 57.1, 71.5, 88.6, 90.5, 93.7, 101.7, 104.4, 159.3, 170.8, 172.1, 176.3, 192.6, 197.8. (See Table 9 and Figures 9-11); HRESIMS m/z 335.1119 $[M+H]^+$ (calc'd for $C_{17}H_{19}O_7$, 335.1125).

6-*O*-desmethyl-7-dechlorogriseofulvin ((2*S*,6'*R*)-6-hydroxy-2',4-dimethoxy-6'-methyl-3H-spiro[benzofuran-2,1'-cyclohexan]-2'-ene-3,4'-dione; **5**): White solid; $[\alpha]_D^{27}$ +221 (*c* 0.1, MeOH); UV (solvent) λ_{max} (log ε) 248 (4.3), 290 (4.2), 322 (4.2) nm; ^{1}H NMR (400 MHz, $CDCl_3$) δ = 0.97 (d, 6.7 Hz, 3H), 2.43 (dd, *J* = 16.7 Hz, 4.8 Hz, 1H), 2.76 (dqd, *J* = 13.2 Hz, 6.7 Hz, 4.8 Hz, 1H), 3.08 (dd, *J* = 16.7 Hz, 13.2 Hz, 1H), 3.64 (s, 3H), 3.90 (s, 3H), 5.55 (s, 1H), 6.05 (d, *J* = 1.9 Hz, 1H), 6.20 (d, *J* = 1.9 Hz, 1H); ^{13}C NMR (100 MHz, $CDCl_3$) δ = 14.4, 36.7, 40.1, 56.3, 56.9, 90.0, 91.7, 93.6, 104.1, 104.7, 159.9, 167.9, 172.2, 175.8, 192.6, 198.4 (See Table 8 and Figure 12); HRESIMS m/z 305.1032 $[M+H]^+$ (calc'd for $C_{16}H_{17}O_6$, 305.1020).

6-*O*-desmethyl-7-griseofulvin ((2*S*,6'*R*)-7-chloro-6-hydroxy-2',4-dimethoxy-6'-methyl-3H-spiro[benzofuran-2,1'-cyclohexan]-2'-ene-3,4'-dione; **6**): White solid; $[\alpha]_D^{27}$ +278 (*c* 0.1, MeOH); UV (solvent) λ_{max} (log ε) 243 (4.3), 288 (4.3), 347 (3.7) nm; ^{1}H NMR (400 MHz, $CDCl_3$) δ = 0.97 (d, *J* = 6.7 Hz, 3H), 2.44 (dd, *J* = 16.6 Hz, 4.7 Hz,

1H), 2.83 (dqd, *J* = 13.3 Hz, 6.7 Hz, 4.7 Hz, 1H), 3.04 (dd, *J* = 16.6 Hz, 13.3 Hz, 1H), 3.63 (s, 3H), 3.92 (s, 3H), 5.55 (s, 1H), 6.25 (s, 1H); ^{13}C NMR (100 MHz, $CDCl_3$) δ = 14.4, 36.5, 40.1, 56.6, 56.8, 91.2, 93.6, 95.2, 105.0, 105.4, 158.0, 161.8, 169.9, 170.7, 192.2, 197.2. (See Table 9 and Figure 13); HRESIMS m/z 339.0646 $[M+H]^+$ (calc'd for $C_{16}H_{16}ClO_6$, 339.0630).

General fluorination procedure with selectfluor. To an ice-cold acetonitrile solution of the natural product was slowly added a freshly prepared acetonitrile solution of Selectfluor. The reaction mixture was allowed to stir at 0 °C for 4 h and then heated to 50 °C and monitored by HPLC. After 24 h, the reaction mixture was cooled to room temperature and the solvent was removed *in vacuo.*

Fluorination of griseofulvin (1). Griseofulvin (**1**) (10.0 mg, 0.028 mmol, 0.02 M) and Selectfluor (15.1 mg, 0.043 mmol, 0.02 M) were reacted via the general method. The residue was purified by preparative HPLC eluting with a linear gradient from 40% to 60% CH_3CN in H_2O (0.1% HCOOH) over 30 min to obtain **7** (t_R =19 min) and **8a**/**8b** (t_R =13 min).

5-Fluorogriseofulvin ((2*S*,6'*R*)-7-chloro-5-fluoro-2',4,6-trimethoxy-6'-methyl-3H-spiro[benzofuran-2,1'-cyclohexan]-2'-ene-3,4'-dione; **7**):White solid $[\alpha]_D^{27}$ +290 (*c* 0.1, MeOH) 1.0 mg (10 % yield, 21 % yield based on recovered starting material); ^{1}H NMR (400 MHz, $CDCl_3$) δ = 0.95 (d, *J* = 6.7 Hz, 3H), 2.45 (dd, *J* = 16.7 Hz, 4.4 Hz, 1H), 2.85 (dqd, *J* = 13.3 Hz, 6.7 Hz, 4.4 Hz, 1H), 2.98 (dd, *J* = 16.7 Hz, 13.3 Hz, 1H), 3.64 (s, 3H), 4.17 (d, *J* = 3.1 Hz, 3H), 4.20 (d, *J* = 3.1 Hz, 3H), 5.56 (s, 1H).^{13}C NMR (100 MHz, $CDCl_3$) δ = 14.4, 36.6, 40.0, 56.9, 62.1 (d, *J* = 7.0 Hz), 62.6 (d, *J* = 6.0 Hz), 90.6, 103.4,

105.2, 108.0, 142.9 (d, J = 244.3 Hz), 144.7 (d, J = 9.0 Hz), 153.9 (d, J = 12.1 Hz), 164.9, 170.5, 193.5 (d, J = 4.0 Hz), 196.8. ^{19}F NMR (470 MHz, $CDCl_3$) δ = -155.5 (sept. J = 3.1 Hz) (See Table 10 and Figure 14-18); HRESIMS m/z 371.0696 $[M+H]^+$ (calc'd for $C_{17}H_{17}ClFO_6$ 371.0692).

(2*S*,6'*R*)-7-chloro-5-fluoro-2',4,6-trimethoxy-6'-methyl-3H-spiro[benzofuran-2,1'-cyclohexan]-2'-ene-3,4'-dione (**8a/8b**):White solid; 2.3 mg (Isolated as a diastereoisomeric mixture of the two compounds with a 2:1 ratio, 23 % yield, 49 % yield based on recovered starting material); white solid; **8a**:^{1}H NMR (400 MHz, $CDCl_3$) δ = 1.00 (d, J = 6.3 Hz, 3H), 2.46 (dd, J = 16.1 Hz, 4.2 Hz, 1H), 2.89 (m, 1H), 2.97 (m, 1H), 3.69 (s, 3H), 3.94 (s, 3H), 5.55 (d, J = 1.8 Hz, 1H), 5.58 (s, 1H). ^{13}C NMR (100 MHz, $CDCl_3$) δ = 14.1, 36.1, 39.7, 57.1, 57.8, 94.1, 94.1 (d, J = 252.3), 102.0 (d, J = 2.0 Hz), 105.4, 110.1 (d, J = 3.0 Hz), 162.8 (d, J = 19.1 Hz), 168.1, 176.9 (d, J = 2.0 Hz), 185.3 (d, J = 21.0 Hz), 191.8, 195.8. ^{19}F NMR (470 MHz, $CDCl_3$) δ = -126.4 (d, J = 1.8 Hz). **8b**:^{1}H NMR (400 MHz, $CDCl_3$) δ = 1.06 (d, J = 6.3 Hz, 3H), 2.46 (dd, J = 16.1 Hz, 4.2 Hz, 1H), 2.95 (m, 1H), 2.97 (m, 1H), 3.67 (s, 3H), 3.94 (s, 3H), 5.55 (d, J = 1.8 Hz, 1H), 5.58 (s, 1H). ^{13}C NMR (100 MHz, $CDCl_3$) δ = 14.1, 36.5, 39.7, 57.2, 57.8, 94.0 (d, J = 254.3), 94.1, 102.0 (d, J = 2.0 Hz), 105.5, 110.0 (d, J = 3.0 Hz), 162.8 (d, J = 19.1 Hz), 167.7, 176.9 (d, J = 2.0 Hz), 185.4 (d, J = 21.0 Hz), 191.7, 195.8. ^{19}F NMR (470 MHz, $CDCl_3$) δ = -127.5 (d, J = 1.8 Hz) (See Table 11 and Figures 19-23); HRESIMS m/z 357.0543 $[M+H]^+$ (calc'd for $C_{16}H_{15}ClFO_6$ 357.0536).

Fluorination of 7-dechlorogriseofulvin (3). 7-Dechlorogriseofulvin (**3**) (7.0 mg, 0.022 mmol) and Selectfluor (11.7 mg, 0.033 mmol) were reacted via the general method.

The residue was purified by preparative HPLC eluting with a linear gradient from 30% to 50% CH_3CN in H_2O (0.1% HCOOH) over 30 min to obtain compounds **9** (t_R =21 min), and **10** (t_R =18 min).

5-Fluoro-7-dechlorogriseofulvin ((2*S*,6'*R*)-5-fluoro-2',4,6-trimethoxy-6'-methyl-3H-spiro[benzofuran-2,1'-cyclohexan]-2'-ene-3,4'-dione; **9**):White solid; $[\alpha]_D^{27}$ +289 (*c* 0.1, MeOH) 2.3 mg (33 % yield, 46 % yield based on recovered starting material); ^{1}H NMR (500 MHz, $CDCl_3$) δ = 0.95 (d, *J* = 6.9 Hz, 3H), 2.75 (dd, *J* = 17.2 Hz, 4.6 Hz, 1H), 2.75 (m, 1H), 3.02 (dd, *J* = 17.2 Hz, 13.2 Hz, 1H), 3.63 (s, 3H), 3.98 (s, 3H), 4.20 (d, *J* = 3.3 Hz, 3H), 5.55 (s, 1H), 6.37 (d, *J* = 5.2 Hz, 1H). ^{13}C NMR (125 MHz, $CDCl_3$) δ = 14.4, 36.7, 40.1, 56.8, 57.0, 62.1 (d, *J* = 7.5 Hz), 89.8, 90.0, 105.0, 105.5, 139.6 (d, *J* = 237.5 Hz), 145.0 (d, *J* = 8.8 Hz), 158.6 (d, *J* = 11.3 Hz), 170.4, 171.1, 193.4, 197.2. ^{19}F NMR (470 MHz, $CDCl_3$) δ = -163.0 (m) (See Table 12 and Figure 24-28); HRESIMS m/z 337.1080 $[M+H]^+$ (calc'd for $C_{17}H_{18}FO_6$ 337.1082).

7-Fluoro-7-dechlorogriseofulvin ((2*S*,6'*R*)-7-fluoro-2',4,6-trimethoxy-6'-methyl-3H-spiro[benzofuran-2,1'-cyclohexan]-2'-ene-3,4'-dione; **10**):White solid; $[\alpha]_D^{27}$ +230 (*c* 0.1, MeOH) 1.3 mg (19 % yield, 26 % yield based on recovered starting material); ^{1}H NMR (700 MHz, $CDCl_3$) δ = 0.98 (d, *J* = 6.7 Hz, 3H), 2.43 (dd, *J* = 17.2 Hz, 4.8 Hz, 1H), 2.81 (m, 1H), 3.03 (dd, *J* = 17.2 Hz, 13.4 Hz, 1H), 3.62 (s, 3H), 3.95 (s, 3H), 4.02 (s, 3H), 5.54 (s, 1H), 6.09 (d, *J* = 5.2 Hz, 1H). ^{13}C NMR (175 MHz, $CDCl_3$) δ = 14.4, 36.6, 40.2, 56.5, 56.8, 57.3, 90.1, 91.0, 105.0, 105.0, 132.4 (d, *J* = 238.0 Hz), 154.7 (d, *J* = 1.8 Hz), 157.4 (d, *J* = 7.0 Hz), 160.3 (d, *J* = 8.8 Hz), 170.9, 192.4 (d, *J* = 2.4 Hz),

197.1. ^{19}F NMR (470 MHz, $CDCl_3$) δ = -171.3 (d, J = 5.2 Hz) (See Table 13 and Figure 29-33); HRESIMS m/z 337.1079 $[M+H]^+$ (calc'd for $C_{17}H_{18}FO_6$ 337.1082).

Fluorination of 7-dechloro-5'-hydroxygriseofulvin (4). 7-dechloro-5'-hydroxygriseofulvin (**4**) (6.2 mg, 0.018 mmol) and Selectfluor (9.8 mg, 0.027 mmol) were reacted via the general method. After purification using preparative HPLC eluting with a linear gradient from 30% to 50% CH_3CN in H_2O (0.1% HCOOH) over 30 min to obtain compounds **11** (t_R =16 min), and **12** (t_R =14 min).

5-Fluoro-5'-hydroxy-7-dechlorogriseofulvin ((2*S*,5'*R*,6'*R*)-5-fluoro-5'-hydroxy-2',4,6-trimethoxy-6'-methyl-3H-spiro[benzofuran-2,1'-cyclohexan]-2'-ene-3,4'-dione; **11**): White solid; $[\alpha]_D^{27}$ +240 (*c* 0.05, MeOH); 1.7 mg (27 % yield, 35 % yield based on recovered starting material); ^{1}H NMR (700 MHz, $CDCl_3$) δ = 1.10 (d, J = 6.9 Hz, 3H), 2.54 (dq, J = 12.0 Hz, 6.9 Hz, 1H), 3.67 (s, 3H), 3.98 (s, 3H), 4.21 (d, J = 3.6 Hz, 3H), 4.67 (d, J = 12.0 Hz, 1H), 5.61 (s, 1H), 6.36 (d, J = 5.4 Hz, 1H). ^{13}C NMR (175 MHz, $CDCl_3$) δ = 11.1, 43.7, 57.1, 57.1, 62.1 (d, J = 6.7 Hz), 71.4, 89.1, 90.4, 101.9, 105.5 (d, J = 1.4 Hz), 139.6 (d, J = 241.6 Hz), 145.1 (d, J = 7.9 Hz), 158.9 (d, J = 11.2 Hz), 170.5, 171.7, 193.4 (d, J = 3.3 Hz), 197.5. ^{19}F NMR (470 MHz, $CDCl_3$) δ = -162.7 (dq, J = 5.4 Hz, 3.6 Hz) (See Table 14 and Figures 34-38); HRESIMS m/z 353.1027 $[M+H]^+$ (calc'd for $C_{17}H_{18}FO_7$ 353.1031).

7-Fluoro-5'-hydroxy-7-dechlorogriseofulvin ((2*S*,5'*R*,6'*R*)-7-fluoro-5'-hydroxy-2',4,6-trimethoxy-6'-methyl-3H-spiro[benzofuran-2,1'-cyclohexan]-2'-ene-3,4'-dione; **12**): White solid;$[\alpha]_D^{27}$ +270 (*c* 0.03, MeOH); 1.0 mg (16% yield, 21 % yield based on recovered starting material); ^{1}H NMR (700 MHz, $CDCl_3$) δ = 1.13 (d, J = 6.3 Hz, 3H),

2.60 (dq, J = 12.0 Hz, 6.3Hz, 1H), 3.66 (s, 3H), 3.95 (s, 3H), 4.03 (s, 3H), 4.68 (d, J = 12.0 Hz, 1H), 5.61 (s, 1H), 6.10 (d, J = 5.1 Hz, 1H); ^{13}C NMR (175 MHz, $CDCl_3$) δ = 11.1, 43.7, 56.6, 57.1, 57.3, 71.4, 90.2, 91.2, 101.8, 104.9, 132.2 (d, J = 237.0 Hz), 154.8 (d, J = 1.8 Hz), 157.6 (d, J = 8.8 Hz), 160.3 (d, J = 10.5 Hz), 171.5, 192.4 (d, J = 2.7 Hz), 197.4. ^{19}F NMR (470 MHz, $CDCl_3$) δ = -171.1 (d, J = 5.1 Hz) (See Table 15 and Figures 39-43); HRESIMS m/z 353.1022 $[M+H]^+$ (calc'd for $C_{17}H_{18}FO_7$ 353.1031).

Cytotoxicity assay. Human melanoma cancer cells (MDA-MB-435), human breast cancer cells (MDA-MB-231) and human cancer cells (OVCAR3) were procured from the American Type Culture Collection (Manassas, VA). The cell lines were cultivated in RPMI 1640 medium, supplemented with fetal bovine serum (10%), penicillin (100 units/mL), and streptomycin (100 µg/mL); and grown at 37°C under 5% CO_2. Huh7.5.1 cells were cultured in DMEM medium as previously described.[100] Cells in log-phase growth were harvested by trypsinization followed by two washing to remove all traces of enzyme. Cells were seeded in 96-well clear, flat-bottom plate (Corning) at a density of 5,000 cells per well, and each plate was incubated overnight at 37°C under 5% CO_2. Samples dissolved in DMSO were diluted and added to the appropriate wells to give final concentrations of 20 and 2 µg/mL (20, 4, 0.8, 0.16, and 0.032 µM for pure compounds) with a total volume of 100 µL and 0.5% DMSO. The cells with the test samples were then incubated for 72 h at 37 °C. Cell viability was examined using a commercial absorbance assay (Cell titer 96® Aqueous One Solution Cell Proliferation Assay, Promega Corp, Madison, WI). For Huh7.5.1 cells, viability was determined by measuring ATP levels in cells using the ATPlite kit (Perkin Elmer, Waltham, MA) as

previously described.[101] Results are expressed as percent survival relative to the solvent (DMSO) control.

Antifungal assay. The test fungal isolate *Microsporum gypseum* was kept at the Fungal Culture Collection at the Department of Chemistry and Biochemistry at the University of North Carolina at Greensboro. The test isolate was maintained on Saboraud dextrose agar plates at rt and sub-cultured monthly throughout this study. The test compounds were dissolved in DMSO and 5 µL were loaded onto a 6 mm filter paper disk to obtain the desired 25 µg sample concentration per disk. Antimycotic activity was carried out by the agar disk diffusion method.[102,103] Following growth of the fungi, the conidia were harvested in sterile distilled deionized water. The inoculum was adjusted to 0.5-1.0 OD (~10^5 cells/ mL) at 600 nm. Mueller-Hinton agar supplemented with 2% glucose and 0.5 µg/ml methylene blue was then seeded with 100 uL of the inoculum. Disks impregnated with the test agent were aseptically added onto the surface of the inoculated plates. The sensitivity of the microorganism to the compounds was determined after 5 d by measuring the diameter (in mm) of the zones of inhibition around the disks.

Principal component analysis. The structures and SMILES where generated with ChemDraw and 11 molecular properties were calculated using QikProp (version 3.5)[104]. The calculated properties can be divided in three main groups: electronic, surface, and solubility descriptors. The electronic descriptors were: calculated electron affinity EA (eV), predicted polarizability (QPpolrz), electrotopological state (Estate) and dipole moment of the molecule (dipole). The surface descriptors were: total solvent accessible

area (SAS), hydrophilic component of the SASA (FISA), carbon and attached hydrogen component of the SASA (PISA), Van der Waals surface area of polar nitrogen and oxygen atoms (PSA), and solvent-accessible surface area of fluorine atoms (SAFluorine). The solubility descriptors were: free energy of solvation in hexadecane (QPlogPC16) and predicted aqueous solubility (QPlogS). To generate a visual representation of the chemical space based on these properties, a principal component analysis was performed using Molecular Operating Environment (version 2014.08)[105], and Data Warrior (version 4.2.2)[106].

Acknowledgements

This research was supported via program project grant P01 CA125066 from the National Cancer Institute/National Institutes of Health, Bethesda, MD, USA. The high-resolution mass spectrometry data were acquired in the Triad Mass Spectrometry Laboratory at the University of North Carolina at Greensboro, Greensboro, NC, USA. We also acknowledge the support of the Universidad Nacional Autónoma de México (UNAM), grant PAPIME PE200116, and the Programa de Apoyo a la Investigación y el Posgrado (PAIP), grant 5000-9163, Facultad de Química, UNAM.

Supporting Information

Table 3. *In Vitro* Cytotoxicity of *X. cubensis* (MSX48662) Extract Against Three Human Cancer Cell Lines.

Sample	MDA-MB-435[a]		MDA-MB-231[b]		OVCAR3[c]	
	20 μg/mL	2 μg/mL	20 μg/mL	2 μg/mL	20 μg/mL	2 μg/mL
MSX48662	25	28	50	62	23	59

[a] melanoma cancer cells; [b] human breast cancer cells;
[c] human ovarian cancer cells

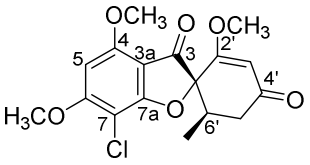

Table 4. NMR Data for Griseofulvin (1) in $CDCl_3$.

Position	δ_C[a]	type	δ_H, mult (*J* in Hz)[b]	HMBC
2	90.9	C		
3	192.6	C		
3a	105.2	C		
4	157.9	C		
5	89.5	CH	6.13, s	3, 3a, 4, 6, 7
6	164.7	C		
7	97.3	C		
7a	169.6	C		
2´	170.9	C		
3´	105.0	CH	5.53, s	2, 2´, 4´, 5´
4´	197.2	C		
5´	40.1	CH_2	α 2.42, dd (16.8, 4.6)	2, 3´, 4´, 6´, 6´-Me
			β 3.03, dd (16.8, 13.4)	2, 4´, 6´, 6´-Me
6´	36.5	CH	2.84, m	2, 3, 5´, 6´-Me
6´-Me	14.4	CH_3	0.96, d (6.8)	2, 3, 5´, 6´
4-OMe	56.5	CH_3	3.98, s	4
6-OMe	57.1	CH_3	4.03, s	6
2´-OMe	56.8	CH_3	3.61, s	3a, 2´

[a] 100 MHz, [b] 400 MHz Jeol NMR Spectrometer

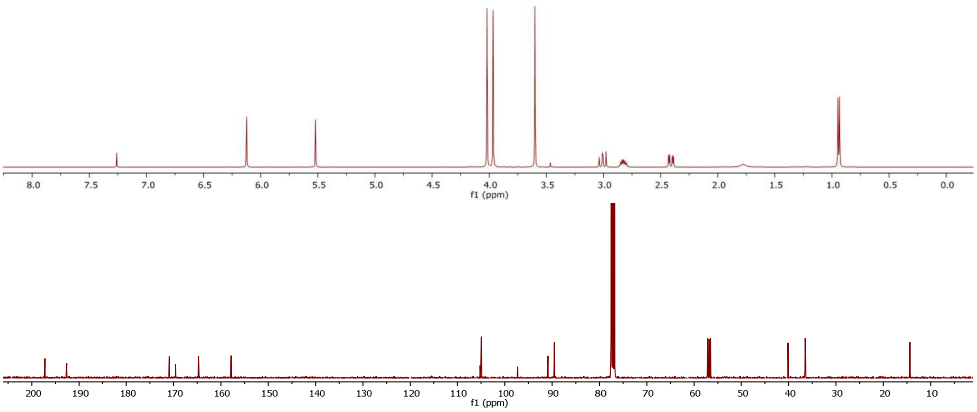

Figure 6. ^{1}H NMR (400 MHz; Top) and ^{13}C NMR (100 MHz; Bottom) Spectra of Griseofulvin (1) in $CDCl_3$.

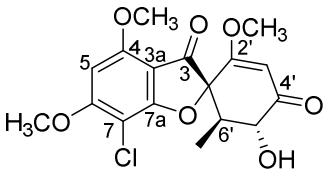

Table 5. NMR Data for 5´-Hydroxygriseofulvin (2) in $CDCl_3$.

Position	δ_C[a]	type	δ_H, mult (*J* in Hz)[b]	HMBC
2	91.2	C		
3	192.6	C		
3a	105.2	C		
4	158.0	C		
5	89.7	CH	6.14, s	3a, 4, 6, 7
6	165.0	C		
7	97.4	C		
7a	169.8	C		
2´	171.5	C		
3´	101.8	CH	5.61, s	2, 2´, 5´
4´	197.5	C		
5´	71.5	CH	4.68, d (12.2)	
6´	43.6	CH	2.64,dq (12.2, 6.7)	2, 5´
6´-Me	11.1	CH_3	1.11, d (6.7)	2, 5´, 6´
4-OMe	56.6	CH_3	3.99, s	4
6-OMe	57.2	CH_3	4.04, s	6
2´-OMe	57.1	CH_3	3.65, s	2´

[a] 175 MHz, [b] 700 MHz Jeol NMR Spectrometer

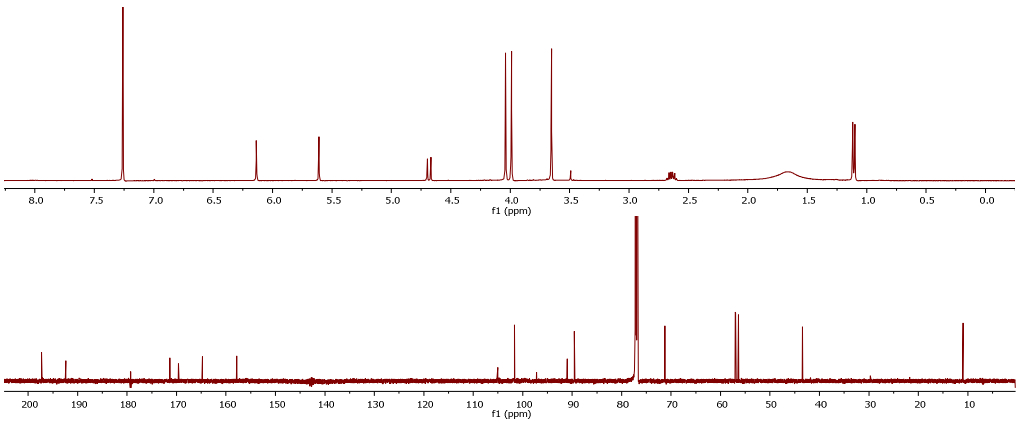

Figure 7. ^{1}H NMR (700 MHz; Top) and ^{13}C NMR (175 MHz; Bottom) Spectra of 5´-Hydroxygriseofulvin (2) in $CDCl_3$.

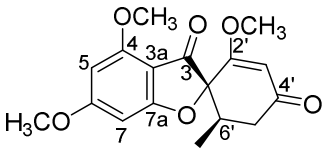

Table 6. NMR Data for 7-Dechlorogriseofulvin (3) in $CDCl_3$.

Position	δ_C[a]	type	δ_H, mult (*J* in Hz)[b]	HMBC
2	90.0	C		
3	192.7	C		
3a	104.4	C		
4	159.2	C		
5	93.5	CH	6.03, d (1.9)	3, 3a, 4, 6, 7
6	170.5	C		
7	88.6	CH	6.23, d (1.9)	3a, 5, 6, 7a
7a	176.2	C		
2´	171.5	C		
3´	104.9	CH	5.53, s	2, 2´, 4´, 5´
4´	197.6	C		
5´	40.2	CH_2	α 2.39, dd (16.8, 4.7) β 3.03, dd (16.8, 13.4)	2, 3´, 4´, 6´, 6´-Me,
6´	36.7	CH	2.74 (m)	2, 3, 2´, 4´, 5´, 6´-Me
6´-Me	14.4	CH_3	0.94, d (6.6)	2, 4´, 5´, 6´
4-OMe	56.2	CH_3	3.90, s	4
6-OMe	56.2	CH_3	3.89, s	6
2´-OMe	56.8	CH_3	3.61, s	2´

[a] 100 MHz, [b] 400 MHz Jeol NMR Spectrometer

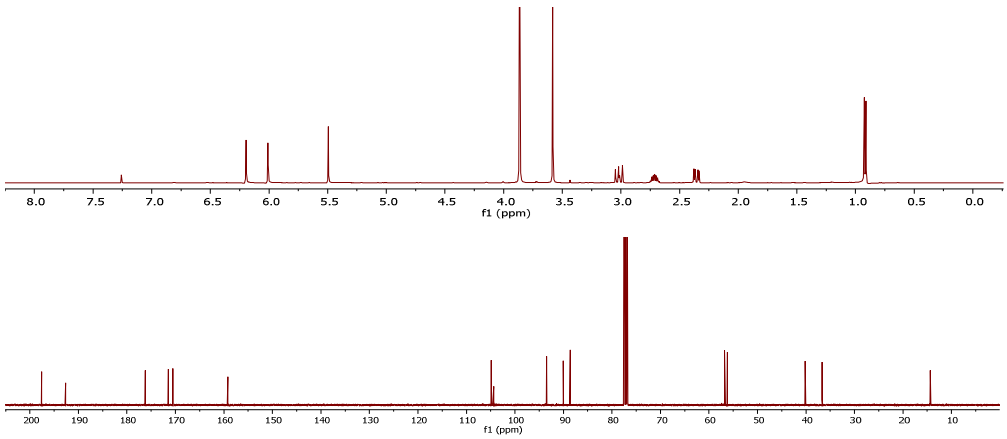

Figure 8. ^{1}H NMR (400 MHz; Top) and ^{13}C NMR (100 MHz; Bottom) Spectra of 7-Dechlorogriseofulvin (3) in $CDCl_3$.

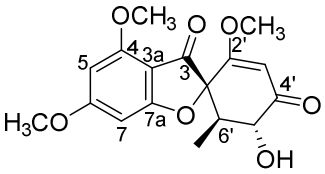

Table 7. NMR Data for 7-Dechloro-5´-hydroxygriseofulvin (4) in $CDCl_3$.

Position	δ_C[a]	type	δ_H, mult (*J* in Hz)[b]	HMBC
2	90.5	C		
3	192.6	C		
3a	104.4	C		
4	159.3	C		
5	93.7	CH	6.06, d (1.1)	3a, 4, 6, 7
6	170.8	C		
7	88.6	CH	6.22, d (1.1)	3a, 5, 6, 7a
7a	176.3	C		
2´	172.1	C		
3´	101.7	CH	5.61, s	2, 2´, 4´, 5´
4´	197.8	C		
5´	71.5	CH	4.71, d (12.1)	4´, 6´, 6´-Me
6´	43.9	CH	2.55, dq (12.1, 6.6)	2, 3, 5´, 6´-Me
6´-Me	11.2	CH_3	1.11, d (6.6)	2, 5´, 6´
4-OMe	56.3	CH_3	3.92, s	4
6-OMe	56.3	CH_3	3.91, s	6
2´-OMe	57.1	CH_3	3.66, s	2´

[a] 100 MHz, [b] 400 MHz Jeol NMR Spectrometer

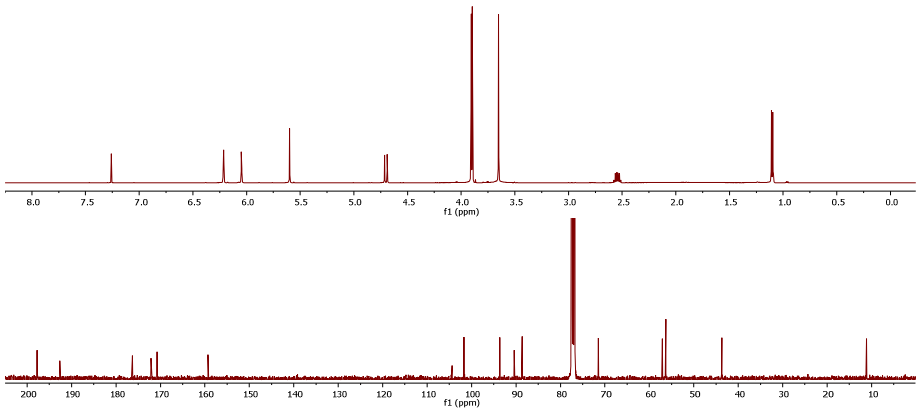

Figure 9. ^{1}H NMR (400 MHz; Top) and ^{13}C NMR (100 MHz; Bottom) Spectra of 7-Dechloro-5´-hydroxygriseofulvin (4) in $CDCl_3$.

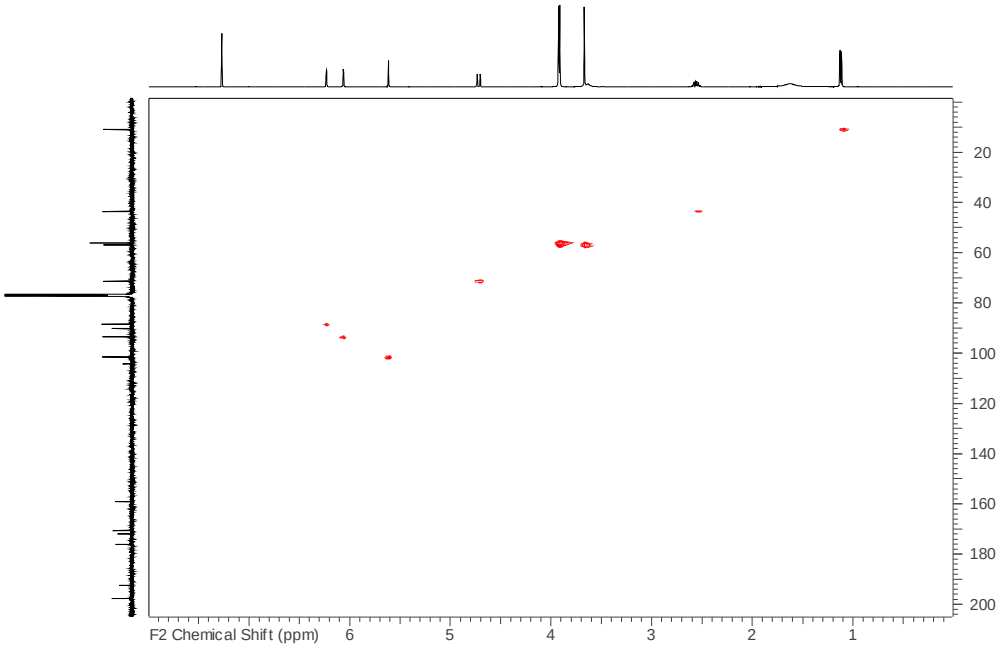

Figure 10. ^{1}H-^{13}C Edited-HSQC Spectrum of 7-Dechloro-5´-hydroxygriseofulvin (4).

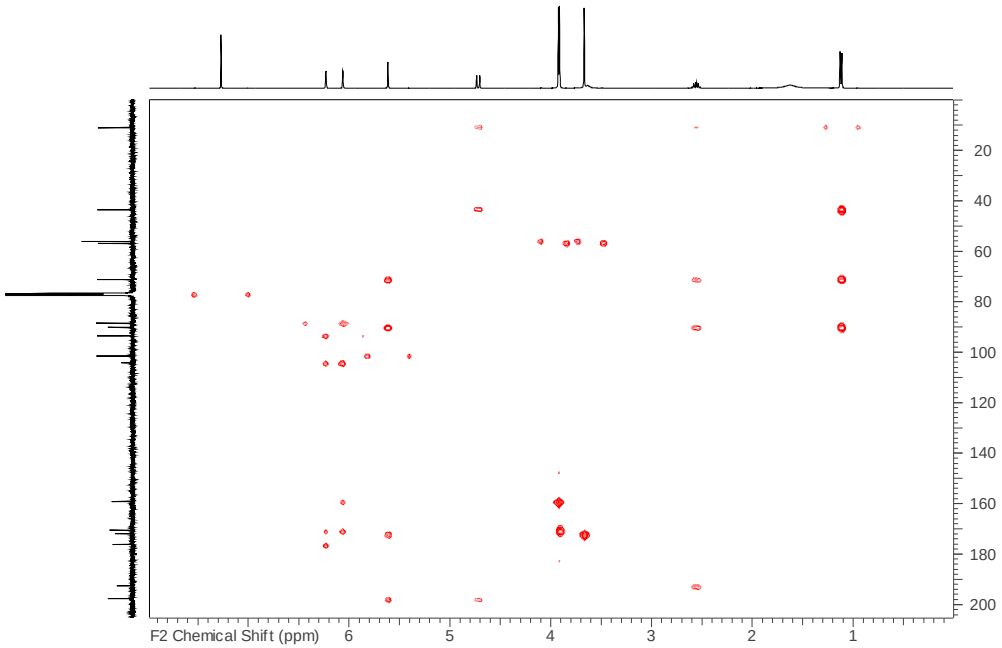

Figure 11. HMBC Spectrum of 7-Dechloro-5´-hydroxygriseofulvin (4).

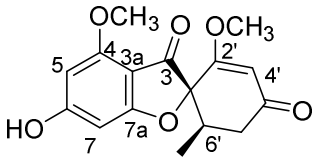

Table 8. NMR Data for 6-O-desmethyl-7-dechlorogriseofulvin (5) in $CDCl_3$.

Position	δ_C[a]	type	δ_H, mult (*J* in Hz)[b]	HMBC
2	90.0	C		
3	192.6	C		
3a	104.1	C		
4	159.9	C		
5	93.6	CH	6.05, d (1.9)	3, 3a, 4, 5, 6
6	167.9	C		
7	91.7	CH	6.20, d (1.9)	3a, 6, 7, 7a
7a	175.8	C		
2´	172.2	C		
3´	104.7	CH	5.55, s	2, 2´, 4´, 5´
4´	198.4	C		
5´	40.1	CH_2	α 2.43, dd (16.7, 4.8)	2, 3´, 4´
			β 3.08, dd (16.7, 13.2)	4´, 6´, 6´-Me
6´	36.7	CH	2.76, dqd (13.2, 6.7, 4.8)	2, 3
6´-Me	14.4	CH_3	0.97, d (6.7)	2, 5´, 6´
4-OMe	56.3	CH_3	3.90, s	4
2´-OMe	56.9	CH_3	3.64, s	2´

[a] 100 MHz, [b] 400 MHz Jeol NMR Spectrometer

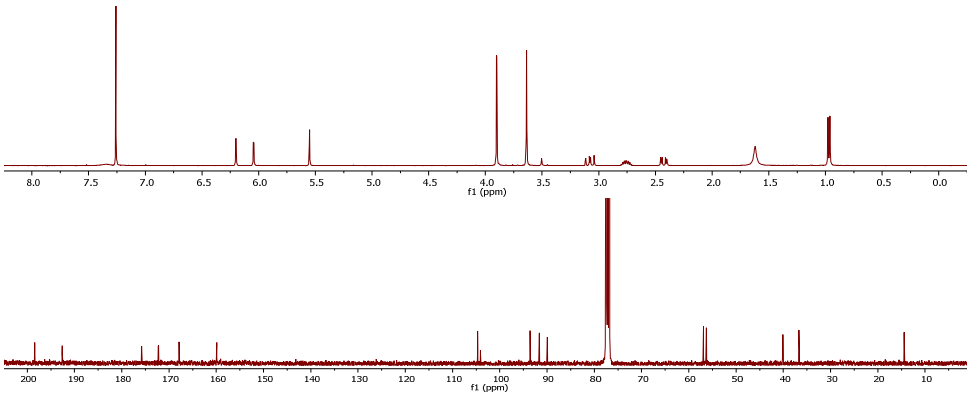

Figure 12. ^{1}H NMR (400 MHz; Top) and ^{13}C NMR (100 MHz; Bottom) Spectra of 6-O-desmethyl-7-dechlorogriseofulvin (5) in $CDCl_3$.

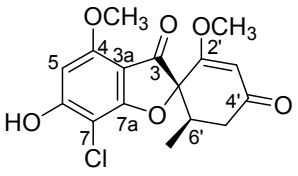

Table 9. NMR Data for 6-O-desmethylgriseofulvin (6) in $CDCl_3$.

Position	δ_C[a]	type	δ_H, mult (*J* in Hz)[b]	HMBC
2	91.2	C		
3	192.2	C		
3a	105.4	C		
4	158.0	C		
5	93.6	CH	6.25, s	3, 3a, 4, 6, 7
6	161.8	C		
7	95.2	C		
7a	169.9	C		
2´	170.7	C		
3´	105.0	CH	5.55, s	2, 2´, 4´, 5´
4´	197.2	C		
5´	40.1	CH_2	α 2.44, dd (16.6, 4.7)	2, 3´, 6´
			β 3.04, dd (16.6, 13.3)	4´, 6´, 6´-Me,
6´	36.5	CH	2.83, dqd (13.3, 6.7, 4.7)	6´-Me, 5´, 2, 3
6´-Me	14.4	CH_3	0.97, d (6.7)	6´, 5´, 2
4-OMe	56.6	CH_3	3.92, s	4
2´-OMe	56.8	CH_3	3.63, s	2´

[a] 100 MHz, [b] 400 MHz Jeol NMR Spectrometer

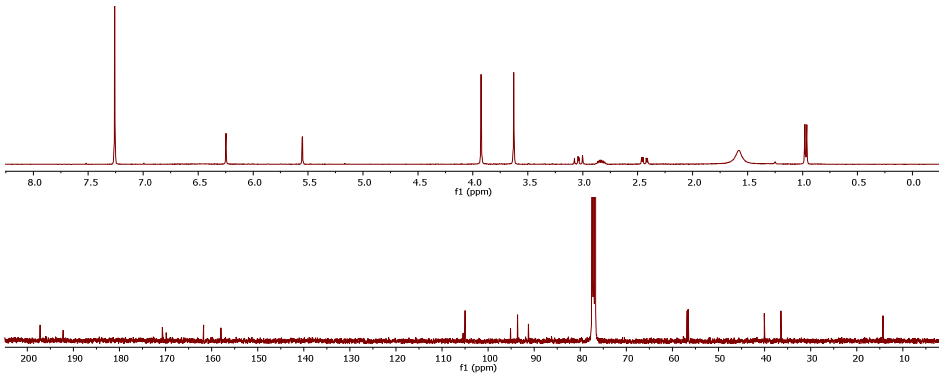

Figure 13. ^{1}H NMR (400 MHz; Top) and ^{13}C NMR (100 MHz; Bottom) Spectra of 6-O-desmethylgriseofulvin (6) in $CDCl_3$.

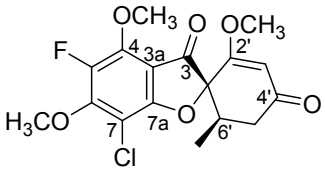

Table 10. NMR Data for Compound 7 in $CDCl_3$.

Position	δ_C mult (*J* in Hz)[a]	type	δ_H, mult (*J* in Hz)[b]	HMBC
2	90.6	C		
3	193.5,d (3.4)	C		
3a	108.0	C		
4	144.7, d (9.0)	C		
5	142.9, d (244.3)	C		
6	153.9, d (12.1)	C		
7	103.4	C		
7a	164.9	C		
2´	170.5	C		
3´	105.2	C	5.56, s	2, 2´, 4´, 5´
4´	196.8	C		
5´	40.0	CH_2	α 2.45, dd (16.7, 4.4)	3´
			β 2.98, dd (16.7, 13.3)	2, 4´, 6´, 6´-Me
6´	36.6	CH	2.85, dqd (13.3, 6.7, 4.4)	2, 3, 6´, 6´-Me
6´-Me	14.4	CH_3	0.95, d (6.7)	2, 5´, 6´
4-OMe	62.6, d (6.0)	CH_3	4.20, d (3.1)	4
6-OMe	62.1, d, (7.0)	CH_3	4.17, d (3.1)	6
2´-OMe	56.9	CH_3	3.64, s	2´

[a] 100 MHz, [b] 400 MHz Jeol NMR Spectrometer

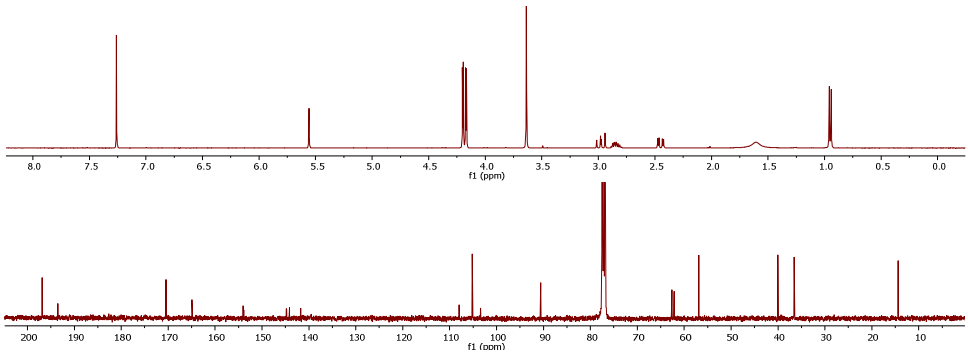

Figure 14. ^{1}H NMR (400 MHz; Top) and ^{13}C NMR (100 MHz; Bottom) Spectra of Compound 7 in $CDCl_3$.

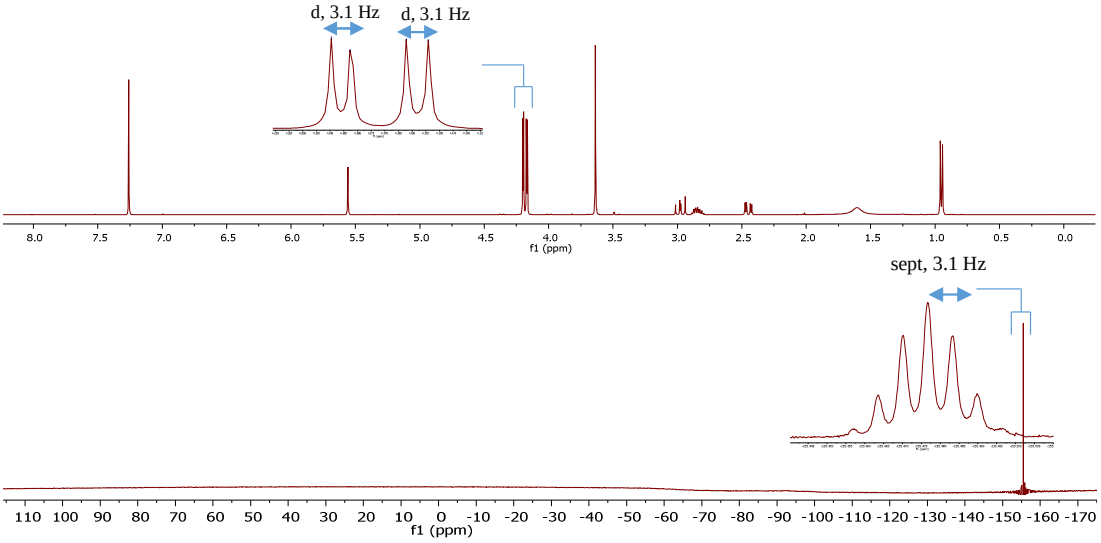

Figure 15. ^{1}H NMR (Top) and ^{19}F NMR (Bottom) Spectra of Compound 7 in $CDCl_3$.

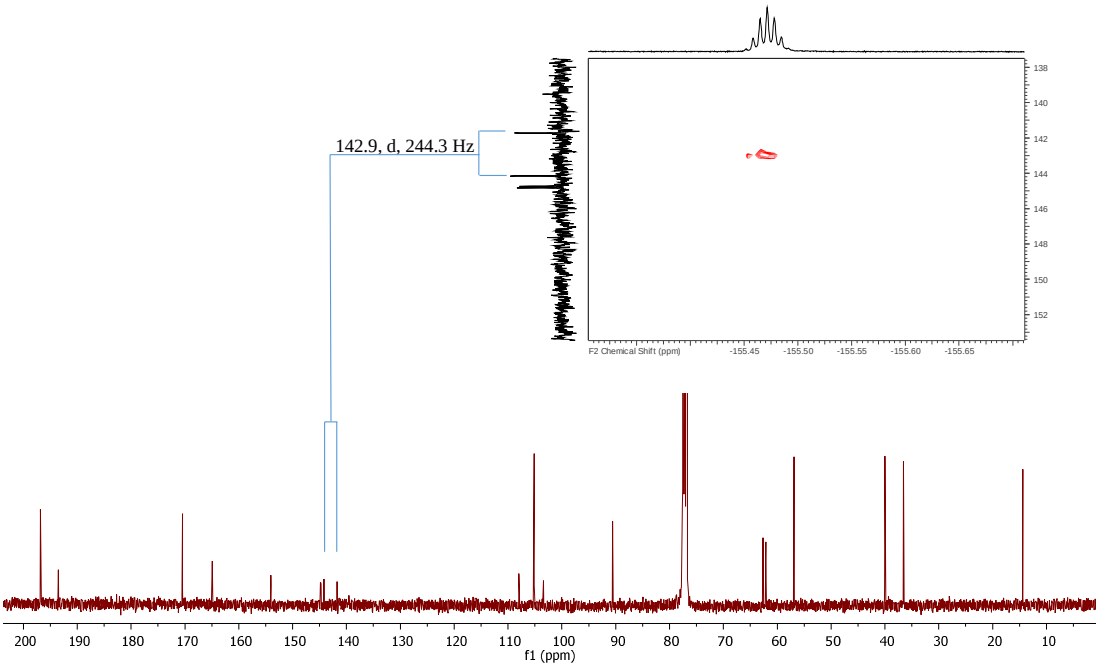

Figure 16. ^{13}C NMR and ^{19}F-^{13}C HMQC Spectrum of Compound 7 in $CDCl_3$.

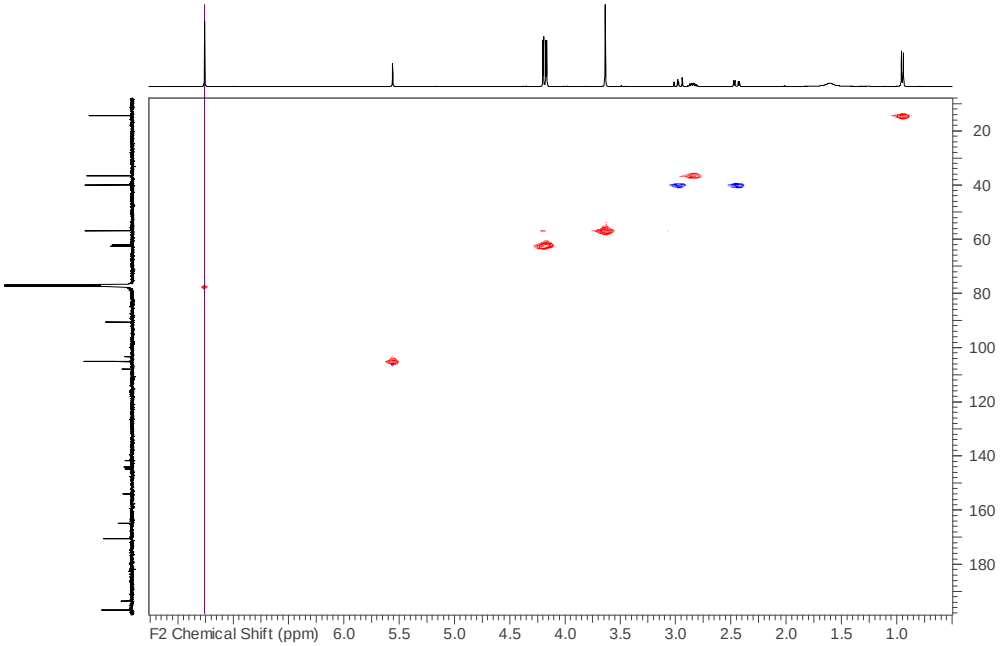

Figure 17. ^{1}H-^{13}C Edited-HSQC Spectrum of Compound 7 in $CDCl_3$.

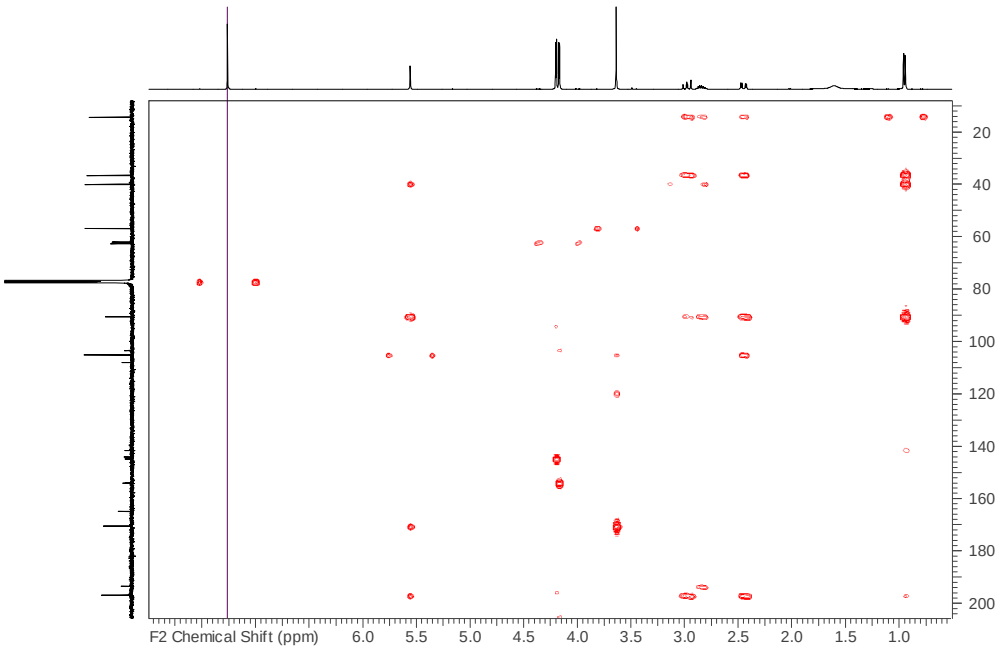

Figure 18. ^{1}H-^{13}C HMBC Spectrum of Compound 7 in $CDCl_3$.

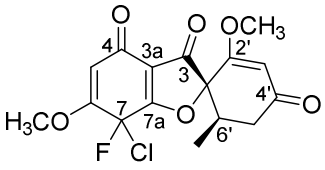

Table 11. NMR Data for Compounds 8a/8b in $CDCl_3$.

Position	8a		8b		
	δ_C, mult (J in Hz)[a]	δ_H, mult (J in Hz)[b]	δ_C, mult (J in Hz)[a]	δ_H, mult (J in Hz)[b]	HMBC
2	94.1		94.1		
3	191.8		191.7		
3a	110.1, d (3.0)		110.0, d (3.0)		
4	176.9, d (2.0)		176.9, d (2.0)		
5	102.0, d (2.0)	5.55, d (1.8)	102.0, d (2.0)	5.55, d (1.8)	3, 3a, 4, 6
6	162.8, d (19.1)		162.8, d (19.1)		
7	94.1, d (252.3)		94.0, d (254.3)		
7a	185.3, d (21.0)		185.4, d (21.0)		
2´	168.1		167.7		
3´	105.4	5.58, s	105.5	5.58, s	2, 2', 4', 5'
4´	195.8		195.8		
5´	39.7	α 2.46, dd (16.1, 4.2) β 2.97, m	39.7	α 2.46, dd (16.1, 4.2) β 2.97, m	4', 6', 6'-Me
6´	36.1	2.89, m	36.5	2.95, m	2, 3, 5', 6'-Me
6´-Me	14.1	1.00, d (6.3)	14.1	1.06, d (6.5)	2, 5', 6'
6-OMe	57.8	3.94, s	57.8	3.94, s	5, 6
2´-OMe	57.1	3.69, s	57.2	3.67, s	2'

[a] 100 MHz, [b] 500 MHz Jeol NMR Spectrometer

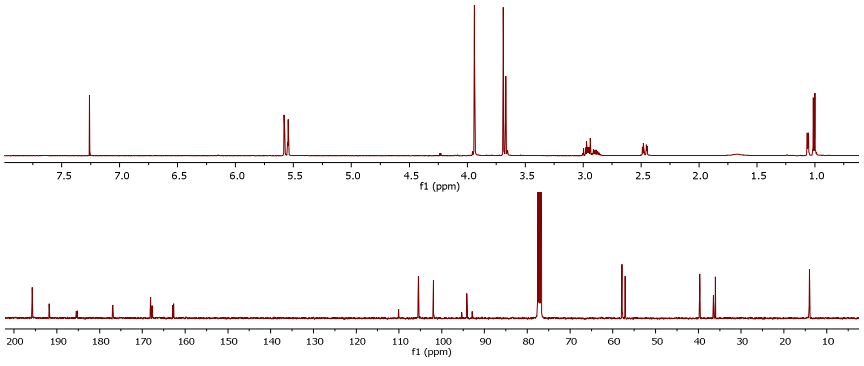

Figure 19. ^{1}H NMR (400 MHz; Top) and ^{13}C NMR (100 MHz; Bottom) Spectra of (8a/8b) in $CDCl_3$.

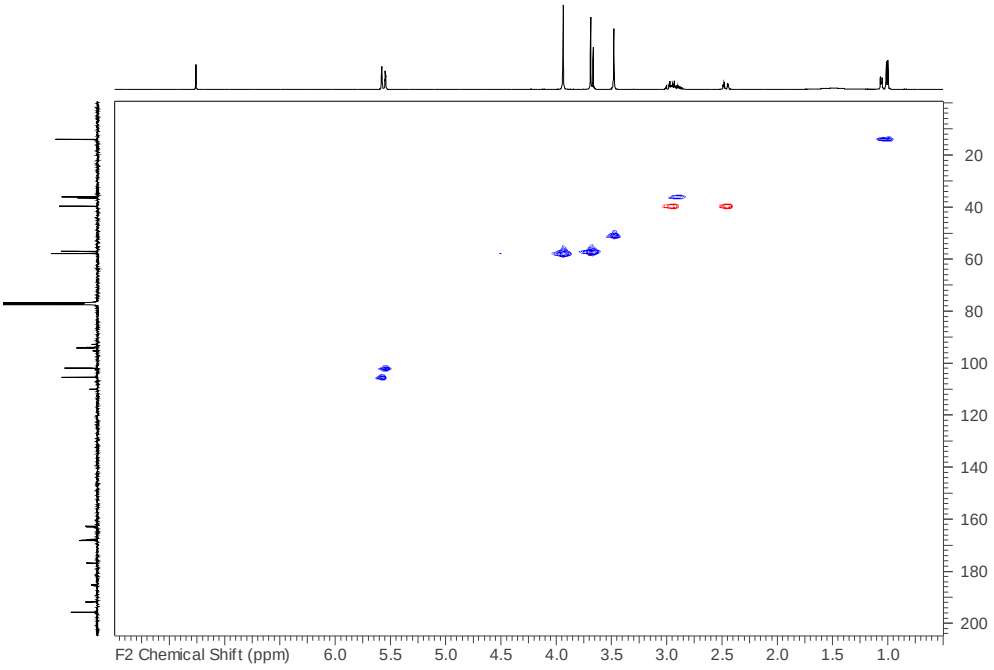

Figure 20. ^{1}H-^{13}C Edited-HSQC Spectrum of Compounds 8a/8b in $CDCl_3$.

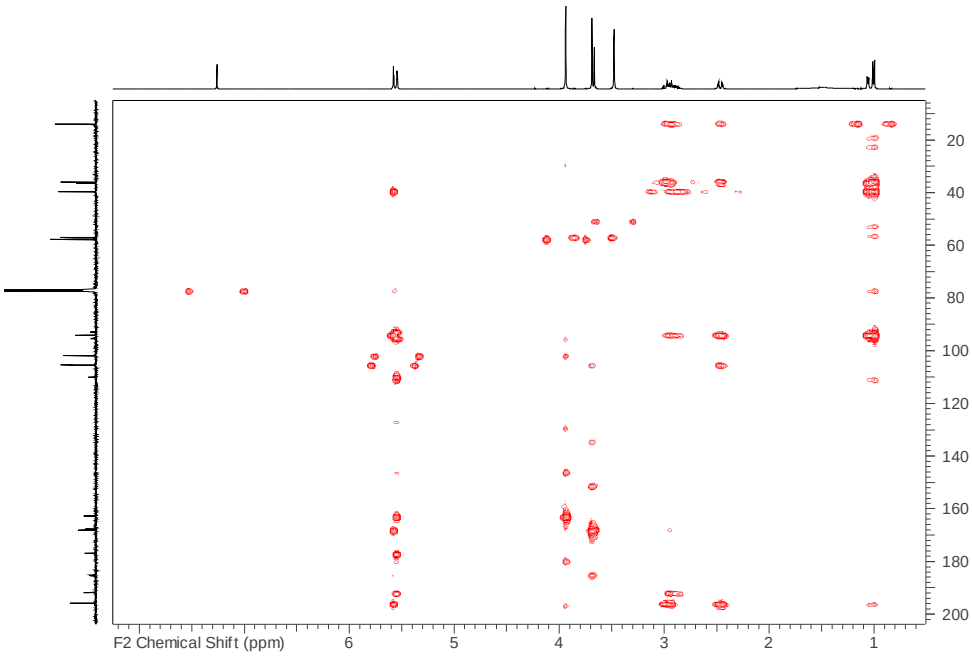

Figure 21. ^{1}H-^{13}C HMBC Spectrum of Compounds 8a/8b in $CDCl_3$.

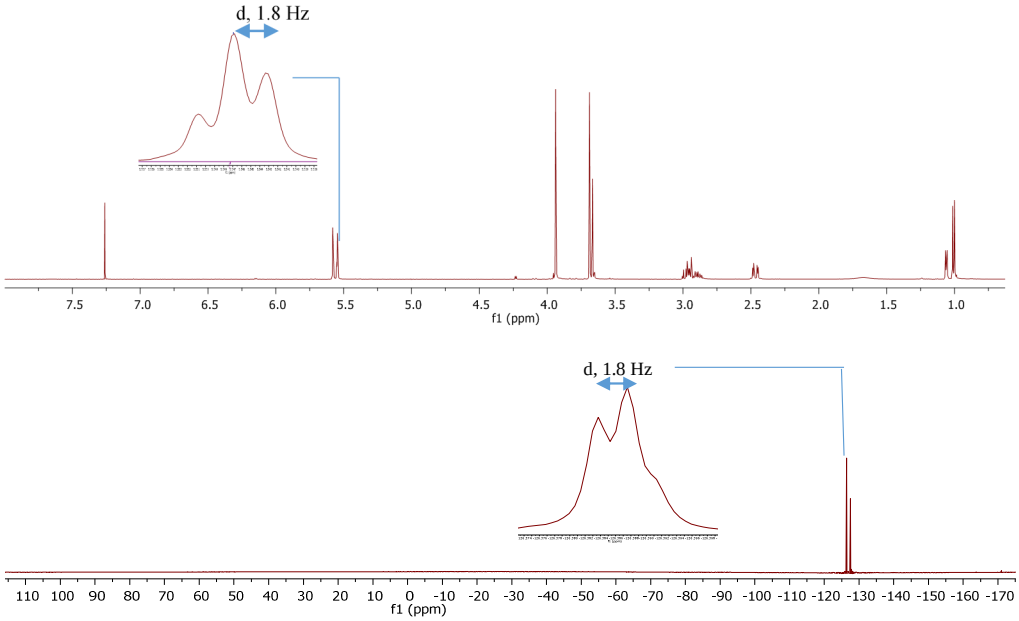

Figure 22. ^{1}H NMR (Top) and ^{19}F NMR (Bottom) Spectra of Compounds 8a/8b in $CDCl_3$.

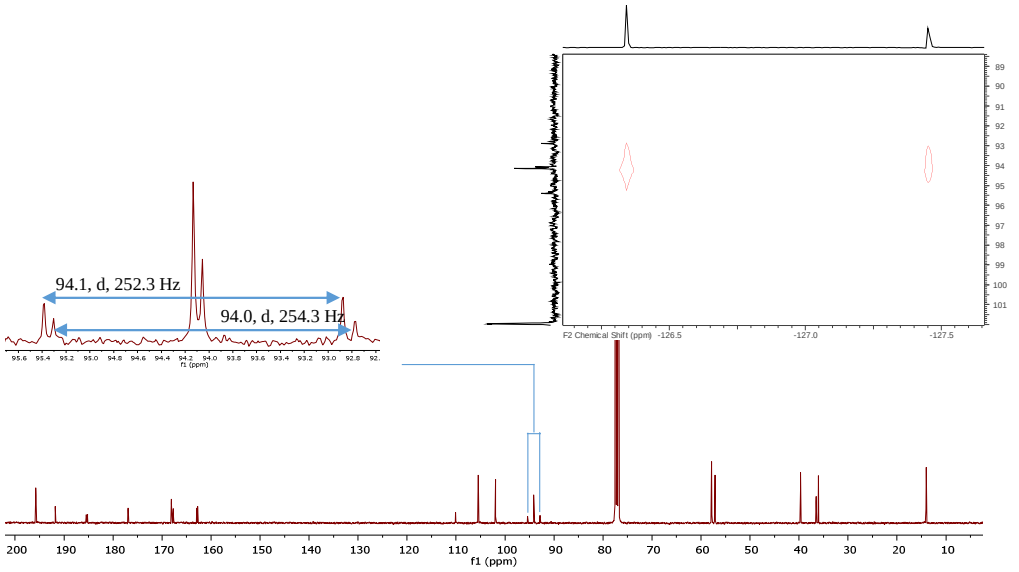

Figure 23. ^{13}C NMR and ^{19}F-^{13}C HMQC Spectrum of Compounds 8a/8b in $CDCl_3$.

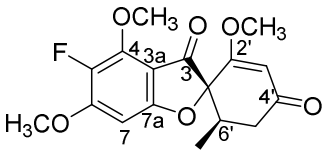

Table 12. NMR Data for Compound 9 in $CDCl_3$.

Position	δ_C, mult (*J* in Hz)[a]	type	δ_H, mult (*J* in Hz)[b]	HMBC
2	90.0	C		
3	193.4, d (3.0)	C		
3a	105.5, d (1.2)	C		
4	145.0, d (8.8)	C		
5	139.6, d (237.5)	C		
6	158.6, d (11.3)	C		
7	89.8	CH	6.37, d (5.2)	3a, 5, 6, 7a
7a	170.4	C		
2′	171.1	C		
3′	105.0	C	5.55, s	2, 2′, 4′, 5′
4′	197.2	C		
5′	40.1	CH_2	α 2.75, dd (17.2, 4.6)	2, 4′, 6′, 6′-Me
			β 3.02, dd (17.2, 13.2)	2, 3′, 4′, 6′, 6′-Me
6′	36.7	CH	2.75, m	2, 3, 2′, 4′
6′-Me	14.4	CH_3	0.95, d (6.9)	2, 5′, 6′
4-OMe	62.1, d (7.5)	CH_3	4.20, d (3.3)	4
6-OMe	57.0	CH_3	3.98, s	6
2′-OMe	56.8	CH_3	3.63, s	2′

[a] 125 MHz, [b] 500 MHz Jeol NMR Spectrometer

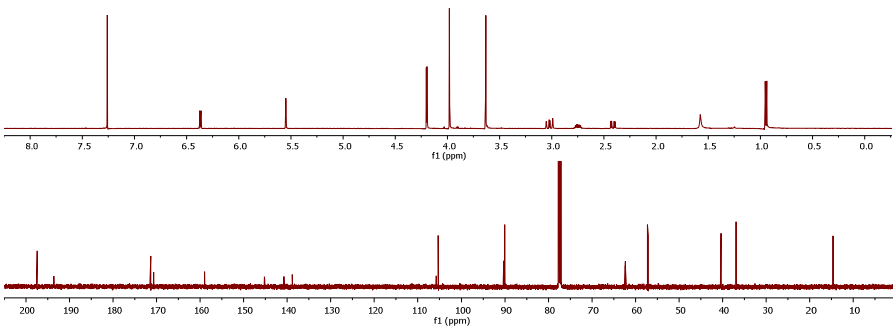

Figure 24. ^{1}H NMR (500 MHz; Top) and ^{13}C NMR (125 MHz; Bottom) Spectra of Compound 9 in $CDCl_3$.

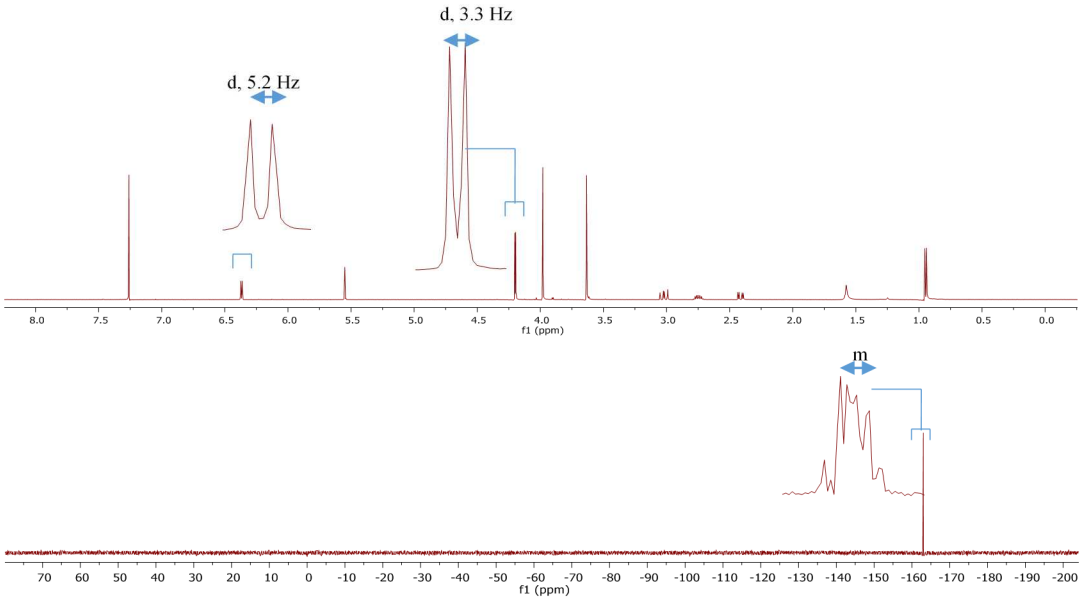

Figure 25. ^{1}H NMR (Top) and ^{19}F NMR (Bottom) Spectra of Compound 9 in $CDCl_3$.

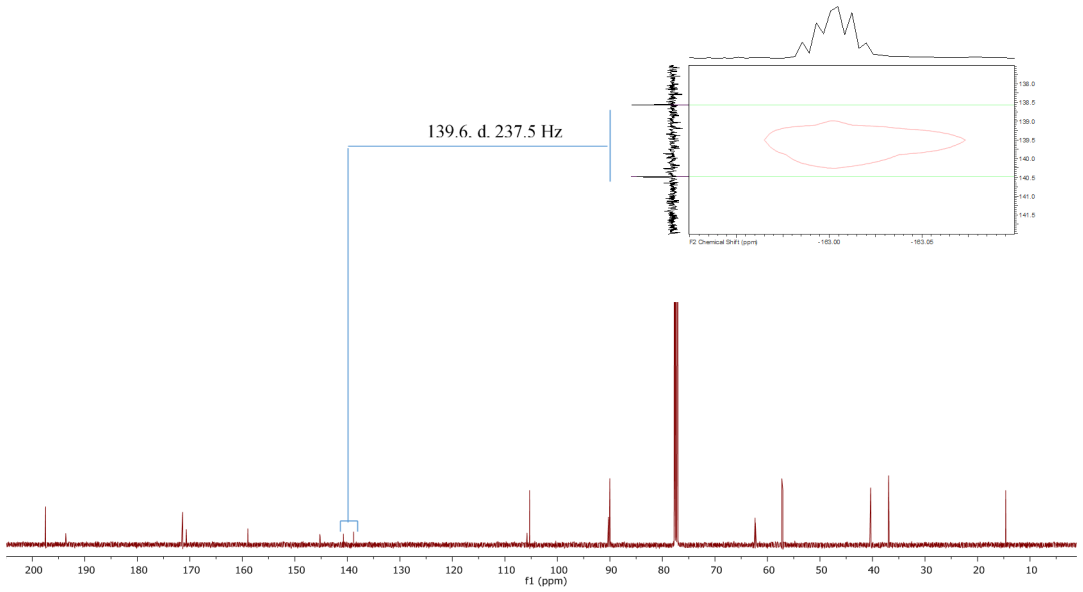

Figure 26. ^{13}C NMR and ^{19}F-^{13}C HMQC Spectrum of Compound 9 in $CDCl_3$.

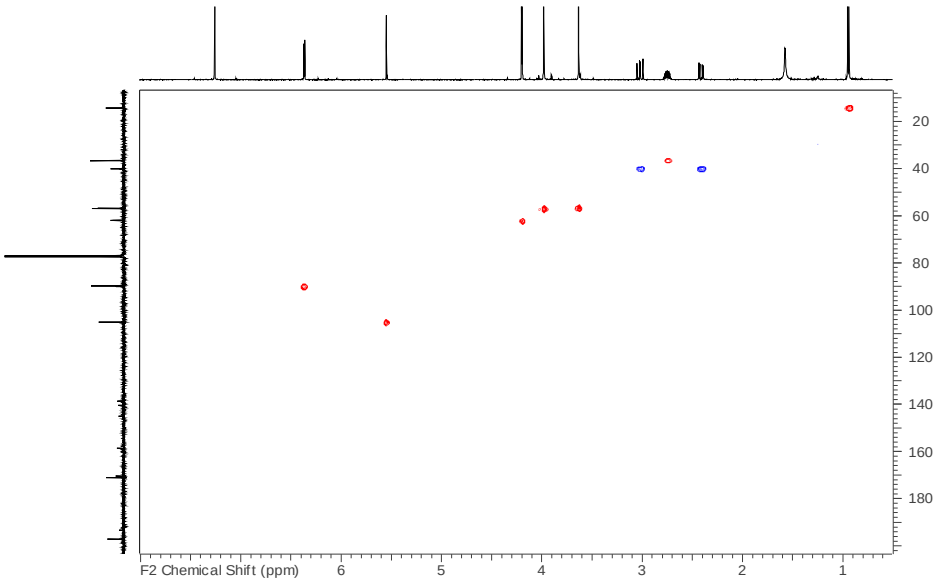

Figure 27. ^{1}H-^{13}C Edited-HSQC Spectrum of Compound 9 in $CDCl_3$.

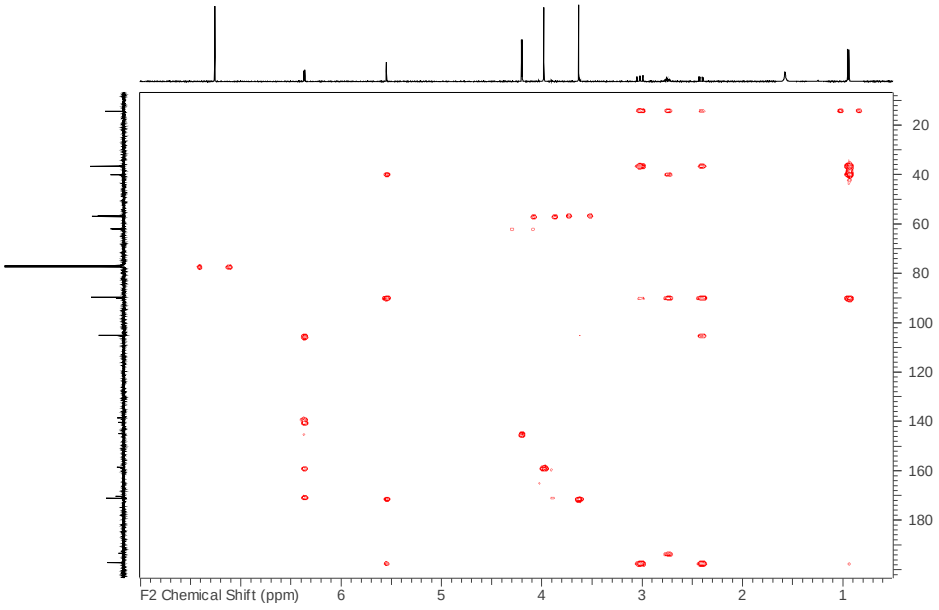

Figure 28. ^{1}H-^{13}C HMBC Spectrum of Compound 9 in $CDCl_3$.

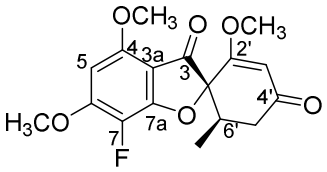

Table 13. NMR Data for Compound 10 in $CDCl_3$.

Position	δ_C, mult (*J* in Hz)[a]	type	δ_H, mult (*J* in Hz)[b]	HMBC
2	91.0	C		
3	192.4, d (2.4)	C		
3a	105.0	C		
4	154.7, d (1.8)	C		
5	90.1	CH	6.09, d (5.2)	3, 3a, 4, 6, 7
6	157.4, d (7.0)	C		
7	132.4, d (238.0)	C		
7a	160.3, d (8.8)	C		
2´	170.9	C		
3´	105.0	CH	5.54, s	2, 2´, 5´
4´	197.1	C		
5´	40.2	CH_2	α 2.43, dd (17.2, 4.8) β 3.03, dd (17.2, 13.4)	2, 3´, 4´, 6´, 6´-Me 2, 4´, 6´, 6´-Me
6´	36.6	CH	2.81, m	2, 3, 2´, 4´, 5´, 6´-Me
6´-Me	14.4	CH_3	0.98, d (6.7)	2, 5´, 6´
6-OMe	57.3	CH_3	4.02, s	6
4-OMe	56.5	CH_3	3.95, s	4
2´-OMe	56.8	CH_3	3.62, s	2´

[a] 175 MHz, [b] 700 MHz Jeol NMR Spectrometer

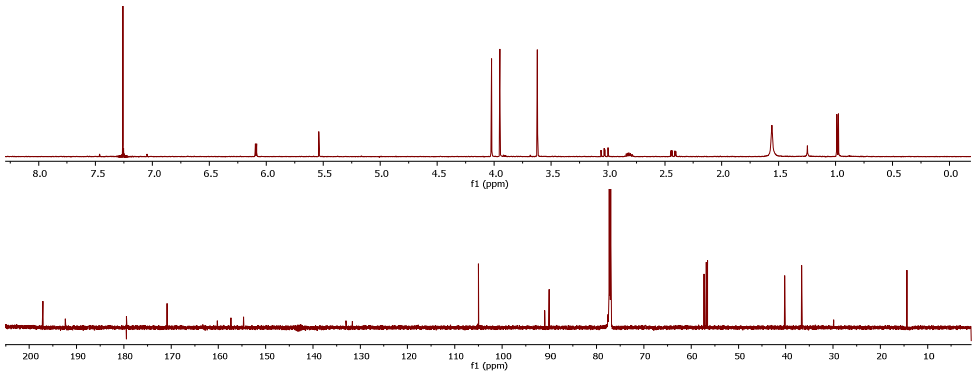

Figure 29. ^{1}H NMR (700 MHz; Top) and ^{13}C NMR (175 MHz; Bottom) Spectra of Compound 10 in $CDCl_3$.

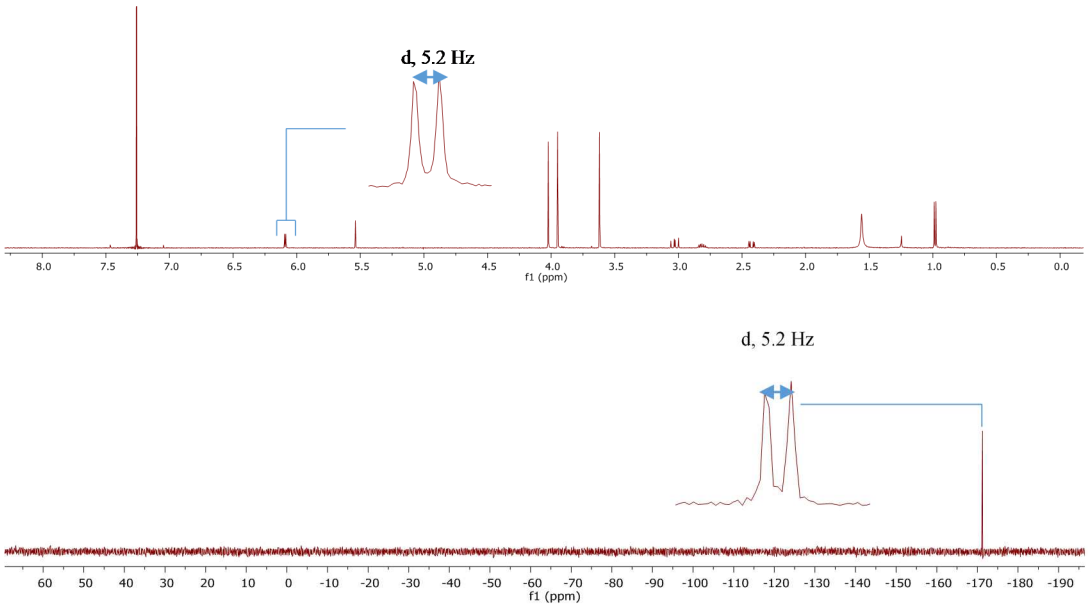

Figure 30. ^{1}H NMR (Top) and ^{19}F NMR (Bottom) Spectra of Compound 10 in $CDCl_3$.

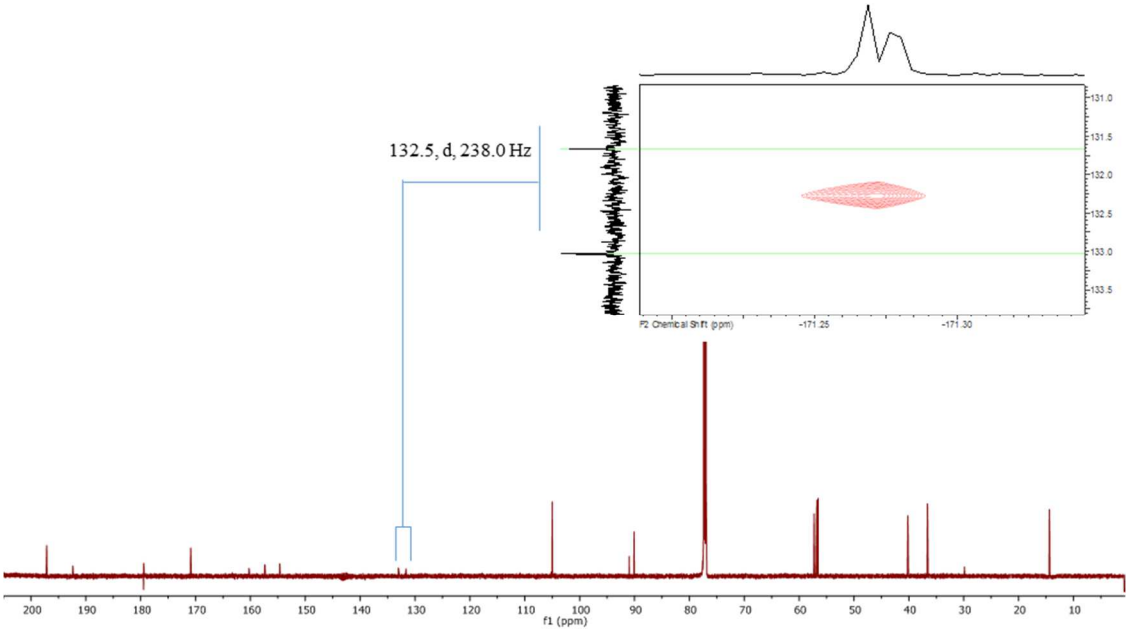

Figure 31. ^{13}C NMR and ^{19}F-^{13}C HMQC Spectrum of Compound 10 in $CDCl_3$.

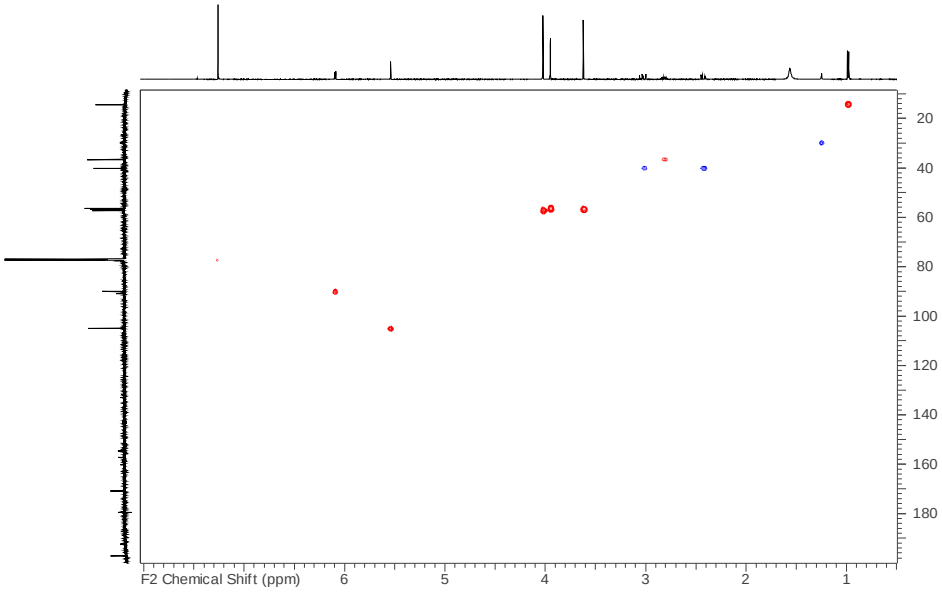

Figure 32. ^{1}H-^{13}C Edited-HSQC Spectrum of Compound 10 in $CDCl_3$.

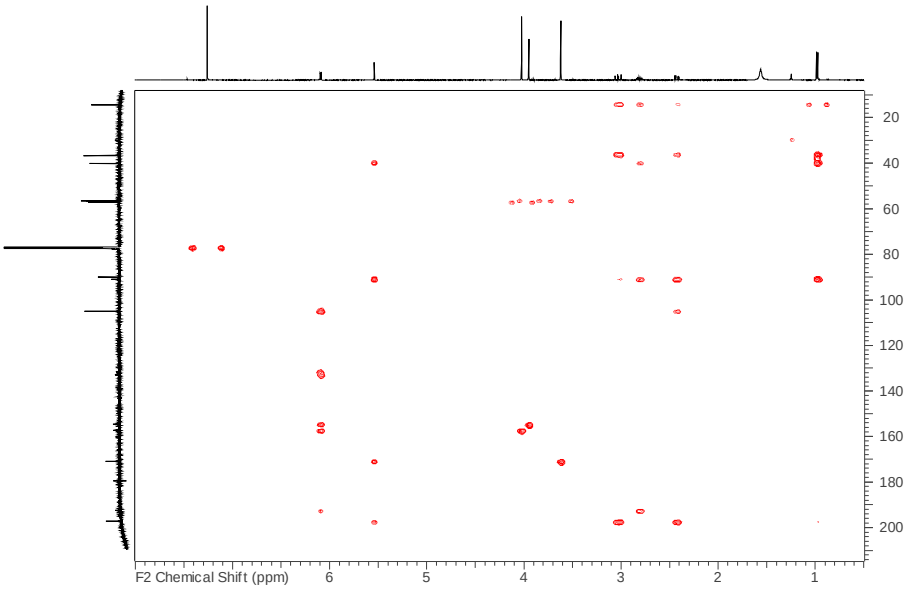

Figure 33. ^{1}H-^{13}C HMBC Spectrum of Compound 10 in $CDCl_3$.

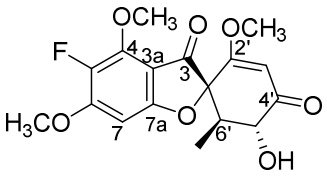

Table 14. NMR Data for Compound 11 in $CDCl_3$.

Position	δ_C, mult (*J* in Hz)[a]	type	δ_H, mult (*J* in Hz)[b]	HMBC
2	90.4	C		
3	193.4, d (3.3)	C		
3a	105.5, d (1.4)	C		
4	145.1, d (7.9)	C		
5	139.6, d (241.6)	C		
6	158.9, d (11.2)	C		
7	89.1	CH	6.36, d (5.4)	3a, 4, 5, 6, 7a
7a	170.5	C		
2′	171.7	C		
3′	101.9	CH	5.61, s	2, 2´, 4´, 5´
4′	197.5	C		
5′	71.4	CH	4.67, d (12.0)	4´, 6´, 6´-Me
6′	43.7	CH	2.54, dq (12.0, 6.9)	2, 3, 5´, 6´-Me
6′-Me	11.1	CH_3	1.10, d (6.9)	2, 5´, 6´
4-OMe	62.1, d (6.7)	CH_3	4.21, d (3.6)	4
6-OMe	57.1	CH_3	3.98, s	6
2′-OMe	57.1	CH_3	3.67, s	2´

[a] 175 MHz, [b] 700 MHz Jeol NMR Spectrometer

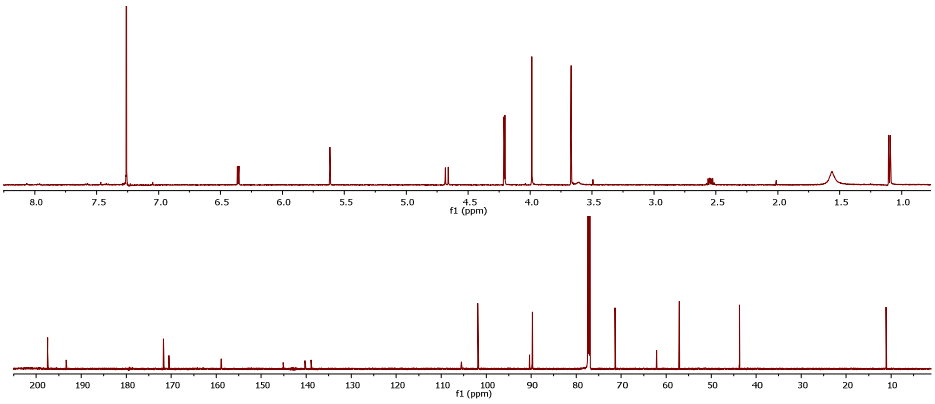

Figure 34. ^{1}H NMR (700 MHz; Top) and ^{13}C NMR (175 MHz; Bottom) Spectra of Compound 11 in $CDCl_3$.

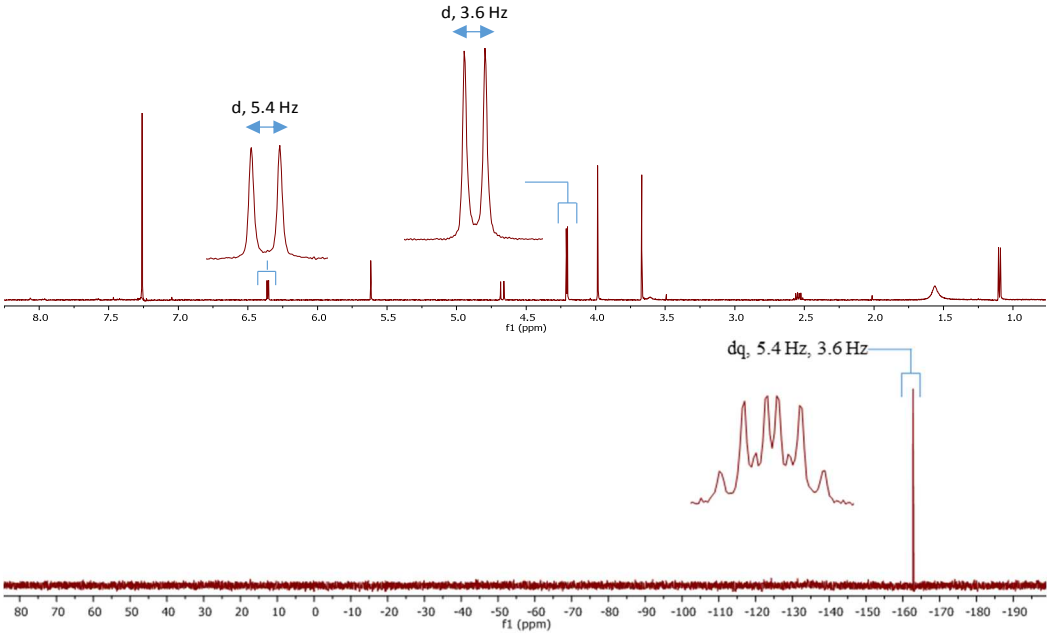

Figure 35. ^{1}H NMR (Top) and ^{19}F NMR (Bottom) Spectra of Compound 11 in $CDCl_3$.

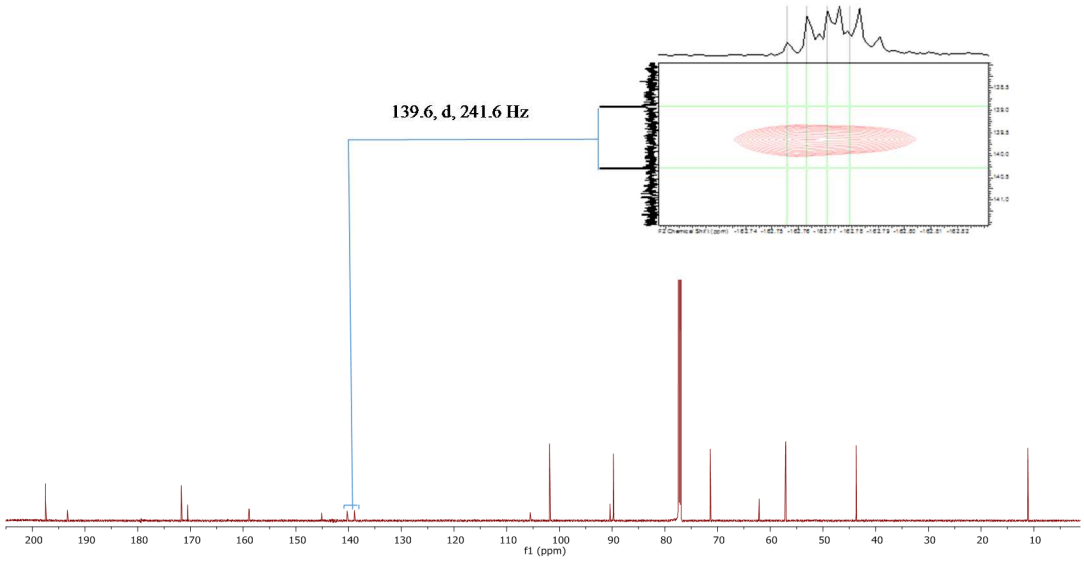

Figure 36. ^{13}C NMR and ^{19}F-^{13}C HMQC Spectrum of Compound 11 in $CDCl_3$.

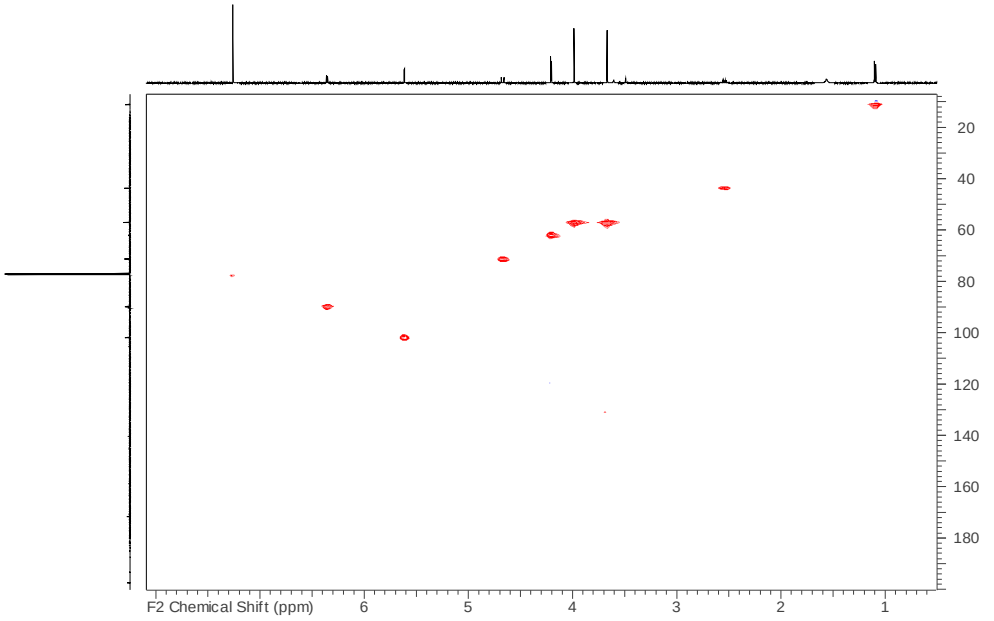

Figure 37. ^{1}H-^{13}C Edited-HSQC Spectrum of Compound 11 in $CDCl_3$.

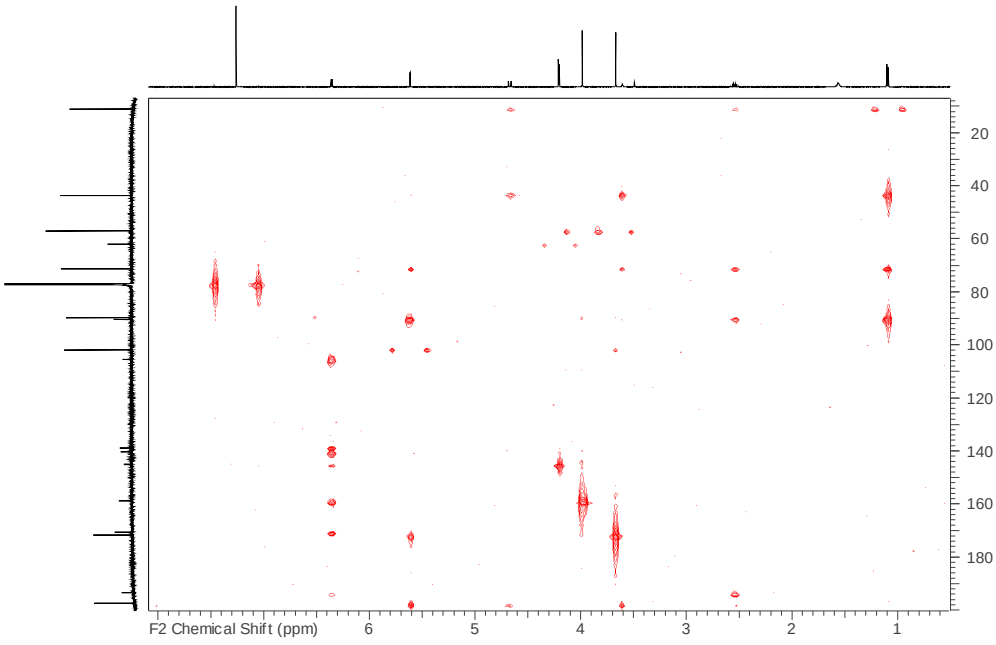

Figure 38. ^{1}H-^{13}C HMBC Spectrum of Compound 11 in $CDCl_3$.

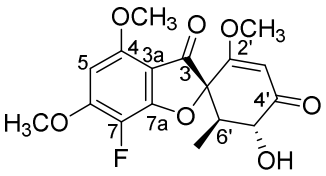

Table 15. NMR Data for Compound 12 in $CDCl_3$.

Position	δ_C, mult (*J* in Hz)[a]	type	δ_H, mult (*J* in Hz)[b]	HMBC
2	91.2	C		
3	192.4, d (2.7)	C		
3a	104.9	C		
4	154.8, d (1.8)	C		
5	90.2	CH	6.10, d (5.1)	3, 3a, 4, 6, 7
6	157.6, d (8.8)	C		
7	132.2, d (237.0)	C		
7a	160.3, d (10.5)	C		
2′	171.5	C		
3′	101.8	CH	5.61, s	2, 2′, 4′, 5′
4′	197.4			
5′	71.4	CH	4.68, d (12.0)	4′, 6′, 6′-Me
6′	43.7	CH	2.60, dq (12.0, 6.3)	2, 3, 2′, 4′, 5′, 6′-Me
6′-Me	11.1	CH_3	1.13, d (6.3)	2, 5′, 6′
6-OMe	57.3	CH_3	4.03, s	6
4-OMe	56.6	CH_3	3.95, s	4
2′-OMe	57.1	CH_3	3.66, s	2′

[a] 175 MHz, [b] 700 MHz Jeol NMR Spectrometer

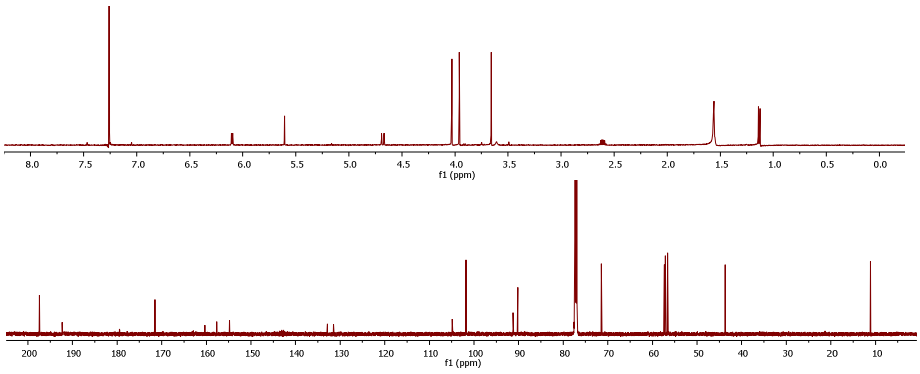

Figure 39. ^{1}H NMR (700 MHz; Top) and ^{13}C NMR (175 MHz; Bottom) Spectra of Compound 12 in $CDCl_3$.

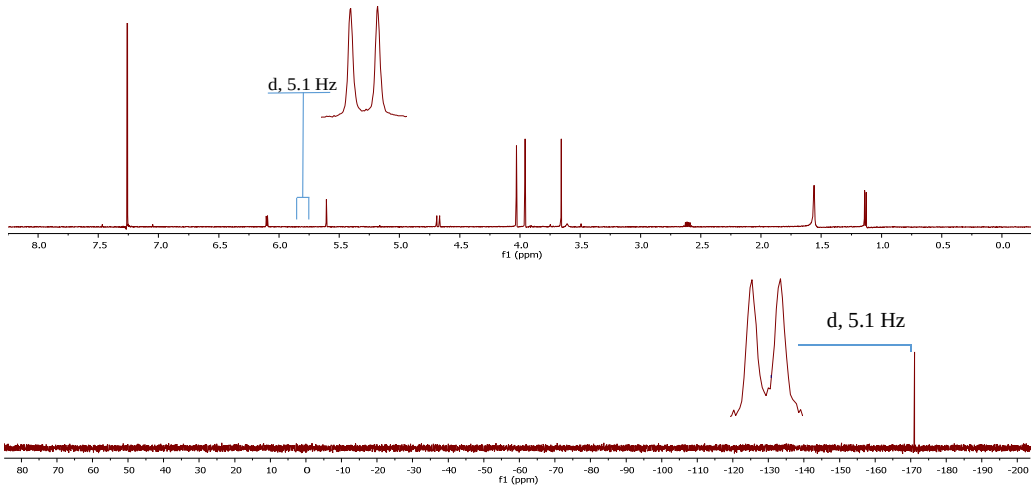

Figure 40. ^{1}H NMR (Top) and ^{19}F NMR (Bottom) Spectra of Compound 12 in $CDCl_3$.

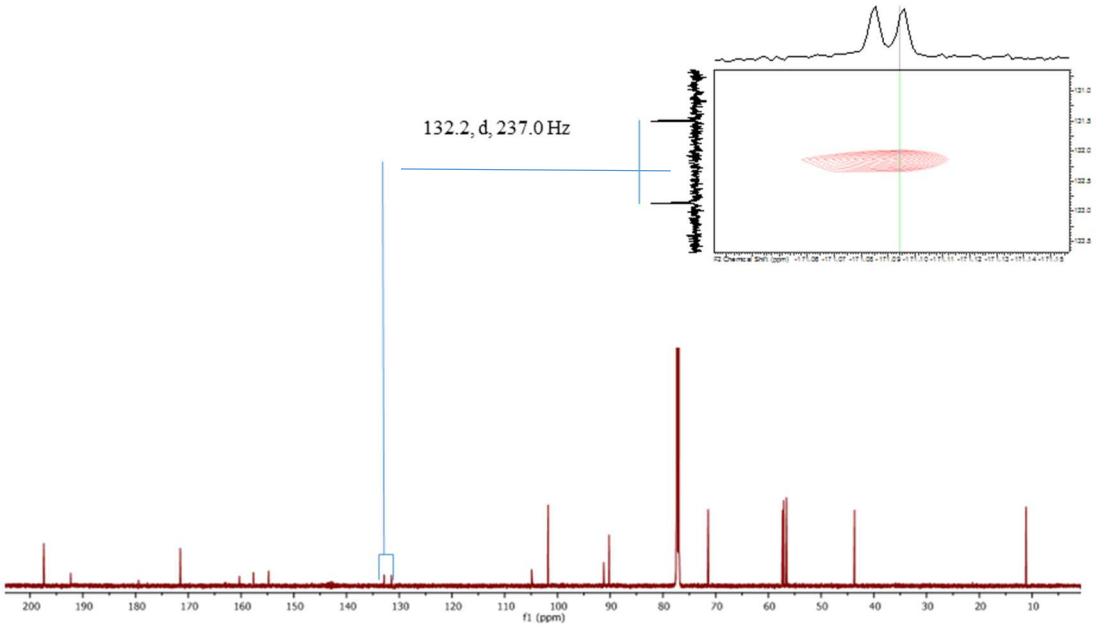

Figure 41. ^{13}C NMR and ^{19}F-^{13}C HMQC Spectrum of Compound 12 in $CDCl_3$.

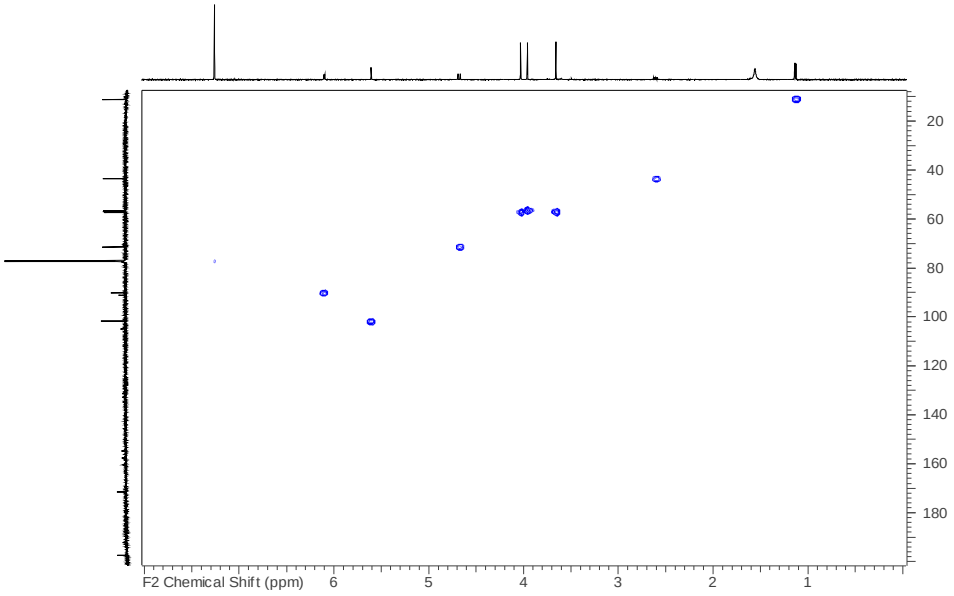

Figure 42. ^{1}H-^{13}C Edited-HSQC Spectrum of Compound 12 in $CDCl_3$.

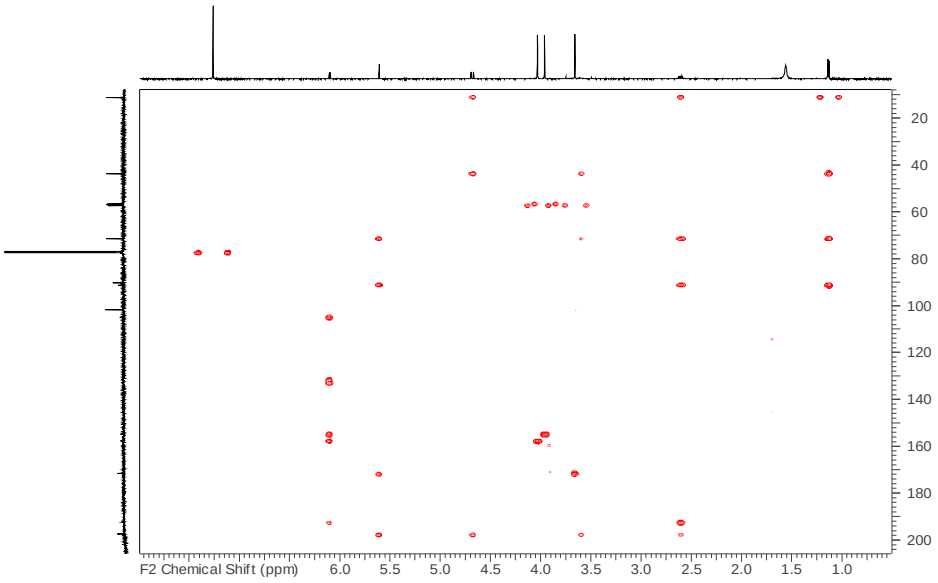

Figure 43. ^{1}H-^{13}C HMBC Spectrum of Compound 12 in $CDCl_3$.

Table 16. *In Vitro* Cytotoxicity of Compounds 1-12 Against Three Human Cancer Cell Lines.[a]

Compound	IC_{50} (µM)		
	MDA-MB-435[c]	MDA-MB-231[d]	OVCAR3[e]
1	6.4 µM	*inactive*	48.5 µM
2	*inactive*	*inactive*	*inactive*
3	*inactive*	*inactive*	*inactive*
4	*inactive*	*inactive*	*inactive*
5	*inactive*	*inactive*	*inactive*
6	*inactive*	*inactive*	*inactive*
7	*inactive*	*inactive*	*inactive*
8a/8b	*inactive*	*inactive*	*inactive*
9	*inactive*	*inactive*	*inactive*
10	22.0 µM	*inactive*	*inactive*
11	*inactive*	*inactive*	*inactive*
12	*inactive*	*inactive*	*inactive*
Vinblastine[b]	0.5 nM	8.8 nM	1.8 nM

[a]A compound is indicated as *inactive* if no activity was observed at 50 µM.
[b]Positive control with inhibition of cell growth expressed as IC_{50} (nM).
[c]Human melanoma cancer cells
[d]Human breast cancer cells
[e]Human ovarian cancer cells

Table 17. Antifungal Activity of Compounds 1-12 Against *Microsporum gypseum.*

Compound	Inhibition Zone Diameter (mm)[a]
1	35 ±1
2	0
3	0
4	0
5	0
6	0
7	23 ± 1
8a/8b	0
9	0
10	34 ± 1
11	0
12	0
Commercial Griseofulvin	35 ± 2

[a]Inhibition diameter expressed as the mean of four replicates ± standard deviation

Table 18. Cytotoxic Activity of Griseofulvin (1) and its Analogues (7-12) Against Human Hepatoma (Huh7.5.1) Cells

Compound	IC_{50} (μM)
1	12.6
2	180.6
3	~6843
4	~723.0
5	>300
6	9.0
7	82.7
9	290.4
10	23.9
11	155.9
12	198.3

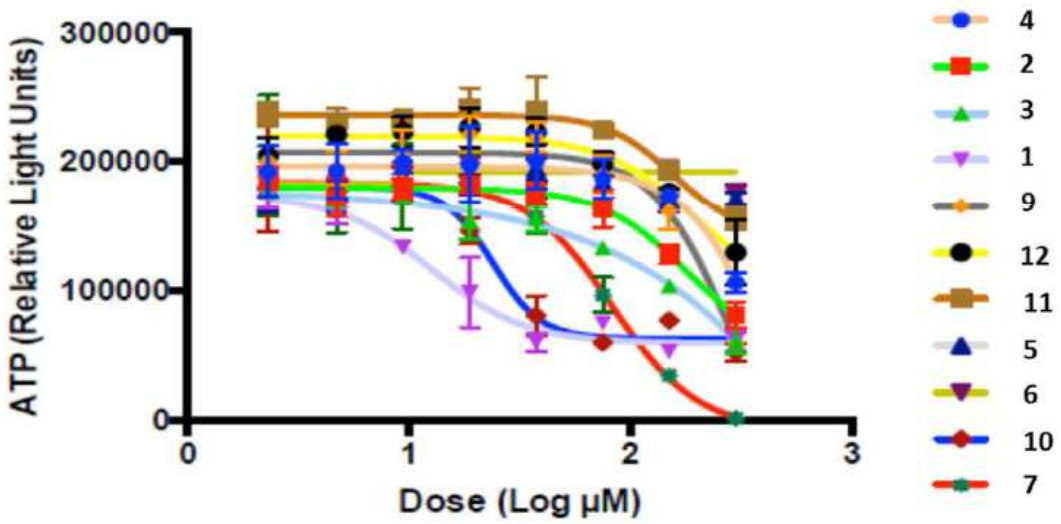

Figure 44. Cytotoxic Activity of Griseofulvin (1) and its Analogues (7-12) Against Human Hepatoma (Huh7.5.1) Cells.

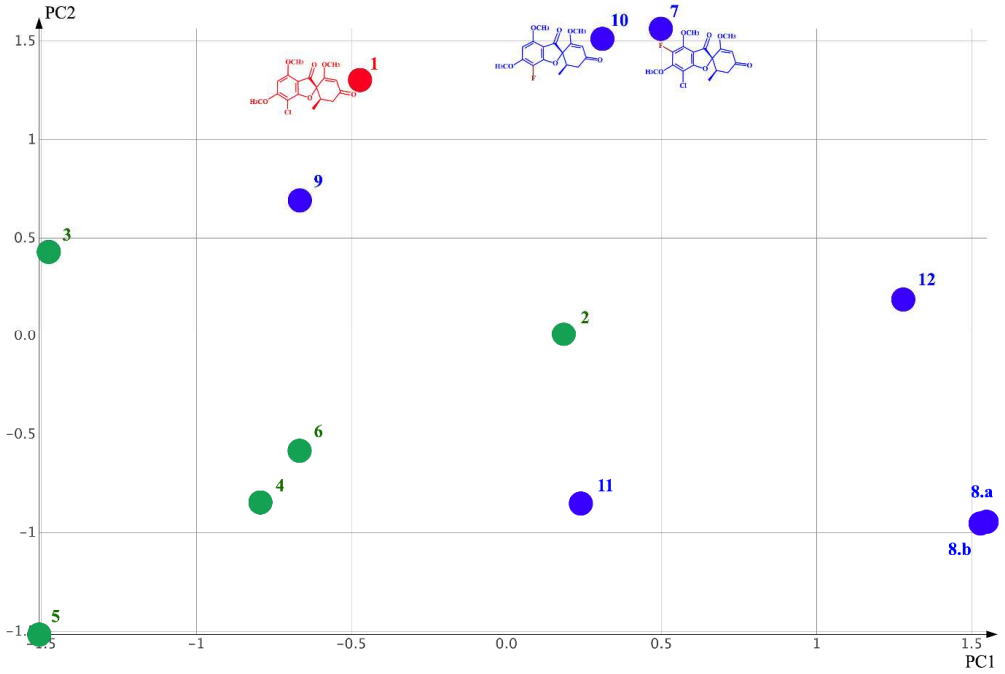

Figure 45. Visual Representation of the Chemical Space of Griseofulvin (1, Red), Structurally Related Fungal Analogues (2-6, Green) and Fluorinated Semisynthetic Derivatives (7-12, Blue). The substructures found on the derivatives and natural products but not on griseofulvin's structure are depicted in red. This 2D plot was generated with the principal component analysis of 11 descriptors. The first two principal components recovered 68% of the covariance. The electron affinity (EA(eV)) and electropological state (Estate) had the highest contribution to the first principal component, while predicted aqueous solubility (QPlogS) had the highest contribution to the second principal component.

CHAPTER III

ACETOPHENONE DERIVATIVES FROM A FRESHWATER FUNGAL ISOLATE OF RECENTLY DESCRIBED *LINDGOMYCES MADISONENSIS* (G416)

This chapter has been published in the journal *Phytochemistry* and is presented in that style. Noemi D. Paguigan, Huzefa A. Raja, Cynthia S. Day, and Nicholas H. Oberlies. *Phytochemistry* (2016) 126, 59-65.

The exploration of freshwater ascomycetes, which have undergone only limited investigation, may provide opportunities both to characterize new genera/species of fungi and to uncover new chemical diversity. In this study, seven acetophenone derivatives (**1**-**7**), madisone (**1**), 4´-methoxymadisone (**2**), dehydromadisone (**3**), 2´´-methoxymadisone (**4**), dihydroallovisnaginone (**5**), dimadisone (**6**), and 4´-methoxydimadisone (**7**) were characterized from an organic extract of a recently described *Lindgomyces madisonensis* (G416) culture, which was isolated from submerged wood collected in a stream in North Carolina. Compounds **1**, **3**, **4**, **6**, and **7** have not been reported previously, while **2** and **5** were isolated for the first time as natural products. The structures were assigned on the basis of NMR and HRESIMS data, with the structure of **1** supported by x-ray crystallography. The antimicrobial activities of compounds **1**, **2**, and **5** were evaluated against a panel of bacteria and fungi. A heat map analysis of the surface of a G416 culture showed that most of the isolated compounds concentrated in the guttate compared with the vegetative mycelium of the fungus.

Introduction

Fungi represent a highly diverse group of organisms, and even though there exists an estimated 5.1 million species, less than 100 thousand have been cultivated and described,[107] and only a fraction of those have been studied with respect to their chemistry.[108] Freshwater ascomycetes are an ecological group that occur on submerged substrates in fresh water and play an important role as decomposers in these habitats.[39,109,110] The number of described ascomycetes has increased dramatically over the past 25 years. Shearer (1993) reported about 200 species from freshwater habitats worldwide; that number doubled to 414 in a 2001 review.[111] Currently, about 640 freshwater ascomycetes have been described.[110] While knowledge regarding the distribution patterns and taxonomy has increased for this ecological group of fungi due to intensive collection over the last two decades, their chemistry, particularly regarding secondary metabolites, has had limited investigation.[112-117] As of 2011, approximately 127 chemical structures had been reported from about 30-40 freshwater fungal species.[11,118,119] To ameliorate this knowledge gap, we have initiated studies on the chemical mycology of freshwater ascomycetes in North Carolina, USA,[118-122] representing the first systematic study of freshwater ascomycetes from this region of North America. Ongoing investigations led to the isolation of five new acetophenones (**1**, **3**, **4**, **6**, and **7**), along with 4´-methoxymadisone (**2**) and dihydroallovisnaginone (**5**), from a fungal isolate recently described as *Lindgomyces madisonensis* (G416) Raja & Oberlies.[123] A heat map analysis by *in situ* sampling via droplet-liquid microjunction-

surface sampling probe (droplet-LMJ-SSP) of a G416 culture showed that the isolated compounds were more abundant in the guttate compared to the fungal mycelium.

Results and Discussion

Structural characterization and bioactivity of compounds 1-7. A culture of *L. madisonensis* (G416) was isolated from decomposing wood collected in the central Piedmont region of North Carolina. The fungus was cultured by solid-substrate fermentation on rice, and this material was extracted with 1:1 $CHCl_3$-CH_3OH. The resulting extract was subjected to partitioning with organic solvents followed by purification using flash chromatography yielding five fractions. These fractions were further purified using preparative HPLC, leading to the isolation of compounds **1-7** (Figure 46). The structures of these were established by analysis of spectroscopic (NMR) and spectrometric (HRESIMS) data.

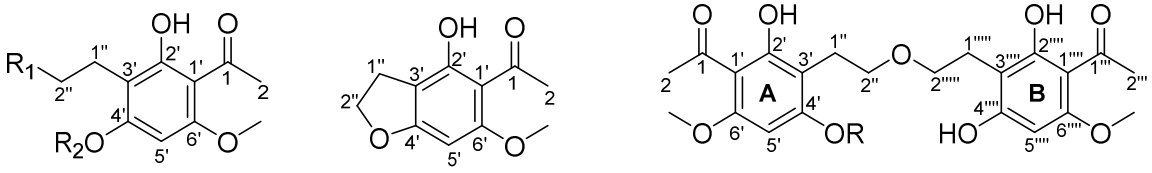

Figure 46. Structures of Compounds 1-7

On the basis of HRESIMS and NMR data (Table 19, Figure 49), compound **1** was found to have the molecular formula $C_{11}H_{14}O_5$ (five degrees of unsaturation). The IR

spectrum of **1** showed absorption bands at 2972 and 1610 cm^{-1}, indicative of an aromatic ring with chelated hydroxy and carbonyl moieties; these functionalities were supported by the observed UV absorption maxima at 306 and 237 nm. ^{13}C NMR and HSQC data, indicated 11 carbon signals, which were attributed to six aromatic carbons (five nonprotonated and one protonated), one ketone carbonyl, and four carbon signals located in the aliphatic region of the spectrum. Furthermore, chemical shift data indicated that three of the aromatic carbons were oxygenated (δ_C 163.3, 166.1, 164.7 for C-6′, C-2′, and C-4′, respectively). The downfield region of the ^1H NMR spectrum of **1** exhibited a singlet at δ_H 5.98 that integrated for one aromatic proton, as expected for a penta-substituted benzene ring. Based on the ^1H NMR data (Table 19), the structure of **1** had one isolated methyl group (δ_H 2.55, singlet), one methoxy, and a hydroxyethyl group. The connections between the subunits were deduced from key HMBC correlations (Figure 47), including those of H-5′ to C-6′, C-1′, C-3′, and C-4′; from the methoxy to C-6′; from the isolated methyl H_3-2 to C-1′; and from H_2-1′′ and H_2-2′′ of the hydroxyethyl group to C-2′, C-3′, and C-4′, and to C-3′, respectively. In further efforts to verify the locations of subunits on the aromatic ring, ^1H NMR data for **1** were recorded in $CDCl_3$, revealing a singlet resonance at δ_H 14.58 that was not observed when recorded in CD_3OD (Figure 56). This result was consistent with the downfield shift associated with intramolecular H-bonding between the proton of the C-2′ hydroxy group and the oxygen of the C-1 carbonyl. The structure of **1**, recrystallized from CH_3OH, was unambiguously assigned by x-ray crystallography (Figure 71) and ascribed the trivial name, madisone.

Table 19. ^{1}H NMR and ^{13}C NMR Data for Compounds 1-3 in CD_3OD.

	1[a]		**2**[a]		**3**[a]	
Position	δ_C	δ_H, mult (*J* in Hz)	δ_C	δ_H, mult (*J* in Hz)	δ_C	δ_H, mult (*J* in Hz)
1	204.2		204.8		204.2	
2	33.1	2.55, s	33.4	2.58, s	33.1	2.56, s
1´	105.9		106.6		105.9	
2´	166.1		164.9		165.6	
3´	105.6		106.6		111.2	
4´	164.7		165.7		164.0	
5´	91.2	5.98, s	87.4	6.16, s	91.0	5.98, s
6´	163.3		163.9		162.8	
1´´	26.7	2.82, t (7.6)	26.6	2.82, t (7.6)	16.3	2.54, q (7.3)
2´´	62.0	3.61, t (7.6)	61.8	3.55, t (7.6)	13.8	1.04, t (7.3)
4´- OCH_3	n/a	-	*56.2	3.91, s	n/a	-
6´- OCH_3	55.9	3.84, s	*56.1	3.93, s	55.8	3.84, s
2´´-OCH_3	n/a	-	n/a	-	n/a	-

[a] Data were collected at 400 MHz (^{1}H) or 100 MHz (^{13}C).
[b] Data were collected at 700 MHz (^{1}H) or 175 MHz (^{13}C).
* May be interchanged.
[#] Value deduced from HMBC
n/a Not applicable

Compound **2** was assigned the molecular formula $C_{12}H_{16}O_5$ (five degrees of unsaturation) on the basis of HRESIMS and NMR data. The NMR spectral data for **2** (Table 19) were nearly identical to that of compound **1**, but with additional signals for a second methoxy group, which were consistent with a 14 amu mass difference. A key HMBC correlation was observed from the methoxy group to C-4´, confirming its connectivity and establishing the structure of **2** (Figures 46, 47, and 58). Compound **2** was first described by Wootton as one of the intermediates in an attempted synthetic oxidative approach to LL-D253α.[124] Their data were acquired in $CDCl_3$; the data herein

(Figure 56) were consistent with the literature with one caveat. It is considered that there was an error in the previous assignment of the C-3´ chemical shift value in the literature. Thus, we have included the NMR shift assignments of **2**. As this is the first report of the isolation of **2** from a natural source, it was given the trivial name 4´-methoxymadisone.

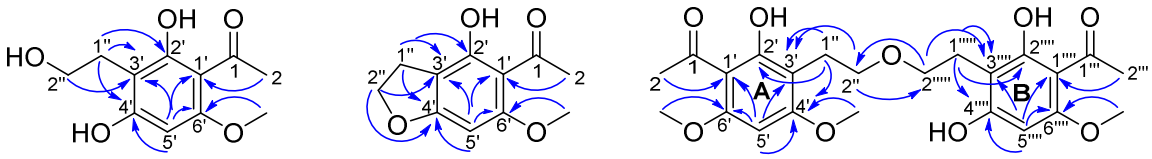

1 **5** **7**

Figure 47. Key HMBC Correlations of Compounds 1, 5, and 7.

The HRESIMS and NMR data (Table 19) established the molecular formula for compound **3** as $C_{11}H_{14}O_4$ (five degrees of unsaturation). Comparison of these data to those of compound **1** indicated the loss of the hydroxy moiety at C-2´´, which was consistent with the associated changes in the shifts and the multiplicities of H_2-1´´ (δ_H 2.54, quartet, 7.3 Hz) and H_3-2´´ (δ_H 1.04, triplet, 7.3 Hz); it also accounted for the 16 amu mass difference between these compounds. As such, compound **3** was identified as shown (Figure 46) and assigned the trivial name dehydromadisone.

Table 20. ^{1}H NMR and ^{13}C NMR Data for Compounds 4-6 in CD_3OD.

	4[b]		**5**[a]		**6**[a]	
Position	δ_C	δ_H, mult (*J* in Hz)	δ_C	δ_H, mult (*J* in Hz)	δ_C	δ_H, mult (*J* in Hz)
1	204.1		204.4		204.2	
2	33.0	2.56, s	33.1	2.55, s	33.1	2.56, s
1´	105.9		106.8		105.9	
2´	166.1		162.7		166.1	
3´	105.4		106.3		105.5	
4´	[#]164.9		169.3		164.7	
5´	91.4	5.99, s	86.7	6.06, s	91.3	5.99, s
6´	163.4		165.8		163.4	
1´´	23.4	2.84, t (7.6)	26.6	3.05, t (7.6)	23.6	2.84, t (7.3)
2´´	72.6	3.48, t (7.6)	74.4	4.65, t (7.6)	70.6	3.55, t (7.3)
4´- OCH_3	n/a	-	n/a	-	n/a	-
6´- OCH_3	55.9	3.85, s	56.3	3.86, s	55.7	3.85, s
2´´-OCH_3	58.5	3.36, s	n/a	-	n/a	-

[a] Data were collected at 400 MHz (^{1}H) or 100 MHz (^{13}C).
[b] Data were collected at 700 MHz (^{1}H) or 175 MHz (^{13}C).
* May be interchanged.
[#] Value deduced from HMBC
n/a Not applicable

The molecular formula of compound **4** was deduced as $C_{12}H_{16}O_5$ (five degrees of unsaturation) based on HRESIMS and NMR data (Table 20). The NMR and HRMS of **4** suggested structural similarities to **1**. However, **4** had an additional methoxy unit (δ_C/δ_H 58.5/3.36) as evidenced by a 14 amu difference in the HRMS between **1** and **4**. Further analysis of the 1- and 2-D NMR data indicated that the 2´´-OH in **1** was replaced with a

methoxy unit in **4**. This substitution was confirmed by the observed more downfield C-2´´ shift in **4** (δ_C 72.6) compared to the C-2´´ shift in **1** (δ_C 62.0). Conversely, C1´´ appeared more upfield in **4** compared to **1** at δ_C 23.4 and δ_C 26.7, respectively. Moreover, an HMBC correlation observed for the methoxy protons to C-2´´ (Figure 47 and Figure 60) established its connectivity. Thus, the structure of compound **4** was assigned (Figure 46) and ascribed the trivial name 2´´-methoxymadisone.

Compound **5** was found to have the molecular formula $C_{11}H_{12}O_4$ (six degrees of unsaturation) on the basis of HRESIMS and NMR data (Table 20). The ^{1}H NMR spectrum of **5** exhibited signals that were almost identical to those of **1** but with more deshielded H_2-1´´ and H_2-2´´ resonances at δ_H 3.05 (triplet, 7.6 Hz) and δ_H 4.65 (triplet, 7.6 Hz), respectively. This distinct change in the chemical shift values suggested a heterocycle, which also accounted for the additional unsaturation and the 18 amu mass difference between **1** and **5** (Figure 46). Although this is the first report of the isolation of **5** from a natural source, Geissman and Hinreiner described it (and named it dihydroallovisnaginone) as one of the derivatives in the monomethylation of 4,6-dihydroxy-5-acetylcoumarane in an attempt to synthesize visnaginone.[125] Although NMR and HRMS data were not available in 1951, the UV data were consistent with the literature.

The ^{1}H and ^{13}C NMR data of **6** (Table 20) showed signals that were nearly identical to those of **1**. However, the HRMS data established the molecular formula to be $C_{22}H_{26}O_9$ (ten degrees of unsaturation), which indicated twice as many carbons, along with 12 additional hydrogen and four more oxygen atoms relative to the formula of **1**.

Compound **6** was presumed to be a homodimer of **1** with an ether linkage connecting the two halves. The HMBC correlation from H_2-2´´ (δ_H 3.55) to C-2´´ (δ_C 70.6) implied that the two symmetrical units of the compound were connected on the hydroxyethyl group comprised of C-1´´ and C-2´´ (Figure 47). Therefore, the structure of **6** was proposed as shown in Figure 46 and ascribed the trivial name dimadisone.

Compound **7** was shown to have the molecular formula $C_{23}H_{28}O_9$ (ten degrees of unsaturation) based on analyses of the HRESIMS and NMR data. The ^{1}H and ^{13}C NMR data (Table 21) displayed two sets of signals, which had close resemblance to those of compounds **1** and **2**, indicating that **7** was a heterodimer of these compounds. In ring A, H-5´ (δ_H 6.17, s) showed HMBC correlations to C-1´ (δ_C 106.7), C-3´ (δ_C 106.6), C-4´ (δ_C 165.7), C-6´ (δ_C 164.0); 6´-OCH_3 (δ_H 3.95, s) to C-6´; H-2 (δ_H 2.59, s) to C-1´; and 4´-OCH_3 (δ_H 3.93, s) to C-4´. Furthermore, in ring A, H-1´´ (δ_H 2.85, m) displayed HMBC correlations to C-2´, C-3´, and C-4´. In ring B, HMBC correlations were observed from H-5´´´´ (δ_H 5.98, s) to C-1´´´´ (δ_C 106.0), C-3´´´´ (δ_C 105.7), C-4´´´´ (δ_C 164.9), C-6´´´´ (δ_C 163.4); from 6´´´´-OCH_3 (δ_H 3.85, s) to C-6´´´´; and H-2´´´ (δ_H 2.56, s) to C-1´´´´ (Figure 47). Additionally, in ring B, H-1´´´´´ (δ_H 2.82, m) showed HMBC correlations to C-2´´´´, C-3´´´´, and C-4´´´´. The observed key HMBC correlations from H_2-2´´ of ring A to C-2´´´´´ of ring B, and from H_2-2´´´´´ (δ_H 3.55, m) of ring B to C-2´´ (δ_C 70.3) of ring A, indicated that an ether linkage connected the two halves, similar to that of **6**. Hence, the structure of **7** was established as shown and was ascribed the trivial name 4´-methoxydimadisone (Figure 46).

Table 21. ^{1}H NMR and ^{13}C NMR Data for Compound 7 in CD_3OD.

	7		
Position	δ_C	type	δ_H, mult (*J* in Hz)
Fragment A			
1	204.8	C	
2	33.3	CH_3	2.59, s
1´	106.7	C	
2´	164.9	C	
3´	106.6	C	
4´	165.7	C	
5´	87.5	CH	6.17, s
6´	164.0	C	
1´´	23.4	CH_2	2.85, m
2´´	**70.3	CH_2	3.54, m
4´-OCH_3	*56.2		3.93, s
6´-OCH_3	*56.1		3.95, s
Fragment B			
1´´´	204.2	C	
2´´´	33.1	CH_3	2.56, s
1´´´´	106.0	C	
2´´´´	166.1	C	
3´´´´	105.7	C	
4´´´´	164.9	C	
5´´´´	91.5	CH	5.98, s
6´´´´	163.4	C	
1´´´´´	23.7	CH_2	2.82, m
2´´´´´	**70.5	CH_2	3.55, m
6´´´´-OCH_3	55.9		3.85, s

Data were collected at 700 MHz (^{1}H) or 175 MHz (^{13}C).
* May be interchanged.
** May be interchanged.

The structure of **1** was confirmed by x-ray crystallography, and the remaining compounds (**2-7**) were structurally related to it via biosynthetic considerations. In particular, the acetophenone moiety was a common motif, noted through the nearly identical NMR data. In addition, when ^{1}H NMR data were acquired in $CDCl_3$, all compounds exhibited a singlet resonance in the range from δ_H 14.00 to δ_H 14.47 (Figure 56), indicative of chelation between the hydroxy and carbonyl moieties in all of the structures.

Compounds **1**, **2** and **5** were evaluated for antimicrobial activity against *Staphylococcus aureus, Escherichia coli, Mycobacterium smegmatis, Candida albicans,* and *Aspergillus niger* (Table 25). All the compounds tested had minimal inhibitory concentrations greater than 55 µg/mL. Compounds **3**, **4**, **6**, **7** were not evaluated for their antimicrobial activity due to the relative paucity of these samples.

***In situ* analysis of the concentration of compounds 1-7 in cultures of G416.** A 3-week old culture of G416 growing on PDA media at room temperature (~22-25˚C) sealed with parafilm was noted to produce a clear guttate (exudate) (Figure 48). Older culture that were grown under the same conditions did not produce any visible guttates. A few recent studies have suggested that guttates are a rich source of secondary metabolites, although their ecological roles and functions in fungi are still uncertain.[126-128] We hypothesized that guttates may serve to store secondary metabolites, concentrating them for interaction with their environment. To test this, the presence and relative concentration of compounds **1-7** were examined *in situ* using a droplet-liquid microjunction-surface sampling probe (droplet-LMJ-SSP), followed by analysis via

UPLC-PDA-HRMS-MS/MS, all according to a previously described procedure.[129] Compounds **1**, **2** and/or **4** (as they have the same molecular weight), **3**, **5**, and **6** were detected and identified in the guttate based on their retention times, accurate *m/z* match (±5 ppm), and MS/MS fragmentation patterns (Figures 65-69). Compound **1** appeared to be the most abundant by *L. madisonensis* (G416), based on its relative intensity compared to **2** and/or **4** and **5**, as shown in Figure 48. Although compounds **3** and **6** were identified in the guttate by droplet-LMJ-SSP, they were only present in trace amounts compared to **1**. Compounds **1**, **2** and/or **4**, and trace amounts of **5** were also detected on the outer mycelium of G416; however, in all cases, these compounds were more concentrated in the guttates. We hypothesize that compound **7** was not detected in the culture, either because the fungus biosynthesized it only when grown on rice or after an extended period of time. This result was not surprising, as it is well known that variation of media conditions can alter the biosynthesis of secondary metabolites in fungi.[130,131] An alternative hypothesis could be that compound **7** was located inside the mycelium, rather than on the surface.[132] Overall, the heat profile (Figure 48) suggested that relatively higher concentrations of the compounds were present in the guttate in comparison with the mycelium. This observation suggested that the fungus could be using the guttates as a reservoir to store and/or concentrate secondary metabolites. Moreover, having a higher concentration of **1**, in general, corroborated the more traditional natural products protocols, where **1** was isolated in the highest yield. With the droplet-LMJ-SSP, the spatial distribution and relative concentration of the compounds were evaluated. This method can provide additional useful information into the metabolism of the fungus *in*

situ, which cannot be obtained with traditional isolation techniques. Unfortunately, it was not possible to assign a biological activity to these compounds, and thus, their potential role in the fungal life cycle is unknown at this time. Further studies to evaluate the biological relevance of these compounds, particularly in relation to their concentration in guttates, are ongoing.

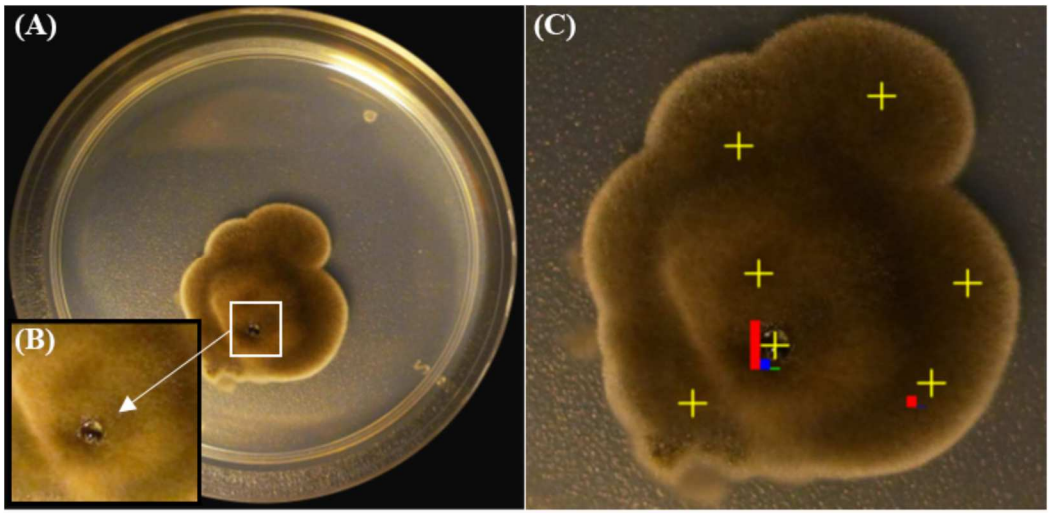

Figure 48. *In situ* Droplet-LMJ-SSP Analysis of G416 Culture. (A) A three-week-old culture of G416 grown on PDA producing a guttate. (B) Arrow showing a magnified view of the guttate. (C) Heat map of compounds **1 (**red), **2** (and/or) **4** (blue), and **5** (green). The height of the bars show the relative amount of signal detected by HRESIMS within a 5 ppm mass tolerance for the given compounds. The crosshairs indicate location of sampling points of the droplet-LMJ-SSP.

Conclusion

Lindgomycetaceae is a recently described family of freshwater ascomycetes, and little is known about the chemistry produced by species in this family.[133] In a previous study, the fatty acid, 6*E*,9*E*-octadecadienoic acid, and the steroid derivative, ergosterol peroxide, were shown to be the major compounds produced by *Lindgomyces*

angustiascus.[120] Additionally, strains phylogenetically related to the Lindgomycetaceae, isolated recently from two different marine habitats produced the newly described compound lindgomycin and ascosetin, both of which have polyketide structures.[134] The isolation and identification of acetophenone derivatives **1-7** from *L. madisonensis* highlights the potential of freshwater ascomycetes as a source of new chemical diversity. The use of droplet-LMJ-SSP demonstrated the concentration of these secondary metabolites in guttates, suggesting that guttates may serve as a reservoir of secondary metabolites, at least under certain growth conditions.

Experimental

General experimental procedures. The NMR data were collected using either a JEOL ECS-400 spectrometer (JEOL USA, Inc.) operating at 400 MHz for ^{1}H and 100 MHz for ^{13}C, and equipped with JEOL normal geometry broadband Royal probe, or an Agilent 700 MHz NMR spectrometer (Agilent Technologies, Inc., Santa Clara, CA, USA) operating at 700 MHz for ^{1}H and 175 MHz for ^{13}C, and equipped with a cryoprobe. NMR chemical shift values were referenced to residual solvent signals for CD_3OD (δ_H/δ_C 3.31/49.0) and $CDCl_3$ (δ_H/δ_C 7.26/77.2). HRESIMS data were obtained using a Thermo QExactive Plus mass spectrometer (ThermoFisher, San Jose, CA, USA) paired with an electrospray ionization source. Analysis of the fungal culture by *in situ* sampling was performed using the CTC/LEAP HTC PAL autosampler (LEAP Technologies Inc.) converted to an automated droplet-LMJ-SSP by using in-house developed software dropletProbe Premium. The droplet-LMJ-SSP was coupled with a Waters Acquity ultraperformance liquid chromatography (UPLC) system (Waters Corp.) and a Thermo

QExactive Plus. The HCD fragmentation used a normalized collision energy of 30 eV for all the compounds to obtain MS/MS data. The UPLC separation was performed using an Acquity BEH C18 column (50 mm x 2.1 mm i.d., 1.7 µm) equilibrated at 40 °C and a flow rate set at 0.3 mL/min. The mobile phase consisted of a linear CH_3CN-H_2O (acidified with 0.1% formic acid) gradient starting at 15% CH_3CN to 100% CH_3CN over 8 min. The mobile phase was held for another 1.5 min at 100% CH_3CN before going back to the starting conditions. The HPLC separations were performed using Varian ProStar HPLC system connected to a ProStar 335 photodiode array detector (PDA) with UV detection set at 210 nm and 254 nm. Preparative HPLC purification of isolated compounds was performed on a Phenomenex Synergi 4 µm particle size C_{18} column (21 x 250 mm) at a flow rate of 21.24 mL/min. Flash column chromatography was carried out with a Teledyne ISCO Combiflash Rf connected to an ELSD and PDA detectors with UV detection set at 200-400 nm. The UV data were acquired using a Varian Cary 100 Bio UV–Vis spectrophotometer (Varian Inc., Walnut Creek, CA, USA). The IR data were recorded using a Perkin-Elmer Spectrum One with Universal ATR attachment (PerkinElmer, Waltham, MA, USA). The melting point data were determined using an SRS DigiMelt Melting Point Apparatus, MPA 160 (Stanford Research Systems, Inc., Sunnyvale, CA, USA), and are uncorrected

Fungal strain isolation and identification. The fungal strain, G416, was isolated from partially decorticated submerged wood collected from Big Beaver Island creek in Madison, North Carolina, USA (36°27'40.0"N 80°01'46.0"W; water pH: 5; water temp 10 °C). Sample collection and isolations were made using procedures outlined earlier.[135]

Identification of strain G416 was accomplished by analysis of molecular sequence data from the nuclear ribosomal internal transcribed spacer region (ITS rDNA). This gene region has been officially designated as the barcoding marker for species identification of fungal strains.[136] In addition, portions of the 18S rDNA (partial SSU) and 28S rDNA (partial LSU) were also sequenced using primers NS1 and NS4 for SSU [137] and LROR and LR6 for LSU.[138,139] The DNA extraction, PCR amplification, sequencing protocols, and phylogenetic analysis were accomplished using methods described previously.[120,126] A BLAST search of the ITS sequence from G416 against GenBank suggested that the fungal strain had affinities with members of the freshwater ascomycetes genus *Lindgomyces*, (Lindgomycetaceae, Dothideomycetes, Ascomycota).[120,133,140,141] Based on examination of morphology, and maximum likelihood analyses using portions of the rDNA gene (partial SSU, and partial LSU; Figure 70), the strain G416 has been identified as new species *Lindgomyces madisonensis* Raja & Oberlies.[123] The Ex-holotype cultures (single ascospore isolate from holotype) of the new species have been deposited in the Deutsche Sammlung von Mikroorganismen und Zellkulturen, Germany (DSMZ) as (DSM-100629) and Centraalbureau voor Schimmelcultures, Netherlands (CBS) as (CBS 140367). A voucher culture of strain G416 is also maintained in the Department of Chemistry and Biochemistry culture collection at the University of North Carolina at Greensboro. The sequence data from the newly established species have been deposited in GenBank (SSU: KT207822, KT207823; ITS: KT207818, KT207819; and LSU: KT207820, KT207821).

Fermentation, Extraction, and Isolation. The fermentation for the fungal strain G416 was performed using procedures described previously with slight modifications.[118] Briefly, a seed culture of G416 was grown on a potato dextrose agar (PDA, Difco) slant for about 14 days. Subsequently, a small agar plug with mycelium was inoculated on liquid YESD media, followed by incubation for approximately 14 days at rt with shaking at 125 rpm using a rotary shaker. Once sufficient fungal growth was observed in the seed culture, it was inoculated into four 250 mL Erlenmeyer flask, each containing 30 mL of autoclaved rice medium (consisting of 10 g of rice and deionized H_2O that was twice the volume of rice) and grown at rt for a period of 28 days.

To each solid fermentation culture of G416, 60 mL of 1:1 CH_3OH-$CHCl_3$ was added, and these were shaken for 16 h on an orbital shaker. The resulting mixtures were filtered under vacuum, and the filtrate from each of the four Erlenmeyer flasks was combined. To the filtrate 360 mL of $CHCl_3$ and 600 mL of H_2O were added, and the mixture was stirred for 30 min and then transferred into a separatory funnel. The organic layer was drawn off and dried *in vacuo*. This dried organic extract was defatted by reconstituting in a mixture of 400 mL of 1:1 CH_3OH-CH_3CN and 400 mL of hexane, and then partitioned in a separatory funnel. The CH_3OH-CH_3CN layer was collected and concentrated *in vacuo*. The resulting CH_3OH-CH_3CN extract (428 mg) was then adsorbed on Celite 545, and subjected to silica flash chromatography on a 12 g RediSep Rf Gold Si-gel column, eluting with an increasing gradient of hexane to $CHCl_3$ at a flow rate of 30 mL/min over 61 column volumes, and for a duration of 34 min to give 48 fractions each containing 22 mL. The resulting fractions were then pooled according to their ELSD and

UV profiles, which resulted in five combined fractions in total. All were examined by analytical HPLC, and fractions 1-3 warranted further purification based on their chromatographic profiles.

Fraction 3 (23 mg) was purified further by preparative reversed phase HPLC eluting with a linear gradient from 40% to 60% CH_3CN in H_2O (0.1% formic acid) at a flow rate of 21.2 mL/min over 30 min to afford compound **1** (14.5 mg, t_R =13.3 min). Fraction 2 (17 mg) was purified using the same preparative RP-HPLC conditions yielding compounds **2** (11.7 mg, t_R =10.4 min) and **6** (1.4 mg, t_R = 26.4 min). Fraction 1 (75 mg) was separated using a linear gradient from 40% to 80% CH_3CN in H_2O (0.1% formic acid) to give compounds **3** (1.4 mg, t_R = 15.4 min), **4** (0.9 mg, t_R = 13.2 min), **5** (8.1 mg, t_R = 16.6 min), and **7** (0.9 mg, t_R = 23.1 min).

madisone (1): White solid;m.p. 174-176 °C; UV (CH_3OH) λ_{max} (log ε) 306 (3.30), 237 (3.25) nm; IR (ATR) ν_{max} 3319, 3012, 2972, 2939, 2754, 1610, 1573, 1449, 1265, 1195, 803 cm^{-1}; ^1H (400 MHz) and ^{13}C NMR (100 MHz) both in CD_3OD, see Table 19; HRESIMS *m/z* 227.09129 $[M+H]^+$ (calc'd for $C_{11}H_{15}O_5$, 227.09140).

4´-methoxymadisone (2): White solid; UV (CH_3OH) λ_{max} (log ε) 293 (3.33), 237 (3.28) nm; IR (ATR) ν_{max} 3275, 3007, 2976, 2940, 2885, 1618, 1579, 1416, 1265, 1122, 866 cm^{-1}; ^1H (400 MHz) and ^{13}C NMR (100 MHz) both in CD_3OD, see Table 19; HRESIMS *m/z* 241.10681 $[M+H]^+$ (calc'd for $C_{12}H_{17}O_5$, 241.10705).

dehydromadisone (3): White solid; UV (CH_3OH) λ_{max} (log ε) 292 (3.27), 231 (3.21) nm; ^1H (400 MHz) and ^{13}C NMR (100 MHz) both in CD_3OD, see Table 19; HRESIMS *m/z* 211.09644 $[M+H]^+$ (calc'd for $C_{11}H_{15}O_4$, 211.09648).

2´´-methoxymadisone (4): White solid; UV (CH_3OH) λ_{max} (log ε) 288 (2.92), 226 (2.95) nm; ^1H (700 MHz) and ^{13}C NMR (175 MHz) both in CD_3OD, see Table 20; HRESIMS *m/z* 241.10678 $[M+H]^+$ (calc'd for $C_{12}H_{17}O_5$, 241.10705).

dihydroallovisnaginone (5): White solid; UV (CH_3OH) λ_{max} (log ε) 307 (3.26), 241 (3.22) nm; IR (ATR) ν_{max} 3106, 2986, 2950, 2908, 2864, 1628, 1594, 1389, 1286, 1242, 1192, 884 cm^{-1}; ^1H (400 MHz) and ^{13}C NMR (100 MHz) both in CD_3OD, see Table 20; HRESIMS *m/z* 209.08083$[M+H]^+$ (calc'd for $C_{11}H_{13}O_4$, 209.08083).

dimadisone (6): White solid; UV (CH_3OH) λ_{max} (log ε) 292 (3.54), 235 (3.49) nm; ^1H (400 MHz) and ^{13}C NMR (100 MHz) both in CD_3OD, see Table 20; HRESIMS *m/z* 435.16467 $[M+H]^+$ (calc'd for $C_{22}H_{27}O_9$, 435.16496).

4´-methoxydimadisone (7): White solid; UV (CH_3OH) λ_{max} (log ε) 292 (3.60), 231 (3.54) nm; ^1H (700 MHz) and ^{13}C NMR (175 MHz) both in CD_3OD, see Table 21; HRESIMS *m/z* 449.18039 $[M+H]^+$ (calc'd for $C_{23}H_{29}O_9$, 449.18061).

X-ray Crystallography. Crystals of compound **1** were grown in CH_3OH at room temperature. A clear colourless irregular-shaped specimen of $C_{11}H_{14}O_5$, approximate dimensions 0.030 mm x 0.160 mm x 0.290 mm, was used for the X-ray crystallographic analysis. The X-ray intensity data were measured on a Bruker APEX CCD system equipped with a graphite monochromator and a Mo Kα sealed x-ray tube (λ = 0.71073 Å). The total exposure time was 20.70 h. The frames were integrated with the Bruker SAINT software package using a narrow-frame algorithm. The integration of the data using an orthorhombic unit cell yielded a total of 15607 reflections to a maximum θ angle

of 30.03° (0.71 Å resolution), of which 3150 were independent (Friedel opposites not merged, average redundancy 4.955, completeness = 99.7%, R_{int} = 4.04%, R_{sig} = 3.01%) and 2720 (86.35%) were greater than $2\sigma(F^2)$. The final cell constants of a = 4.3710(4) Å, b = 11.6045(11) Å, c = 21.2672(19) Å, volume = 1078.74(17) $Å^3$, are based upon the refinement of the XYZ-centroids of 4245 reflections above 20 σ (I) with 7.022° < 2θ < 56.44°. Data were corrected for scaling and absorption effects using the multi-scan method (SADABS). The ratio of minimum to maximum apparent transmission was 0.986. The calculated minimum and maximum transmission coefficients (based on crystal size) are 0.9690 and 0.9970. The structure was solved and refined using the Bruker SHELXTL Software Package, using the space group $P2_12_12_1$, with Z = 4 for the formula unit, $C_{11}H_{14}O_5$. The final anisotropic full-matrix least-squares refinement on F^2 with 159 variables converged at R_1 = 4.22%, for the observed data and wR_2 = 10.90% for all data. The goodness-of-fit was 1.031. The largest peak in the final difference electron density synthesis was 0.318 $e^-/Å^3$ and the largest hole was -0.140 $e^-/Å^3$ with an RMS deviation of 0.047 $e^-/Å^3$. On the basis of the final model, the calculated density was 1.393 g/cm^3 and F (000), 480 e^-. Crystal data, data collection, and structure refinement details are summarized in Table 22-24.

Antimicrobial assay. Determination of the minimum inhibitory concentrations (MICs) of compounds **1, 2**, and **5** against *S. aureus, E. coli, M. smegmatis, C. albicans,* and *A. niger* were performed according to previously described methods.[142,143]

Acknowledgements. We thank Mr. David Sprinkle for permission to collect samples on his property, Dr. Joe Falkinham (Virginia Polytechnic Institute and State

University) for the *in vitro* antibacterial and antifungal testing of the isolated compounds, Dr. Tamam El-Elimat (University of North Carolina at Greensboro; UNCG) for helpful suggestions, and Drs. Vilmos Kertesz and Gary J. Van Berkel (Mass Spectrometry and Laser Spectroscopy Group, Chemical Sciences Division, Oak Ridge National Laboratory) for inspiration and guidance with the droplet-LMJ-SSP. The high resolution mass spectrometry data were collected at the Triad Mass Spectrometry Laboratory at UNCG. The Wake Forest University *X*–ray Facility thanks the National Science Foundation (grant CHE–0234489) for funds to purchase the *X*–ray instrument and computers.

Supplementary Data

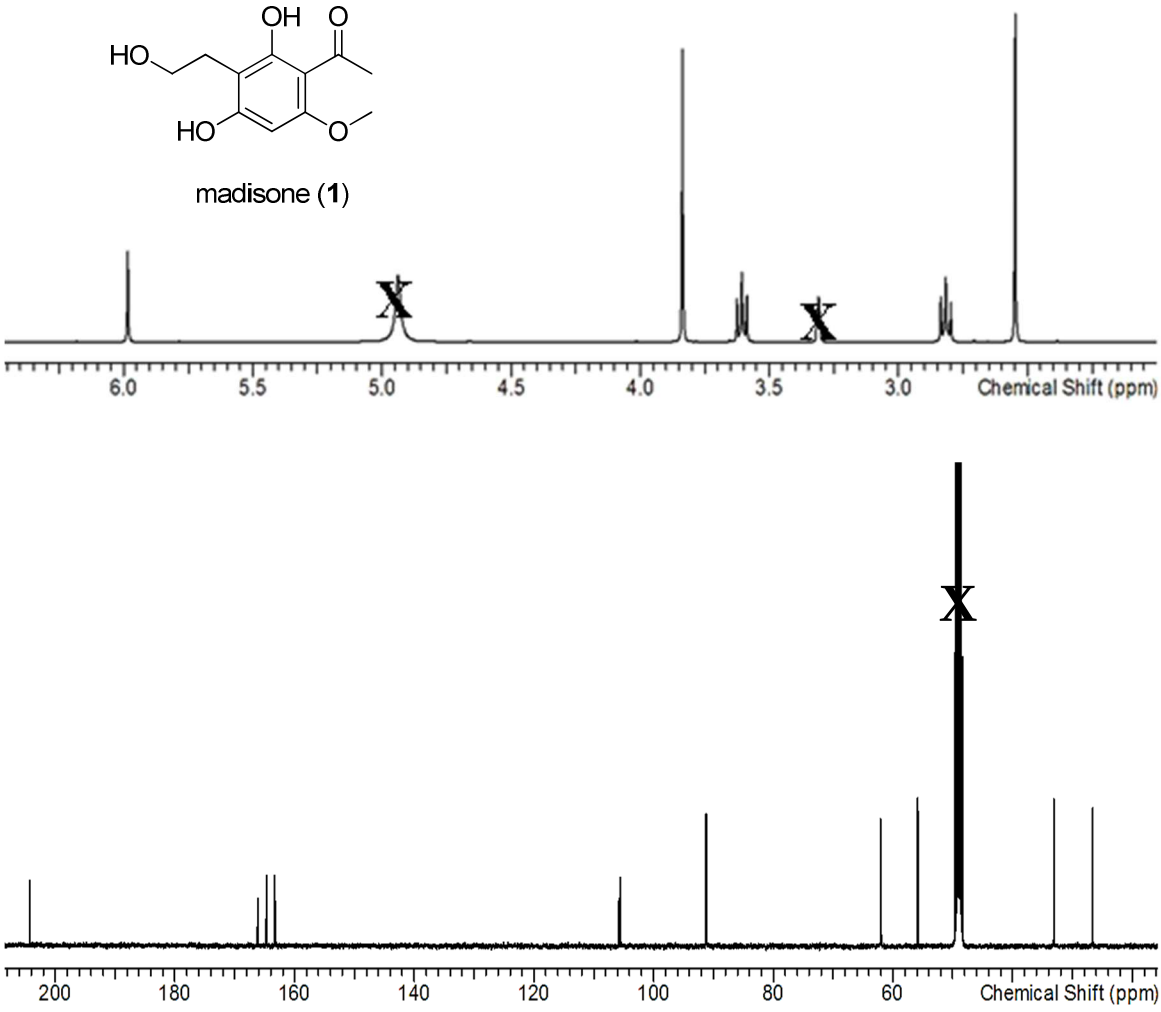

Figure 49. ^{1}H NMR (400 MHz; Top) and ^{13}C NMR (100 MHz; Bottom) Spectra of Madisone (1) in CD_3OD.

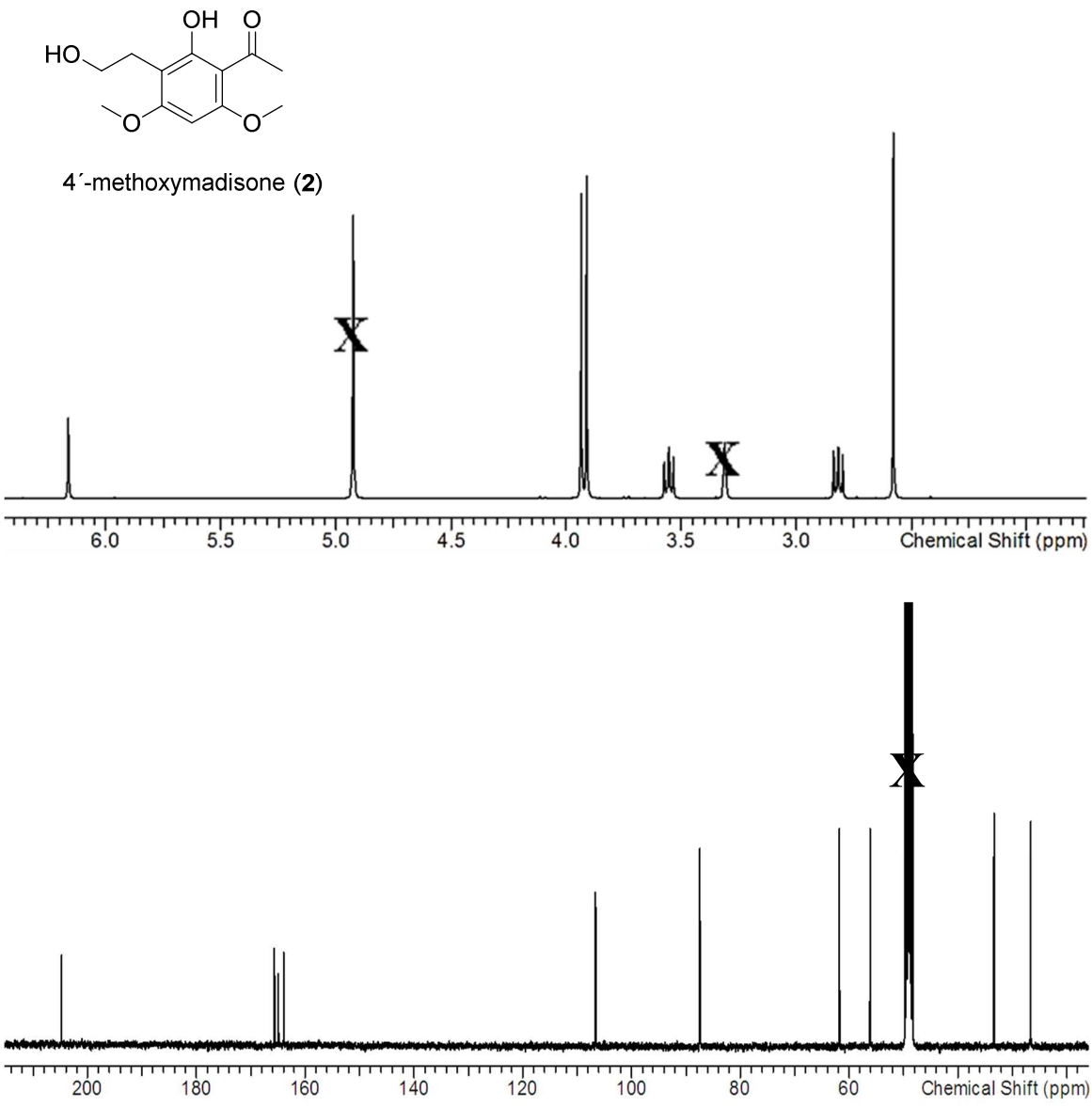

Figure 50. ^{1}H NMR (400 MHz; Top) and ^{13}C NMR (100 MHz; Bottom) Spectra of 4´-Methoxymadisone (2) in CD_3OD.

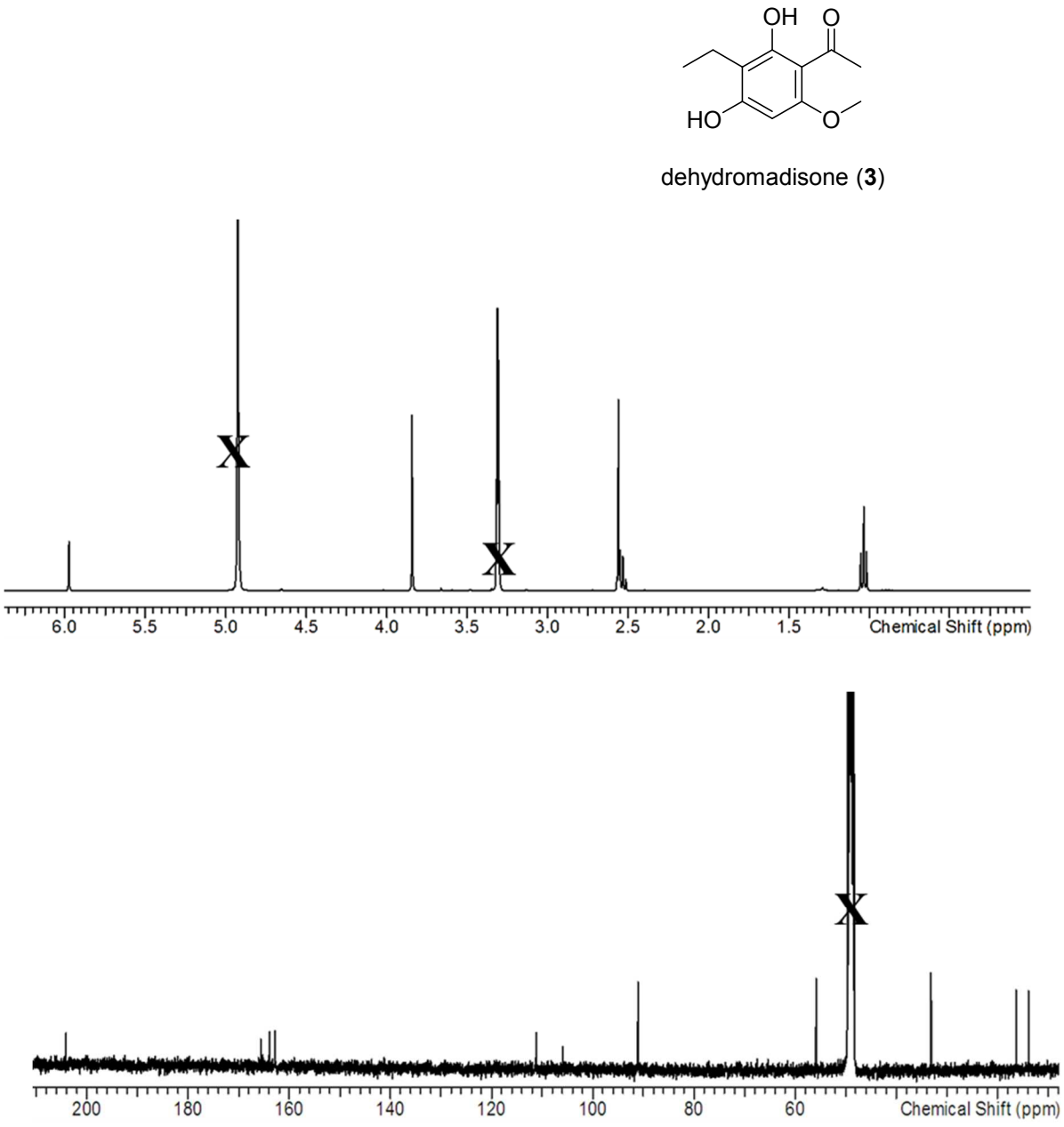

Figure 51. ^{1}H NMR (400 MHz; Top) and ^{13}C NMR (100 MHz; Bottom) Spectra of Dehydromadisone (3) in CD_3OD.

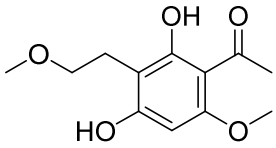

2´´-methoxymadisone (**4**)

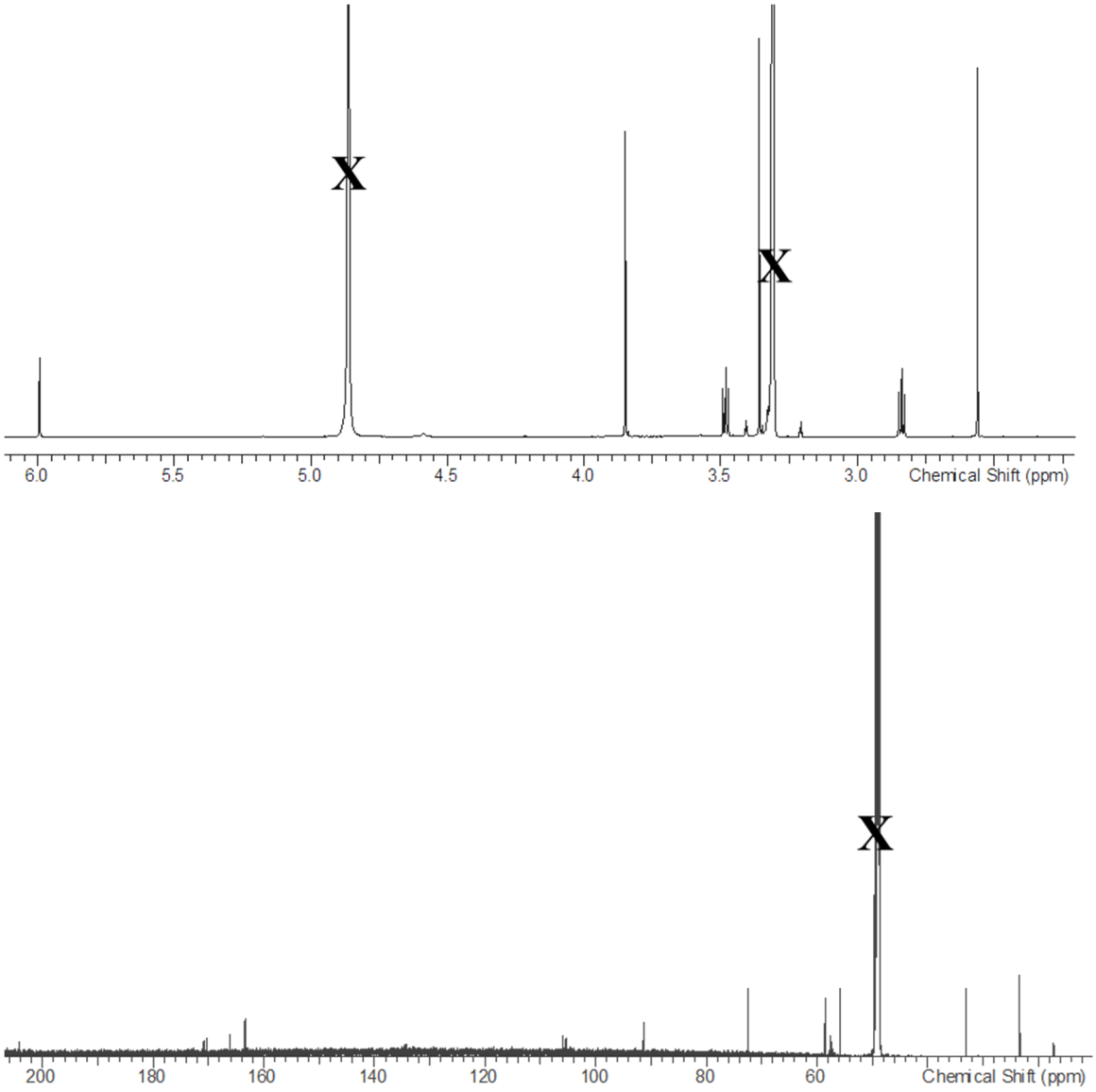

Figure 52. ^{1}H NMR (700 MHz; Top) and ^{13}C NMR (175 MHz; Bottom) Spectra of 2´´-Methoxymadisone (4) in CD_3OD.

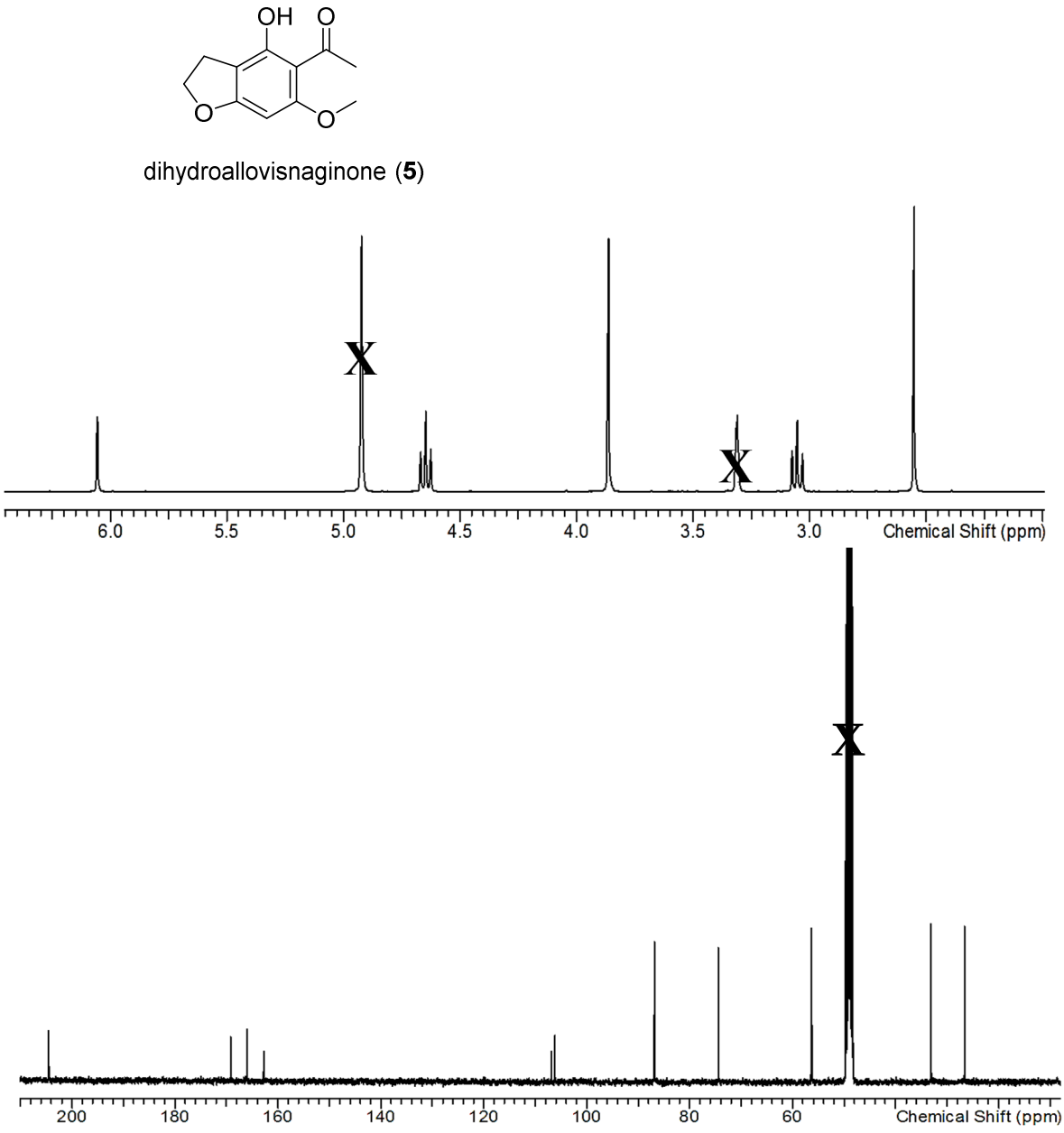

Figure 53. ^{1}H NMR (400 MHz; Top) and ^{13}C NMR (100 MHz; Bottom) Spectra of Dihydroallovisnaginone (5) in CD_3OD.

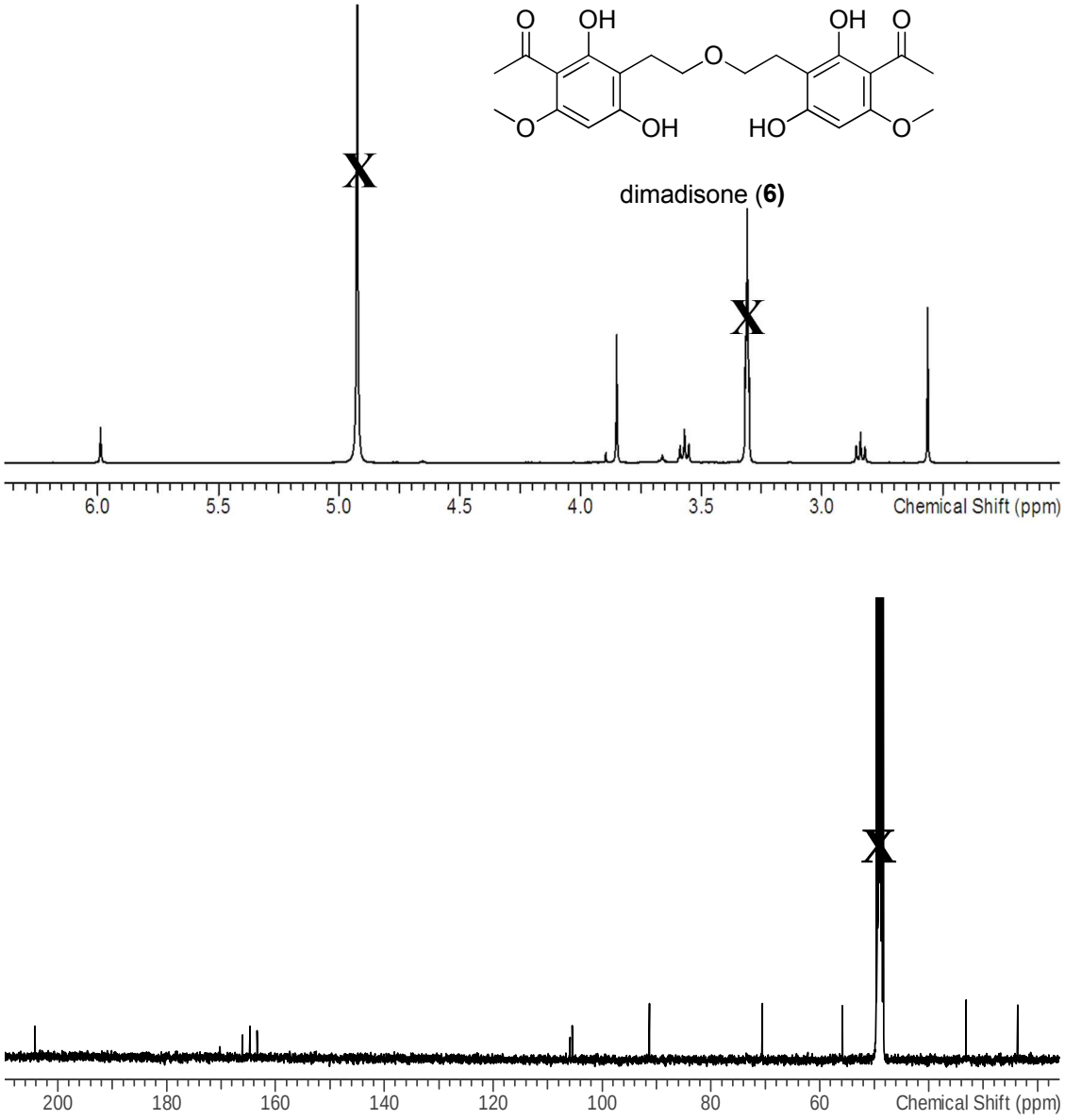

Figure 54. ^{1}H NMR (400 MHz; Top) and ^{13}C NMR (100 MHz; Bottom) Spectra of Dimadisone (6) in CD_3OD.

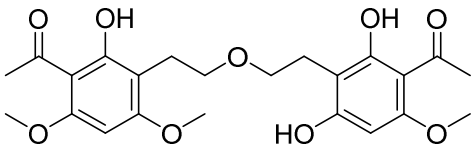

4´-methoxydimadisone (**7)**

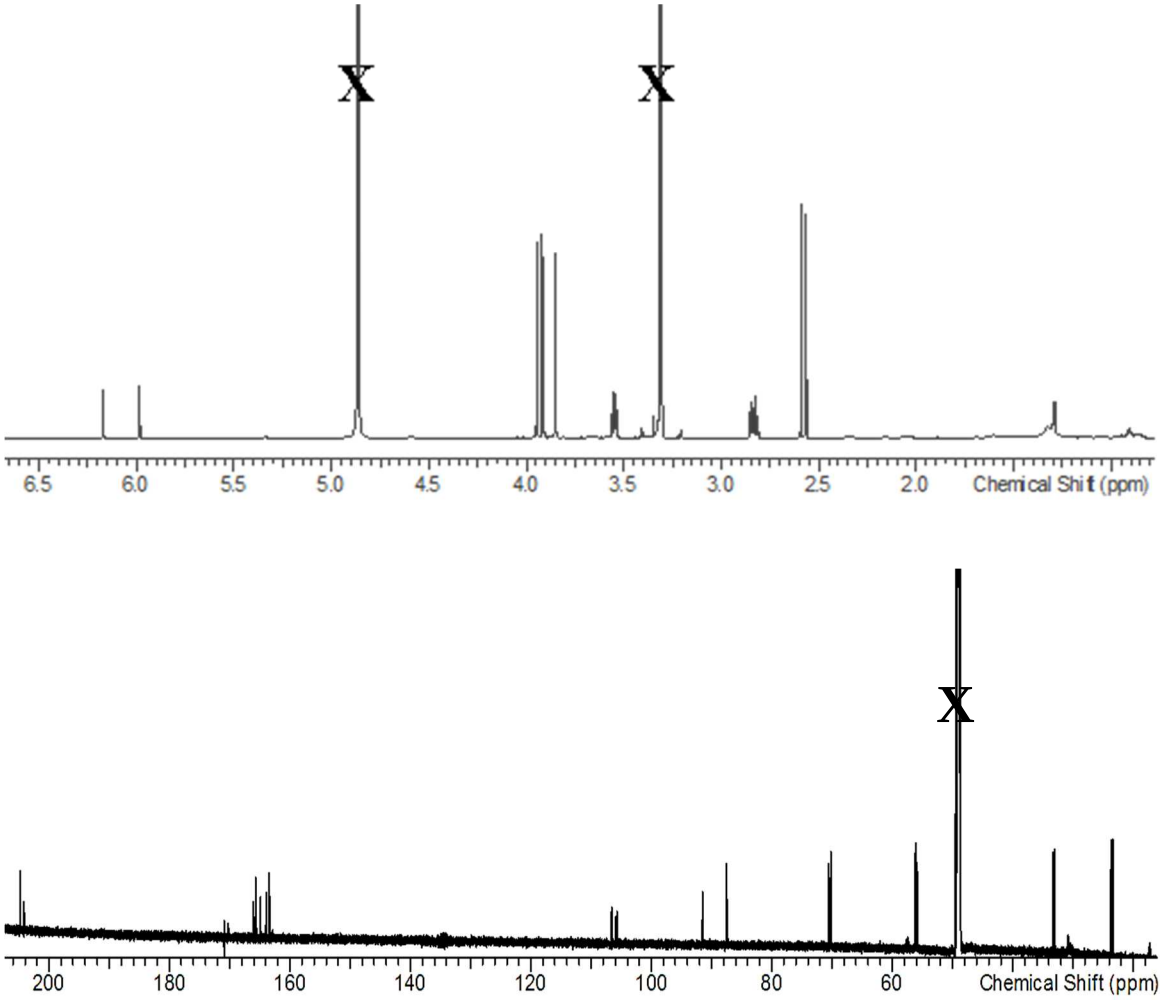

Figure 55. ^{1}H NMR (700 MHz; Top) and ^{13}C NMR (175 MHz; Bottom) Spectra of 4´-Methoxydimadisone (7) in CD_3OD.

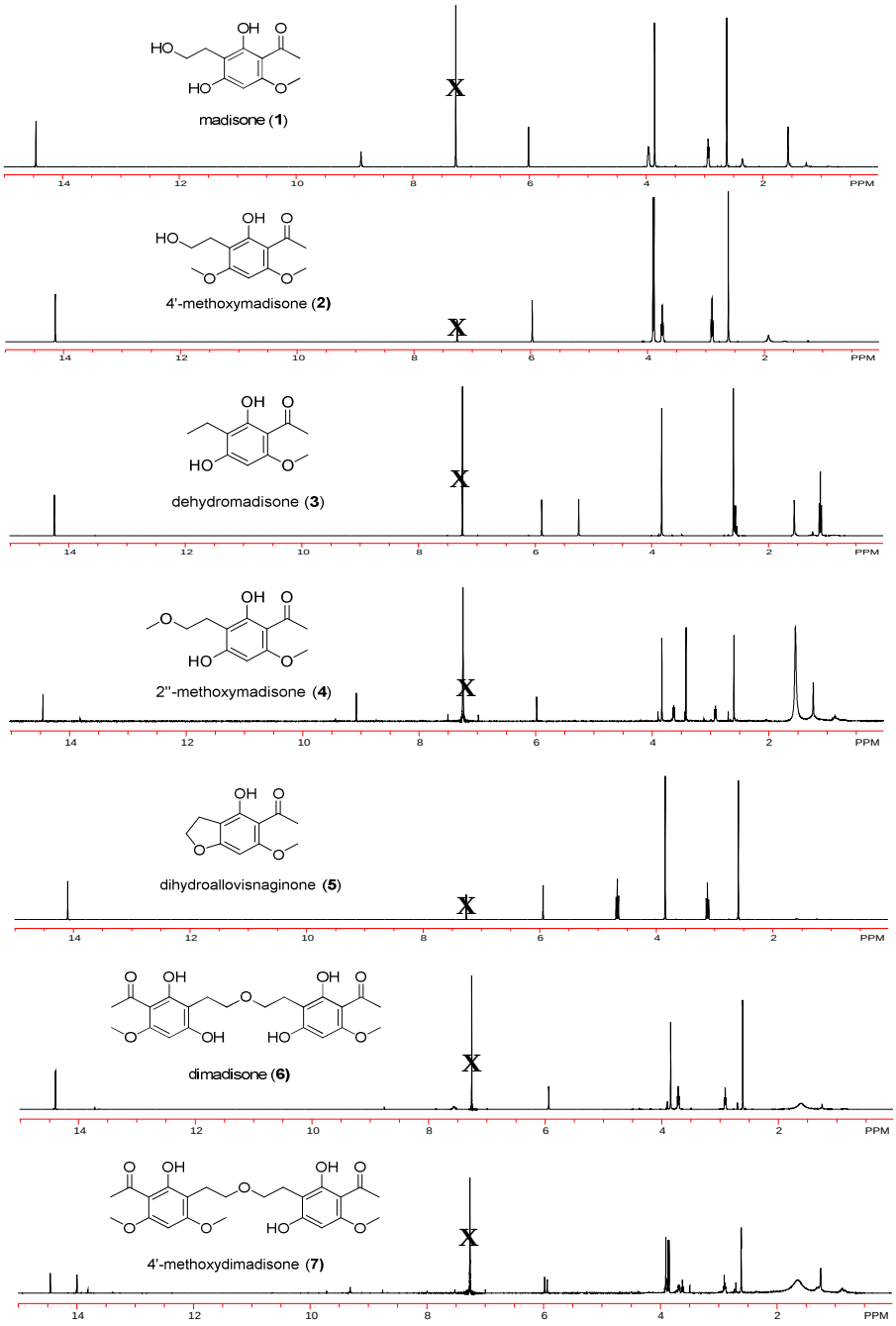

Figure 56. ^{1}H NMR (400 MHz) Spectra of Compounds 1-7 in $CDCl_3$.

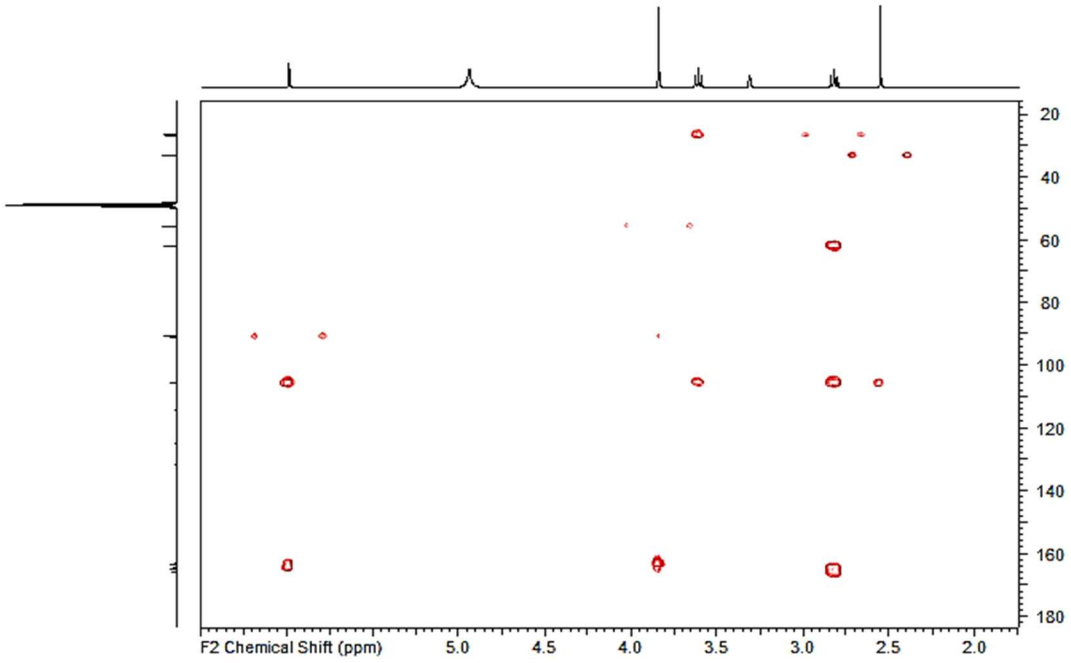

Figure 57. The HMBC (400 MHz/100 MHz) Spectrum of Madisone (1) in CD_3OD.

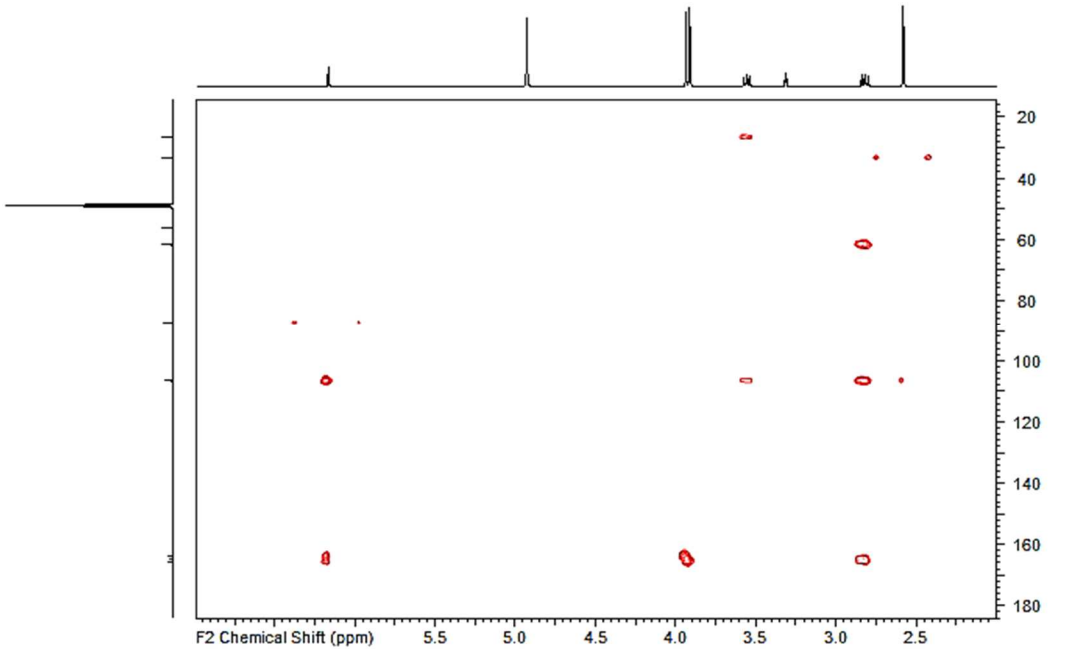

Figure 58. The HMBC (400 MHz/100 MHz) Spectrum of 4´-Methoxymadisone (2) in CD_3OD.

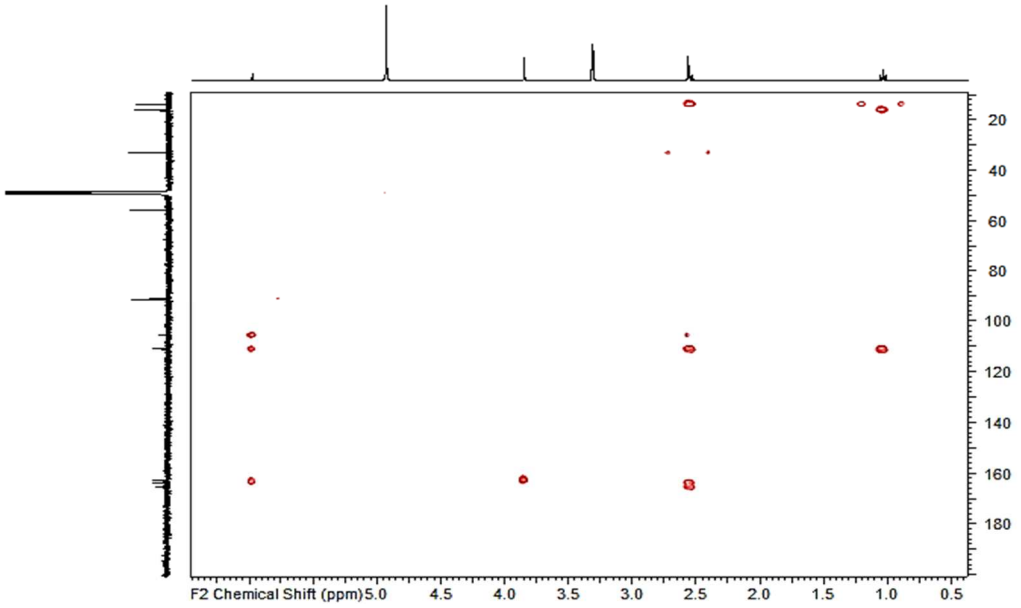

Figure 59. The HMBC (400 MHz/100 MHz) Spectrum of Dehydromadisone (3) in CD_3OD.

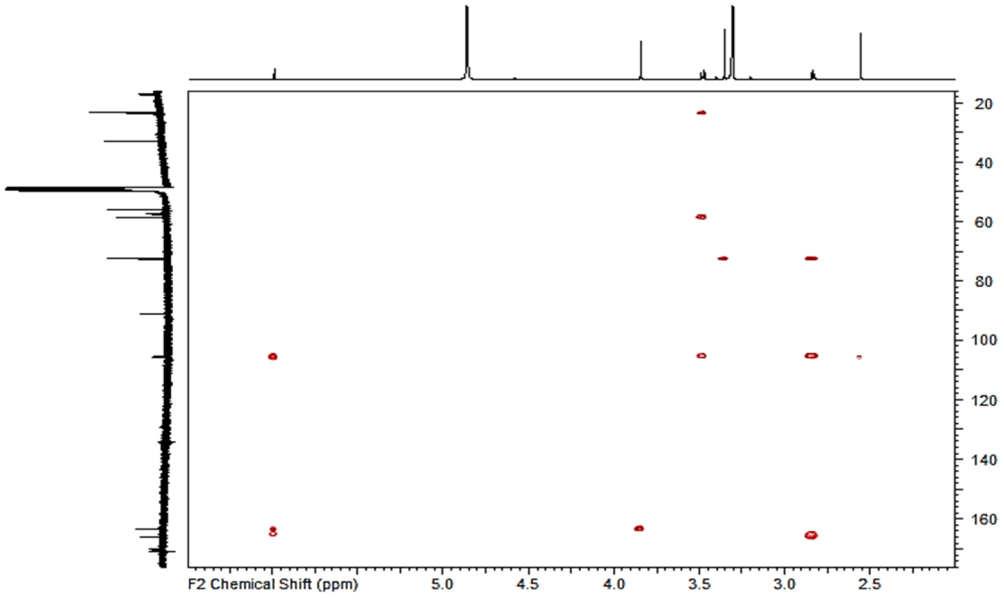

Figure 60. The HMBC (700 MHz/175 MHz) Spectrum of 2´´-Methoxymadisone (4) in CD_3OD.

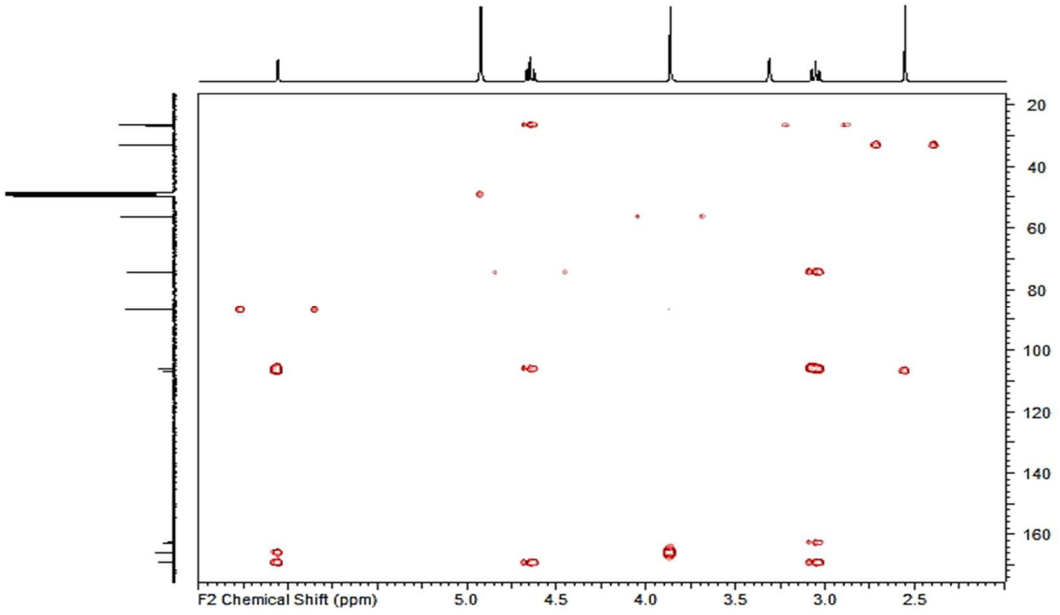

Figure 61. The HMBC (400 MHz/100 MHz) Spectrum of Dihydroallovisnaginone (5) in CD_3OD.

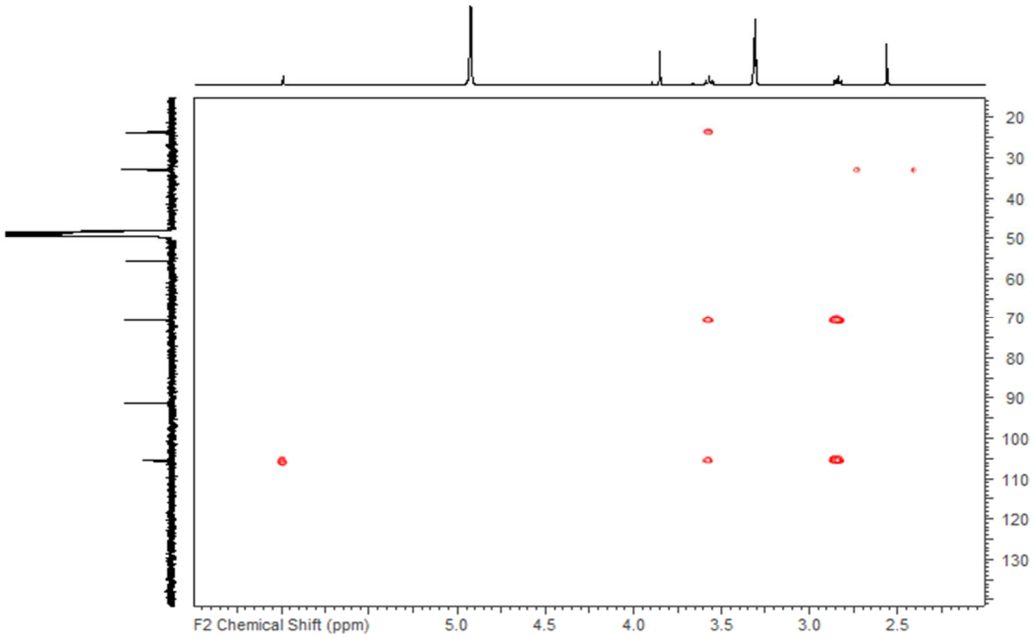

Figure 62. The HMBC (400 MHz/100 MHz) Spectrum of Dimadisone (6) in CD_3OD.

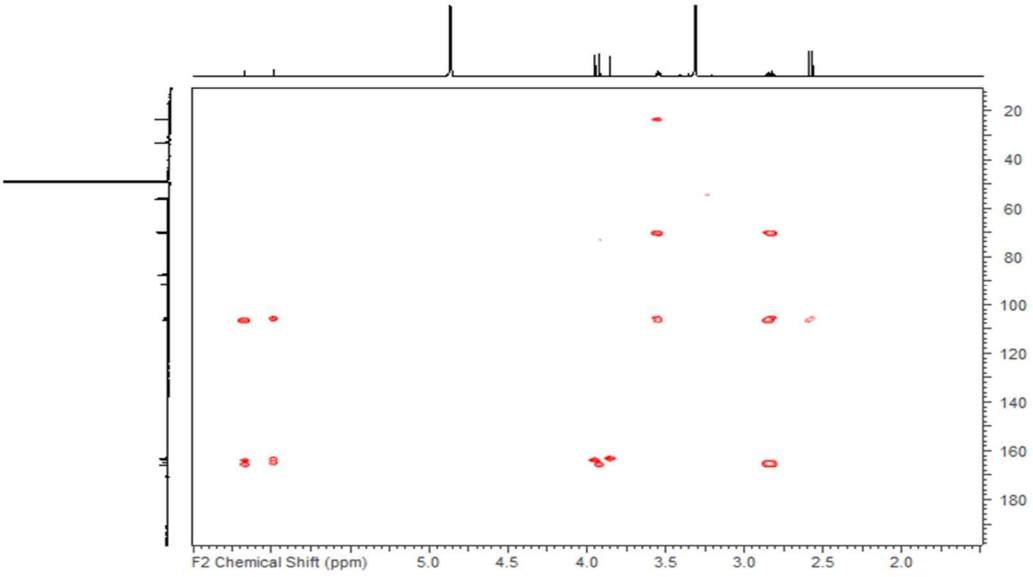

Figure 63. The HMBC (700 MHz/175 MHz) Spectrum of 4´-Methoxydimadisone (7) in CD_3OD.

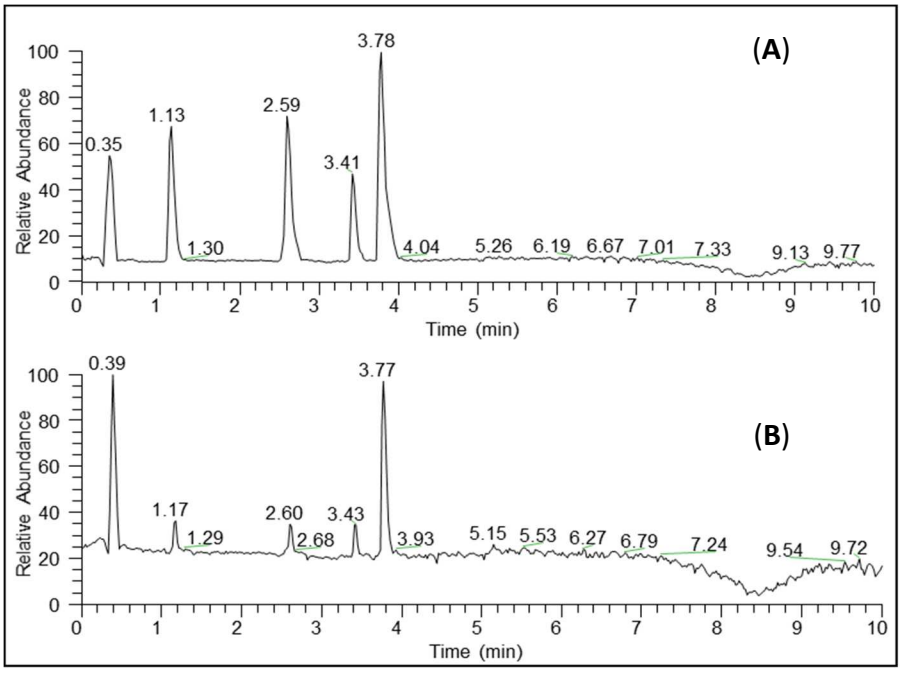

Figure 64. Base Peak Chromatograms for G416 Sampled by the Droplet-LMJ-SSP. (A) Guttate Produced by G416 (B) Outer Mycelium of G416.

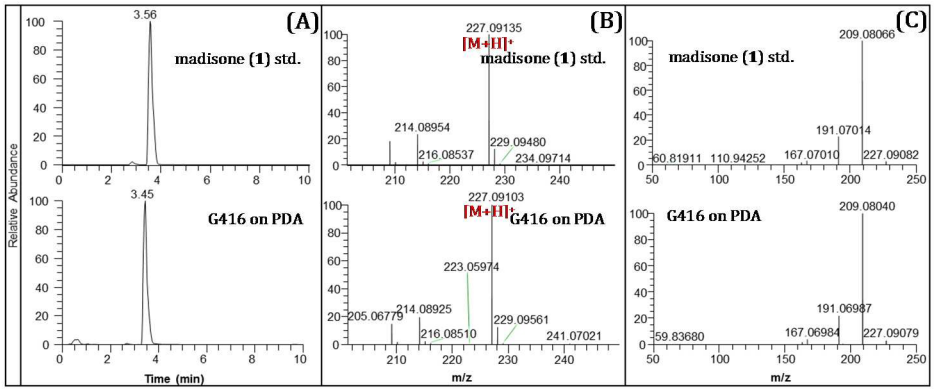

Figure 65. Data for the Reference Standard 1 (Top) and *In Situ* Analysis of G416 Grown on PDA (Bottom). Overlay of chromatographic peaks of **1** (B) (+)-HRESIMS of **1** (C) MS/MS HCD fragmentation of **1.**

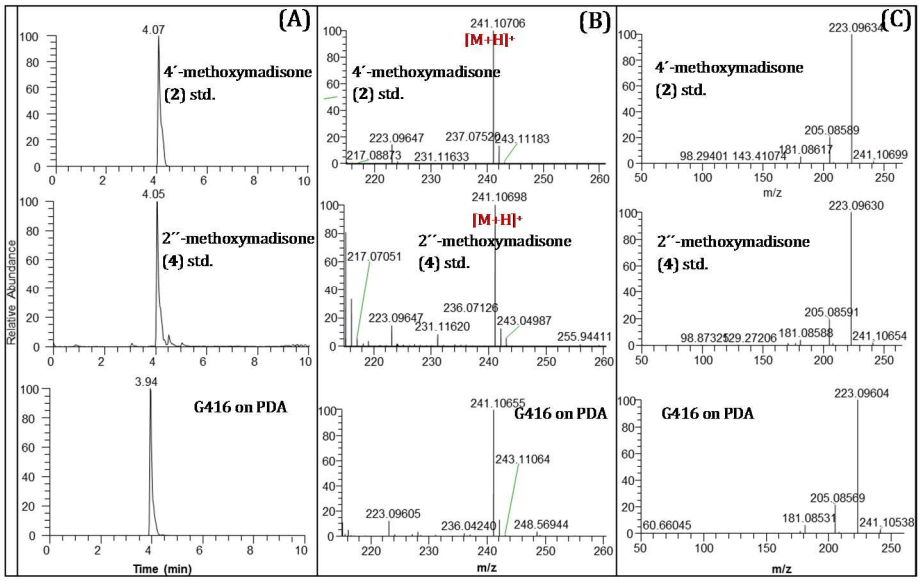

Figure 66. Data for the Reference Standard 2 (Top) and *In Situ* Analysis of G416 Grown on PDA (Bottom). (A) Overlay of chromatographic peaks of **2** and **4** (B) (+)-HRESIMS of **2** and **4** (C) MS/MS HCD fragmentation of **2** and **4**.

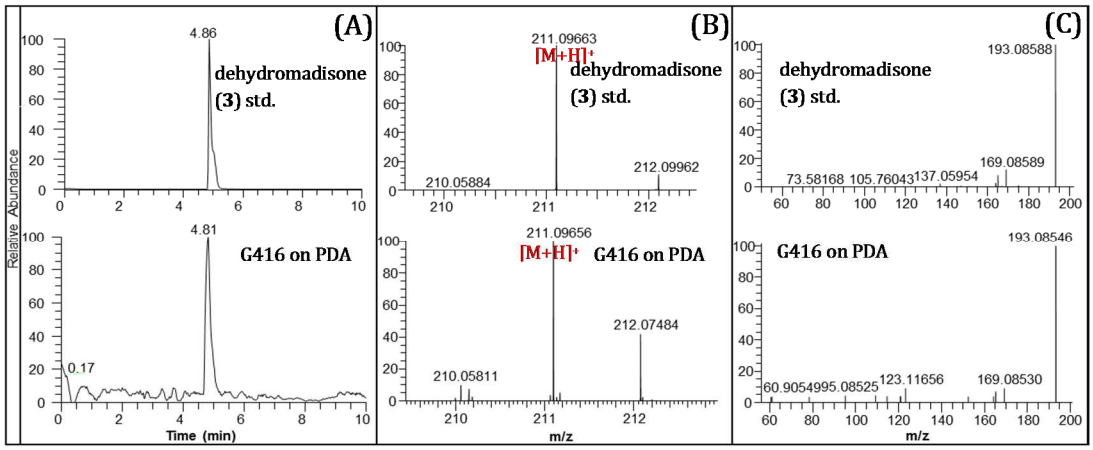

Figure 67. Data for the Reference Standard 3 (Top) and *In Situ* Analysis of G416 Grown on PDA (Bottom). (A) Overlay of chromatographic peaks of **3** (B) (+)-HRESIMS of **3** (C) MS/MS HCD fragmentation of **3.** The top and bottom show the data for the reference standard and *in situ* analysis of G416 grown on PDA, respectively.

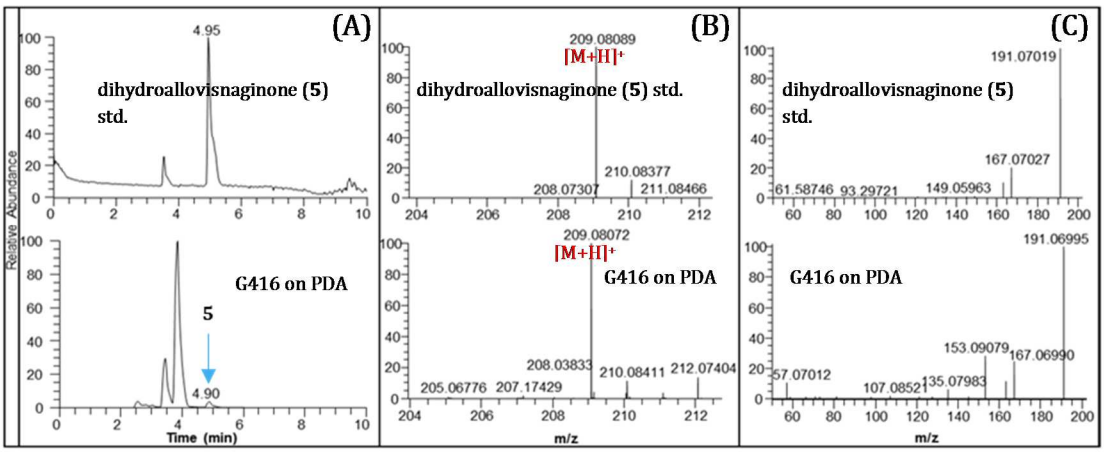

Figure 68. Data for the Reference Standard 5 (Top) and *In Situ* Analysis of G416 Grown on PDA (Bottom). (A) Overlay of chromatographic peaks of **5** (B) (+)-HRESIMS of **5** (C) MS/MS HCD fragmentation of **5.**

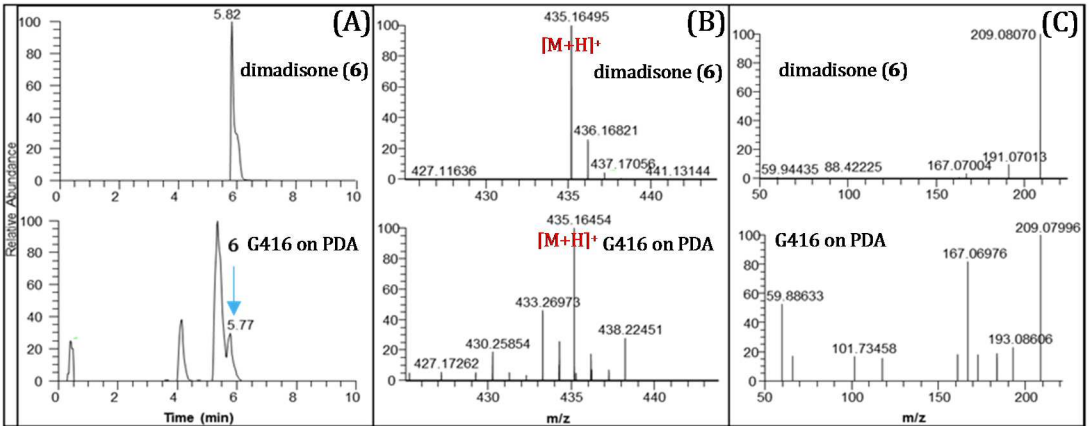

Figure 69. Data for the Reference Standard 6 (Top) and *In Situ* Analysis of G416 Grown on PDA (Bottom). (A) Overlay of chromatographic peaks of **6** (B) (+)-HRESIMS of **6** (C) MS/MS HCD fragmentation of **6.**

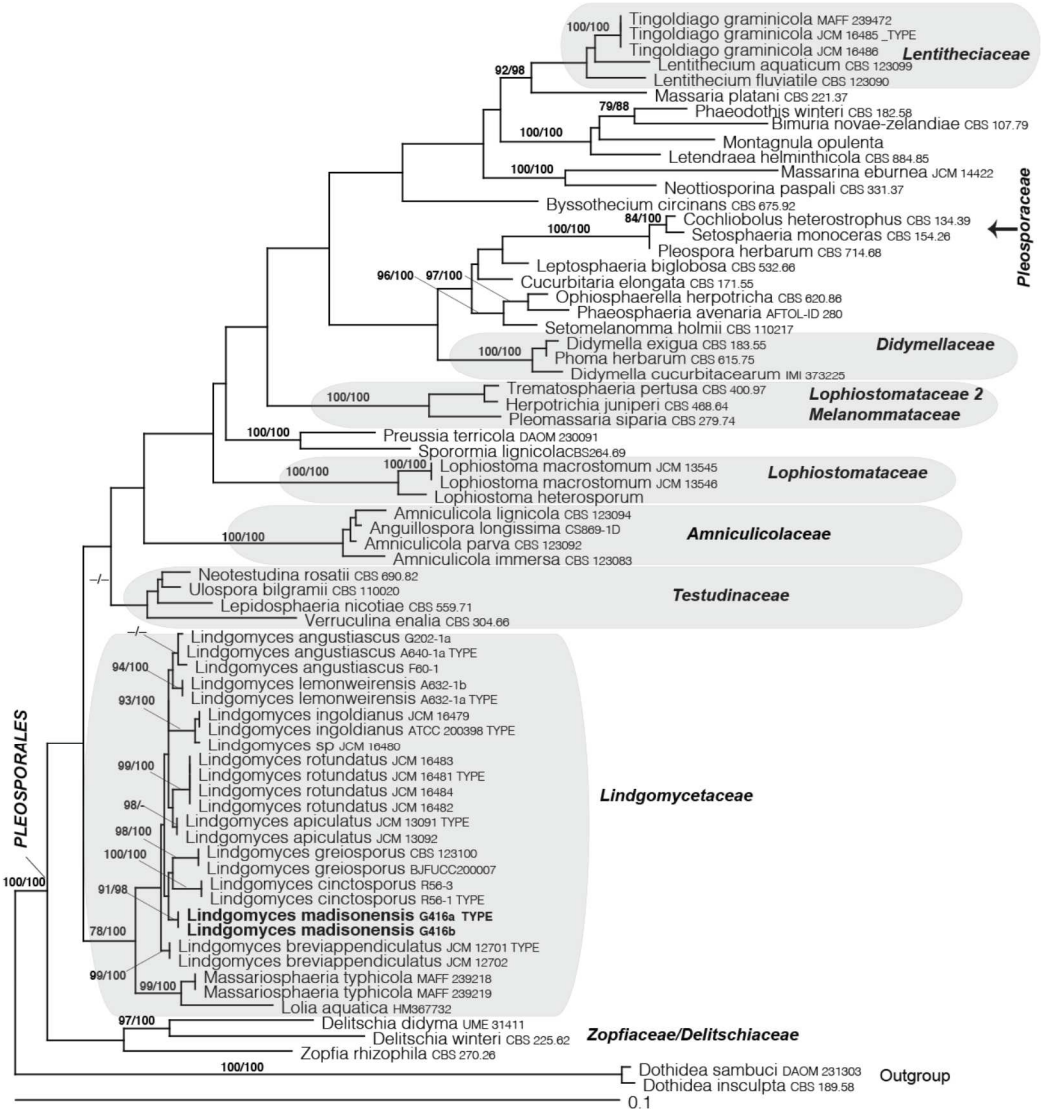

Figure 70. Phylogram of The Most Likely Tree (-lnL = 10047.29) From a RAxML Analysis of 70 Taxa Based on Combined SSU and LSU nrDNA Sequence Data (2309 bp). Numbers refer to RAxML bootstrap support values ≥ 70 % based on 1000 replicates and significant Bayesian posterior probabilities ≥ 95 %. New species of strain G416 is indicated in bold and is identified as having phylogenetic affinities to members of the freshwater ascomycete genus *Lindgomyces.* Bar indicates nucleotide substitutions per site.

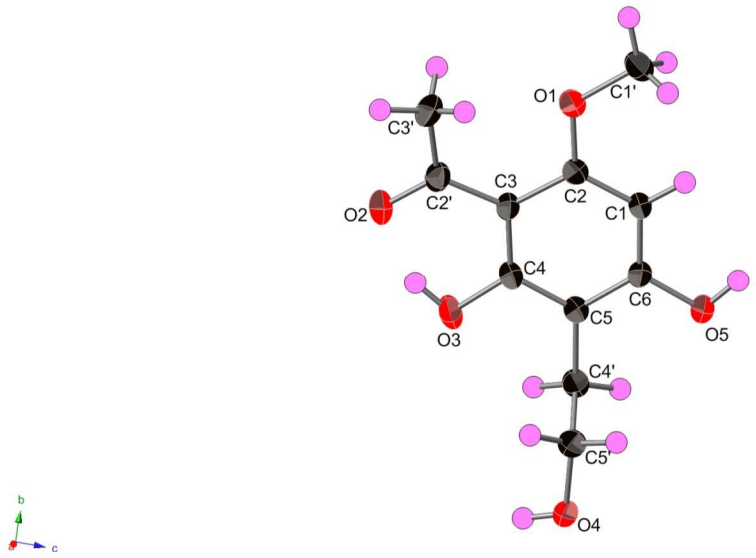

Figure 71. The Molecular Structure of 1 Depicted with 50% Probability Displacement Ellipsoids.

Table 22. Crystal Data for Compound 1.

$C_{11}H_{14}O_5$	D_x = 1.393 Mg m^{-3}
M_r = 226.22	Mo $K\alpha$ radiation, λ = 0.71073 Å
Orthorhombic, $P2_12_12_1$	Cell parameters from 4245 reflections
a = 4.3710 (4) Å	θ = 3.5–28.2°
b = 11.6045 (11) Å	μ = 0.11 mm^{-1}
c = 21.2672 (19) Å	T = 193 K
V = 1078.74 (17) Å^3	Irregular, colourless
Z = 4	0.29 × 0.16 × 0.03 mm
F(000) = 480	

Table 23. Crystal Data Collection Parameters for Compound 1.

Bruker APEX CCD diffractometer	3150 independent reflections
Radiation source: sealed tube	2720 reflections with $I > 2\sigma(I)$
Graphite monochromator	R_{int} = 0.040
ϕ and ω scans	θ_{max} = 30.0°, θ_{min} = 3.5°
Absorption correction: multi-scan data were corrected for scaling and absorption effects using the multi-scan technique (*SADABS*). The ratio of minimum to maximum apparent transmission was 0.986. The calculated minimum and maximum transmission coefficients (based on crystal size) are 0.969 and 0.997.	h = -6→6
T_{min} = 0.735, T_{max} = 0.986	k = -16→16
15607 measured reflections	l = -29→29

Table 24. Refinement Details for Crystal Data Collection for Compound 1.

Refinement on F^2	Primary atom site location: structure-invariant direct methods
Least-squares matrix: full	Secondary atom site location: difference Fourier map
$R[F^2 > 2\ \sigma(F^2)] = 0.042$	Hydrogen site location: mixed
$wR(F^2) = 0.109$	H atoms treated by a mixture of independent and constrained refinement
$S = 1.03$	$w = 1/[\sigma^2(F_o^2) + (0.0583P)^2 + 0.116P]$ where $P = (F_o^2 + 2F_c^2)/3$
3150 reflections	$(\Delta/\ \sigma)_{max} = 0.001$
159 parameters	$\Delta\rangle_{max} = 0.32$ e Å^{-3}
0 restraints	$\Delta\rangle_{min} = -0.14$ e Å^{-3}
Special details *Geometry*. All esds (except the esd in the dihedral angle between two l.s. planes) are estimated using the full covariance matrix. The cell esds are taken into account individually in the estimation of esds in distances, angles and torsion angles; correlations between esds in cell parameters are only used when they are defined by crystal symmetry. An approximate (isotropic) treatment of cell esds is used for estimating esds involving l.s. planes.	

Table 25. Antimicrobial Activities of Compounds 1, 2, and 5.

Compound	Minimum inhibitory concentration (µg/mL)				
	S. aureus	*E. coli*	*M. smegmatis*	*C. albicans*	*A. niger*
1	>55	>55	>55	>55	>55
2	>55	>55	>55	>55	>55
5	>55	>55	>55	>55	>55

CHAPTER IV

PRENYLATED XANTHENES AS QUORUM SENSING INHIBITORS FROM A FRESHWATER LEOTIOMYCETES SP.

This chapter is intended for publication to *Journal of Natural Products* (2017) and is presented in that style. Coauthors include José Rivera-Chávez, Justin Stempin, Mario Augustinovic, Aleksandra I. Noras, Huzefa A. Raja, Daniel A. Todd, Kathleen Triplett, Cynthia Day, Mario Figueroa, Pamela R. Hall, Nadja B. Cech and Nicholas H. Oberlies.

Freshwater fungi are an underexplored ecological group with a high potential for discovery of new bioactive secondary metabolites. In the course of our investigation of freshwater fungi from North Carolina, we investigated an isolate of Leotiomycetes sp. which led to the isolation of three new prenylated xanthenes (**1**-**3**) along with two known compounds 4*R*-regiolone (**4**), and decarboxycitrinone (**5**). Their structures were assigned on the basis of HRESIMS and NMR experiments. The structure of compound **1** was confirmed via x-ray diffraction analysis, and its absolute configuration was established by TDDFT-ECD calculations. Compounds **1**-**3** suppressed quorum sensing in a clinical isolate of methicillin-resistant *Staphylococcus aureus* (MRSA), with IC_{50} values ranging from 0.3 to 12.5 μM suggesting potential antivirulence activity for the compounds.

The prevalence of methicillin-resistant *Staphylococcus aureus* (MRSA) infections is a major public health burden, exacerbated by the emergence of community-associated (CA) MRSA, which causes significant morbidity and mortality worldwide.[144,145] In the

US, the Centers for Disease Control and Prevention estimated that there are at least 80,000 incidences of severe MRSA infections per year, with about 11,000 cases leading to death.[146] Addressing this urgent health threat an executive order was issued by the White House in 2014, launching an interagency task force charged with developing a five-year national action plan to combat the emergence and spread of antibiotic-resistant bacteria.[147] Part of the strategy depends on the acceleration of research on the development of new antibacterial drugs and other novel therapeutics.[147] In 2017, the World Health Organization listed MRSA as one of the priority pathogens that cause the greatest threat to human health, and they called for the development of new antibiotics and better treatment options to reduce the severity of the impact of these pathogens.[148]

Several alternative approaches have been explored for combating bacterial infections, and one of these is focused on blocking bacterial pathogenesis without killing or inhibiting bacterial growth.[149-155] By controlling bacterial virulence, it has been proposed that selective pressure toward resistance development would be prevented or minimized, thereby decreasing antibiotic use and, in theory, decreasing the occurrence of infections with drug-resistant pathogens.[149,150] In *Staphylococcus aureus* the expression of virulence factors is mediated by the accessory gene regulator (*agr*) quorum sensing system,[156] which regulates the secretion of the virulence factors that lead to pathogenicity. Therefore, disrupting the *agr* system is a promising target to combat *S. aureus* infections.[157]

Natural products continue to be a prolific source of therapeutics as a large extent of the world's biodiversity has been untapped for chemical diversity and biological

activity.[1,158] Current studies have identified a few small molecules with anti-virulence activity against *S. aureus*, including ambuic acid[159] and ω-hydroxyemodin,[160,161] both of which are fungal secondary metabolites. It is known that bacteria and fungi in their natural environment can interact with each other via chemical communication.[162] These interactions often result in changes in the production of small molecules that either affect the pathogenicity of one or both organisms. This concept led us to hypothesize that fungi inherently have the ability to produce compounds that can modulate bacterial quorum sensing. Thus we predicted that fungal metabolites could play a significant role in the discovery of antivirulence agents.

Freshwater ascomycetes are an ecological group of fungi with about 1500 described species to date.[163,164] These fungi are adapted to lentic and lotic habitats, primarily as parasites and endophytes of aquatic macrophytes and algae, and as organic matter decomposers.[39,163-165] Our earlier studies of the freshwater ascomycetes from North Carolina have been productive from both mycological and chemical perspectives,[122,166-171] but far from exhaustive, representing only a minor fraction of the immense potential of these organisms. As part of our ongoing studies to further explore the chemical diversity of these organisms and identify fungal natural products that target virulence in MRSA, we investigated an isolate identified as Leotiomycetes sp. (accessioned as G730). The fungal isolate (G730) was collected from submerged wood in a freshwater lake in Hanging Rock State Park, North Carolina. Investigation of the secondary metabolites from Leotiomycetes sp. led to the isolation of three new prenylated xanthenes **1**-**3** and two known compounds (**4**-**5**). The structures of these

metabolites were assigned by NMR and HRESIMS. The structural assignments of **1** based on NMR data were confirmed by X-ray crystal diffraction analysis. The absolute configuration of **1** was determined using ECD spectroscopy combined with time-dependent density functional theory and quantum chemical ECD calculations (TDDFT-ECD). The new prenylated xanthenes (**1**-**3**) were tested for antivirulence against MRSA strain USA300 LAC strain (AH1263)[172] and showed promising results.

Results and Discussion

An organic extract from G730 showed promising antivirulence activity when tested in a quorum sensing inhibition assay against a clinical isolate of a USA300 LAC strain of MRSA (AH1263)[172]. Conventional bioassay guided fractionation of the extract using chromatographic procedures led to the isolation of three new prenylated xanthenes (**1**-**3**) which were ascribed the trivial names Leotiomyxene A-C, respectively. Moreover, the known compounds 4*R*-regiolone (**4**),[173] and decarboxycitrinone (**5**)[174] were also isolated and identified based on NMR, HRMS, and optical rotation data, which were in agreement to the literature.

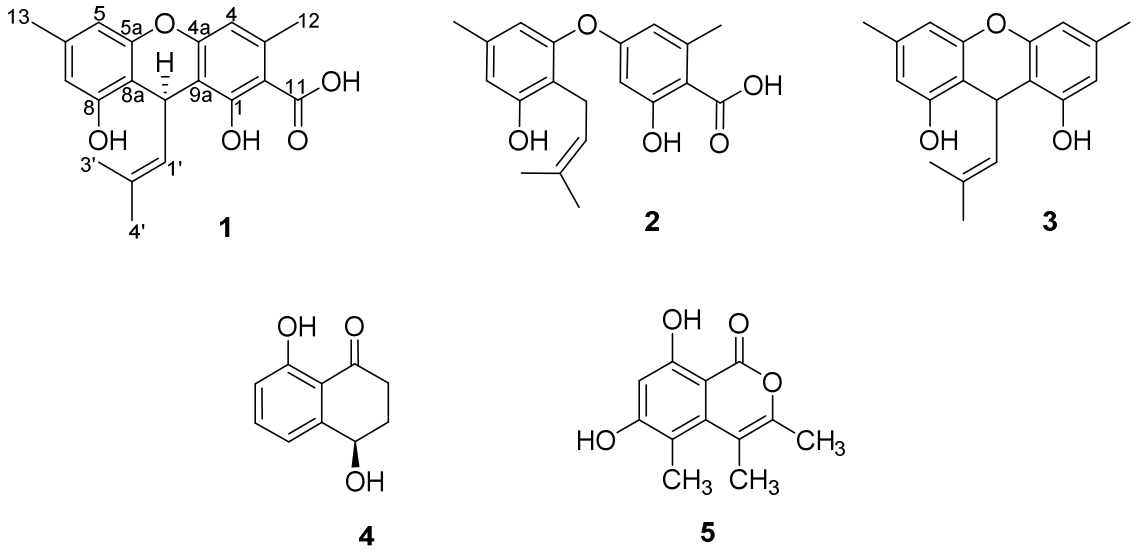

Figure 72. Structures of Compounds 1-5 Isolated and Identified From an Organic Extract of G730.

Leotiomycene A (**1**) was obtained as whitish yellow, amorphous powder. The molecular formula for **1** was established as $C_{20}H_{20}O_5$ based on HRESIMS data ($[M+H]^+$ ion at m/z 341.1380, calcd 341.1384) and NMR data, indicating an index of hydrogen deficiency of eleven. Analysis of the ^{1}H and ^{13}C NMR data indicated the presence of 20 carbon atoms, consisting of four methyl groups, five methines (three aromatic, one olefinic, and one aliphatic), and eleven non-protonated carbons (nine aromatic, one olefinic, and one carbonyl). Based on 1D and 2D NMR data (Table 26, Figures 78-81) three partial structures of **1** were elucidated (Figure 73).

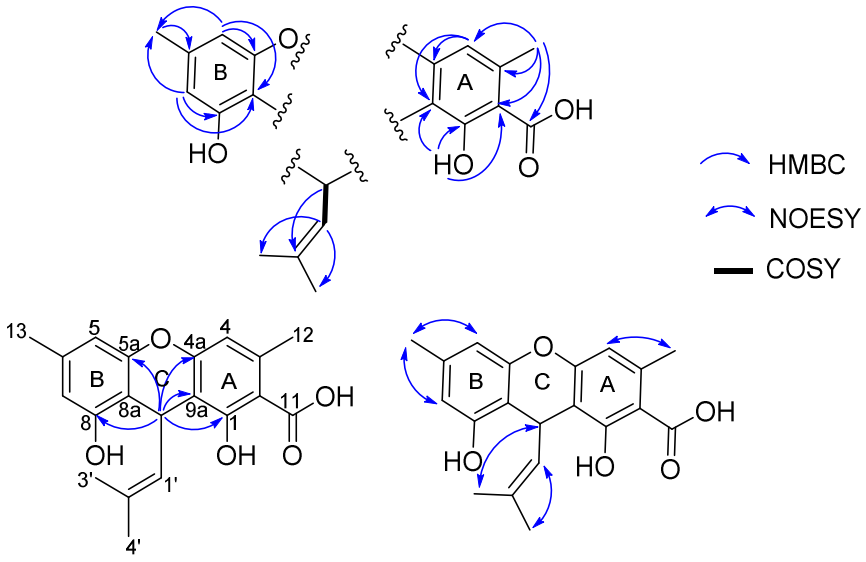

Figure 73. Partial Structures, Selected HMBC and NOESY Correlations of Compound 1.

Table 26. ^{1}H (400 Mhz) and ^{13}C (100 MHz) NMR Data for Compound 1 in $CDCl_3$.

	1			
position	**δ_C**	**Type**	**δ_H, mult (*J* in Hz)**	**HMBC**
1	164.1	C		
2	105.4	C		
3	142.6	C		
4	111.8	CH	6.48, s	2, 4a, 9a, 11, 12
4a	155.9	C		
5	109.8	CH	6.52, bs	5a, 7, 8, 8a, 13
5a	150.7	C		
6	138.6	C		
7	112.3	CH	6.45, bs	5, 8, 8a, 13
8	154.3	C		
8a	108.5	C		
9	28.3	CH	4.96, d (10.4)	1, 4a, 5a, 1´, 2´
9a	109.1	C		
11	175.4	C		
12	24.4	CH_3	2.58, s	1, 2, 3, 4, 11
13	21.4	CH_3	2.28, s	5, 6, 7
1´	125.4	CH	5.01, dm (10.4)	3´, 4´
2´	132.6	C		
3´	18.2	CH_3	2.04, s	1´, 2´, 4´
4´	25.9	CH_3	1.69, s	1´, 2´, 3´
1-OH			11.90, s	1, 2, 4a, 9a
8-OH				

Resonances for a pentasubstituted and 1,2,3,5-tetrasubstituted aromatic rings were identified based on the singlet resonance at δ_H 6.48 (H-4) and signals for meta-coupled protons at δ_H 6.52 (H-5) and δ_H 6.45 (H-7) (both observed as broad singlets). Furthermore, the ^{13}C NMR shifts (δ_C 164.1, 155.9, 150.7, 154.3) observed for the aromatic moieties C-1, C-4a, C-5a, and C-8, respectively indicated that they are both dioxygenated. HMBC correlations from H-4 to C-4a/C-9a; H_3-12 to C-2/C-4/C-11/ C-

12, in combination with the NOESY cross-peaks between H-4 and H_3-12, and the presence of a phenolic hydroxy resonance at δ_H 11.90 (1-OH) chelated with the carboxylic acid moiety at δ_C 175.4 (C-11) allowed the assembly of ring A. Similarly, ring B was assigned based on the HMBC from H-5 to C-5a/C-8a/C-13 and from H-7 to C-8/C-8a/ C-13, and the NOESY cross peaks observed between H_3-13 and H-5, and H_3-13 and H-7. The remaining fragment in **1** was elucidated as a prenyl moiety based on HMBC and ^{1}H-^{1}H COSY experiments. This prenyl moiety was attached to C-8a of ring A and C-9a of ring B as supported by HMBC correlations observed from H-9 to C-1/C-4a/C-5a/C-8/C-8a/C-9. Consideration of the molecular formula and the unsaturation requirement of **1**, along with the downfield shifts of C-4a (δ_C 155.9) and C-5a (δ_C 150.7) indicated the ether linkage between rings A and B at C-4a and C-5a forming ring C which established the 9*H*-xanthene skeleton. Altogether, these correlations resulted in the planar structure of the new metabolite **1**. During the course of this study, crystals were obtained from a concentrated 1:1 acetone-hexane solution of **1**. X-ray diffraction analysis of a suitable crystal confirmed the proposed structural assignments of **1** as shown in Figure 74.

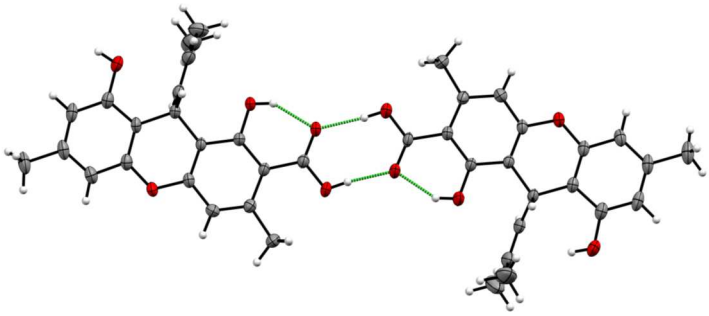

Figure 74. ORTEP Drawing of Two Molecules of Compound 1 Showing Intra- and Intermolecular H-bonding Indicated by Green Dashed Lines.

In order to determine the absolute configuration of **1** at C-9, the experimental ECD of **1** and the time-dependent density functional theory-calculated (TDDFT) ECD spectra for enantiomer 9*R* and 9*S* of **1** were compared. In brief, TDDFT calculations were performed by minimization of the structure of each enantiomer, followed by a conformational search using a Monte Carlo protocol. Conformers for each enantiomer that were within a 10 kcal/mol window were selected and reoptimized using DFT calculations at the B3LYP/6-311+G (2d,p) level of theory. Finally, the theoretical ECD spectra of each conformer of the *9R* and 9*S* enantiomers were calculated using TDDFT at the same level of theory with the polarizable continuum model in CH_3CN. The specific optical rotation values for enantiomers 9*R* and 9*S* were also calculated. The calculated ECD spectrum based on TDDFT for the 9*S* enantiomer matched well with the experimentally measured data, which displayed a positive and a negative Cotton effect at ~210 and ~230, respectively (Figure 75). Furthermore, the calculated specific optical rotation value for the 9*S* enantiomer ($[\alpha]^{25}_{D}$ +117) was in agreement with the

experimental data ($[\alpha]^{25}_{D}$ +90). Thus, the absolute configuration of **1** at C-9 was assigned as *S*.

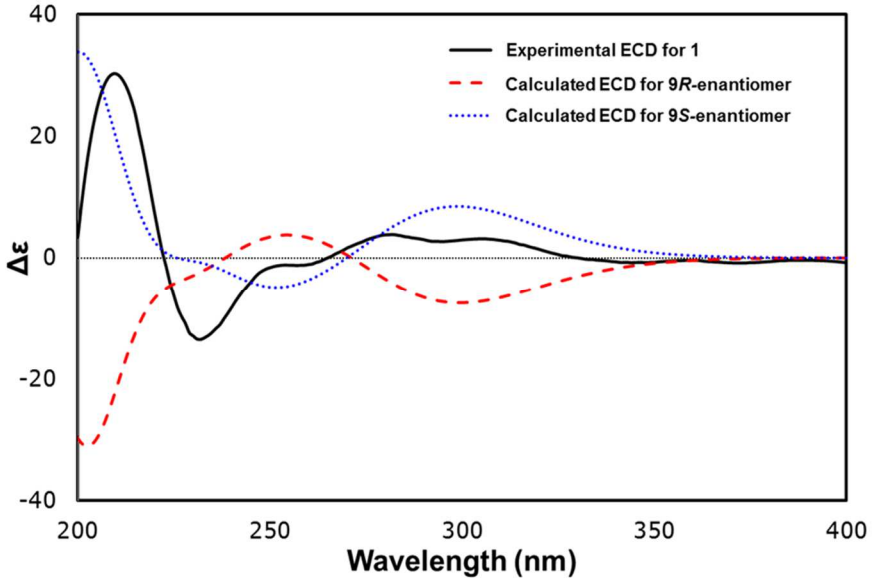

Figure 75. Comparison of the Experimental and Calculated (at the B3LYP/6-311+G(2d,p) Level) ECD Spectra of 1 in MeCN.

A molecular formula consisting of $C_{20}H_{22}O_5$ (ten unsaturations) was assigned for leotiomycene B (**2**) based on HRESIMS data ($[M+H]^+$ ion at m/z 343.1530, calcd 343.1540) and NMR data (Table 27, Figure 82-84). The ^{1}H NMR spectrum of **2** displayed signals similar to those of **1**, with notable differences consisting of an additional aromatic proton signal H-9a (δ_H 6.20, d, J = 2.4 Hz), and an upfield shifted signal for methylene protons H_2-9 (δ_H 3.24, d, J = 7.1 Hz) in contrast to a methine (δ_H 4.96, d, J=10.4 Hz) in **1** in the prenyl portion of the molecule. Considering these changes in the ^{1}H NMR spectrum and a decrease of an unsaturation count in **2** relative to **1**, a loss

of the *9H*-xanthene skeleton was proposed for **2**. This was later confirmed on the basis of the meta-coupling observed (J= 2.4 Hz) between H-9a and H-4 (δ_H 6.37, d) and the HMBC correlations from H-9a to C-1/C-2/C-4/C-4a, and from H-9 to C-5a/C-8/C-8a. Overall, the detected HMBC correlations for **2** were almost identical to **1.** The main difference was the lack of cross peaks from H_2-9 to C-9a, suggesting **2** to be the *seco* derivative of **1**. Thus, the structure of **2** was established as illustrated.

Table 27. ^{1}H (400 MHz) and ^{13}C (100 MHz) NMR Data for Compound 2 in $CDCl_3$.

			2	
position	**δ_C**	**Type**	**δ_H, mult (*J* in Hz)**	**HMBC**
1	166.3	C		
2	105.0	C		
3	145.3	C		
4	112.5	CH	6.37, d (2.4)	2, 4a, 9a
4a	164.2	C		
5	114.7	CH	6.43, bs	5a, 7, 8a, 13
5a	152.3	C		
6	138.4	C		
7	114.1	CH	6.56, bs	5, 8, 8a, 13
8	156.0	C		
8a	117.0	C		
9	23.1	CH_2	3.24, d (7.1)	5a, 8, 8a, 1´, 2´
9a	102.0	CH	6.20, d (2.4)	1, 2, 4, 4a
11	175.0	C		
12	24.6	CH_3	2.57, s	2, 3, 4, 11
13	21.3	CH_3	2.26, s	5, 6, 7
1´	121.3	CH	5.16, tm (7.1)	3´, 4´, 9
2´	135.3	C		
3´	18.0	CH_3	1.71, bs	1´, 2´, 4´
4´	25.9	CH_3	1.69, bs	1´, 2´, 3´
1-OH			11.44, s	1, 2, 4a, 9a
8-OH			5.26 bs	

Table 28. ^{1}H (500 MHz) and ^{13}C (125 MHz) NMR Data for Compound 3 in $CDCl_3$

position	δ_C	Type	δ_H, mult (*J* in Hz)	HMBC
1/8	154.3	C		
2/7	111.2	CH	6.36, bs	1, 4, 9a, 11/5, 8, 8a, 12
3/6	138.6	C		
4/5	109.8	CH	6.49, bs	2, 4a, 9a,11/7, 5a, 8a, 12
4a/5a	151.6	C		
8a/9a	107.5	C		
9	28.7	CH	4.91, d (10.4)	1/8, 4a/5a, 8a/9a, 1´, 2
11/12	21.3	CH_3	2.26, s	2, 3, 4/5, 6, 7
1´	126.4	CH	5.16, dm (10.4)	3´, 4´
2´	132.2	C		
3´	18.0	CH_3	2.05, d (1.4)	1´, 2´, 4´
4´	25.9	CH_3	1.73, d (1.1)	1´, 2´, 3´
1-OH/8-OH			4.88, s	1, 2, 9a/7, 8, 8a

Leotiomycene C (**3**) was isolated as an optically inactive white powder. Its molecular formula, $C_{19}H_{20}O_3$, established from HRESIMS data ($[M+H]^+$ ion at m/z 297.1480, calcd 297.1485) and NMR data (Table 28, Figure 85-87), indicated a structure with ten degrees of unsaturation. These data were consistent with compound **3** being a decarboxylated analogue of **1**. The ^{1}H NMR spectrum of **3** displayed only one set of signals for the meta-coupled protons H-2/7 and H-4/5 (broad singlets δ_H 6.36 and δ_H 6.49, respectively) in rings A and B, as well as the methyl H_3-11/12 (δ_H 2.26, s) and hydroxyl 1-OH/8-OH (δ_H 4.88, s) groups. Likewise, the ^{13}C NMR spectrum only displayed one set of signals for the aromatic carbons C-1/8, C-2/7, C-3/6, C-4/5 (δ_C 154.3, 111.2, 138.6, 109.8, respectively) in both rings. Based on these data, along with the analysis of the 2D NMR data, it was concluded that decarboxylation at C-2 rendered the two halves of the molecule symmetrical. This therefore indicated that compound **3** do not have a chiral

center at C-9 which was supported by the lack of optical activity observed for the compound. Altogether, the structure of **3** was assigned as shown.

Compounds **1-3** were evaluated as quorum sensing inhibitors against AH1263 at below growth-inhibitory concentrations. As shown in Table 29, **1-3** suppressed quorum sensing with IC_{50} values in the 0.3-12.5 μM range. The most potent activity was detected for compound **1** with an IC_{50} of 0.3 ± 0.1 μM. The results also indicated that **1** was more potent than the positive controls ambuic acid and ω-hydroxyemodin.

Table 29. Activity of Compounds 1-3 as *Agr* Quorum Sensing Inhibitors

Compound	IC_{50} (μM)
1	0.3 ± 0.1
2	4.6 ± 2.3
3	6.3-12.5
*ambuic acid	1.3 ± 0.1
*ω-hydroxyemodin	6.3-12.5

*Positive control

To support the antivirulence activity observed mainly for compound **1**, it was evaluated for the suppression of the transcription of the *agr* effector RNAIII and *agr*-regulated virulence factors, including phenol soluble modulin alpha (psmα) and alpha-hemolysin (hla) in the same MRSA strain (AH1263). RNAIII is the intracellular effector of the quorum sensing system in *S. aureus* that controls the expression of >200 virulence factors that lead to invasive infections.[161] Based on the results (Figure 76), compound **1** decreased the transcription of RNAIII at 9.0 and 16.0 μM concentrations. As anticipated based on the inhibition of RNAIII transcription, compound **1** suppressed the production of both psmα and hla (Figure 76) at 2.9, 9.0 and 16.0 μM concentrations. These results

indicated that compound **1** was inhibiting *S. aureus* quorum sensing-mediated pathogenesis by disrupting part of the *agr* system that modulates production of virulence factors that target adaptive immunity during invasive infections.

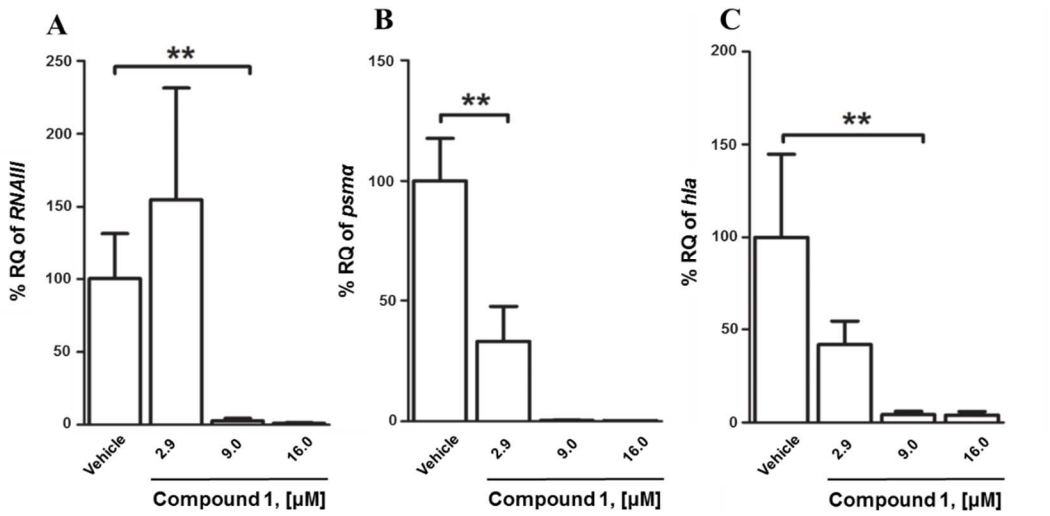

Figure 76. Relative Quantification of (A) RNAIII, (B) Psmα, and (C) Hla by qRT-PCR Relative to 16S rRNA Following a 5 h Incubation of USA300 LAC (2 x 10^7 CFU/mL) and Compound 1 or Vehicle. Data are represented as the fold change relative to 16S rRNA as compared to inoculum bacteria. Data are represented as the mean ± SEM, n = 3 replicates of a representative experiment of two independent experiments. ** $p<0.01$ based on Mann Whitney U test.

Due to structural similarities of **1** to a fragment compound (9*H*-xanthene-9-carboxylic acid) identified previously as an inhibitor of AgrA (cytoplasmic response regulator protein of the *agr* quorum sensing system),[176] we hypothesized that **1** would be an inhibitor of the same component of the *agr* quorum sensing system. To predict the mode of inhibition for **1**, the potential binding sites on the crystal structure of the C-terminal AgrA DNA binding domain (PDB ID 4G4K) were evaluated via *in silico* docking calculations (Figure 77A). The compound was predicted to dock in a pocket

(binding energy (ΔG) = -5.5 kcal/mol) between the side chains of Thr142, Lys146, Phe182, Asn185, Leu189, and Leu192, and formed hydrogen bonds between Glu144 and Leu145 (Figure 77A-B).

The polyhydroxyanthraquinone ω-hydroxyemodin is a fungal secondary metabolite that has been recently shown to have *in vivo* efficacy against quorum sensing in *S. aureus.*[161] Comparison of the putative mode of binding of **1** and ω-hydroxyemodin on $AgrA_C$ indicated that these compounds have the same potential binding sites on the protein structure (Figure 77C). The calculated binding energy for the best docking pose for ω-hydroxyemodin was -5.95 kcal/mol. The compound was observed to bind in a pocket bounded by the side chains of Thr142, Tyr156, Lys146, Gly184, Leu189, Leu192, and had hydrogen bond interactions with Ile143, Glu144, Asn185, and Glu188.

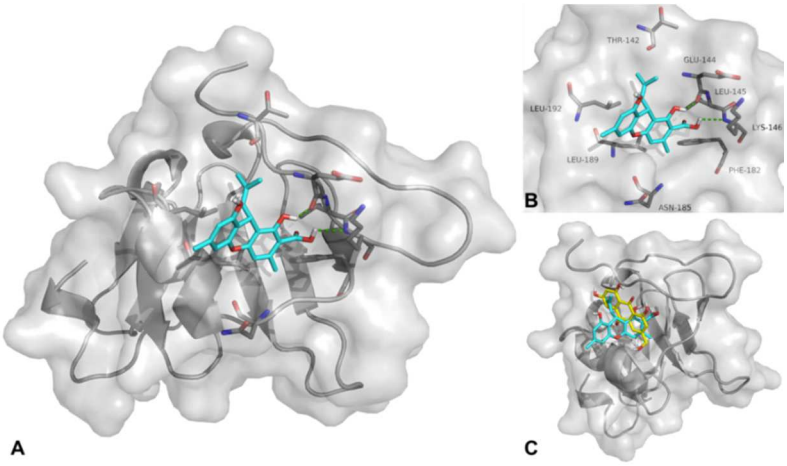

Figure 77. Compound 1 *In Silico* Binding Predictions on AgrA. (A) The putative mode of binding for compound **1** on $AgrA_c$ crystal structure (PDB ID 4G4K) as predicted by *in silico* docking calculations. (B) Optimized view of the binding mode for **1**. Predicted hydrogen bonds between **1** and the amino acids (Leu145 and Glu144) are indicated by green dashed lines. (C) The known AgrA inhibitor ω-hydroxyemodin (yellow) and compound **1** bound to the same pocket on AgrA.

The similarities in the predicted binding pockets on $AgrA_C$ for **1** and ω-hydroxyemodin indicated that the two compounds could potentially have the same mode of action in suppressing quorum sensing in MRSA. To address this possibility, it will be important to experimentally characterize the mechanisms of action of **1** with more confirmatory assays.[161] Overall, the isolation and characterization of the new prenylated xanthenes **1-3** from Leotiomycetes sp. highlighted the importance of freshwater fungi as a potential source for new drug leads. The identification of the antivirulence activity of **1-3** could possibly contribute to the promotion of antibiotic stewardship.

Experimental Section

General experimental procedures. All solvents and chemicals were purchased from standard suppliers and were used without any further purification. The NMR data were collected using either a JEOL ECS-400 spectrometer (JEOL USA, Inc.) operating at 400 MHz for ^{1}H and 100 MHz for ^{13}C, and equipped with JEOL normal geometry broadband Royal probe; or a JEOL ECA-500 spectrometer (JEOL USA, Inc.) operating at 500 MHz for ^{1}H and 125 MHz for ^{13}C; or an Agilent 700 MHz NMR spectrometer (Agilent Technologies, Inc., Santa Clara, CA, USA) operating at 700 MHz for ^{1}H and 175 MHz for ^{13}C, and equipped with a cryoprobe. NMR chemical shift values were referenced to residual solvent signals for $CDCl_3$ (δ_H/δ_C 7.26/77.2). HRESIMS data were obtained using a Thermo QExactive Plus mass spectrometer (ThermoFisher, San Jose, CA, USA) with an electrospray ionization source coupled with a Waters Acquity ultraperformance liquid chromatography (UPLC) system (Waters Corp.). The UPLC separation was performed using an Acquity BEH C18 column (50 mm x 2.1 mm i.d., 1.7

µm) equilibrated at 40 °C and a flow rate set at 0.3 mL/min. The mobile phase consisted of a linear CH_3CN-H_2O (acidified with 0.1% HCOOH) gradient starting at 15% CH_3CN to 100% CH_3CN over 8 min. The mobile phase was held for another 1.5 min at 100% CH_3CN before going back to the starting conditions. The HPLC separations were performed using Varian ProStar HPLC system connected to a ProStar 335 photodiode array detector (PDA) with UV detection set at 210 nm and 254 nm. Preparative reversed phase HPLC purification of samples was performed on an Atlantis® Prep T3 (5 µm; 250 × 19 mm) column using a 17 mL/min flow rate of the mobile phase consisting of a mixture of CH_3CN and H_2O (with 0.1% HCOOH). Flash column chromatography was carried out with a Teledyne ISCO Combiflash Rf connected to an evaporative light scattering detector and PDA detectors with UV detection set at 200-400 nm. Optical rotation data were acquired on a Rudolph Research Autopol III polarimeter (Rudolph Research Analytical, Flanders, NJ, USA). The UV data were acquired using a Varian Cary 100 Bio UV–Vis spectrophotometer (Varian Inc., Walnut Creek, CA, USA). The ECD data were collected with an Olis DSM 17 ECD spectrophotometer (Olis, Inc., Bogard, GA, USA).

Fungal strain isolation and identification. The fungal strain, G730 was isolated serendipitously from a sample of submerged wood collected in March of 2015 from a freshwater lake in Hanging Rock State Park, North Carolina (N 36 23.433, W 80 16.64), while attempting to isolate a new genus of freshwater ascomycetes (data not shown). The single spore isolation of the new fungal genus failed as it was contaminated by hyphal growth from strain G730, which was subsequently purified and isolated using antibiotic

water agar (AWA; agar 20 g, streptomycin sulfate 250 mg/L, penicillin G 250 mg/L, distilled water 1L; antibiotics were added to the molten agar immediately after autoclaving). A culture of strain G730 is preserved in the Department of Chemistry and Biochemistry culture collection at the University of North Carolina at Greensboro. For isolation of freshwater fungi, previously outlined collection and isolation methods by Shearer *et al*.[177] were implemented. Morphological examination of fungal cultures grown on different nutrient media types, such as Potato Dextrose Agar (PDA; Difco), Potato Carrot Agar (PCA; Himedia) indicated that the strain G730 grew only as sterile mycelia. Fruiting body formation was induced by adding a piece of sterilized balsa to the nutrient media[177]; however, after two/three months no ascoma were observed on the balsa wood or the PDA plates. Since no morphological data were available for identification of fungal strain G730, molecular sequencing was performed. Molecular data for strain G730 were obtained by sequencing the internal transcribed spacer regions 1 and 2 and 5.8S nrDNA (ITS)[178] along with the D1 and D2 regions of the 28S nuclear ribosomal large subunit rRNA gene (LSU).[139,179] The ITS region was used for DNA barcoding[180], while the LSU region was utilized for phylogenetic analysis.[96] DNA extraction, PCR amplification, and sequencing were performed according to previously published procedures.[96] A BLAST search in GenBank using the complete ITS rDNA sequence showed low homology (81% similarity) with members of Leotiomycetes sp. genotype 727 JMUR-2016 voucher ARIZ: FL1722 (KX908942), Leotiomycetes sp. genotype 730 JMUR-2016 voucher ARIZ: FL1746 (KX908694), and *Phialocephala fortinii* (LC131022). To better predict the phylogenetic affiliations of G730 to taxa within

the Leotiomycetes, Ascomycota, a molecular phylogenetic analysis using maximum likelihood was undertaken using LSU data for strain G730, along with sequences of the diverse aquatic and terrestrial Helotialean taxa of the Leotiomycetes from previous molecular phylogenetic studies.[181-185] Maximum Likelihood analysis was implemented using RAxML v. 7.0.4[186] run on the CIPRES portal[187] with the default rapid hill-climbing algorithm and GTR model employing 1000 fast bootstrap searches. Clades with bootstrap values ≥70% were considered to be significant and strongly supported.[188] In addition, Bayesian analysis using Markov Chain Monte Carlo (MCMC) algorithm was performed using Mr. Bayes[189,190] as an additional measure of branch support assessment using the GTR+I+G model of evolution[191]. Detailed methodology of the phylogenetic analysis has been outlined previously.[96] Results of the phylogenetic analysis indicated that strain G730 has phylogenetic affinities to the *Vibrissea-Loramyces* Clade sensu Wang et al[182]; G730 was nested within a clade containing genera such as, *Vibrissea, Loramyces, Mollisia, Strossmayeria,* with moderate RAxML bootstrap support (69%), but without Bayesian posterior probability support (Figure 90). On the basis of these data, G730 is tentatively identified as Leotiomycetes sp., Ascomycota. A number of freshwater fungi belonging to the Leotiomycetes have been isolated from submerged wood previously.[192] Based on the distant homology to ribosomal sequences present in NCBI GenBank, it is likely that strain G730 may represent a new genus and/or species; however, since G730 only occurs only as sterile mycelia, it is conservatively referred to as Leotiomycetes sp. The complete ITS and combined ITS-LSU sequences were deposited in GenBank (accession no. ITS: XXXX; ITS-LSU:XXXX, XXXX).

Fermentation, extraction, and isolation. A fresh culture of G730 was grown on potato dextrose agar and maintained at rt. Once good growth was observed, a culture plug was subsequently inoculated into a 15 mL liquid medium consisting of 2% soy peptone, 2% dextrose, and 1% yeast extract (YESD). This was followed by incubation with agitation at rt for about 7 days using a rotary shaker. Once sufficient fungal growth was observed the seed culture was used to inoculate a 250 mL Erlenmeyer flask containing an autoclaved rice medium (10 g rice added with 25 mL deionized H_2O). The fermentation culture was allowed to grow at rt for a period of 30 days. Six fermentation cultures of G730 were prepared, each was extracted by addition of 1:1 CH_3OH-$CHCl_3$ (60 mL) with overnight shaking, filtered, and then all the filtrates were combined.

To the combined filtrate, 500 mL of $CHCl_3$ and 900 mL of H_2O were added, stirred for 0.5 h, partitioned, the $CHCl_3$-soluble layer collected and dried *in vacuo.* The resulting extract was further partitioned between CH_3OH-CH_3CN (1:1, 300 mL) and hexanes (300 mL) to remove lipids, and then the CH_3OH-CH_3CN soluble layer was dried *in vacuo*. The dried material (1.2 g) was adsorbed on Celite 545, and subjected to silica flash chromatography on a 24 g RediSep Rf Gold Si-gel column, eluting with use of a gradient solvent system of hexane-$CHCl_3$-CH_3OH at a flow rate of 35 mL/min over 41 column volumes, and for a duration of 40 min to give 100 fractions each containing 15 mL. The fractions were then pooled according to their ELSD and UV profiles, which resulted into six fractions.

Fraction 2 (556 mg) was subjected to preparative reversed-phase HPLC eluting with a linear gradient from 50% to 60% CH_3CN in H_2O (0.1% HCOOH) over 30 min to afford 11 fractions, with the ninth and seventh fraction being compounds **1** (190 mg) and **2** (7.0 mg), respectively. Fraction eight (142 mg) was repurified using an isocratic condition consisting of 50% CH_3CN in H_2O (0.1% HCOOH) over 60 min to afford compound **3** (0.9 mg) and more of compounds **1** (115 mg) and **2** (2.4 mg).

Leotiomycene A (**1**): white solid; $[\alpha]^{27}_D$ +90 (*c* 0.1, MeCN); UV (MeCN) λ_{max} (log ε) 215 (4.5), 291 (4.1) nm; ^1H and ^{13}C NMR, see Table 26; HRESIMS m/z 341.1379 $[M+H]^+$ (calcd for $C_{20}H_{21}O_5$, 341.1384).

Leotiomycene B (**2**): white solid; UV (MeCN) λ_{max} (log ε) 210 (4.8), 265 (4.2), 307 (3.9) nm; ^1H and ^{13}C NMR, see Table 27; HRESIMS m/z 343.1530 $[M+H]^+$ (calcd for $C_{20}H_{23}O_5$, 343.1540).

Leotiomycene C (**3**): white solid; UV (MeCN) λ_{max} (log ε) 221 (4.3), 282 (3.3) nm; ^1H and ^{13}C NMR, see Table 28; HRESIMS m/z 297.1480 $[M+H]^+$ (calcd for $C_{19}H_{21}O_3$, 297.1485).

The agr quorum sensing system inhibition assay. A Synergy H1 Multi-Mode Reader (Biotek Instruments, Inc., Winooski, VT) was used to obtain optical density (OD_{600}) readings. Liquid chromatography-mass spectrometry (LC-MS) was performed using an Aquity ultra-high performance liquid chromatography (UPLC) system (Waters Corporation, Milford, MA) coupled to a QExactive Plus Hybrid Quadrupole-Orbitrap mass spectrometer (Thermo Fisher Scientific, Waltham, MA). The positive control ambuic acid was purchased from Adipogen International, San Diego, CA.

Mass spectrometric measurements to evaluate AIP production inhibition was performed according to a method described previously.[175] Briefly, the bacteria were cultured in the presence of the test substance in triplicate wells in a 96 well plate format. The bacterial cell growth was monitored at 1 h interval by measurement of OD_{600} to determine growth inhibition or delay. At the end of log-phase growth, the cells were filtered and the filtrate analyzed using a UPLC coupled to MS. IC_{50} values were determined from a four parameter logistic function in Sigmaplot.

Quantitative PCR for *S. aureus* gene transcription. For the quantification of *S. aureus* gene transcription, 500-µl cultures at 2×10^7 CFU/mL of USA300 LAC (AH1263) were grown in TSB at 37°C, with aeration, and treatments (vehicle versus Compound **1**). The bacteria were stored at −20°C in RNAprotect cell reagent, according to the manufacturer's recommendations (Qiagen), until the RNA was purified as previously described.[193] Quantitative PCR (qPCR) were performed using an ABI 7900HT real-time PCR system with TaqMan Gene expression master mix, according to the manufacturer's directions (Applied Biosystems). Predesigned primer and probe sets (Integrated DNA Technologies, Coralville, IA) were used for the quantitation of RNAIII, psmα, and hla. The data are represented as the fold change relative to the concentration of 16S rRNA. The primer and probe sets for the quantification of the *S. aureus* genes are listed in a previous publication.[161]

***In silico* docking on AgrA$_C$.** *In silico* docking calculations for each ligand (**1** and ω-hydroxyemodin) was performed using the AutoDock 4.0 systems to predict the putative mode of binding on AgrA$_C$. Compound **1** was prepared by assigning the

Gasteiger−Marsili atomic charges and nonpolar hydrogens on the crystal structure of the compound (XXX.cif) using AutoDockTools 1.5.4 (http://mgltools.scripps.edu/). Meanwhile, ω-hydroxyemodin was prepared for docking calculations in the same manner but applying a geometrically optimized structure for the compound. The optimized structure was built using Spartan'10 (www.wavefunction.com) with the optimization performed utilizing the software Gaussian 09 (Gaussian Inc., Wallingford, CT, USA) at the DFT B3LYP/6-311+G(2d,p) level of theory. On the other hand, the $AgrA_C$ crystal structure (RSCB Protein Data Bank [www.pdb.org], PDB ID 4G4K) was set by assigning all the non-polar hydrogens and Koleman charges to the receptor. A blind docking approach was performed to initiate the prediction, the best energy obtained from which was used as the initial conformation for subsequent simulations. Docking studies were done with Lamarckian Genetic Algorithm (LGA). The grid box for docking was set around a central atom of the ligand with dimensions of 40 × 40 × 40 Å. Parameters were set to an LGA calculation of 100 runs, whereas energy evaluations were set to 2,500,000 and 27,000 generations (repetitions of the process). The resulting docked poses were analyzed with AutoDockTools using cluster analysis, PyMOL.24. Molecular modeling images were prepared using PDB ID 3BS1 and PyMOL.

X-ray crystal diffraction analysis of compound 1. A specimen of $C_{20}H_{20}O_5$, approximate dimensions 0.140 mm x 0.200 mm x 0.300 mm, was used for the X-ray crystallographic analysis. The X-ray intensity data were measured on a Bruker APEX CCD[194] system equipped with a graphite monochromator and a MoKα sealed tube (λ = 0.71073 Å). The frames were integrated with the Bruker SAINT software[195] package

using a narrow-frame algorithm. The integration of the data using a triclinic unit cell yielded a total of 17054 reflections to a maximum θ angle of 29.99° (0.71 Å resolution), of which 9966 were independent (average redundancy 1.711, completeness = 98.7%, R_{int} = 2.33%, R_{sig} = 4.66%) and 8084 (81.12%) were greater than 2σ (F^2). The final cell constants of a = 7.3973 (5) Å, b = 11.0738 (8) Å, c = 12.0820 (9) Å, α = 69.8100 (10)°, β = 77.6290 (10)°, γ = 77.2120 (10)°, volume = 895.52 (11) $Å^3$, are based upon the refinement of the XYZ-centroids of 4964 reflections above 20 σ(I). Data were corrected for scaling using the multi-scan method (SADABS)[196]. The calculated minimum and maximum transmission coefficients (based on crystal size) are 0.9730 and 0.9870.

The structure was solved and refined using the Bruker SHELXTL Software Package, using the space group P 1, with Z = 2 for the formula unit, $C_{20}H_{20}O_5$. The final anisotropic full-matrix least-squares refinement on F^2 with 465 variables converged at R1 = 4.63%, for the observed data and wR2 = 12.30% for all data. The goodness-of-fit was 1.040. The final structural model was refined as an inversion twin with a BASF value of 0.4(8). The largest peak in the final difference electron density synthesis was 0.334 $e^-/Å^3$ and the largest hole was -0.207 $e^-/Å^3$ with an RMS deviation of 0.043 $e^-/Å^3$. On the basis of the final model, the calculated density was 1.262 g/cm^3 and F(000), 360 e^-. Crystal data, data collection and structure refinement details are summarized in the supplementary material. The x-ray crystallographic data for **1** have been deposited with the Cambridge Crystallographic Data Center under accession number CCDC####. These data can be accessed free of charge at http://www.ccdc.cam.ac.uk/.

Computational details. The TDDFT calculations, such as ECD and optical rotation, were performed according to a previous work utilizing Gaussian'09 program package.[197] A 3D model of **1** was built and geometry optimized using Spartan'10 software (www.wavefunction.com). Conformational analysis was performed by a Monte Carlo search protocol as implemented in the same software under semiempirical method (PM3). The resulting conformers were filtered, checked for duplicity, and minimized using a DFT force field at the B3LYP/6-311+G(2d,p) level of theory. ECD calculations using the self-consistent reaction field with conductor-like continuum solvent model in CH_3CN were subsequently performed on the obtained DFT-minimized major conformers of both 9*R* and 9*S* enantiomers of compound **1**. Following which, the excitation energy (nm), rotatory strength (*R*) in dipole velocity (R_{vel}) and dipole length (R_{len}) forms obtained from the calculations were then used to simulate the ECD curves.

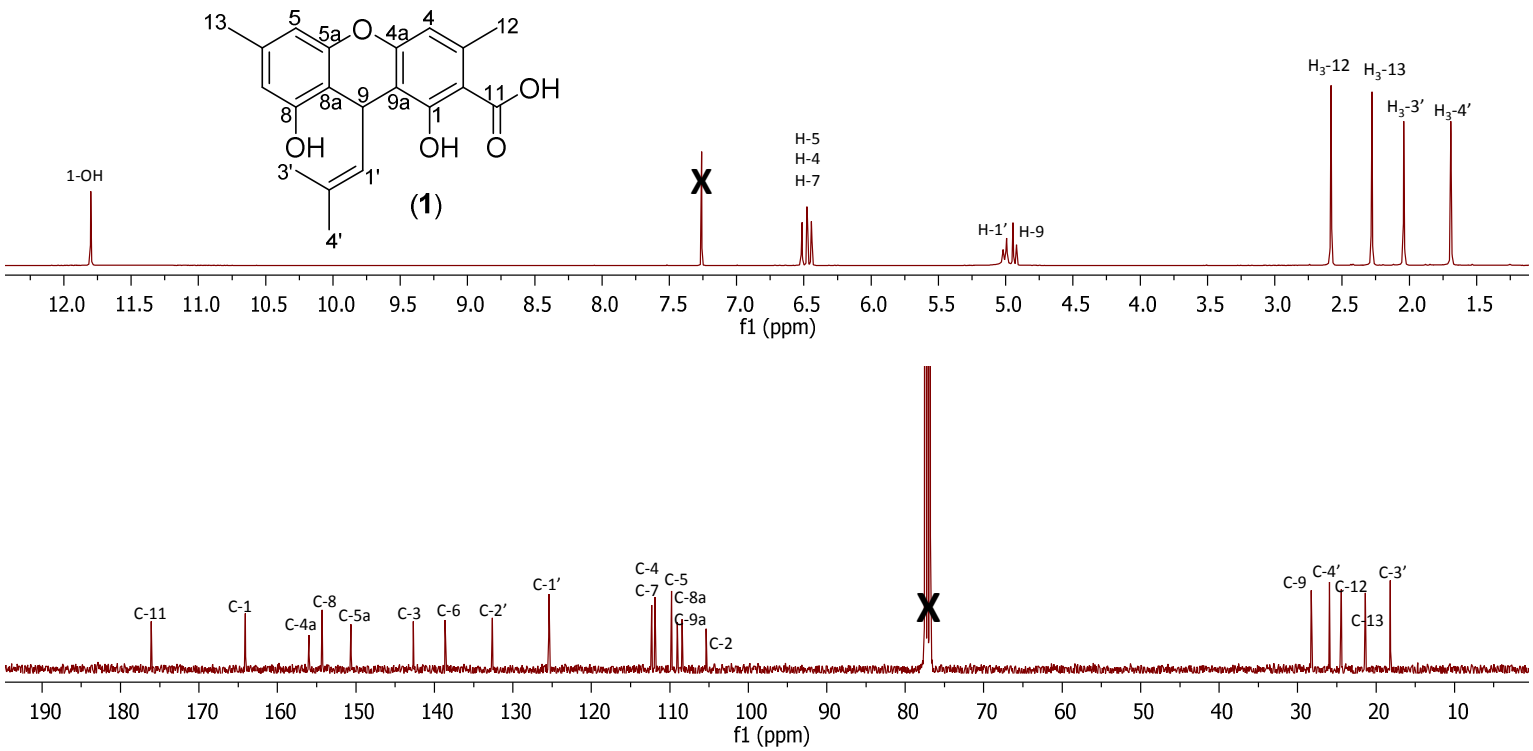

Figure 78. ^{1}H NMR (400 MHz; Top) and ^{13}C NMR (100 MHz; Bottom) Spectra of 1 in $CDCl_3$.

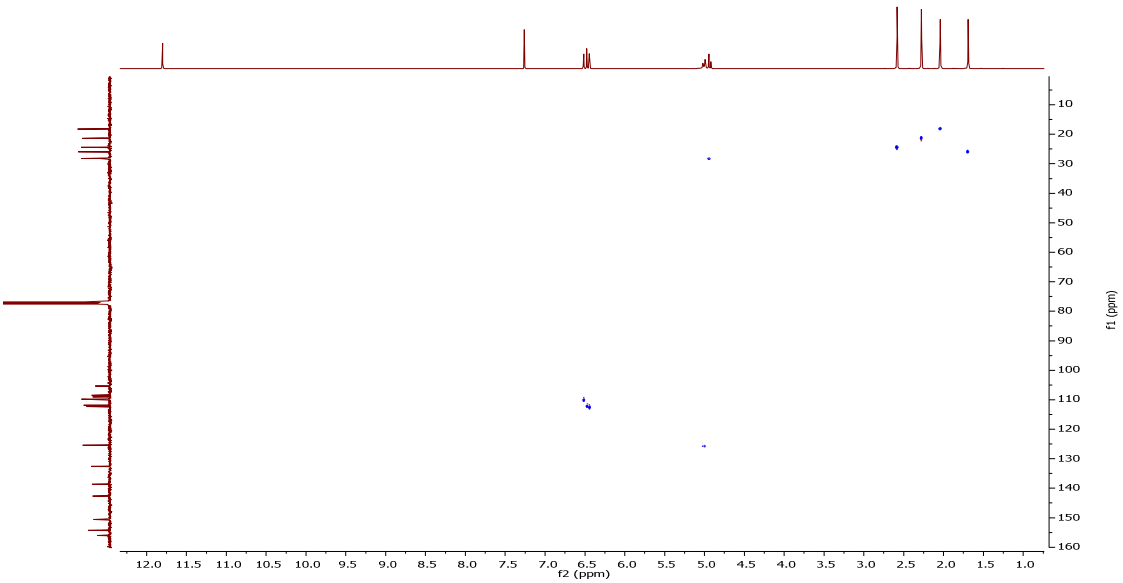

Figure 79. ^{1}H-^{13}C Edited-HSQC Spectrum of 1 in $CDCl_3$.

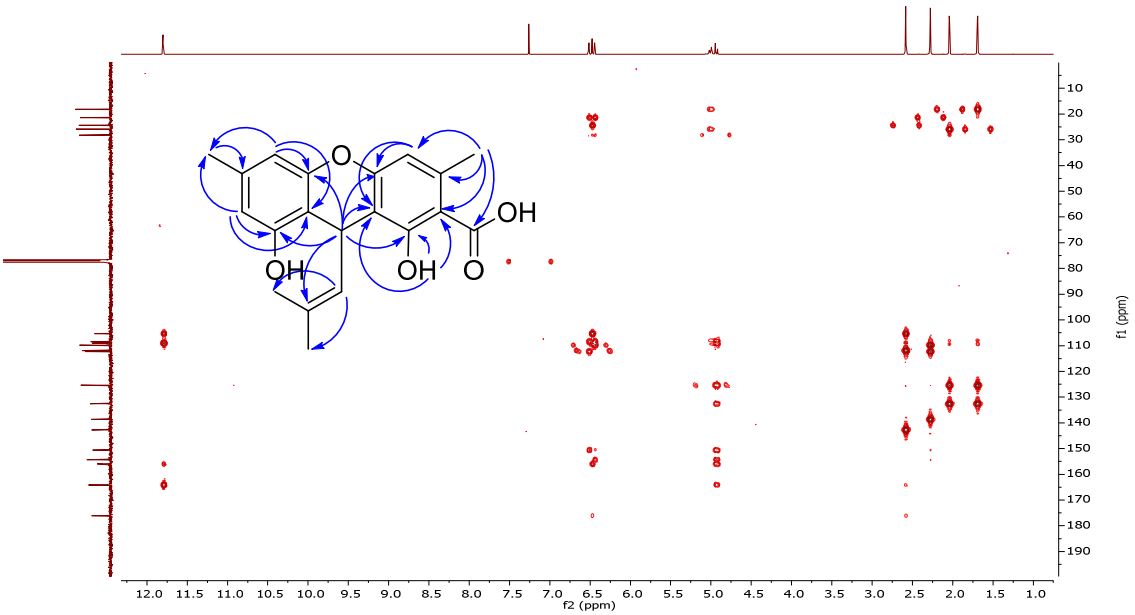

Figure 80. HMBC Spectrum of 1 in $CDCl_3$.

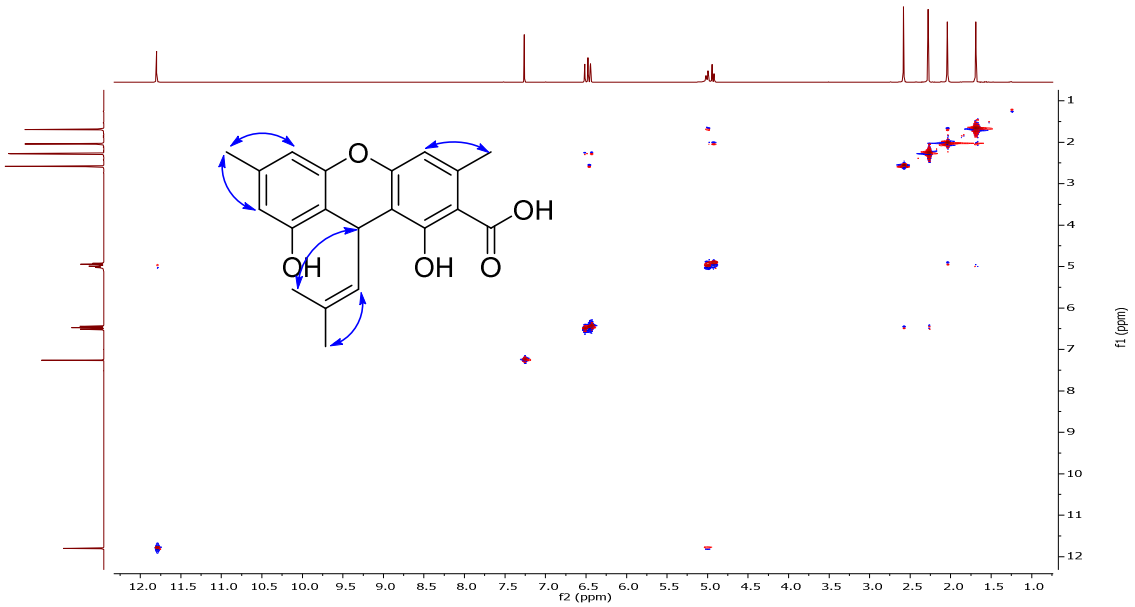

Figure 81. NOESY Spectrum of 1 in $CDCl_3$.

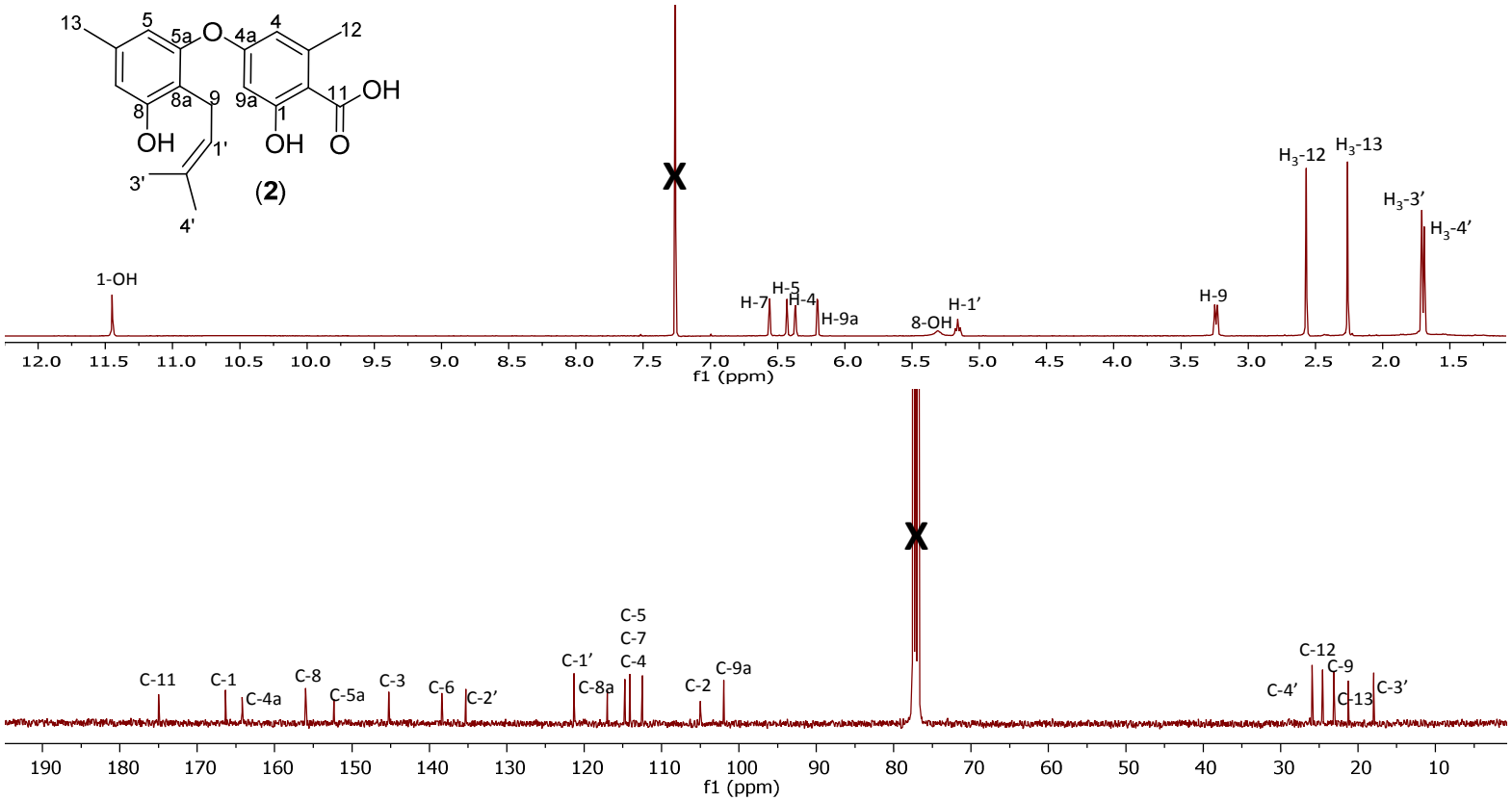

Figure 82. ^{1}H NMR (400 MHz; Top) and ^{13}C NMR (100 MHz; Bottom) Spectra of 2 in $CDCl_3$.

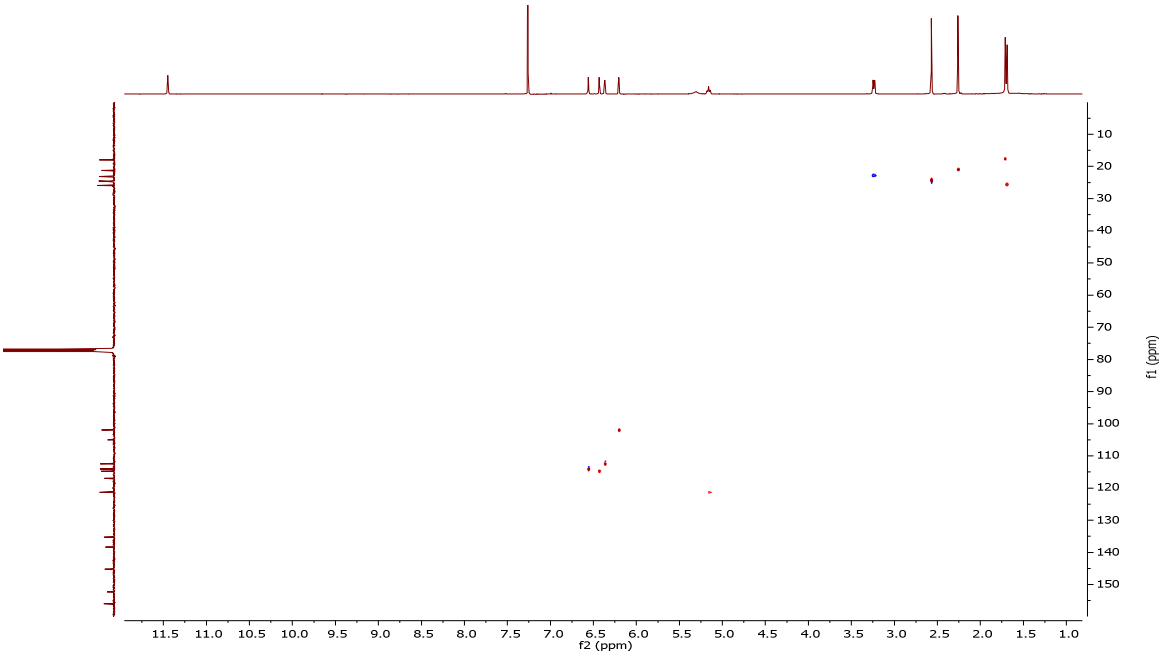

Figure 83. ^{1}H-^{13}C Edited-HSQC Spectrum of 2 in $CDCl_3$.

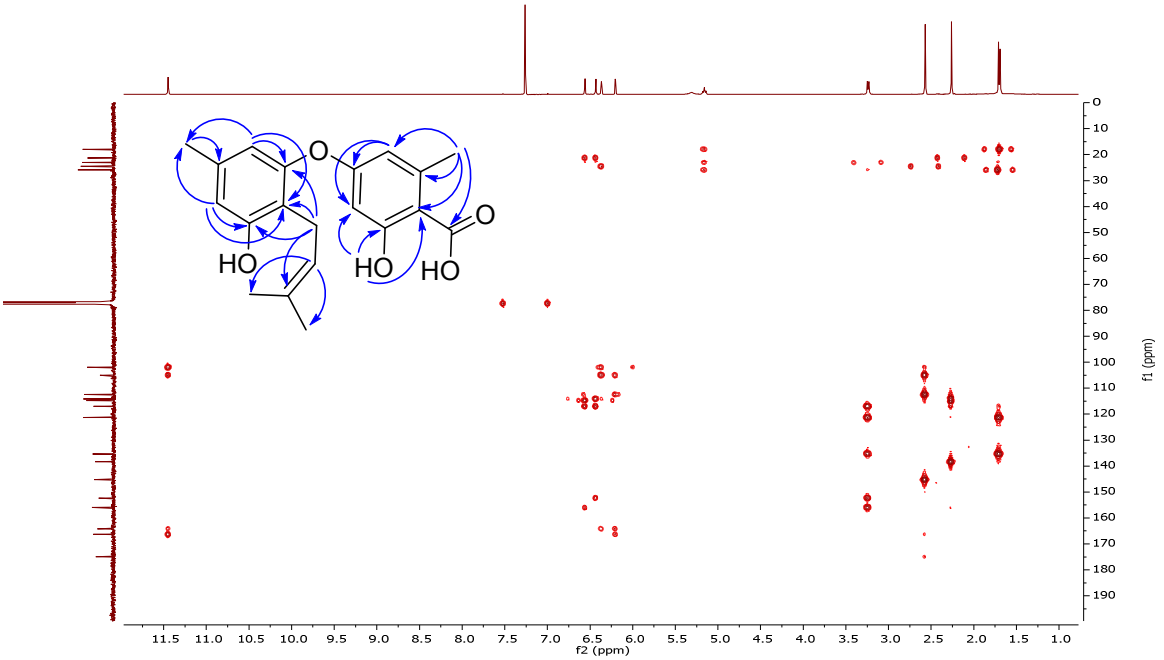

Figure 84. HMBC Spectrum of 2 in $CDCl_3$.

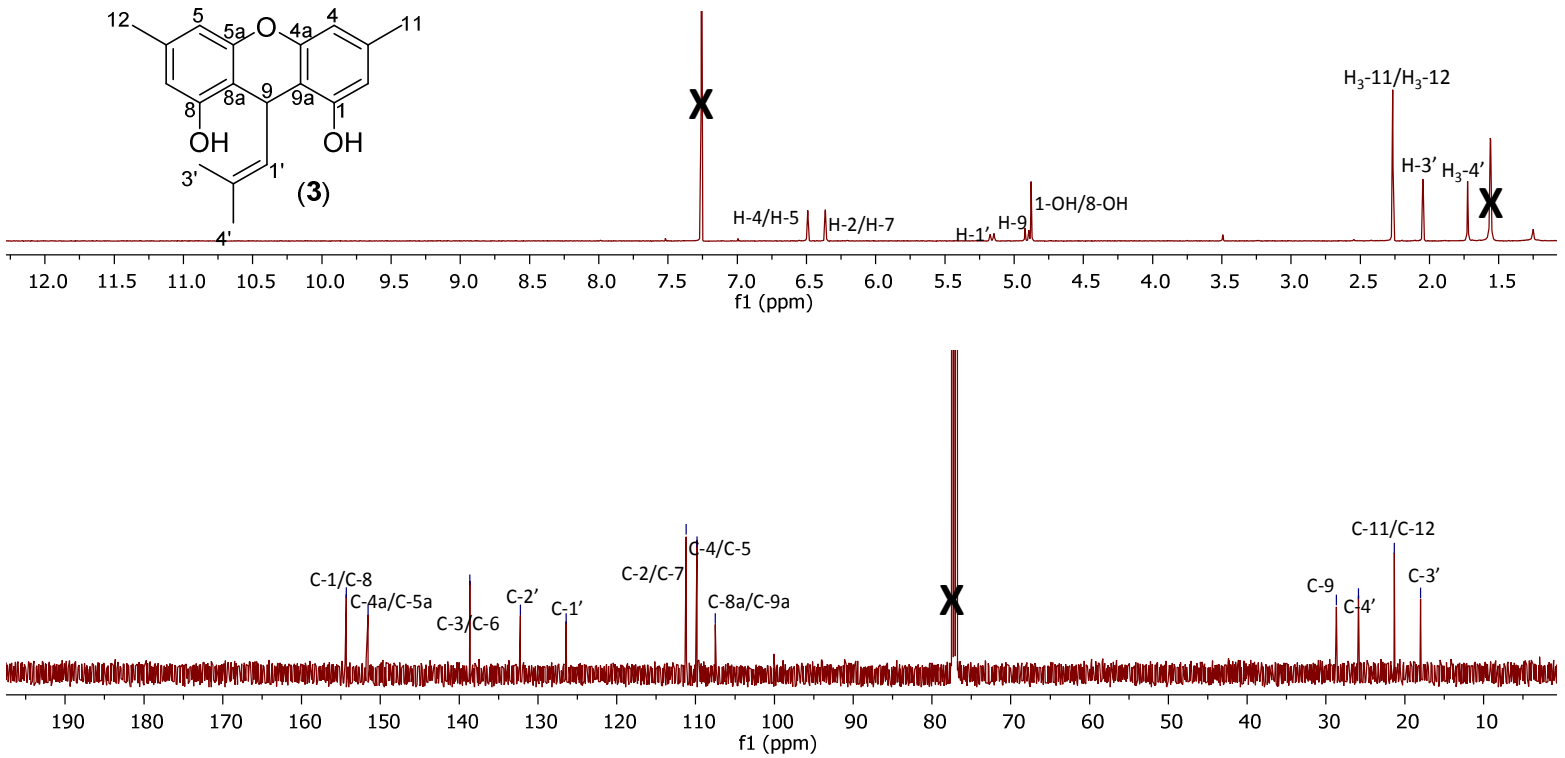

Figure 85. ^{1}H NMR (500 MHz; Top) and ^{13}C NMR (125 MHz; Bottom) Spectra of 3 in $CDCl_3$.

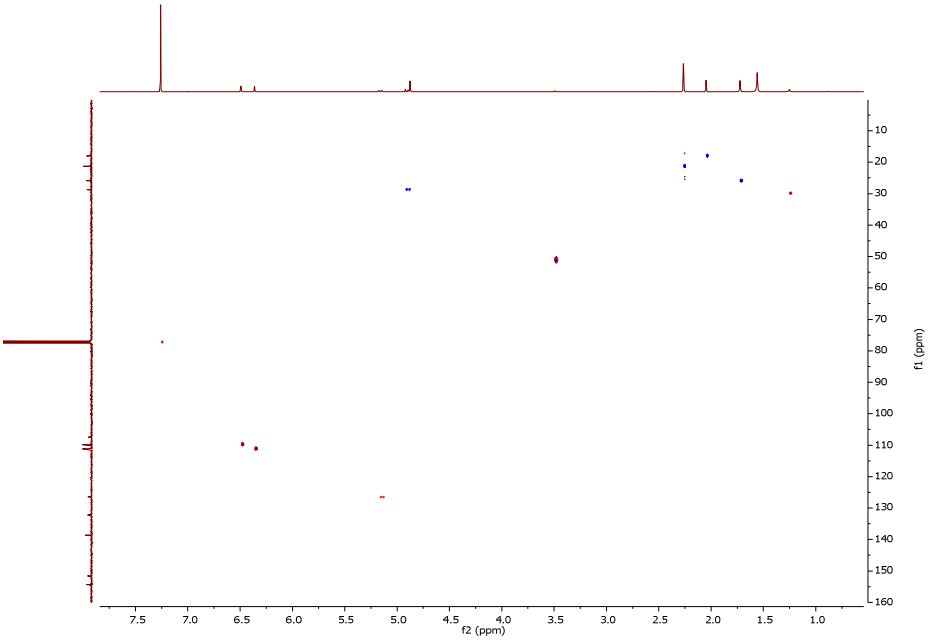

Figure 86. ^{1}H-^{13}C Edited-HSQC Spectrum of 3 in $CDCl_3$.

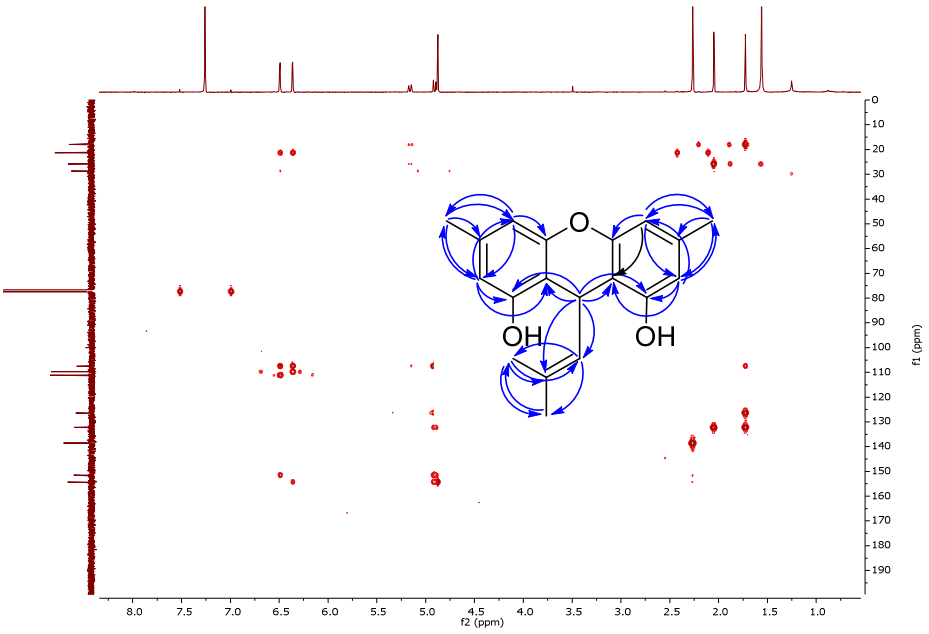

Figure 87. HMBC Spectrum of 3 in $CDCl_3$.

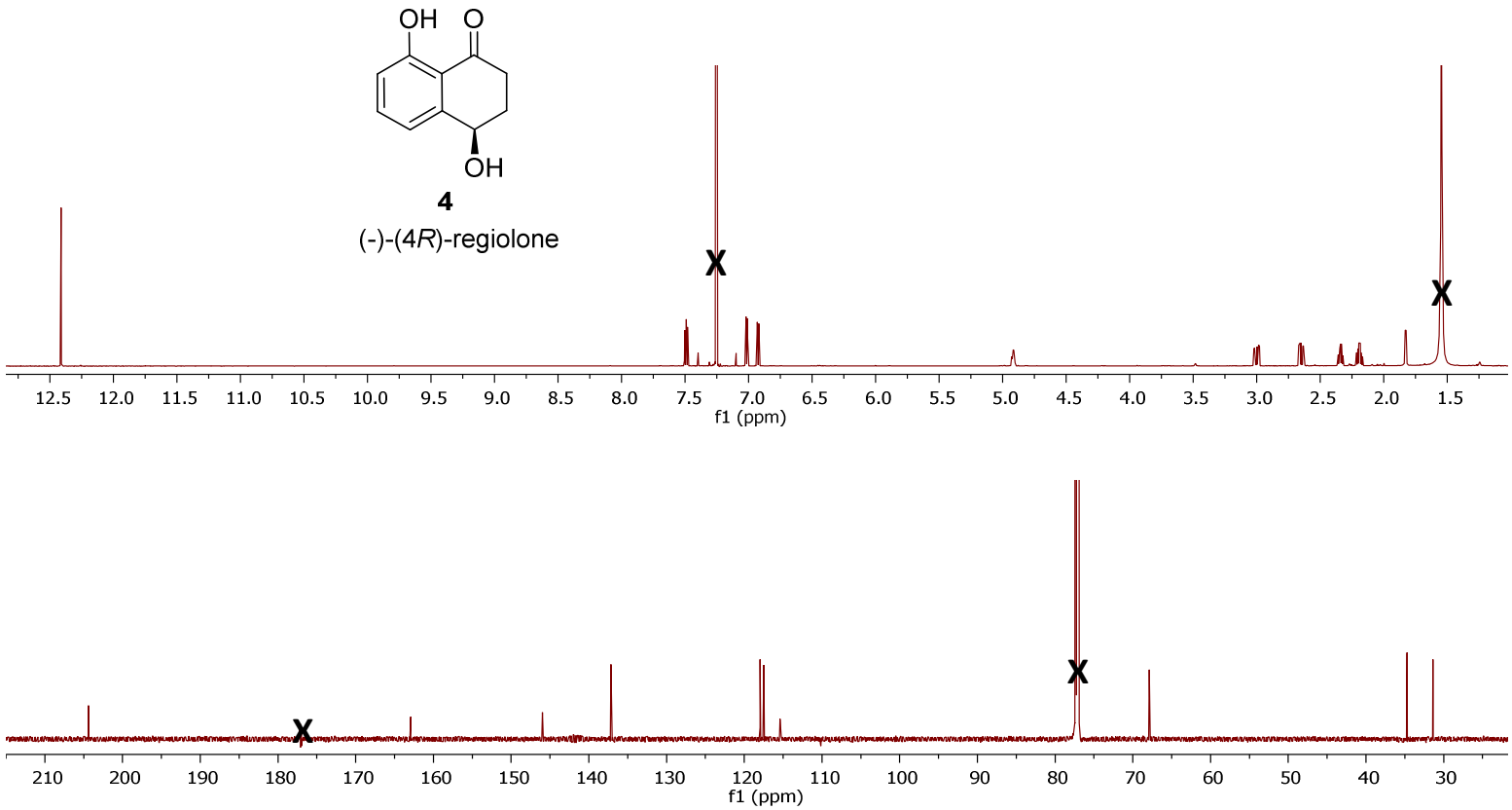

Figure 88. ^{1}H NMR (700 MHz; Top) and ^{13}C NMR (175 MHz; Bottom) Spectra of 4 in $CDCl_3$.

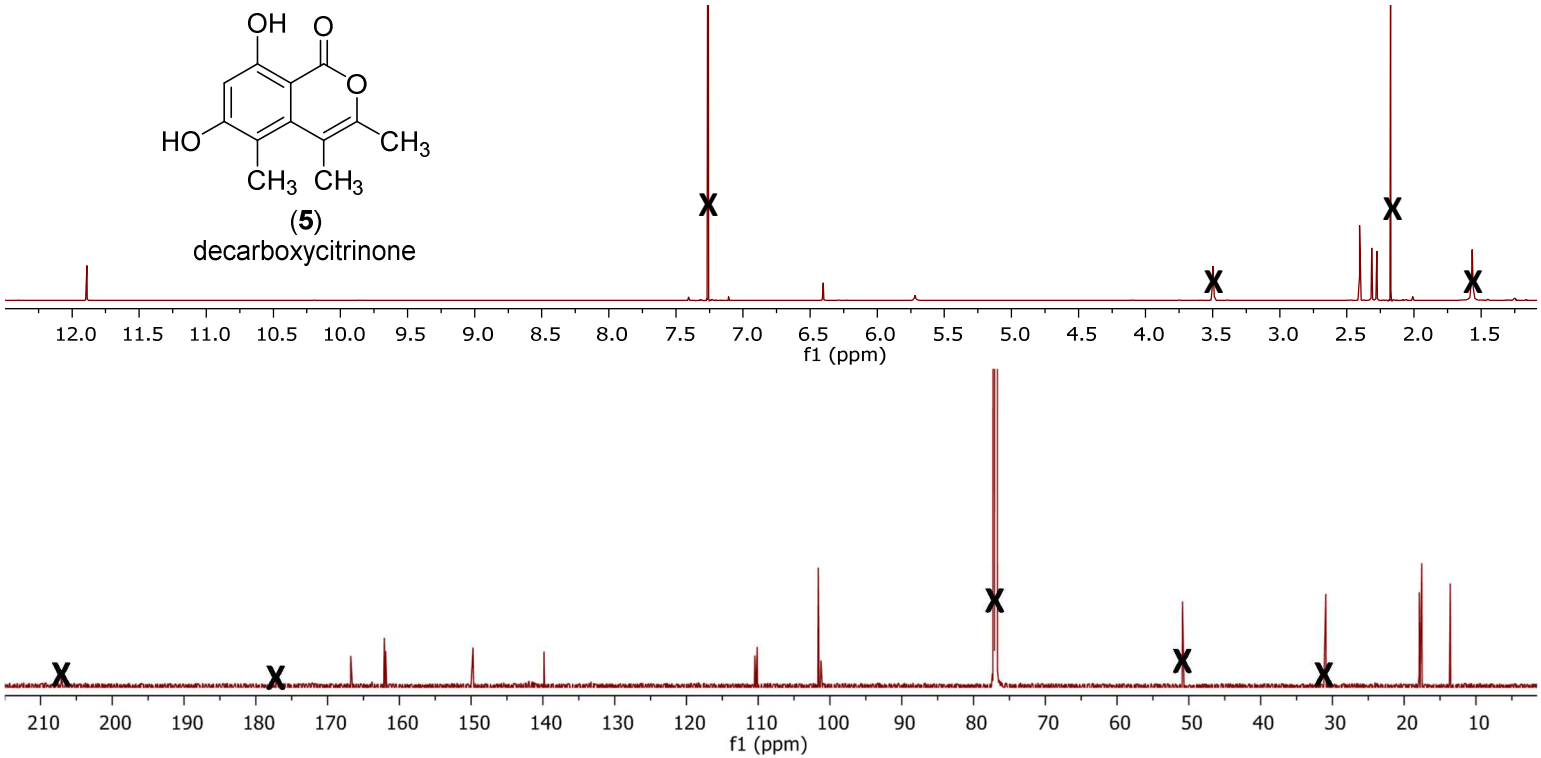

Figure 89. ^{1}H NMR (700 MHz; Top) and ^{13}C NMR (175 MHz; Bottom) Spectra of 5 in $CDCl_3$.

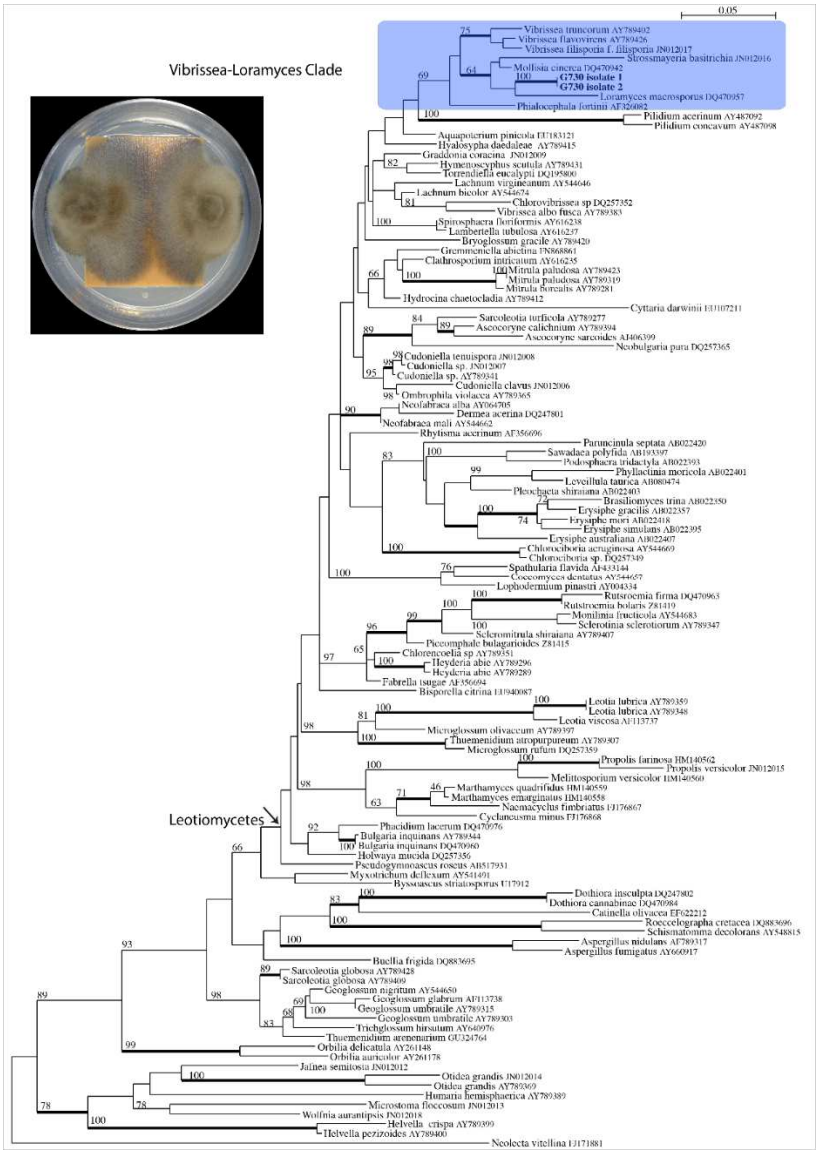

Figure 90. Phylogram of the Most Likely Tree (-lnL = 14302.40) From a RAxML Analysis of 117 Taxa Based on Partial LSU Sequence Data (830 bp). Numbers refer to RAxML bootstrap support values ≥ 65% based on 1000 replicates. Thickened branches indicate Bayesian Probabilities ≥95%; strain G730 is identified as *Leotiomycetes* sp. (Bold, highlighted in blue. A 30 d old culture on Potato Dextrose Agar media is shown on the left. Bar indicates nucleotide substitutions per site.

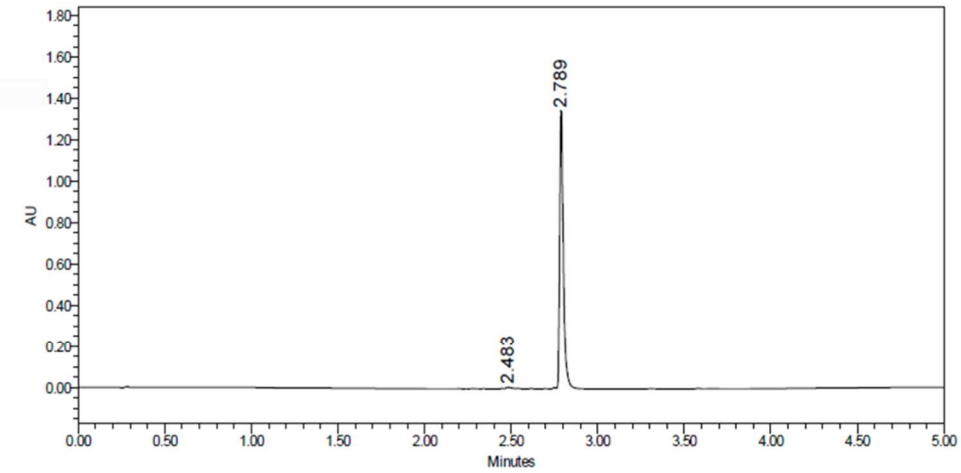

Peak Results

	RT	Name	Height	Width (sec)	Area	% Area
1	2.483		8503	4.0	19769	0.99
2	2.789		1348542	5.9	1972390	99.01

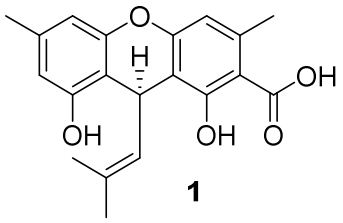

1

Figure 91. The Purity Evaluation of Compound 1 (99%) Data was obtained via a Waters Acquity UPLC system (Waters Corp., Milford, MA, USA) utilizing a Waters BEH C18 column (1.7 μm; 2.1 x 50 mm) and a CH_3CN-H_2O from 15% to 100% CH_3CN over 4.0 min. The UV absorbance was monitored at 254 nm.

Table 30. Crystal Data for Compound 1.

$C_{20}H_{20}O_5$	$Z = 2$
$M_r = 340.36$	$F(000) = 360$
Triclinic, $P1$	$D_x = 1.262$ Mg m^{-3}
$a = 7.3973$ (5) Å	Mo $K\alpha$ radiation, $\lambda = 0.71073$ Å
$b = 11.0738$ (8) Å	Cell parameters from 4964 reflections
$c = 12.0820$ (9) Å	$\theta = 3.6–29.9°$
$\alpha = 69.810$ (1)°	$\mu = 0.09$ mm^{-1}
$\beta = 77.629$ (1)°	$T = 193$ K
$\gamma = 77.212$ (1)°	Irregular, colourless
$V = 895.52$ (11) Å^3	0.30 × 0.20 × 0.14 mm

Table 31. Crystal Data Collection Parmeters for Compound 1.

Data collection	
Bruker APEX CCD diffractometer	8084 reflections with $I > 2\sigma(I)$
Radiation source: sealed tube	$R_{int} = 0.023$
Graphite monochromator	$\theta_{max} = 30.0°$, $\theta_{min} = 3.6°$
ϕ and ω scans	$h = -10$–>10
17054 measured reflections	$k = -15$–>15
9966 independent reflections	$l = -16$–>16

Table 32. Refinement Details for Compound 1.

Refinement	
Refinement on F^2	Secondary atom site location: difference Fourier map
Least-squares matrix: full	Hydrogen site location: inferred from neighbouring sites
$R[F^2 > 2\sigma(F^2)] = 0.046$	H-atom parameters constrained
$wR(F^2) = 0.123$	$w = 1/[\sigma^2(F_o^2) + (0.0675P)^2]$ where $P = (F_o^2 + 2F_c^2)/3$
$S = 1.04$	$(\Delta/\sigma)_{max} < 0.001$
9966 reflections	$\Delta>_{max} = 0.33$ e Å^{-3}
465 parameters	$\Delta>_{min} = -0.21$ e Å^{-3}
3 restraints	Absolute structure: Refined as an inversion twin.
Primary atom site location: structure-invariant direct methods	Absolute structure parameter: 0.4 (8)
Special details	
Geometry. All esds (except the esd in the dihedral angle between two l.s. planes) are estimated using the full covariance matrix. The cell esds are taken into account individually in the estimation of esds in distances, angles and torsion angles; correlations between esds in cell parameters are only used when they are defined by crystal symmetry. An approximate (isotropic) treatment of cell esds is used for estimating esds involving l.s. planes.	
Refinement. Refined as a 2-component inversion twin.	

CHAPTER V

ENHANCED DEREPLICATION OF FUNGAL CULTURES VIA USE OF MASS DEFECT FILTERING

This chapter has been published in *The Journal of Antibiotics* and is presented in that style. Noemi D. Paguigan, Tamam El-Elimat, Diana Kao, Huzefa A. Raja, Cedric J. Pearce, Nicholas H. Oberlies. *The Journal of Antibiotics* (2017) 70, 553–561.

Effective and rapid dereplication is a hallmark of present-day drug discovery from natural sources. This project strove to both decrease the time and expand the structural diversity associated with dereplication methodologies. A 5 min liquid chromatographic run time employing heated electrospray ionization (HESI) was evaluated to determine whether it could be used as a faster alternative over the 10 min ESI method we reported previously. Results revealed that the 5 min method was as sensitive as the 10 min method and, obviously, was twice as fast. To facilitate dereplication, the retention times, UV absorption maxima, full-scan HRMS and MS/MS were cross-referenced with an in-house database of over 300 fungal secondary metabolites. However, this strategy was dependent upon the makeup of the screening in-house database. Thus, mass defect filtering (MDF) was explored as an additional targeted screening strategy to permit identification of structurally related components. The use of a dereplication platform incorporating the 5 min chromatographic method together with MDF facilitated rapid and effective

identification of known compounds and detection of structurally related analogs in extracts of fungal cultures.

Introduction

As Ōmura and colleagues showed the world via their research on avermectins[198-200] (and many other compounds), Nature is a prolific source of chemical diversity, providing humanity with many drugs and drug leads for a suite of diseases.[2,3,201] A common characteristic of natural product extracts is that they consist of a mixture of compounds, often structurally related, although present at varying abundance. As such, it is desirable to have a means to prioritize samples, such that valuable time and financial resources can be focused on those extracts most likely to yield new structural diversity. An important part of this discovery process involves dereplication, a rapid identification of known compounds in extracts in order to focus on the isolation of new chemical entities. Several recent advancements in dereplication strategies, most involving hyphenated spectroscopic techniques, have been pivotal to the increased efficiency in natural products-based drug discovery.[202-204] In particular, mass spectrometry coupled with electrospray ionization (ESI) has become increasingly more important in natural products drug discovery, especially for chemical profiling of complex extracts.[205-207] Hyphenation of liquid chromatography with ESI-MS has increased the pace of dereplication by providing an efficient means of identifying the multiple components of complex extracts prior to further purification and isolation work.[204,208]

Our research team has been working on the dereplication of fungal cultures for about a decade, particularly within a drug discovery program that aims to identify new

anticancer lead compounds.[50,209] This started with a generalized dereplication methodology utilizing UV and ^{1}H NMR spectra and targeting distinct classes of mycotoxins,[210] as these nuisance compounds yield positive results in cytotoxicity-based assays. This protocol evolved significantly to target a wider range of secondary metabolites in fungal extracts using a complementary suite of hyphenated techniques, specifically ultraperformance liquid chromatography-photodiode array-high resolution tandem mass spectrometry (UPLC-PDA-HRMS-MS/MS). Finally, the latter was augmented with a droplet-liquid microjunction-surface sampling probe (droplet-LMJ-SSP), so as to analyze the secondary metabolite profile of fungal cultures *in situ*.[129]

Mass defect filtering was developed recently and is finding growing use in drug metabolite profiling studies.[211-213] This approach utilizes the full scan-HRMS data, and detection of drug metabolites is accomplished via data mining post acquisition. Mass defect filtering is based on the fact that each isotope of every element has a defined mass defect (i.e. the non-integral portion of an *m/z* value). This is why each molecule of a defined elemental composition will have a unique exact mass, typically observed in the 1000ths to 10,000ths place.

The useful application of mass defect filtering in drug metabolism studies is centered on the observation that the core structure of a drug does not change significantly during biotransformation.[211,214,215] Thus, the mass defect between the parent drug and its metabolites will fall within a narrow range (typically within 50 mDa). If a mass defect filter window is centered on the mass defect of the parent drug, then ions with a mass defect outside of this window will be excluded, resulting in the removal of interference

signals in the total ion chromatogram (TIC). Importantly, this then facilitates the selective identification of drug metabolite peaks from the noise in complex biological matrices.

Aside from drug metabolite identification, mass defect filtering has been adapted for use in the qualitative examination of natural products, particularly those based on herbals.[216-218] However, this data-mining tool has not been used in the analysis of fungal secondary metabolites. Theoretically, compounds produced by fungi can be classified into distinct classes, each class sharing the same core structure. Thus, if a filter reference and substituents around the core structure are carefully defined, then mass defect filters can be constructed to exclude the majority of unrelated ions. This should, in turn, facilitate the identification of structural analogues in the extract.

In this study, mass defect filtering is presented as an additional approach for the targeted screening of secondary metabolites in fungal extracts. The merger of UPLC-PDA-HRMS-MS/MS dereplication with mass defect filtering permits additional profiling for structurally related components in the sample based on their mass defects (Figure 92). This workflow enhances the dereplication methods so as to screen for a wider range of secondary metabolites produced by fungal cultures.

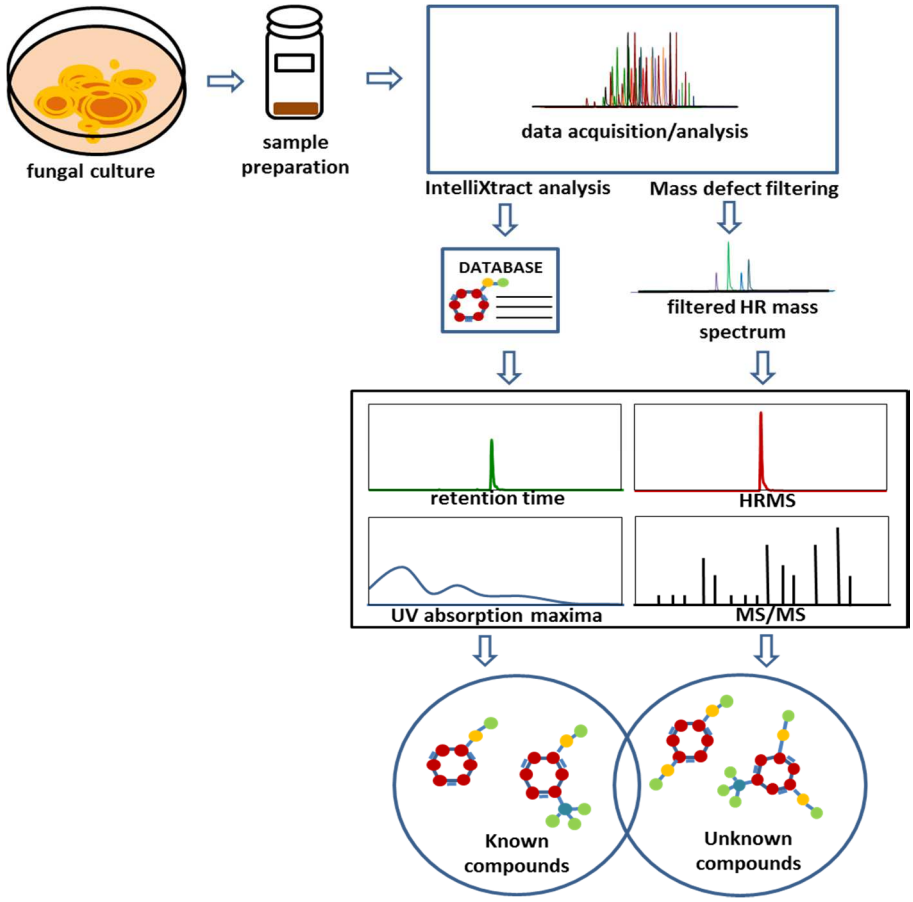

Figure 92. Proposed Workflow for Dereplication of Fungal Extracts Including a 5-Minute UPLC-PDA-HRMS-MS/MS Methodology. HRMS and MS/MS (CID 30) data were acquired by LTQ Orbitrap using data dependent scan. A post-acquisition data analysis using IntelliXtract, an add-in feature of ACD MS Manager, cross-references the molecular-ion peaks and retention times to identify compounds known to the in-house database. For targeted-analysis of a specific class of compounds, a user-defined mass defect filtering criteria was designed based on accurate masses and mass defects centered around a core structure. The HRMS data were filtered with Compound Discoverer™ software to identify components related to the known compounds. The identity of the known compounds were verified based on HRMS, MS/MS fragmentation pattern, retention time, and UV absorption maxima. The tentative identity of the discovered unknown compounds were assigned based on the interpretation of their CID-MS/MS (30 eV) fragmentation patterns.

Results and Discussion

5-min HESI method. Previously, we developed a dereplication method for diverse classes of fungal secondary metabolites[50] in extracts on an LTQ Orbitrap.[219] That protocol utilized a 10-min liquid chromatographic run time to acquire full-scan HRMS and MS/MS (using a normalized collision energy of 30) spectra in both positive and negative electrospray ionization (ESI) modes, with UV absorption maxima and retention times used as orthogonal data. To facilitate dereplication, these data were uploaded into ACD MS Manager with add-in Intelliextract software, which cross-references the molecular-ion peaks and retention times with an in-house database of over 300 fungal secondary metabolites. Molecular ions identified by the software that matched the database were confirmed by comparison of the HRMS, MS/MS, retention time, and UV data to that of the standard in the database. With this method, nearly all of the fungal metabolites (>98 %) in the in-house database ionized efficiently in the ESI^+ mode, while about 90% of the samples ionized in the ESI^- mode. In total, this suggested the ESI^+ mode as the ionization of choice for sample dereplication, unless knowledge of the samples or extracts indicated ionization in ESI^- mode.

While valuable for routine analysis of a large number of samples (batches of > 50 samples), the 10-min liquid chromatographic method was not ideal, particularly for shared instruments. Thus, a dereplication method utilizing a 5-min run time at a 0.6 mL/min flow rate via heated electrospray ionization (HESI) was evaluated to determine if it could be used as a faster alternative. The use of HESI was important,[220,221] as it would

allow better desolvation, given that a higher flow rate (twice as fast) was used for the 5-min method compared to the 0.3 mL/min flow rate utilized in the 10-min method.

As proof of concept, about a third of the fungal library (>100 compounds) was analyzed in the $HESI^+$ using the 5-min method to obtain the retention times, UV absorption maxima, full-scan HRMS and MS/MS spectra. In general, data obtained for all compounds matched with data in the database built using the 10-min dereplication method,[219] except for the retention times.

To compare the performance characteristics of the 10-min ESI dereplication method to the 5-min HESI dereplication, the two related parameters, limit of detection (LOD) and limit of quantitation (LOQ), were measured for each method, both in the positive ionization mode. The LOD and LOQ values were obtained from the calibration data and regression line directly (Supplementary Figures 99 and 100). Five representative compounds (**1**-**5**) were tested that had molecular weights ranging from 373 amu to 1963 amu, and this included compounds that were based on polyketide building blocks, amino acid building blocks, and those with both in their scaffolds (Supplementary Table 33). In general, the 5-min HESI method had comparable sensitivity to the 10-min ESI method based on the LOD and LOQ values obtained for the five analytes tested (Supplementary Table 33).

Dereplication of fungal extracts. An extract of MSX40080 was dereplicated and determined to contain aflatoxins, thus explaining its potent cytotoxicity.[219] To test if the 5-min method would be able to identify the same aflatoxins, the extract was re-analyzed

(Figure 93). Five aflatoxins, including sterigmatocystin (**6**), 5-methoxysterigmatocystin (**7**), aversin (**8**), brevianamide P (**9**), and 6, 8-di-O-methyl averufin (**10**) were identified, consistent with previous results.[219] Comparison of data obtained from both methods indicated that only the retention times were different for the detected compounds, as shown for **6** (Figure 94) and **7**-**10** (Supplementary Figure 101). In the context of discovering leads for an anticancer drug discovery program, aflatoxins are an obvious nuisance, making their rapid dereplication critical.

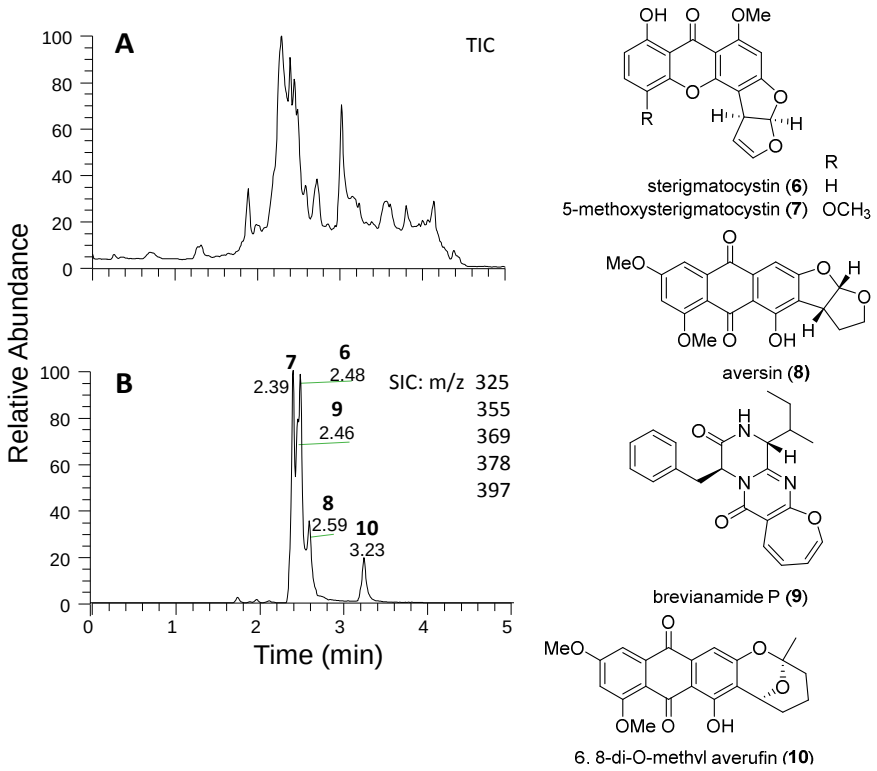

Figure 93. (A) (+)-ESI-TIC of MSX40080. (B) The Selected Ion Chromatogram (SIC) of Dereplicated Aflatoxins (6-10) in MSX40080.

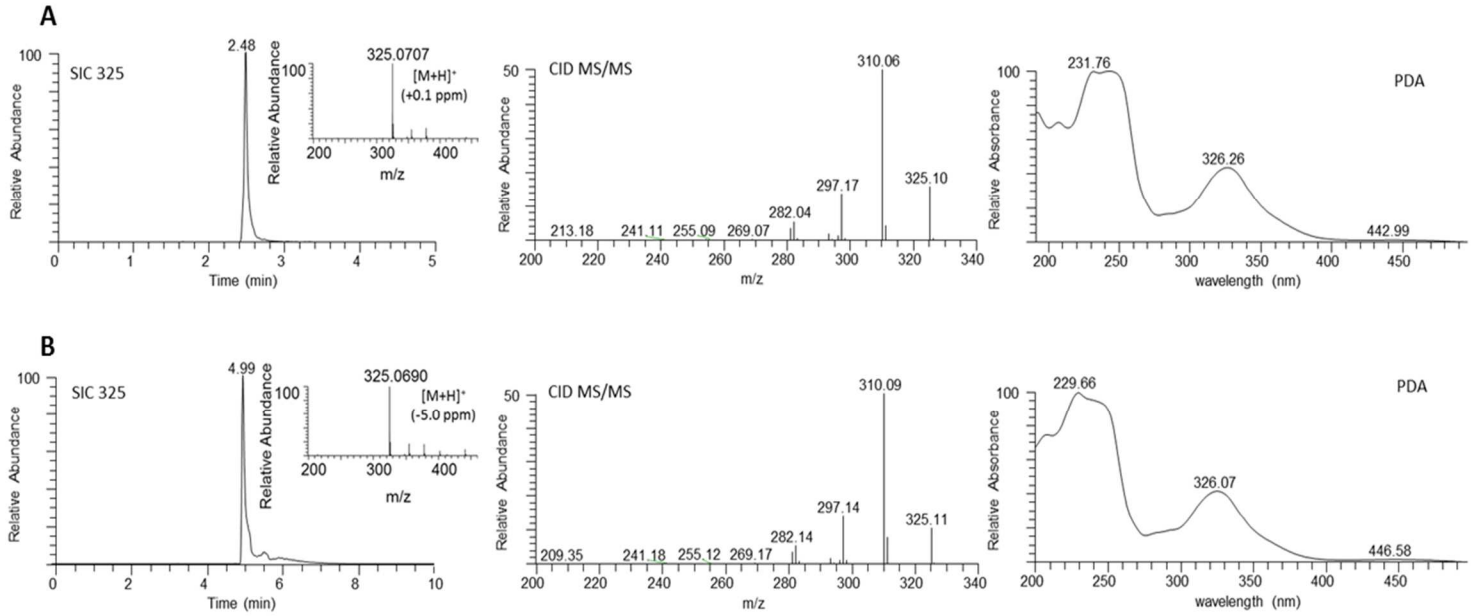

Figure 94. Comparison of SIC (m/z 325), (+)-HRMS, CID MS/MS (30 eV), and UPLC PDA Data of Sterigmatocystin (6) Detected in MSX40080 Using (A) the 5-Minute and (B) the 10-Minute Dereplication Protocols.

Dereplication using UPLC-PDA-HRMS-MS/MS with mass defect filtering.

The first step of the dereplication strategy was focused on the targeted screening of secondary metabolites in our library using the 5-min UPLC-HRMS-MS/MS methodology. To take this dereplication strategy a step further, identified hits were expanded upon by screening for potential analogues with the aid of Compound Discoverer^{TM} data-processing software utilizing mass defect filtering (MDF). MDF was essential to remove the majority of interfering ions and facilitate detection of the potential structural class of related compounds via post-acquisition processing of HRMS data. Theoretically, each structural analogue possessed relatively minor and well-defined changes in the mass defect from filter reference compounds. Therefore the mass defects between the reference skeletons and related analogues should fall within a defined mass defect window.

The case of identifying epipolythiodioxopiperazine (ETP) alkaloid analogues in different fungal cultures illustrates the use of the UPLC-PDA-HRMS-MS/MS dereplication strategy and the benefits of mass defect filtering. Recent studies have identified verticillin A (**11**) as an effective tumor suppressor, inducing tumor cell apoptosis in metastatic human colorectal cancer cells at nanomolar concentrations,[222,223] and structurally-related analogues have been shown to have potent biological activities.[224,225,226] Therefore it was valuable to identify these compounds in extracts, and at the same time, determine the presence of structurally-related analogues that were not part of our library. In this case we were using dereplication as a means to identify other

fungi that biosynthesize these compounds, with the aim of enhancing scale up and production, as will be reported in the future.

A common characteristic of the 15 analogues, all being dimeric ETPs, is a polysulfide bridge in the molecule (Dictionary of Natural Products, Taylor and Francis Group, UK). Supplementary Figure 102 is a graphical representation of the accurate masses and the corresponding mass defects of these compounds. As summarized in Supplementary Table 34, the compounds fall into a narrow range of nominal masses and mass defects. To identify these analogues, a filtering template was set using the structure of Sch 52901 (**12**) having a nominal mass that is the midpoint of the target compounds, and setting a mass window of ± 150 Da. The analogues show a narrow range of mass shifts as a result of modifications in the structures, yielding only a small difference in mass defects relative to the template core structure **12** (Supplementary Table 34). Using a slightly wider mass defect range covering all the potential target compounds (Supplementary Table 34), a mass defect window of ± 50 mDa was used.

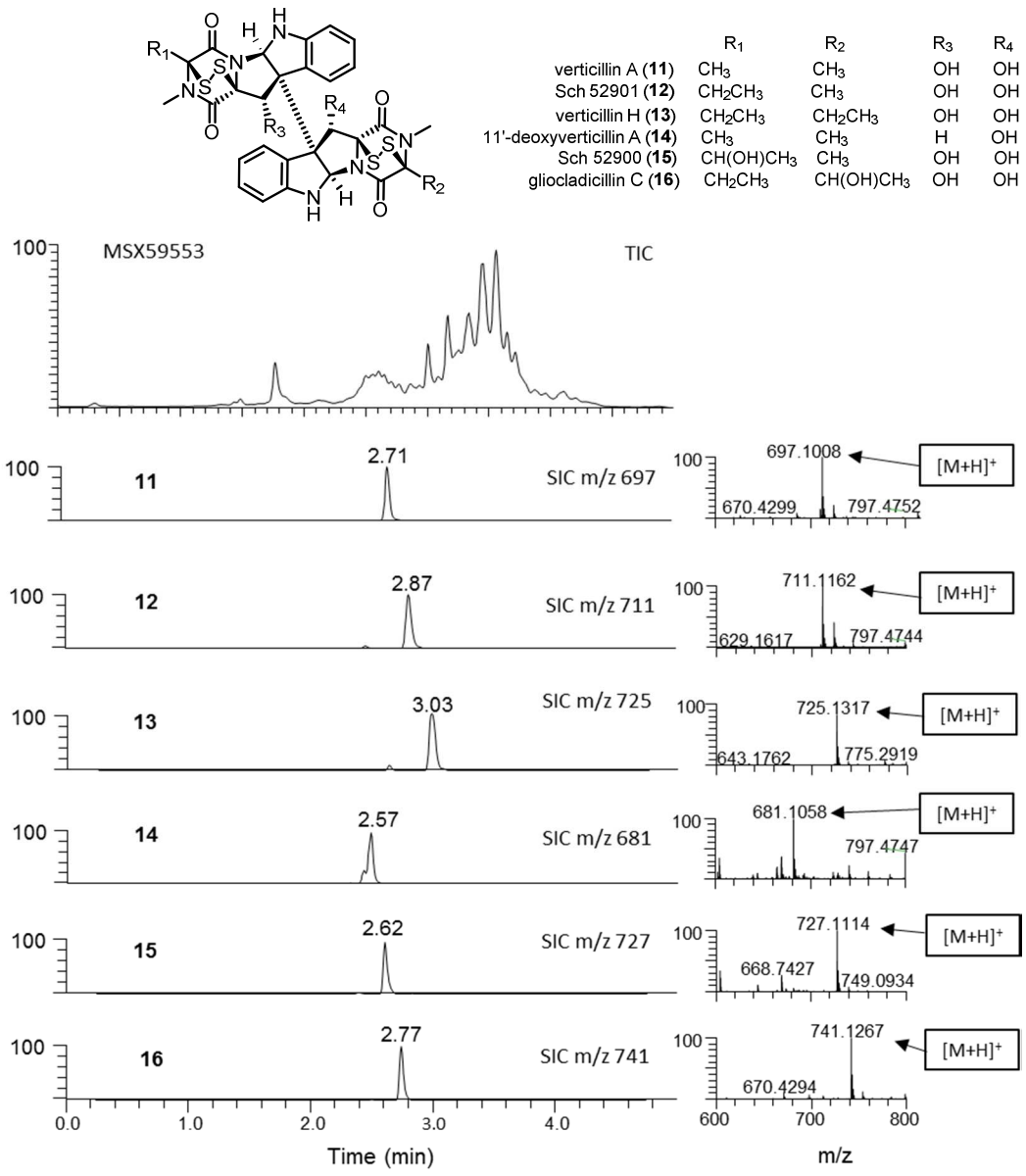

Figure 95. The (+)-ESI-TIC of MSX59553 and Epipolythiodioxopiperazine Analogues (11-16) Dereplicated via the 5-Min UPLC-PDA-HRMS-MS/MS (CID 30 eV) Method.

The applicability of mass defect filtering for detecting these analogues was illustrated with the analysis of an extract obtained from a culture of *Clonostachys rogersoniana* (MSX59553), which was previously identified by our research group as a

Bionectriaceae sp. (Hypocreales) based on partial 28S rDNA sequence data, JQ749725 and known to biosynthesize ETP alkaloids.[226] Dereplication of this strain using the 5-min $HESI^+$ method identified six known ETPs, including verticillin A (**11**), Sch 52901 (**12**), verticillin H (**13**), 11´-deoxyverticillin (**14**), Sch 52900 (**15**), and gliocladicillin C (**16**) based on retention times, HRMS, and MS/MS data (Figure 95 and Supplementary Figure 103). The TIC of MSX59553 was analyzed further by mass defect filtering with the aim of revealing additional structurally-related analogues. Mass defect filtering significantly reduced the amount of interfering ions (Supplementary Figure 104), facilitating identification of related analogues that were present in the extract. The characteristic peaks of ETPs captured by mass defect filtering was consistent with the verticillins identified in the previous analysis.

Identification of the fragmentation pattern for ETP alkaloids. The benefit of using mass defect filtering in conjunction with the traditional targeted dereplication strategy is that it gives additional insight into the remaining unknown compounds present in the extract by simplifying the data. Once a potential structurally-related compound based on mass defect is identified, its structure must be confirmed. But, with the absence of a standard, this might be a challenging task. Thus, to facilitate characterization within the context of an extract, the characteristic CID fragmentation can be analyzed to tentatively assign a structure. In the literature, several studies have been reported that use a CID-MS/MS-based workflow for structural elucidation of natural products.[227-229] Implementation of this strategy requires knowledge of the fragmentation patterns of compounds in the same structural class.

Compounds having the same core substructure generally exhibit similar mass fragmentation patterns, and thus, can be identified based on their diagnostic fragment ions.[218] For the case of ETP alkaloids, the recurrent fragmentation pattern was characterized based on the MS/MS CID fragmentation taken in positive mode (Supplementary Figure 103). In general, desulfurization of the precursor ion peak ([M-2S+H]$^+$, arising from the polysulfide bridge in each of the dioxopiperazine rings, were observed in all CID-MS/MS analyses. Nearly all compounds exhibited dehydration of the [M-2S+H]$^+$ ion, whereas the compound 11´-deoxyverticillin A (**14**), which possessed one hydroxy group, did not. This may indicate that the removal of a H_2O was dependent on the number of hydroxy moieties in the compounds. After H_2O loss, a fragment peak, indicating loss of one of the dioxopiperazine moieties was observed. For instance in verticillin A, the fragment peak at *m/z* 615.18 was followed by a peak at *m/z* 465.08, corresponding to a difference of 150 Da and accounting for the loss of a dioxopiperazine moiety ($C_7H_6N_2O_2$). After this observed dissociation, dehydration and desulfurization occurred, most likely in the other dioxopiperazine moiety of the core.

With the examination of the CID diagnostic fragment ions of the ETP standards (Supplementary Figure 103), we sought to apply this to the rapid characterization of analogues of the ETPs in other complex mixtures, where no available laboratory standard was available.

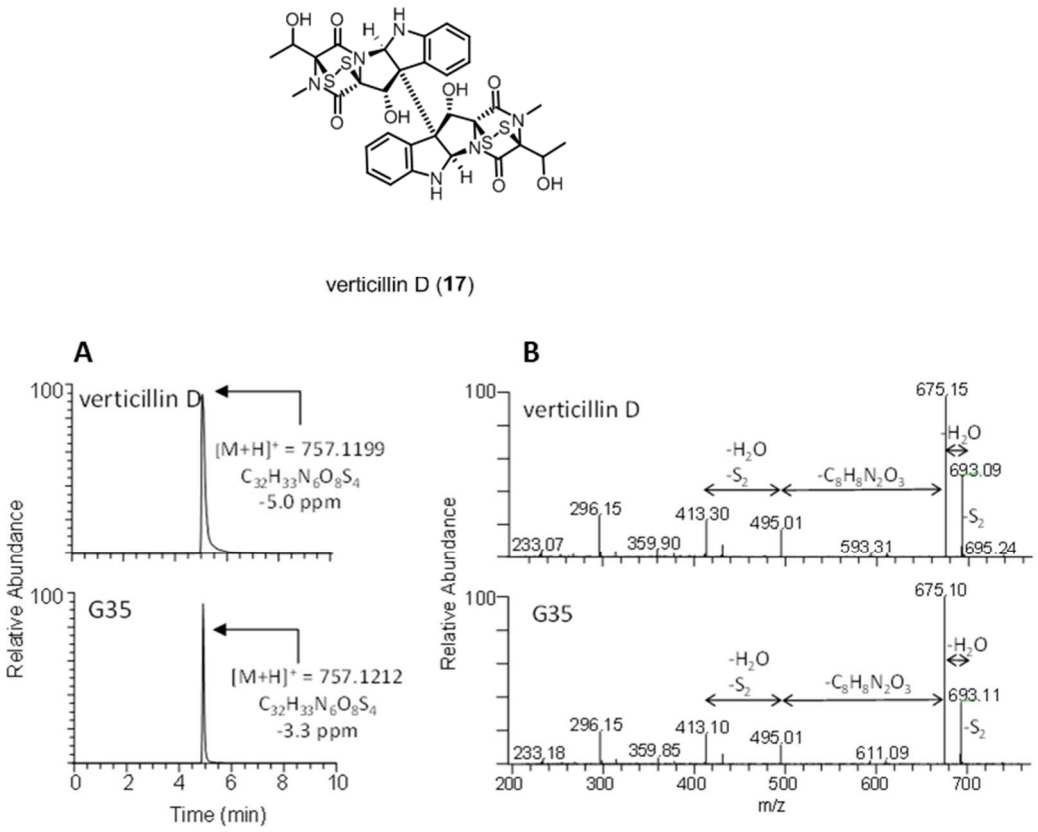

Figure 96. Detection of Verticillin D (17) in G35 Grown in Oatmeal Agar After Mass Defect Filtering. (A) Overlay of (+)-ESI TIC of 17. (B) CID MS/MS (30 eV) Spectra of 17.

Analysis of verticillin production in G35. A culture of *Colletotrichum fioriniae* (G35) was identified previously by dereplication to produce **11** and **15**.[230] However, refermentation of the culture using the standard rice culture conditions failed to produce any structurally-related analogues. In order to revive the ETP biosynthetic pathway, the one strain-many compounds (OSMAC) approach was applied.[231] Using this strategy, 12 different growth conditions providing different nutrients were tested to identify the most

favorable condition that would lead to the revival of the biosynthetic pathway. Still, no analogues were dereplicated in any of the extracts.

Upon analysis of the HRMS data with mass defect filtering, a culture of G35 grown in oatmeal agar showed a peak that had a corresponding value at *m/z* 757.1212, which matched the monoisotopic mass of protonated verticillin D (**17**) with +3.3 ppm mass accuracy (Figure 96). The peak with *m/z* 757.1212 was identified as an ETP alkaloid based on comparison of the characteristic losses observed in its MS/MS spectrum (Figure 96), exhibiting a distinctive fragmentation pattern similar to that of verticillin A (Supplementary Figure 103). In particular the fragment ions at *m/z* 693.11 and *m/z* 675.10 indicated desulfurization and dehydration, respectively.

Coincidentally, **17** was isolated from a freshwater Ascomycete fungal culture of a *Clonostachys* sp. (G600), and this presented an opportunity to verify the identity of the peak observed in G35. The HRMS and MS/MS data for **17** were analyzed and matched that of the compound with *m/z* 757.1212 from G35 (Figure 96). This result verified that **17** was indeed being produced in low quantities by G35 in oatmeal agar, an observation that would not be possible without mass defect filtering.

This result demonstrated the advantages of incorporating mass defect filtering as a processing technique in the dereplication platform. Verticillin D (**17**) was not part of the database when the samples were dereplicated and processed originally. Since mass defect filtering is a post-acquisition data mining technique that analyzes solely the HRMS data, samples can be re-evaluated as more data become available.

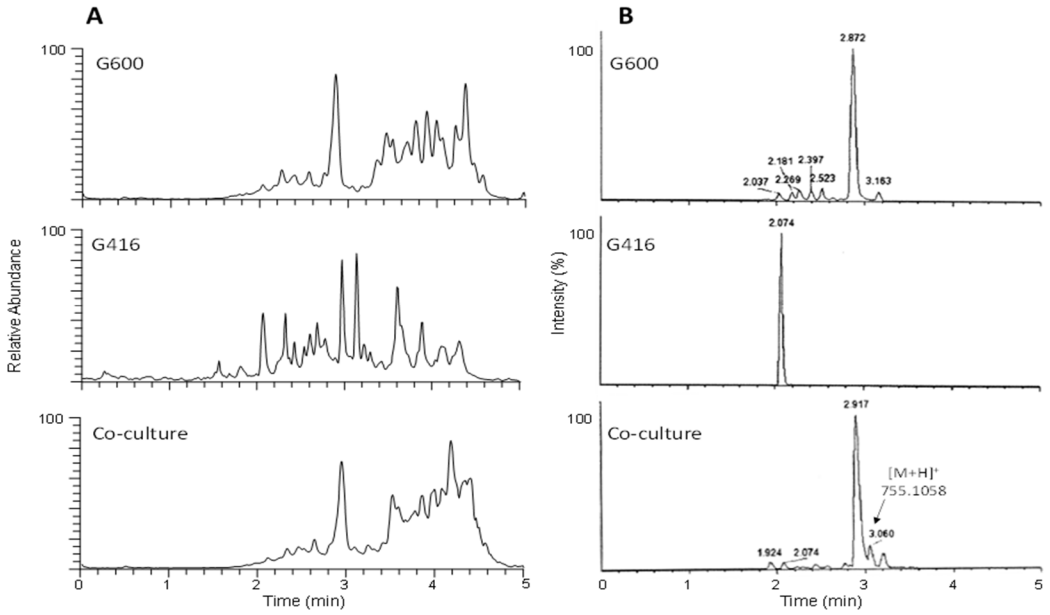

Figure 97. Analysis of the Extract of G600 and G416 Grown Alone and In Co-culture Using Dereplication with Mass Defect Filtering to Determine the Production of Induced Secondary Metabolites. (A) Overlay of (+)-ESI TIC of the samples. (B) Overlay of (+)-ESI TIC of the samples after mass defect filtering.

Co-culture analysis using dereplication with mass defect filtering. Analysis of the extract of G600 and a strain of *Lindgomyces madisonensis* (G416) grown in co-culture illustrates the use of dereplication with mass defect filtering to determine the production of induced secondary metabolites. In this case, the goal was to determine the presence of structurally-related ETPs in the extract. As mentioned previously, G600 was determined to biosynthesize **17**; G416, on the other hand, was known to produce mainly polyketides.[171] The co-culture was analyzed, and the resulting mass defect profile was compared with separate cultures of G600 and G416 (Figure 97). As expected, **17** was identified and appeared to be the most abundant in both G600 and in the co-culture (Supplementary Figure 105). Further inspection of the mass defect profile of the cultures

indicated that the co-culture had a peak at *m/z* 755.1062 that was not detected in a monoculture of G600. The accurate mass for the detected molecular ion peak matched that of verticillin F (**18**), a dimeric ETP alkaloid, at -3.0 ppm mass accuracy (Figure 98). The MS/MS fragmentation for the peak indicated desulfurization of the precursor ion peak (*m/z* 690.16), followed by dehydration (*m/z* 673.03), possible loss of one of the dioxopiperazine moieties (*m/z* 495.01), and then desulfurization and dehydration (*m/z* 413.22), all consistent with the distinctive dissociation of ETPs (Figure 98). Based on this observation, the molecular ion peak identified could be tentatively assigned as verticillin F (**18**) with the absence of a standard for confirmation.

Interestingly, the mass defect profile for a monoculture of G416 exhibited a peak at *m/z* 683.1545. However, the MS/MS profile for that peak did not display the characteristic pattern indicative of an ETP alkaloid (Supplementary Figure 106). This suggested that the detected peak was a false positive and illustrates how MS/MS data can be used to either verify or refute potential hits.

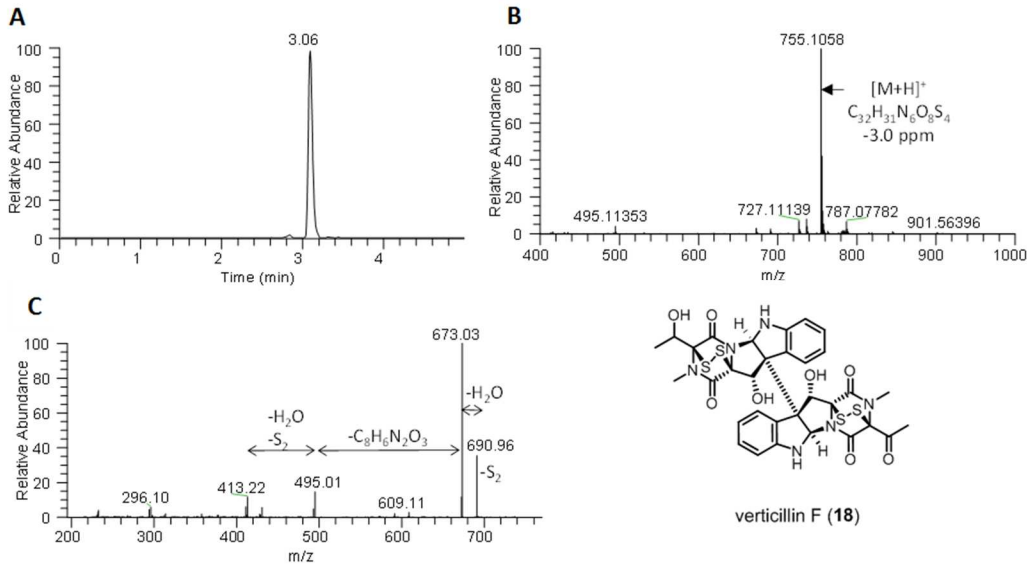

Figure 98. Verticillin F Detected by Mass Defect Filtering in Co-Culture G416 and G600. (A) (+)-ESI SIC of m/z 755.1058 within a ± 5 ppm accuracy. (B) (+)-HRMS of peak at 3.06 min with predicted elemental composition matching the protonated mass of verticillin F with -3.0 ppm accuracy. (C) CID MS/MS (30 eV) spectrum of m/z 755 showing the distinct fragmentation pattern of an ETP alkaloid and consistent with the structure of **18**.

Conclusion

A method to dereplicate fungal extracts was further optimized. This methodology improves a previous dereplication strategy by combining two schemes: a) Targeted screening of compounds known to an in-house built database using a 5-min UPLC-PDA-HRMS-MS/MS where a heated electrospray ionization source (HESI) was utilized and ACD/IntelliXtract software to facilitate the dereplication; b) Mass defect filtering of resulting accurate mass full-scan raw data for a targeted identification of selected known natural products. In particular, mass defect filtering is a data mining technique that can

be applied post acquisition, permitting the re-evaluation of data when future compounds of interest are identified.

Experimental Section

Fungal samples. All fungal samples used in this study were from either the Mycosynthetix (MSX) culture collection (Hillsborough, NC, USA) or the University of North Carolina at Greensboro, Department of Chemistry and Biochemistry, Fungal Culture Collection.

Isolation and identification of fungal strains. Dr Barry Katz isolated Mycosynthetix fungal strain MSX59553 in January of 1992 from leaf litter,[226] while strain MSX40080 was isolated from oak leaf litter on September of 1988. Strain G600 was isolated from submerged wood from fresh water in Knight-Brown Nature Preserve in North Carolina, USA (N 36 18.861', W 80 0.423'). Strain G35 was isolated and identified from surface sterilized seeds of *Hydrastis canadensis* (goldenseal) as *Colletotrichum fioriniae* (KX110401).[230] In addition to examining the micro-morphological characteristics, for molecular identification of new strains dereplicated in the present study (MSX59553 and G600), the internal transcribed spacers (ITS) region of the nuclear RNA operon was sequenced and analyzed via BLAST search. In addition, we constructed a Maximum Likelihood (ML) phylogenetic tree by incorporating ITS sequences from the newly sequenced strains along with ITS sequences used in a recent study on molecular identification of *Clonostachys* spp[232] based on the outcome of results from BLAST search. Methods for sequencing of the strains, BLAST search, and ML phylogenetic analysis have been summarized previously.[122,233-235] Based on morphological and

molecular data, MSX59553 is identified as *Clonostachys rogersoniana*,[236] since it occurred in a strongly supported clade (99% PHYML bootstrap support) with other sequences of *C. rogersoniana* including a reference strain CBS 582.89, while G600 is identified as *Clonostachys* sp. Maximum Likelihood tree along with micro morphological characters of the newly sequenced strains are presented in the Supplementary Figure 107 and 108. The newly obtained sequences from this study have been deposited in GenBank (accession no. KX845687, KX845688).

Fermentation and extraction of fungal cultures. Fungal cultures were grown as described previously.[99,226] Once the screener cultures were generated, 60 mL of 1:1 CH_3OH-$CHCl_3$ was added into each flask, followed by shaking for ~16 h at rt on an orbital shaker set at ~100 rpm. The resulting mixtures were filtered under vacuum. To the filtrate 90 mL of $CHCl_3$ and 150 mL of H_2O were added, and the mixture was stirred for 30 min and then transferred into a separatory funnel. The bottom layers were drawn off and dried *in vacuo*. The dried organic extracts were defatted by reconstituting in a mixture of 100 mL of 1:1 CH_3OH-CH_3CN and 100 mL of hexane, and then partitioned. The CH_3OH-CH_3CN layers were collected and concentrated *in vacuo*.

For G35, from the seed culture, an inoculum was transferred onto five 100 mm x 15 mm Petri dishes with solid oatmeal agar mix. The cultures were then allowed to grow for 28 days at rt before they were extracted. Extraction of these samples were performed in the same way as the screener cultures.

UPLC-PDA-HRMS-MS/MS. Fungal extracts were dissolved with CH_3OH-dioxane (1:1, v/v) to obtain a final concentration of 2 mg/mL. UPLC-HESI-HRMS-MS/MS was performed on an Acquity UPLC system (Waters, Massachussets, USA) equipped with a cooled autosampler kept at 10 °C, photodiode array detector (PDA), column manager, and binary solvent manager; all coupled to an LTQ-Orbitrap XL mass spectrometry system (Thermo Finnigan, San Jose, CA, USA) with a heated electrospray ionization source (HESI).

UPLC separations were performed at 40 °C on a 50 mm x 2.1 mm i.d., 1.7 µm, Acquity BEH C_{18} column (Waters, Massachusetts, USA) equipped with a security guard pre-column. A linear CH_3CN-H_2O gradient of 15% CH_3CN-H_2O to 100% CH_3CN in 4 min was applied at a constant flow rate of 0.6 mL/min; then 100% CH_3CN was maintained for 0.75 min before returning to the starting conditions in 0.25 min. All solvents used were acidified with 0.1% formic acid. PDA data were collected from 191 to 499 nm with resolution of 3.6 nm at a 5 point per second sampling rate.

The HESI source was operated in the positive ionization mode with the following conditions: vaporizer temperature set at 300 °C; capillary temperature set at 275 °C; 4.0 kV for the source voltage; 9.0 V for the capillary voltage; and 100.0 V for the tube lens; Nitrogen sheath gas flow rate set at 35.00 arb. Full-scan HRMS data were acquired from *m/z* 100 to 2000. A collision-induced (CID) energy of 30 eV in the ion trap was used to obtain MS/MS fragmentation data. The system was controlled with Thermo Xcalibur software ver. 2.2.

The LC-MS raw data were processed by the add-in IntelliXtract feature of the ACD MS Manager (Advanced Chemistry Developments, Inc., Toronto, Canada). Mass defect filtering of the HRMS data was performed with Thermo Scientific Compound Discoverer software ver. 1.0. (Thermo Scientific, Inc, San Jose, CA).

Limit of detection and limit of quantitation data analysis. Calibration curves were obtained by preparing two-fold serial dilutions of the standards, which were analyzed in triplicate via 3 µL injections. All LC-HRMS data were processed using Thermo Xcalibur to automatically integrate and calculate the MS signal peak area of each analyte over noise (S/N). Linearity of the calibration curve was assessed by least-squares analysis. The concentration of the analyte that gives the LOD (C_{LOD}) and the concentration at LOQ (C_{LOQ}) were calculated as 3 times the standard error of the regression line ($s_{y/x}$) divided by the slope (b), and 10 times $s_{y/x}$ divided by b, respectively. The standards, alamethicin F50 (**1**), trichokonin VI (**2**), equisetin (**3**), acremonidin A (**4**), and acuminatum B (**5**) were dissolved separately in a 1:1 CH_3CN-dioxane mixture to produce a 15726 µM stock solution of each. An aliquot from each standard solution was taken to prepare a 2621 µM multi-standard stock solution. A two-fold serial dilution of the multi-standard stock solution was prepared to make 20 standard solutions at concentrations ranging from 0.0025 µM to 1310 µM.

Supplementary Material

Table 33. Comparison of Performance Characteristics of the 10-Min and 5-Min Dereplication Methods

Analyte Structure and Molecular Weight (g/mol)	10-min ESI method		5-min HESI method	
	LOD[a] (µM)	LOQ[b] (µM)	LOD[a] (µM)	LOQ[b] (µM)
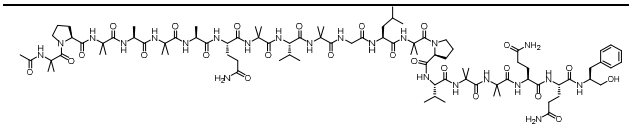 Alamethicin F50 (**1**) (1963.35)	0.04	0.1	0.07	0.2
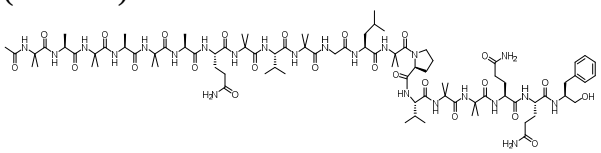 Trichokonin VI (**2**) (1937.32)	0.06	0.2	0.09	0.3
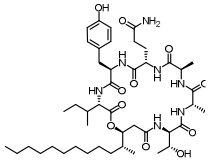 Acuminatum B (**3**) (888.12)	0.07	0.2	0.07	0.2
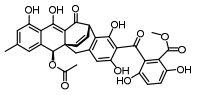 Acremonidin A (**4**) (614.56)	0.2	0.4	0.1	0.4
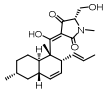 Equisetin (**5**) (373.49)	0.4	1	0.8	3

[a]LOD, limit of detection as calculated by three times the standard error of the regression line divided by the slope ($C_{LOD} = 3s_{y/x} \div b$). [b]LOQ, limit of quantitation as calculated by ten times the standard error of the regression line divided by the slope ($C_{LOQ} = 10s_{y/x} \div b$).

Table 34. Nominal Mass and Corresponding Mass Defects for a Series of Epipolythiodioxopiperazine Alkaloid Analogues.

Compound	Nominal Mass (Da)	Mass Defect (mDa)	ΔMD[a] (mDa)
Verticillin A	696	95.3	-15.7
11'-Deoxyverticillin A	680	100.4	-10.6
11, 11'-Dideoxyverticillin A	664	105.5	-5.5
Verticillin B	712	90.2	-20.7
Verticillin C	744	67.4	-48.7
Verticillin D	756	116.0	5.5
Verticillin F	754	62.3	-10.2
Verticillin E	752	116.4	-25.8
Verticillin G	712	100.8	-20.7
Verticillin H	724	85.1	15.7
Sch 52900	726	90.2	-5.1
Sch 52901	710	105.9	0.0
Gliocladicillin A	694	111.0	5.1
Gliocladicillin B	678	116.1	10.1
Gliocladicillin C	740	121.1	10.6

[a] ΔMD = (Mass defect of a compound – Mass defect of template structure)

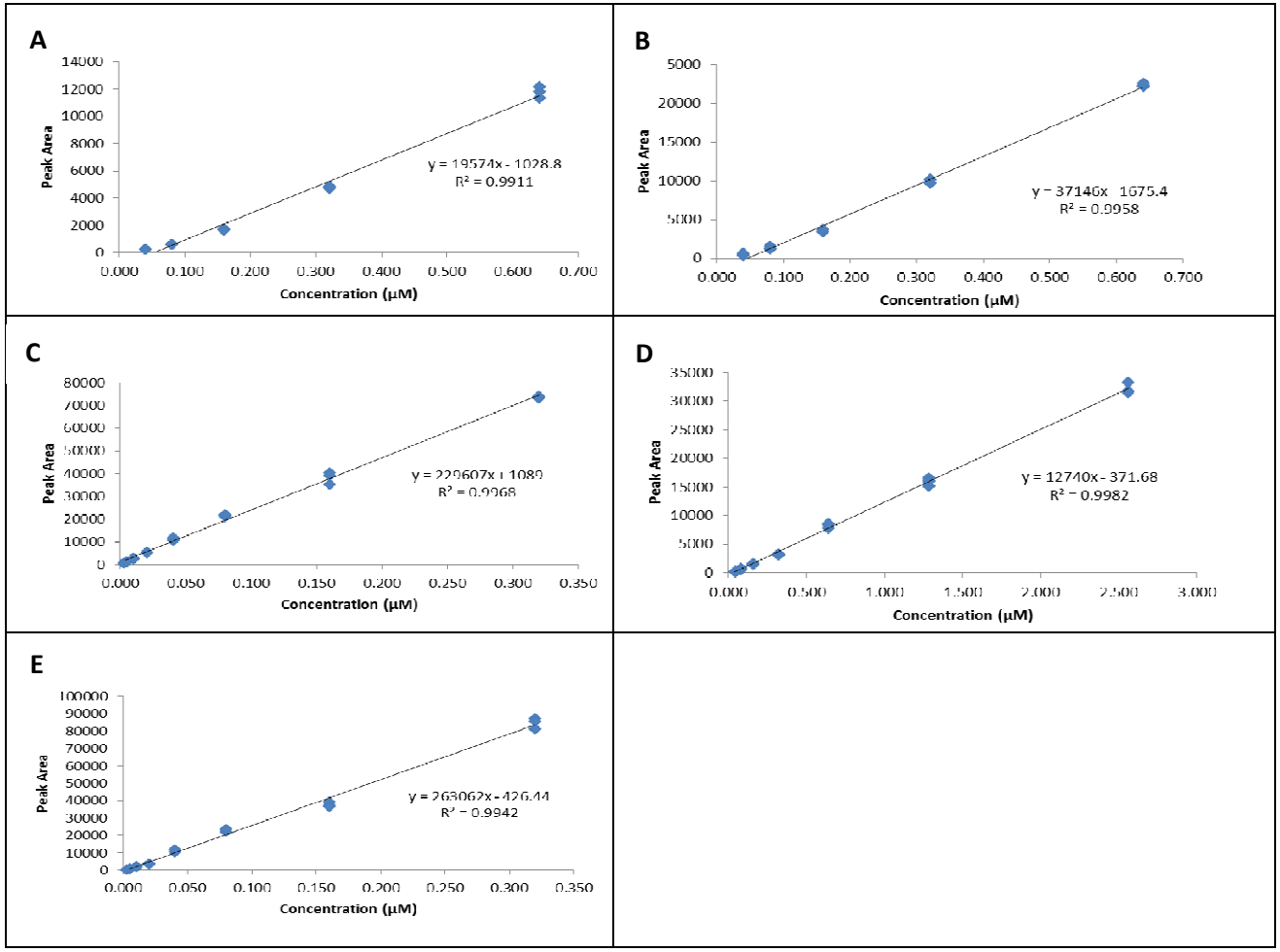

Figure 99. Calibration Curves for (A) Alamethicin F50 (1), (B) Trichokonin VI (2), (C) Acuminatum B (3), (D) Acremonidin A (4), and (E) Equisetin (5) Generated Using the 5-Min HESI Method.

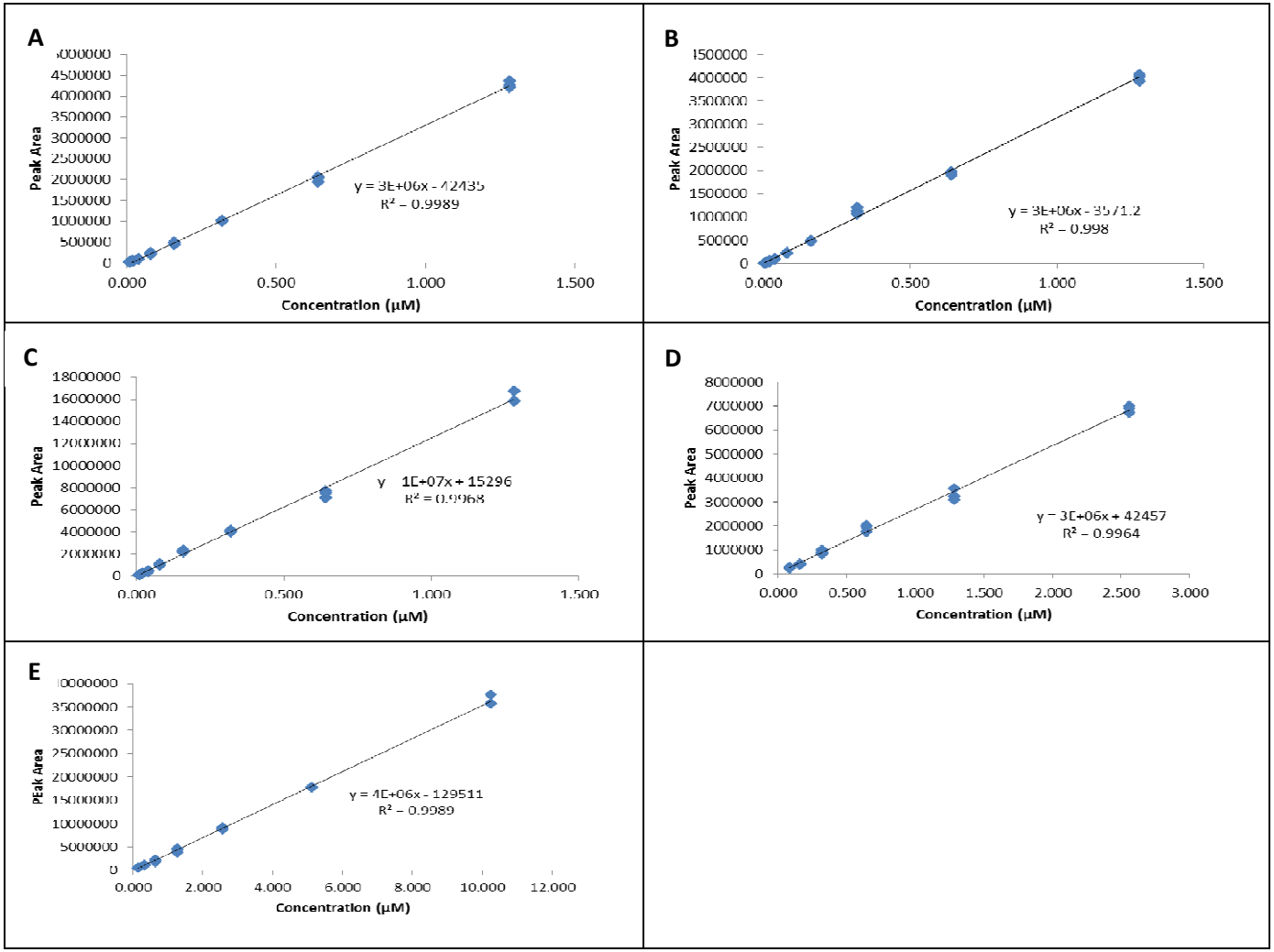

Figure 100. Calibration Curves for (A) Alamethicin F50 (1), (B) Trichokonin VI (2), (C) Acuminatum B (3), (D) Acremonidin A (4), and (E) Equisetin (5) Generated Using the 10-Min ESI Method.

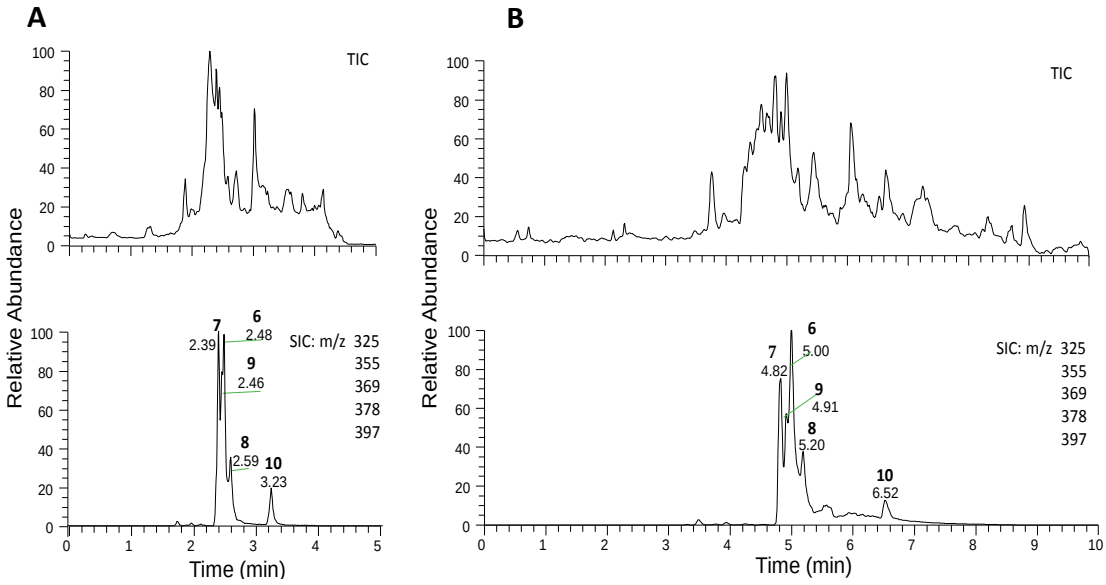

Figure 101. Dereplication Analysis of MSX40080. (A) Overlay of the (+)-ESI-TIC and SIC (m/z 325, 355, 369, 378, 397) of MSX40080 analyzed using the 5-min UPLC-PDA-HRMS-MS/MS method. (B) Overlay of the (+)-ESI-TIC and SIC (m/z 325, 355, 369, 378, 397) of MSX40080 analyzed using the 10-min UPLC-PDA-HRMS-MS/MS method. Dereplication analysis identified the aflatoxins as sterigmatocystin (**6**), 5-methoxysterigmatocystin (**7**), aversin (**8**), brevianamide P (**9**), and 6, 8-di-O-methyl averufin (**10**) in MSX40080.

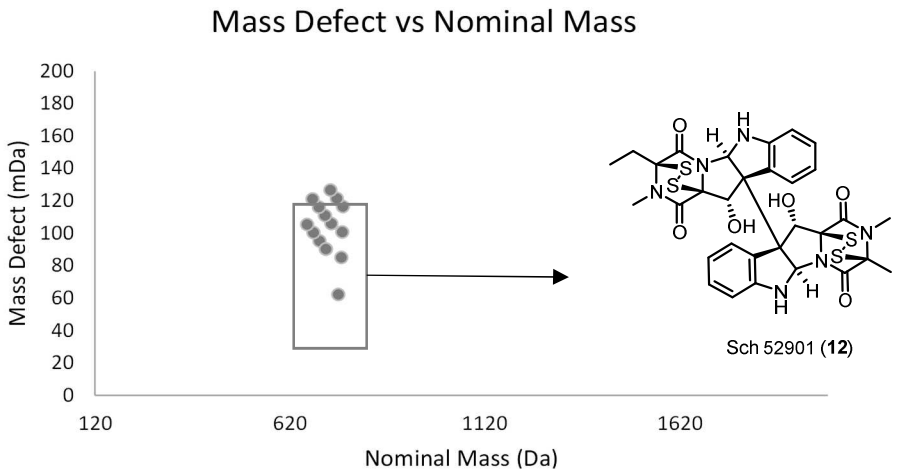

Figure 102. Parameters Used in Mass Defect Filtering Analysis to Detect Epipolythiodioxopiperazine Alkaloid Analogues. Based on the structures of a series of epipolythiodioxopiperazine alkaloid analogues (Table S2) a mass defect filtering reference was defined according to the structure of **12** ($C_{31}H_{30}N_6O_6S_4$). The mass defect filter window was then set at a mass tolerance of $C_{31}H_{30}N_6O_6S_4 \pm 150$ Da at ± 50 mDa mass defect.

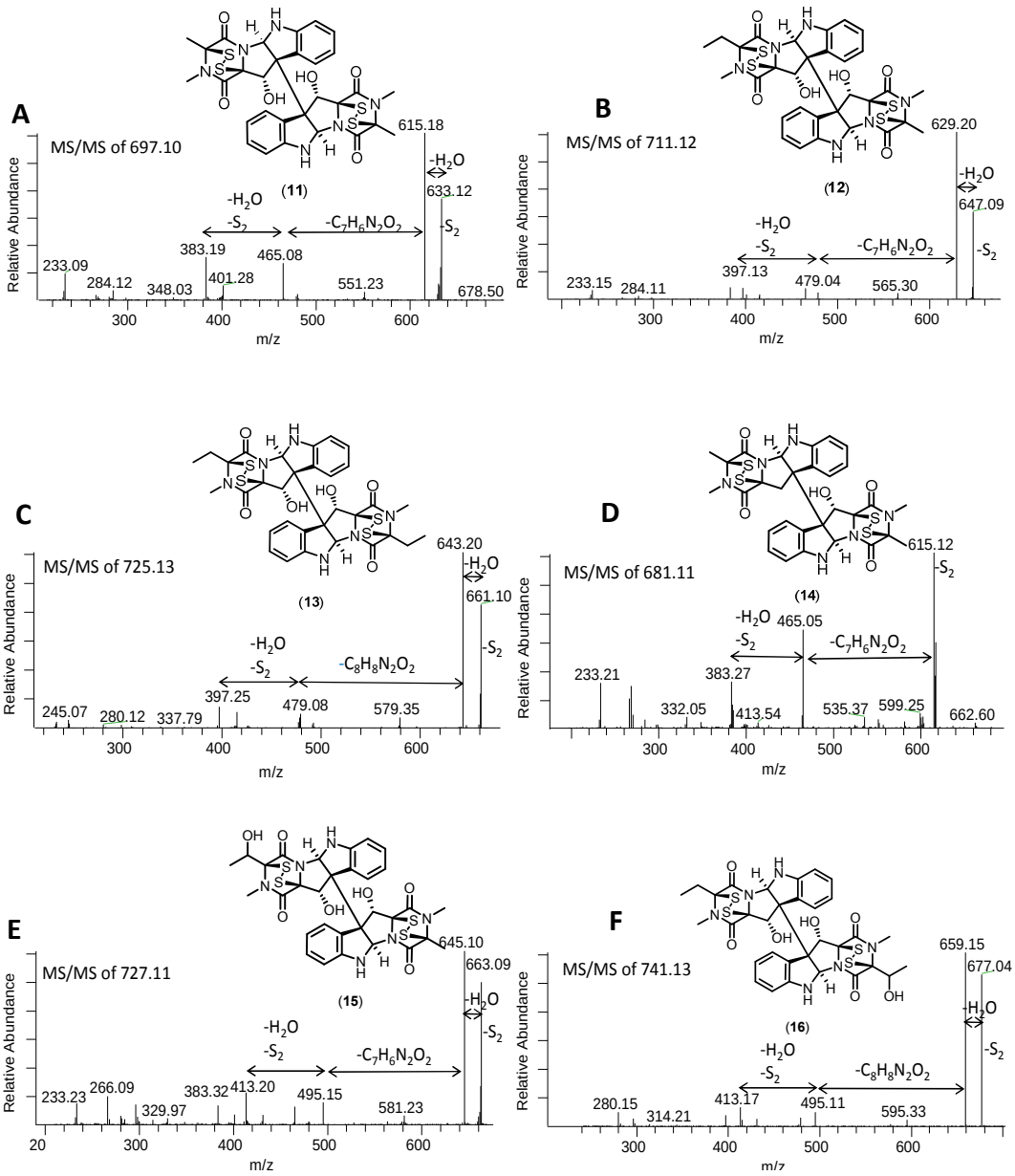

Figure 103. The CID MS/MS (30 eV) Spectra of Compounds 11-16 (Displayed in Panels A-F, Respectively) Showing the Similarity of Their Characteristic Neutral Losses.

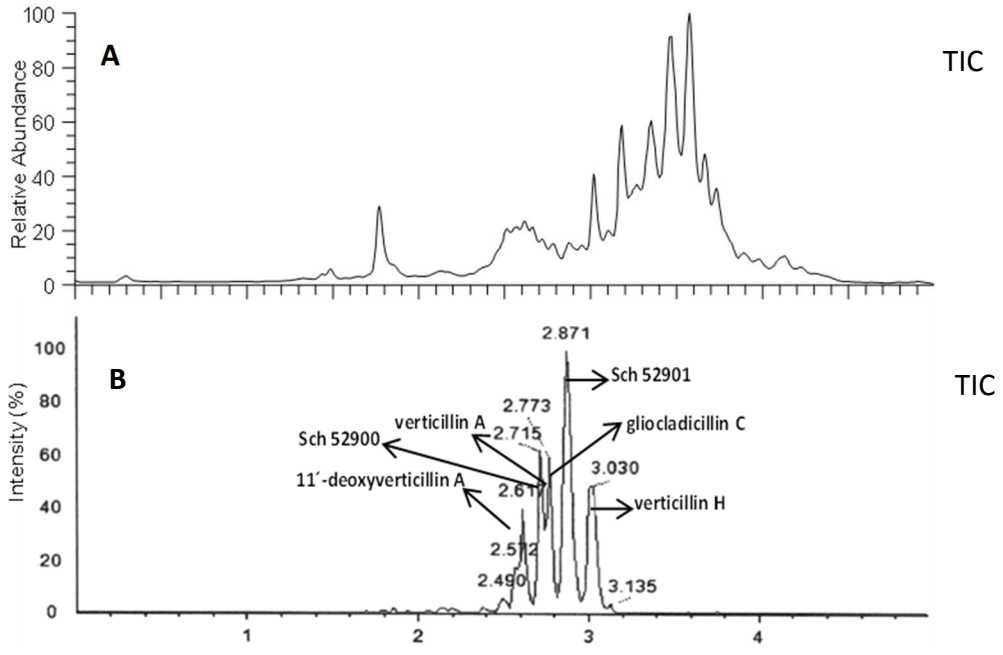

Figure 104. Overlay of (A) (+)-ESI TIC of MSX59553 and (B) (+)-ESI TIC of MSX59553 After Mass Defect Filtering.

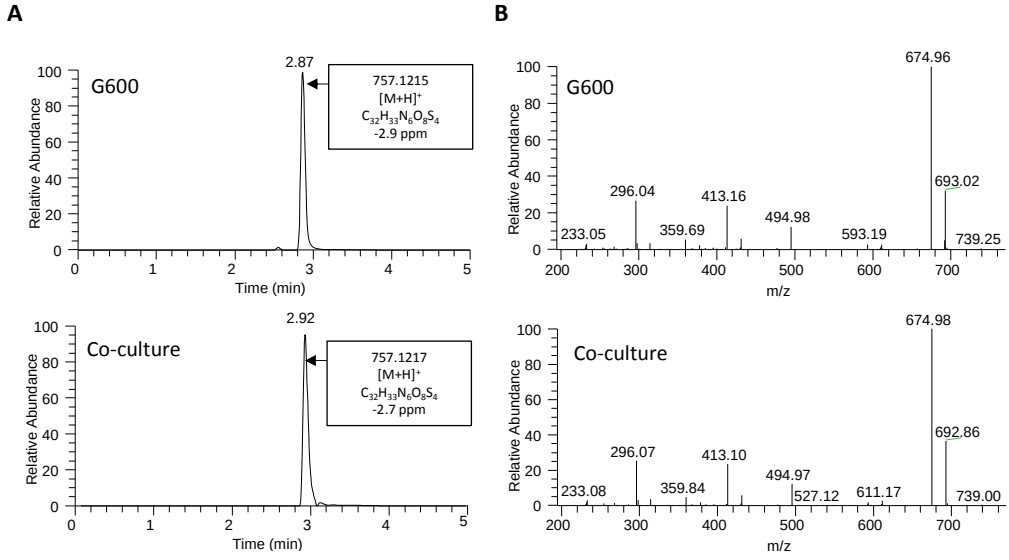

Figure 105. (A) Overlay of Chromatographic Peaks of Verticillin D (17). (B) CID MS/MS (30 eV) Spectra of 17.

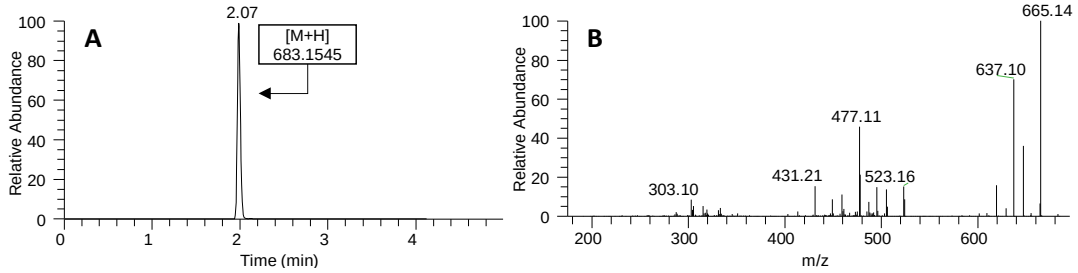

Figure 106. (A) (+)-ESI TIC of G416 After Mass Defect Filtering. (B) CID MS/MS (30 eV) of m/z 683.15.

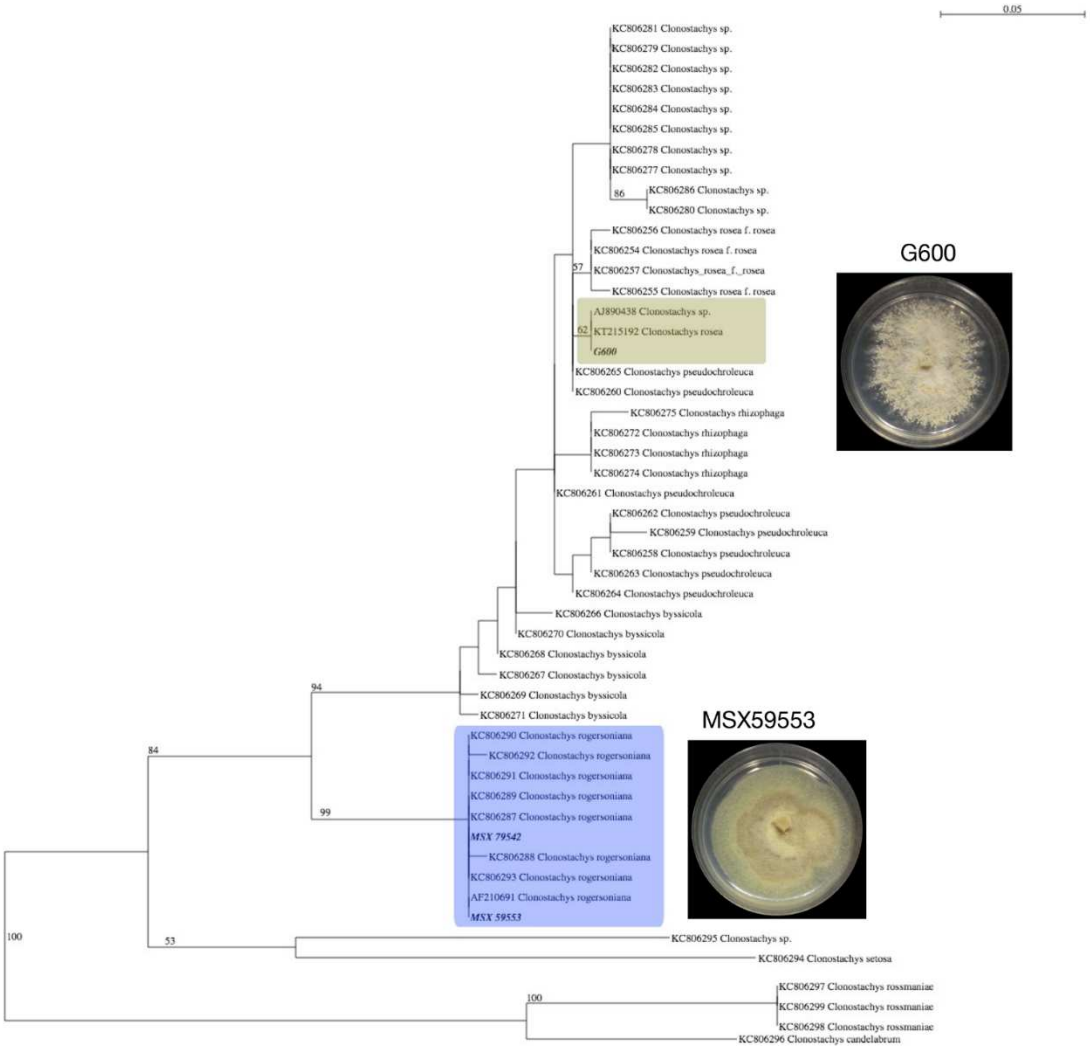

Figure 107. Phylogram of the Most Likely Tree (-lnL = 1507.85) from a PHYML Analysis of 51 Isolates Based on Partial ITS rDNA (520 bp). Numbers refer to PHYML bootstrap support values ≥ 50% based on 1000 replicates. Newly sequenced strains MSX59553 and G600 are highlighted in colored boxes. A 3-week old culture of MSX59553 and G600 on Potato Dextrose Agar (Difco) is shown on the right. Bar indicates nucleotide substitutions per site.

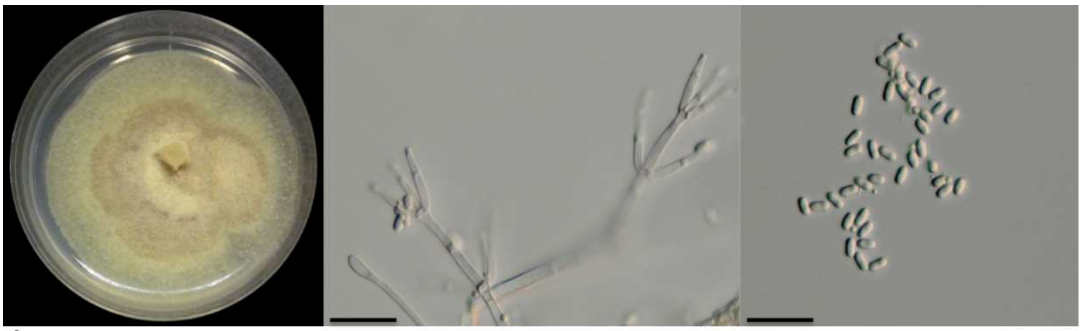

A

B

Figure 108. Micromorphological Features of MSX59553 and G600 Cultures. (A) 3-week culture of *Clonostachys rogersoniana* (MSX59553) on Potato Dextrose Agar (Difco) and micromorphological features such as conidiophores showing phialides and conidia; Scale bars = 20 µm. (B**).** A 3-week culture of *Clonostachys* sp. (G600) on Potato Dextrose Agar (Difco) showing conidia; Scale bars = 20 µm.

Acknowledgements

This research was supported by grant P01 CA125066 from the National Cancer Institute/National Institutes of Health, Bethesda, MD, USA.

CHAPTER VI

CONCLUSIONS

The studies presented here have demonstrated the value of filamentous ascomycetes as an incredibly rich source of structural diversity for drug discovery. Different approaches to optimize the process of drug discovery were used and these included use of structure-activity relationship studies starting with a known bioactive pharmacophore; exploration of understudied ecological groups for new chemistry; and development of dereplication strategies.

In Chapter II we investigated the effect of fluorine substitution as a strategy to expand the medicinally relevant chemical space of isolated fungal metabolites starting with a known bioactive pharmacophore. Griseofulvin and five analogues (with one being new to literature) were isolated from *Xylaria cubensis*, and a series of fluorinated analogues were chemoselectively synthesized using Selectfluor. Principal component analysis (PCA) captured the variation in the molecular and physicochemical properties brought about by incorporation of a fluorine atom to the fungal secondary metabolites; and demonstrated that the fluorinated analogues occupied a different region of space than the isolated fungal metabolites. In Chapters III and IV, as part of our ongoing studies to explore the chemical mycology of freshwater ascomycetes from North Carolina, we investigated the chemical mycology of *Lindgomyces madisonensis* (strain G416) and

Leotiomycetes sp. (accessioned as G730). From *L. madisonensis,* collected from Big Beaver Island creek in Madison, North Carolina, seven acetophenone derivatives (five new to literature and two newly reported as natural products) were isolated and characterized (Chapter III). In Chapter IV, chemical investigation of Leotiomycetes sp., collected from a freshwater lake in Hanging Rock State Park, North Carolina, led to the isolation and identification of three new prenylated xanthenes and two known compounds. Biological evaluation of the new prenylated xanthenes indicated potential anti-virulence activity against a clinically relevant strain of methicillin resistant staphylococcus aureus. Overall, the studies presented in Chapters III and IV highlighted the importance of freshwater ascomycetes as source of new chemistry and new drug leads. Lastly, in Chapter V, a method using a complementary suite of hyphenated techniques, specifically ultra-performance liquid chromatography-photodiode array-high resolution tandem mass spectrometry to dereplicate fungal extracts was further optimized. This methodology improved a previous dereplication strategy by combining two schemes including targeted screening of compounds known to an in-house built library followed by mass defect filtering that allowed screening for potential analogues.

REFERENCES

(1) Newman, D. J.; Cragg, G. M. *J. Nat. Prod.* **2016**, *79*, 629-661.

(2) Newman, D. J.; Cragg, G. M. *J. Nat. Prod.* **2012**, *75*, 311-335.

(3) Cragg, G. M.; Newman, D. J. *Biochim. Biophys. Acta* **2013**, *1830*, 3670-3695.

(4) Cragg, G. M.; Pezzuto, J. M. *Med. Princ. Pract.* **2016**, *25(suppl 2)*, 41-59.

(5) Donadio, S.; Maffioli, S.; Monciardini, P.; Sosio, M.; Jabes, D. *J. Antibiot.* **2010**, *63*, 423-430.

(6) Clardy, J.; Fischbach, M. A.; Walsh, C. T. *Nat. Biotechnol.* **2006**, *24*, 1541-1550.

(7) Newman, D. J.; Cragg, G. M.; Snader, K. M. *J. Nat. Prod.* **2003**, *66*, 1022-1037.

(8) Drewry, D. H.; Macarron, R. *Curr. Opin. Chem. Biol.* **2010**, *14*, 289-298.

(9) Chin, Y.-W.; Balunas, M. J.; Chai, H. B.; Kinghorn, A. D. *AAPS J.* **2006**, *8*, E239-E253.

(10) Blackwell, M.; Spatafora, J. W. In *Biodiversity of Fungi*; Bills, G. F.; Foster, M. S., Eds.; Academic Press: Burlington, 2004; pp 7-21.

(11) Hernández-Carlos, B.; Gamboa-Angulo, M. M. *Phytochem. Rev.* **2011**, *10*, 261-286.

(12) Blackwell, M. *Am. J. Bot.* **2011**, *98*, 426-38.

(13) Hibbett, D.; Abarenkov, K.; Kõljalg, U.; Öpik, M.; Chai, B.; Cole, J.; Wang, Q.; Crous, P.; Robert, V.; Helgason, T.; Herr, J. R.; Kirk, P.; Lueschow, S.; O'Donnell, K.;

Nilsson, R. H.; Oono, R.; Schoch, C.; Smyth, C.; Walker, D. M.; Porras-Alfaro, A.; Taylor, J. W.; Geiser, D. M. *Mycologia* **2016**, *108*, 1049-1068.

(14) Zhong, J. J.; Xiao, J. H. *Adv. Biochem. Eng. Biotechnol.* **2009**, *113*, 79-150.

(15) De Lucca, A. J. *Rev. Iberoam. Micol.* **2007**, *24*, 3-13.

(16) Wright, A. J. *Mayo Clin. Proc. 74*, 290-307.

(17) Marshall, W. F.; Blair, J. E. *Mayo Clin. Proc.* **1999**, *74*, 187-195.

(18) Agathos, S. N.; Madhosingh, C.; Marshall, J. W.; Lee, J. *Ann. N. Y. Acad. Sci.* **1987**, *506*, 657-62.

(19) Laupacis, A.; Keown, P. A.; Ulan, R. A.; McKenzie, N.; Stiller, C. R. *Can. Med. Assoc. J.* **1982**, *126*, 1041-1046.

(20) Campbell, C. D.; Vederas, J. C. *Biopolymers* **2010**, *93*, 755-763.

(21) Endo, A. *J. Antibiot.* **1980**, *33*, 334-6.

(22) Rea, P. A. *Am. Sci.* **2008**, *96*, 408-415.

(23) Manzoni, M.; Rollini, M. *Appl. Microbiol. Biotechnol.* **2002**, *58*, 555-564.

(24) Oxford, A. E.; Raistrick, H.; Simonart, P. *Biochem. J.* **1939**, *33*, 240-8.

(25) Rønnest, M. H.; Raab, M. S.; Anderhub, S.; Boesen, S.; Krämer, A.; Larsen, T. O.; Clausen, M. H. *J. Med. Chem.* **2012**, *55*, 652-660.

(26) Ho, Y. S.; Duh, J. S.; Jeng, J. H.; Wang, Y. J.; Liang, Y. C.; Lin, C. H.; Tseng, C. J.; Yu, C. F.; Chen, R. J.; Lin, J. K. *Int. J. Cancer* **2001**, *91*, 393-401.

(27) Rebacz, B.; Larsen, T. O.; Clausen, M. H.; Ronnest, M. H.; Loffler, H.; Ho, A. D.; Kramer, A. *Cancer Res.* **2007**, *67*, 6342-50.

(28) Rathinasamy, K.; Jindal, B.; Asthana, J.; Singh, P.; Balaji, P. V.; Panda, D. *BMC Cancer* **2010**, *10*, 213-213.

(29) Mauro, V.; Carette, D.; Pontier-Bres, R.; Dompierre, J.; Czerucka, D.; Segretain, D.; Gilleron, J.; Pointis, G. *Apoptosis* **2013**, *18*, 480-91.

(30) Raab, M. S.; Breitkreutz, I.; Anderhub, S.; Ronnest, M. H.; Leber, B.; Larsen, T. O.; Weiz, L.; Konotop, G.; Hayden, P. J.; Podar, K.; Fruehauf, J.; Nissen, F.; Mier, W.; Haberkorn, U.; Ho, A. D.; Goldschmidt, H.; Anderson, K. C.; Clausen, M. H.; Kramer, A. *Cancer Res.* **2012**, *72*, 5374-85.

(31) Zomorodian, K.; Uthman, U.; Tarazooie, B.; Rezaie, S. *J. Infect. Chemother.* **2007**, *13*, 373-379.

(32) Eckerman, S. J.; Graham, K. J. In *Studies in Natural Products Chemistry*; Atta ur, R., Ed.; Elsevier: 2000; Vol. Volume 22, Part C, pp 55-92.

(33) Gloer, J. *Environmental and Microbial Relationships* **2007**, *4*, 257.

(34) Gloer, J. B. *Can. J. Bot.* **1995**, *73*, 1265-1274.

(35) Fritsche, W. *J. Basic Microbiol.* **1983**, *23*, 208-208.

(36) Shearer, C. A. *Can. J. Bot.* **1995**, *73*, 1259-1264.

(37) Raja, H.; Schoch, C. L.; Hustad, V.; Shearer, C.; Miller, A. *MycoKeys* **2011**, *1*.

(38) Wong, M. K. M.; Goh, T.-K.; Hodgkiss, I. J.; Hyde, K. D.; Ranghoo, V. M.; Tsui, C. K. M.; Ho, W.-H.; Wong, W. S. W.; Yuen, T.-K. *Biodivers. Conserv.* **1998**, *7*, 1187-1206.

(39) Shearer, C. A. *Nova Hedwigia* **1993**, *56*, 1-33.

(40) Wong, M. K. M.; Goh, T. K.; Hodgkiss, I. J.; Hyde, K. D.; Ranghoo, V. M.; Tsui, C. K. M.; Ho, W. H.; Wong, W. S. W.; Yuen, T. K. *Biodivers. Conserv.* **1998**, *7*, 1187-1206.

(41) Goh, T. K.; Hyde, K. D. *J. Ind. Microbiol. Biotechnol.* **1996**, *17*, 328-345.

(42) Shearer, C. A.; Raja, H. A.; Miller, A. N.; Nelson, P.; Tanaka, K.; Hirayama, K.; Marvanová, L.; Hyde, K. D.; Zhang, Y. *Stud. Mycol.* **2009**, *64*, 145-153-S4.

(43) Shearer, C. A.; Raja, H. A. Freshwater Ascomycetes Database. http://fungi.life.illinois.edu/ (April 23, 2017)

(44) Hubert, J.; Nuzillard, J.-M.; Renault, J.-H. *Phytochem. Rev.* **2017**, *16*, 55-95.

(45) Harvey, A. L.; Clark, R. L.; Mackay, S. P.; Johnston, B. F. *Expert Opin. Drug Discov.* **2010**, *5*, 559-68.

(46) Ganesan, A. *Curr. Opin. Chem. Biol.* **2008**, *12*, 306-17.

(47) Evans, B. E.; Rittle, K. E.; Bock, M. G.; DiPardo, R. M.; Freidinger, R. M.; Whitter, W. L.; Lundell, G. F.; Veber, D. F.; Anderson, P. S. *J. Med. Chem.* **1988**, *31*, 2235-2246.

(48) Nicolaou, K. C.; Pfefferkorn, J. A.; Roecker, A. J.; Cao, G. Q.; Barluenga, S.; Mitchell, H. J. *J. Am. Chem. Soc.* **2000**, *122*, 9939-9953.

(49) Newman, D. J.; Cragg, G. M. *J. Nat. Prod.* **2012**, *75*, 311-35.

(50) El-Elimat, T.; Zhang, X.; Jarjoura, D.; Moy, F. J.; Orjala, J.; Kinghorn, A. D.; Pearce, C. J.; Oberlies, N. H. *ACS Med. Chem. Lett.* **2012**, *3*, 645-649.

(51) González-Medina, M.; Prieto-Martínez, F. D.; Naveja, J. J.; Méndez-Lucio, O.; El-Elimat, T.; Pearce, C. J.; Oberlies, N. H.; Figueroa, M.; Medina-Franco, J. L. *Future Med. Chem.* **2016**, *8*, 1399-1412.

(52) González-Medina, M.; Owen, J.; El-Elimat, T.; Pearce, C.; Oberlies, N.; Figueroa, M.; Medina-Franco, J. *Front. Pharmacol.* **2017**, *8*.

(53) Fakhouri, L.; El-Elimat, T.; Hurst, D. P.; Reggio, P. H.; Pearce, C. J.; Oberlies, N. H.; Croatt, M. P. *Bioorg. Med. Chem.* **2015**, *23*, 6993-9.

(54) Ayers, S.; Graf, T. N.; Adcock, A. F.; Kroll, D. J.; Matthew, S.; Carcache de Blanco, E. J.; Shen, Q.; Swanson, S. M.; Wani, M. C.; Pearce, C. J.; Oberlies, N. H. *J. Nat. Prod.* **2011**, *74*, 1126-1131.

(55) Huang, D. B.; Ostrosky-Zeichner, L.; Wu, J. J.; Pang, K. R.; Tyring, S. K. *Dermatol. Ther.* **2004**, *17*, 517-22.

(56) Petersen, A. B.; Rønnest, M. H.; Larsen, T. O.; Clausen, M. H. *Chem. Rev.* **2014**, *114*, 12088-12107.

(57) Di Santo, R. *Nat. Prod. Rep.* **2010**, *27*, 1084-1098.

(58) Gentles, J. C. *Nature* **1958**, *182*, 476-7.

(59) Rathinasamy, K.; Jindal, B.; Asthana, J.; Singh, P.; Balaji, P. V.; Panda, D. *BMC Cancer* **2010**, *10*, 213.

(60) Singh, P.; Rathinasamy, K.; Mohan, R.; Panda, D. *IUBMB life* **2008**, *60*, 368-75.

(61) Pasquier, E.; Kavallaris, M. *IUBMB life* **2008**, *60*, 165-70.

(62) Dumontet, C.; Jordan, M. A. *Nat. Rev. Drug Discovery* **2010**, *9*, 790-803.

(63) Wang, J.; Sanchez-Rosello, M.; Acena, J. L.; del Pozo, C.; Sorochinsky, A. E.; Fustero, S.; Soloshonok, V. A.; Liu, H. *Chem. Rev.* **2014**, *114*, 2432-506.

(64) Zhou, P.; Zou, J.; Tian, F.; Shang, Z. *J. Chem. Inf. Model.* **2009**, *49*, 2344-2355.

(65) Zhou, Y.; Wang, J.; Gu, Z.; Wang, S.; Zhu, W.; Aceña, J. L.; Soloshonok, V. A.; Izawa, K.; Liu, H. *Chem. Rev.* **2016**, *116*, 422-518.

(66) Isanbor, C.; O'Hagan, D. *J. Fluor. Chem.* **2006**, *127*, 303-319.

(67) Brooks, W. C.; Paguigan, N. D.; Raja, H. A.; Moy, F. J.; Cech, N. B.; Pearce, C. J.; Oberlies, N. H. *Magn. Reson. Chem.* **2016**, DOI: 10.1002/mrc.4571.

(68) Zhong, J.; Gastaminza, P.; Cheng, G.; Kapadia, S.; Kato, T.; Burton, D. R.; Wieland, S. F.; Uprichard, S. L.; Wakita, T.; Chisari, F. V. *Proc. Natl. Acad. Sci. U.S.A.* **2005**, *102*, 9294-9.

(69) Townley, E. R. In *Analytical Profiles of Drug Substances*; KlausFlorey, F., Ed.; Academic Press: 1979; Vol. Volume 8, pp 219-249.

(70) Chooi, Y.-H.; Cacho, R.; Tang, Y. *Chem. Biol.* **2010**, *17*, 483-494.

(71) Taub, D.; Kuo, C. H.; Wendler, N. L. *J. Org. Chem.* **1963**, *28*, 2752-2755.

(72) Barton, D. H. R.; Hesse, R. H.; Ogunkoya, L.; Westcott, N. D.; Pechet, M. M. *J. Chem. Soc., Perkin Trans. 1* **1972**, 2889-2891.

(73) Barton, D. H. R.; Ganguly, A. K.; Hesse, R. H.; Loo, S. N.; Pechet, M. M. *Chem. Comm.* **1968**, 806-808.

(74) Schack, C. J.; Christe, K. O. *Inorg. Chem.* **1979**, *18*, 2619-2620.

(75) Barton, D. H. R.; Godinho, L. S.; Hesse, R. H.; Pechet, M. M. *Chem. Comm.* **1968**, 804-806.

(76) Nyffeler, P. T.; Duron, S. G.; Burkart, M. D.; Vincent, S. P.; Wong, C. H. *Angew. Chem.* **2005**, *44*, 192-212.

(77) Woodhead, A. J.; Angove, H.; Carr, M. G.; Chessari, G.; Congreve, M.; Coyle, J. E.; Cosme, J.; Graham, B.; Day, P. J.; Downham, R.; Fazal, L.; Feltell, R.; Figueroa, E.; Frederickson, M.; Lewis, J.; McMenamin, R.; Murray, C. W.; O'Brien, M. A.; Parra, L.; Patel, S.; Phillips, T.; Rees, D. C.; Rich, S.; Smith, D.-M.; Trewartha, G.; Vinkovic, M.; Williams, B.; Woolford, A. J. A. *J. Med. Chem.* **2010**, *53*, 5956-5969.

(78) Singh, R. P.; Shreeve, J. n. M. *Acc. Chem. Res.* **2004**, *37*, 31-44.

(79) Hierso, J.-C. *Chem. Rev.* **2014**, *114*, 4838-4867.

(80) Weigert, F. J.; Roberts, J. D. *J. Am. Chem. Soc.* **1971**, *93*, 2361-2369.

(81) Stavber, S.; Jereb, M.; Zupan, M. *Synlett* **1999**, *1999*, 1375-1378.

(82) Fukuhara, T.; Akiyama, Y.; Yoneda, N.; Tada, T.; Hara, S. *Tetrahedron Lett.* **2002**, *43*, 6583-6585.

(83) Meurs, J. H. H.; Sopher, D. W.; Eilenberg, W. *Angew. Chem.* **1989**, *101*, 955-956.

(84) Norihiko, Y.; Tsuyoshi, F. *Chem. Lett.* **2001**, *30*, 222-223.

(85) Karam, O.; Martin-Mingot, A.; Jouannetaud, M.-P.; Jacquesy, J.-C.; Cousson, A. *Tetrahedron* **2004**, *60*, 6629-6638.

(86) Kovtonyuk, V. N.; Kobrina, L. S.; Yakobson, G. G. *J. Fluor. Chem.* **1985**, *28*, 89-98.

(87) Gao, Z.; Lim, Y. H.; Tredwell, M.; Li, L.; Verhoog, S.; Hopkinson, M.; Kaluza, W.; Collier, T. L.; Passchier, J.; Huiban, M.; Gouverneur, V. *Angew. Chem. Int. Ed.* **2012**, *51*, 6733-6737.

(88) Soelch, R. R.; Mauer, G. W.; Lemal, D. M. *J. Org. Chem.* **1985**, *50*, 5845-5852.

(89) Holl, M. G.; Struble, M. D.; Siegler, M. A.; Lectka, T. *J. Fluor. Chem.* **2016**, *188*, 126-130.

(90) Naumann, K. *Pest Manage. Sci.* **2000**, *56*, 3-21.

(91) Oda, T. *J. Antibiot.* **2006**, *59*, 114-6.

(92) Singh, C. J. *Mycoses* **2011**, *54*, e183-e188.

(93) Achterman, R. R.; Smith, A. R.; Oliver, B. G.; White, T. C. *Fungal Genet. Biol.* **2011**, *48*, 335-341.

(94) Gillis, E. P.; Eastman, K. J.; Hill, M. D.; Donnelly, D. J.; Meanwell, N. A. *J. Med. Chem.* **2015**, *58*, 8315-8359.

(95) Rønnest, M. H.; Rebacz, B.; Markworth, L.; Terp, A. H.; Larsen, T. O.; Krämer, A.; Clausen, M. H. *J. Med. Chem.* **2009**, *52*, 3342-3347.

(96) Raja, H. A.; Miller, A. N.; Pearce, C. J.; Oberlies, N. H. *J. Nat. Prod.* **2017**, *80*, 756-770.

(97) El-Elimat, T.; Figueroa, M.; Raja, H. A.; Graf, T. N.; Swanson, S. M.; Falkinham, J. O.; Wani, M. C.; Pearce, C. J.; Oberlies, N. H. *Eur. J. Org. Chem.* **2015**, *2015*, 109-121.

(98) Figueroa, M.; Graf, T. N.; Ayers, S.; Adcock, A. F.; Kroll, D. J.; Yang, J.; Swanson, S. M.; Munoz-Acuna, U.; Carcache de Blanco, E. J.; Agrawal, R.; Wani, M. C.; Darveaux, B. A.; Pearce, C. J.; Oberlies, N. H. *J. Antibiot.* **2012**, *65*, 559-564.

(99) Kaur, A.; Raja, H. A.; Darveaux, B. A.; Chen, W.-L.; Swanson, S. M.; Pearce, C. J.; Oberlies, N. H. *Magn. Reson. Chem.* **2015**, *53*, 616-619.

(100) Polyak, S. J.; Morishima, C.; Lohmann, V.; Pal, S.; Lee, D. Y.; Liu, Y.; Graf, T. N.; Oberlies, N. H. *Proc. Natl. Acad. Sci. U.S.A.* **2010**, *107*, 5995-9.

(101) Lovelace, E. S.; Wagoner, J.; MacDonald, J.; Bammler, T.; Bruckner, J.; Brownell, J.; Beyer, R. P.; Zink, E. M.; Kim, Y. M.; Kyle, J. E.; Webb-Robertson, B. J.; Waters, K. M.; Metz, T. O.; Farin, F.; Oberlies, N. H.; Polyak, S. J. *J. Nat. Prod.* **2015**, *78*, 1990-2000.

(102) Balouiri, M.; Sadiki, M.; Ibnsouda, S. K. *J. Pharm. Anal.* **2016**, *6*, 71-79.

(103) Nweze, E. I.; Mukherjee, P. K.; Ghannoum, M. A. *J. Clin. Microbiol.* **2010**, *48*, 3750-3752.

(104) Piddock, L. J. *Nat. Rev. Microbiol.* **2006**, *4*, 629-636.

(105) Padilla, E. *Antimicrob. Agents Chemother.* **2010**, *54*, 177-183.

(106) Sander, T.; Freyss, J.; von Korff, M.; Rufener, C. *J. Chem. Inf. Model.* **2015**, *55*, 460-73.

(107) Blackwell, M. *Am. J. Bot.* **2011**, *98*, 426-438.

(108) Aly, A.; Debbab, A.; Proksch, P. *Fungal Divers.* **2011**, *50*, 3-19.

(109) Shearer, C. A. *Biodivers. Conserv.* **2007**, *16*, 49-67.

(110) Shearer, C. A.; Raja, H. A. Freshwater Ascomycetes Database. http: //fungi.life.illinois.edu/

(111) Shearer, C. A. In Science Publishers, Plymouth, UK: 2001; pp 225-292.

(112) Hosoe, T.; Gloer, J. B.; Wicklow, D. T.; Raja, H. A.; Shearer, C. A. *Heterocycles* **2010**, *81*, 2123-2130.

(113) Jiao, P.; Swenson, D. C.; Gloer, J. B.; Campbell, J.; Shearer, C. A. *J. Nat. Prod.* **2006**, *69*, 1667-71.

(114) Mudur, S. V.; Swenson, D. C.; Gloer, J. B.; Campbell, J.; Shearer, C. A. *Org. Lett.* **2006**, *8*, 3191-4.

(115) Li, C.; Nitka, M. V.; Gloer, J. B.; Campbell, J.; Shearer, C. A. *J. Nat. Prod.* **2003**, *66*, 1302-6.

(116) Oh, H.; Kwon, T. O.; Gloer, J. B.; Marvanova, L.; Shearer, C. A. *J. Nat. Prod.* **1999**, *62*, 580-3.

(117) Reategui, R. F.; Gloer, J. B.; Campbell, J.; Shearer, C. A. *J. Nat. Prod.* **2005**, *68*, 701-5.

(118) El-Elimat, T.; Raja, H. A.; Day, C. S.; Chen, W. L.; Swanson, S. M.; Oberlies, N. H. *J. Nat. Prod.* **2014**, *77*, 2088-98.

(119) El-Elimat, T.; Raja, H. A.; Figueroa, M.; Falkinham 3rd, J. O.; Oberlies, N. H. *Phytochemistry* **2014**, *104*, 114-20.

(120) Raja, H. A.; Oberlies, N. H.; El-Elimat, T.; Miller, A. N.; Zelski, S. E.; Shearer, C. A. *Mycoscience* **2013**, *54*, 353-361.

(121) Raja, H. A.; Oberlies, N. H.; Figueroa, M.; Tanaka, K.; Hirayama, K.; Hashimoto, A.; Miller, A. N.; Zelski, S. E.; Shearer, C. A. *Mycologia* **2013**, *105*, 959-76.

(122) Raja, H. A.; El-Elimat, T.; Oberlies, N. H.; Shearer, C. A.; Miller, A. N.; Tanaka, K.; Hashimoto, A.; Fournier, J. *Mycologia* **2015**, *107*, 845-62.

(123) Crous, P. W.; Wingfield, M. J.; Le Roux, J. J.; Richardson, D. M.; Strasberg, D.; Shivas, R. G.; Alvarado, P.; Edwards, J.; Moreno, G.; Sharma, R.; Sonawane, M. S.; Tan,

Y. P.; Altés, A.; Barasubiye, B.; Barnes, C. W.; Blanchette, R. A.; Boertmann, D.; Bogo, A.; Carlavilla, J. R.; Cheewangkoon, R.; Daniel, R.; de Beer, Z. W.; de Jesús Yáñez-Morales, M.; Duong, T. A.; Fernández-Vicente, J.; Geering, A. D. W.; Guest, D. I.; Held, B. W.; Heykoop, M.; Hubka, V.; Ismail, A. M.; Kajale, S.; Khemmuk, W.; Kolařík, M.; Kurli, R.; Lebeuf, R.; Lévesque, C. A.; Lombard, L.; Magista, D.; Manjón, J. L.; Marincowitz, S.; Mohedano, J. M.; Nováková, A.; Oberlies, N. H.; Otto, E. C.; Paguigan, N. D.; Pascoe, I. G.; Pérez-Butrón, J. L.; Perrone, G.; Rahi, P.; Raja, H. A.; Rintoul, T.; Sanhueza, R. M. V.; Scarlett, K.; Shouche, Y. S.; Shuttleworth, L. A.; Taylor, P. W. J.; Thorn, R. G.; Vawdrey, L. L.; Vidal, R. S.; Voitk, A.; Wong, P. T. W.; Wood, A. R.; Zamora, J. C.; Groenewald, J. Z. *Persoonia* **2015**, *35*, 264-327.

(124) Wootton, R. C. R. Synthetic approaches to polyoxygenated chromone and chromanone natural products (Doctoral dissertation). Doctor of Philosophy, University of Salford, UK, 2000.

(125) Geissman, T. A.; Hinreiner, E. *J. Am. Chem. Soc.* **1951**, *73*, 782-786.

(126) Figueroa, M.; Jarmusch, A. K.; Raja, H. A.; El-Elimat, T.; Kavanaugh, J. S.; Horswill, A. R.; Cooks, R. G.; Cech, N. B.; Oberlies, N. H. *J. Nat. Prod.* **2014**, *77*, 1351-8.

(127) Gareis, M.; Gareis, E.-M. *Mycopathologia* **2007**, *163*, 207-214.

(128) Wang, X.; Sena Filho, J. G.; Hoover, A. R.; King, J. B.; Ellis, T. K.; Powell, D. R.; Cichewicz, R. H. *J. Nat. Prod.* **2010**, *73*, 942-8.

(129) Sica, V. P.; Raja, H. A.; El-Elimat, T.; Kertesz, V.; Van Berkel, G. J.; Pearce, C. J.; Oberlies, N. H. *J. Nat. Prod.* **2015**, *78*, 1926-1936.

(130) Du, L.; King, J. B.; Morrow, B. H.; Shen, J. K.; Miller, A. N.; Cichewicz, R. H. *J. Nat. Prod.* **2012**, *75*, 1819-23.

(131) Vandermolen, K. M.; Raja, H. A.; El-Elimat, T.; Oberlies, N. H. *AMB Express* **2013**, *3*, 71.

(132) Sica, V. P.; Raja, H. A.; El-Elimat, T.; Oberlies, N. H. *RSC Adv.* **2014**, *4*, 63221-63227.

(133) Hirayama, K.; Tanaka, K.; Raja, H. A.; Miller, A. N.; Shearer, C. A. *Mycologia* **2010**, *102*, 729-46.

(134) Wu, B.; Wiese, J.; Labes, A.; Kramer, A.; Schmaljohann, R.; Imhoff, J. F. *Mar. Drugs* **2015**, *13*, 4617-32.

(135) Shearer, C. A.; Langsam, D. M.; Longcore, J. E. In *Measuring and Monitoring Biological Diversity: Standard Methods for Fungi*; Mueller, G. M.; Bills, G. F.; Foster, M. S., Eds.; Smithsonian Institution Press: Washington, D.C., 2004; pp 513-531.

(136) Schoch, C. L.; Seifert, K. A.; Huhndorf, S.; Robert, V.; Spouge, J. L.; Levesque, C. A.; Chen, W. *Proc. Natl. Acad. Sci. U.S.A.* **2012**, *109*, 6241-6.

(137) White, T. J.; Bruns, T.; Lee, S.; Taylor, J. In *PCR Protocols: A Guide to Methods and Applications*; Innis, M.; Gelfand, D.; Shinsky, J.; White, T., Eds.; Academic Press: 1990; pp 315-322.

(138) Rehner, S. A.; Samuels, G. J. *Can. J. Bot.* **1995**, *73*, 816-823.

(139) Vilgalys, R.; Hester, M. *J. Bacteriol.* **1990**, *172*, 4238-4246.

(140) Raja, H. A.; Tanaka, K.; Hirayama, K.; Miller, A. N.; Shearer, C. A. *Mycologia* **2011**, *103*, 1421-32.

(141) Zhang, Y.; Zhang, X.; Fournier, J.; Chen, J.; Hyde, K. D. *Mycoscience* **2014**, *55*, 43-48.

(142) Ayers, S.; Ehrmann, B. M.; Adcock, A. F.; Kroll, D. J.; Carcache de Blanco, E. J.; Shen, Q.; Swanson, S. M.; Falkinham, J. O., 3rd; Wani, M. C.; Mitchell, S. M.; Pearce, C. J.; Oberlies, N. H. *J. Pept. Sci.* **2012**, *18*, 500-10.

(143) Williams, A. A.; Sugandhi, E. W.; Macri, R. V.; Falkinham, J. O., 3rd; Gandour, R. D. *J. Antimicrob. Chemother.* **2007**, *59*, 451-8.

(144) Mediavilla, J. R.; Chen, L.; Mathema, B.; Kreiswirth, B. N. *Curr. Opin. Microbiol.* **2012**, *15*, 588-595.

(145) David, M. Z.; Daum, R. S. *Clin. Microbiol. Rev.* **2010**, *23*, 616-687.

(146) Centers for Disease Control and Prevention. Antibiotic / Antimicrobial Resistance. https://www.cdc.gov/drugresistance/biggest_threats.html (April 21, 2017)

(147) The White House. Executive Order 13676: Combating Antibiotic-Resistant Bacteria. Fed Regist. **2014**, Sep 18;184(79):56931–5.

(148) World Health Organization. WHO Publishes List of Bacteria for Which New Antibiotics Are Urgently Needed. http://www.who.int/mediacentre/news/releases/2017/bacteria-antibiotics-needed/en/ (April 21, 2017)

(149) Maura, D.; Ballok, A. E.; Rahme, L. G. *Curr. Opin. Microbiol.* **2016**, *33*, 41-46.

(150) Rasko, D. A.; Sperandio, V. *Nat. Rev. Drug Discovery* **2010**, *9*, 117-128.

(151) Yang, T.; Tal-Gan, Y.; Paharik, A. E.; Horswill, A. R.; Blackwell, H. E. *ACS Chem. Biol.* **2016**, *11*, 1982-1991.

(152) Tal-Gan, Y.; Ivancic, M.; Cornilescu, G.; Cornilescu, C. C.; Blackwell, H. E. *J. Am. Chem. Soc.* **2013**, *135*, 18436-18444.

(153) Cegelski, L.; Marshall, G. R.; Eldridge, G. R.; Hultgren, S. J. *Nat. Rev. Microbiol.* **2008**, *6*, 17-27.

(154) George, E. A.; Muir, T. W. *ChemBioChem* **2007**, *8*, 847-855.

(155) Czaplewski, L.; Bax, R.; Clokie, M.; Dawson, M.; Fairhead, H.; Fischetti, V. A.; Foster, S.; Gilmore, B. F.; Hancock, R. E.; Harper, D.; Henderson, I. R.; Hilpert, K.; Jones, B. V.; Kadioglu, A.; Knowles, D.; Olafsdottir, S.; Payne, D.; Projan, S.; Shaunak, S.; Silverman, J.; Thomas, C. M.; Trust, T. J.; Warn, P.; Rex, J. H. *Lancet Infect. Dis.* **2016**, *16*, 239-51.

(156) Thoendel, M.; Kavanaugh, J. S.; Flack, C. E.; Horswill, A. R. *Chem. Rev.* **2011**, *111*, 117-151.

(157) Cech, N. B.; Horswill, A. R. *Future Microbiol.* **2013**, *8*, 1511-1514.

(158) Cragg, G. M.; Newman, D. J. *Biochim. Biophys. Acta* **2013**, *1830*, 3670-3695.

(159) Nakayama, J.; Uemura, Y.; Nishiguchi, K.; Yoshimura, N.; Igarashi, Y.; Sonomoto, K. *Antimicrob. Agents Chemother.* **2009**, *53*, 580-586.

(160) Figueroa, M.; Jarmusch, A. K.; Raja, H. A.; El-Elimat, T.; Kavanaugh, J. S.; Horswill, A. R.; Cooks, R. G.; Cech, N. B.; Oberlies, N. H. *J. Nat. Prod.* **2014**, *77*, 1351-1358.

(161) Daly, S. M.; Elmore, B. O.; Kavanaugh, J. S.; Triplett, K. D.; Figueroa, M.; Raja, H. A.; El-Elimat, T.; Crosby, H. A.; Femling, J. K.; Cech, N. B.; Horswill, A. R.; Oberlies, N. H.; Hall, P. R. *Antimicrob. Agents Chemother.* **2015**, *59*, 2223-2235.

(162) Frey-Klett, P.; Burlinson, P.; Deveau, A.; Barret, M.; Tarkka, M.; Sarniguet, A. *Microbiol. Mol. Biol. Rev.* **2011**, *75*, 583-609.

(163) Shearer, C. A.; Raja, H. A. Freshwater Ascomycetes Database: http://fungi.life.illinois.edu/ (March 1, 2017)

(164) Shearer, C. A.; Descals, E.; Kohlmeyer, B.; Kohlmeyer, J.; Marvanová, L.; Padgett, D.; Porter, D.; Raja, H. A.; Schmit, J. P.; Thorton, H. A.; Voglymayr, H. *Biodivers. Conserv.* **2007**, *16*, 49-67.

(165) Vijaykrishna, D.; Jeewon, R.; Hyde, K. D. *Fungal Divers.* **2006**, *23*, 351-390.

(166) El-Elimat, T.; Raja, H. A.; Figueroa, M.; Falkinham, J. O., 3rd; Oberlies, N. H. *Phytochemistry* **2014**, *104*, 114-120.

(167) El-Elimat, T.; Raja, H. A.; Day, C. S.; Chen, W. L.; Swanson, S. M.; Oberlies, N. H. *J. Nat. Prod.* **2014**, *77*, 2088-2098.

(168) Raja, H. A.; Oberlies, N. H.; Figueroa, M.; Tanaka, K.; Hirayama, K.; Hashimoto, A.; Miller, A. N.; Zelski, S. E.; Shearer, C. A. *Mycologia* **2013**, *105*, 959-976.

(169) El-Elimat, T.; Raja, H. A.; Day, C. S.; McFeeters, H.; McFeeters, R. L.; Oberlies, N. H. *Bioorg. Med. Chem.* **2017**, *25*, 795-804.

(170) Crous, P. W.; Wingfield, M. J.; Burgess, T. I.; Hardy, G. E. S. J.; Crane, C.; Barrett, S.; Cano-Lira, J. F.; Le Roux, J. J.; Thangavel, R.; Guarro, J.; Stchigel, A. M.; Martín, M. P.; Alfredo, D. S.; Barber, P. A.; Barreto, R. W.; Baseia, I. G.; Cano-Canals, J.; Cheewangkoon, R.; Ferreira, R. J.; Gené, J.; Lechat, C.; Moreno, G.; Roets, F.; Shivas, R. G.; Sousa, J. O.; Tan, Y. P.; Wiederhold, N. P.; Abell, S. E.; Accioly, T.; Albizu, J. L.; Alves, J. L.; Antoniolli, Z. I.; Aplin, N.; Araújo, J.; Arzanlou, M.; Bezerra, J. D. P.;

Bouchara, J. P.; Carlavilla, J. R.; Castillo, A.; Castroagudín, V. L.; Ceresini, P. C.; Claridge, G. F.; Coelho, G.; Coimbra, V. R. M.; Costa, L. A.; da Cunha, K. C.; da Silva, S. S.; Daniel, R.; de Beer, Z. W.; Dueñas, M.; Edwards, J.; Enwistle, P.; Fiuza, P. O.; Fournier, J.; García, D.; Gibertoni, T. B.; Giraud, S.; Guevara-Suarez, M.; Gusmão, L. F. P.; Haituk, S.; Heykoop, M.; Hirooka, Y.; Hofmann, T. A.; Houbraken, J.; Hughes, D. P.; Kautmanová, I.; Koppel, O.; Koukol, O.; Larsson, E.; Latha, K. P. D.; Lee, D. H.; Lisboa, D. O.; Lisboa, W. S.; López-Villalba, Á.; Maciel, J. L. N.; Manimohan, P.; Manjón, J. L.; Marincowitz, S.; Marney, T. S.; Meijer, M.; Miller, A. N.; Olariaga, I.; Paiva, L. M.; Piepenbring, M.; Poveda-Molero, J. C.; Raj, K. N. A.; Raja, H. A.; Rougeron, A.; Salcedo, I.; Samadi, R.; Santos, T. A. B.; Scarlett, K.; Seifert, K. A.; Shuttleworth, L.; Silva, G. A.; Silva, M.; Siqueira, J. P. Z.; Souza-Motta, C. M.; Stephenson, S. L.; Sutton, D. A.; Tamakeaw, N.; Telleria, M. T.; Valenzuela-Lopez, N.; Viljoen, A.; Visagie, C. M.; Vizzini, A.; Wartchow, F.; Wingfield, B. D.; Yurchenko, E.; Zamora, J. C.; Groenewald, J. Z. *Persoonia* **2016**, *37*, 218-403.

(171) Paguigan, N. D.; Raja, H. A.; Day, C. S.; Oberlies, N. H. *Phytochemistry* **2016**, *126*, 59-65.

(172) Boles, B. R.; Thoendel, M.; Roth, A. J.; Horswill, A. R. *PLoS ONE* **2010**, *5*, e10146.

(173) Talapatra, S. K.; Karmacharya, B.; De, S. C.; Talapatra, B. *Phytochemistry* **1988**, *27*, 3929-3932.

(174) Whyte, A. C.; Gloer, J. B.; Scott, J. A.; Malloch, D. *J. Nat. Prod.* **1996**, *59*, 765-769.

(175) Todd, D. A. *J. Microbiol. Methods* **2016**, *127*, 89-94.

(176) Leonard, P. G.; Bezar, I. F.; Sidote, D. J.; Stock, A. M. *Biochemistry* **2012**, *51*, 10035-10043.

(177) Shearer, C. A.; Langsam, D. M.; Longcore, J. E. In *Measuring and Monitoring Biological Diversity: Standard Methods for Fungi*; Mueller, G. M.; Bills, G. F.; Foster, M. S., Eds.; Smithsonian institution press: Washington, D.C, **2004**; pp 513–531.

(178) White, T. J.; Bruns, T.; Lee, S. H.; Taylor, J. W. *PCR Protocols: A Guide To Methods and Application*; San Diego, **1990**, 315-322.

(179) Rehner, S. A.; Samuels, G. J. *Can. J. Bot.* **1995**, *73*, S816-S823.

(180) Schoch, C. L.; Seifert, K. A.; Huhndorf, S.; Robert, V.; Spouge, J. L.; Levesque, C. A.; Chen, W.; Fungal Barcoding, C.; Fungal Barcoding Consortium Author, L. *Proc. Natl. Acad. Sci. U.S.A.* **2012**, *109*, 6241–6246.

(181) Wang, Z.; Johnston, P. R.; Takamatsu, S.; Spatafora, J. W.; Hibbett, D. S. *Mycologia* **2006**, *98*, 1065-1075.

(182) Wang, Z.; Binder, M.; Schoch, C. L.; Johnston, P. R.; Spatafora, J. W.; Hibbett, D. S. *Mol. Phylogenet. Evol.* **2006**, *41*, 295-312.

(183) Hustad, V. P.; Miller, A. N. *North American Fungi* **2011**, *6*, 1-13.

(184) Raja, H. A.; Miller, A. N.; Shearer, C. A. *Mycologia* **2008**, *100*, 141-148.

(185) Gnavi, G.; Ercole, E.; Panno, L.; Vizzini, A.; Varese, G. C. *SpringerPlus* **2014**, *3*, 508.

(186) Stamatakis, A. *Bioinformatics* **2006**, *22*, 2688-2690.

(187) Miller, M. A.; Pfeiffer, W.; Schwartz, T., Creating the CIPRES Science Gateway For Inference of Large Phylogenetic Trees. In *Proceedings of the Gateway Computing Environments Workshop (GCE)*, **2010**; pp 1–8.

(188) Hillis, D. M.; Bull, J. J. *Syst. Biol.* **1993**, *42*, 182-192.

(189) Huelsenbeck, J. P.; Ronquist, F. *Bioinformatics* **2001**, *17*, 754-755.

(190) Huelsenbeck, J. P.; Ronquist, F. *Bayesian Analysis of Molecular Evolution Using Mr. Bayes*; Springer: **2005**, 186-226.

(191) Posada, D. *Mol. Biol. Evol.* **2008**, *25*, 1253-1256.

(192) Shearer, C. A.; Raja, H. A. Freshwater Ascomycetes and Their Anamorphs. (August 1, 2016)

(193) Sully, E. K.; Malachowa, N.; Elmore, B. O.; Alexander, S. M.; Femling, J. K.; Gray, B. M.; DeLeo, F. R.; Otto, M.; Cheung, A. L.; Edwards, B. S.; Sklar, L. A.; Horswill, A. R.; Hall, P. R.; Gresham, H. D. *PLoS Pathog.* **2014**, *10*, e1004174.

(194) *Bruker APEX2* version 2014.11-0. Bruker AXS Inc., Madison, Wisconsin, USA; **2014**.

(195) *Bruker SAINT* version 8.34A. Bruker AXS Inc., Madison, Wisconsin, USA; **2014**.

(196) Krause, L.; Herbst-Irmer, R.; Sheldrick, G. M.; Stalke, D. *J. Appl. Crystallogr.* **2015**, *48*, 3-10.

(197) Rivera-Chávez, J.; Figueroa, M.; González, M. d. C.; Glenn, A. E.; Mata, R. *J. Nat. Prod.* **2015**, *78*, 730-735.

(198) Burg, R. W.; Miller, B. M.; Baker, E. E.; Birnbaum, J.; Currie, S. A.; Hartman, R.; Kong, Y. L.; Monaghan, R. L.; Olson, G.; Putter, I.; Tunac, J. B.; Wallick, H.; Stapley, E. O.; Oiwa, R.; Omura, S. *Antimicrob. Agents Chemother.* **1979**, *15*, 361-367.

(199) Egerton, J. R.; Ostlind, D. A.; Blair, L. S.; Eary, C. H.; Suhayda, D.; Cifelli, S.; Riek, R. F.; Campbell, W. C. *Antimicrob. Agents Chemother.* **1979**, *15*, 372-378.

(200) Campbell, W. C.; Burg, R. W.; Fisher, M. H.; Dybas, R. A. In *Pesticide Synthesis Through Rational Approaches*; Magee, P. S., Kohn, G. K., Menn, J.J., Ed.; American Chemical Society: 1984; Vol. 255, pp 5-20.

(201) Harvey, A. L.; Edrada-Ebel, R.; Quinn, R. J. *Nat. Rev. Drug Discovery* **2015**, *14*, 111-129.

(202) Hubert, J.; Nuzillard, J.-M.; Renault, J.-H. *Phytochem. Rev.* **2015**, *15*, 1-41.

(203) Gaudencio, S. P.; Pereira, F. *Nat. Prod. Rep.* **2015**, *32*, 779-810.

(204) Ito, T.; Masubuchi, M. *J. Antibiot.* **2014**, *67*, 353-360.

(205) Kellogg, J. J.; Todd, D. A.; Egan, J. M.; Raja, H. A.; Oberlies, N. H.; Kvalheim, O. M.; Cech, N. B. *J. Nat. Prod.* **2016**, *79*, 376-386.

(206) Wolfender, J.-L.; Marti, G.; Thomas, A.; Bertrand, S. *J. Chromatogr. A* **2015**, *1382*, 136-164.

(207) Ernst, M.; Silva, D. B.; Silva, R. R.; Vencio, R. Z. N.; Lopes, N. P. *Nat. Prod. Rep.* **2014**, *31*, 784-806.

(208) Tchoumtchoua, J.; Njamen, D.; Mbanya, J. C.; Skaltsounis, A. L.; Halabalaki, M. *J. Mass Spectrom.* **2013**, *48*, 561-575.

(209) Kinghorn, A. D. *Pure Appl. Chem.* **2009**, *81*, 1051-1063.

(210) Sy-Cordero, A. A.; Graf, T. N.; Wani, M. C.; Kroll, D. J.; Pearce, C. J.; Oberlies, N. H. *J. Antibiot.* **2010**, *63*, 539-544.

(211) Zhang, H.; Zhang, D.; Ray, K.; Zhu, M. *J. Mass Spectrom.* **2009**, *44*, 999-1016.

(212) Zhu, M.; Ma, L.; Zhang, D.; Ray, K.; Zhao, W.; Humphreys, W. G.; Skiles, G.; Sanders, M.; Zhang, H. *Drug Metab. Dispos.* **2006**, *34*, 1722-1733.

(213) Xing, J.; Zang, M.; Zhang, H.; Zhu, M. *Anal. Chim. Acta* **2015**, *897*, 34-44.

(214) Pähler, A.; Brink, A. *Drug Discov. Today: Technol.* **2013**, *10*, e207-e217.

(215) Sleno, L. *J. Mass Spectrom.* **2012**, *47*, 226-36.

(216) Ekanayaka, E. A. P.; Celiz, M. D.; Jones, A. D. *Plant Physiol.* **2015**, *167*, 1221-1232.

(217) Xu, H.; Niu, H.; He, B.; Cui, C.; Li, Q.; Bi, K. *Molecules* **2016**, *21*, 664.

(218) Xie, T.; Liang, Y.; Hao, H.; A, J.; Xie, L.; Gong, P.; Dai, C.; Liu, L.; Kang, A.; Zheng, X.; Wang, G. *J. Chromatogr. A* **2012**, *1227*, 234-244.

(219) El-Elimat, T.; Figueroa, M.; Ehrmann, B. M.; Cech, N. B.; Pearce, C. J.; Oberlies, N. H. *J. Nat. Prod.* **2013**, *76*, 1709-1716.

(220) Lu, W.; Bennett, B. D.; Rabinowitz, J. D. *J. Chromatogr. B: Anal. Technol. Biomed. Life Sci.* **2008**, *871*, 236-242.

(221) Page, J. S. *J. Am. Soc. Mass Spectrom.* **2007**, *18*, 1582-1590.

(222) Liu, F.; Liu, Q.; Yang, D.; Bollag, W. B.; Robertson, K.; Wu, P.; Liu, K. *Cancer Res.* **2011**, *71*, 6807-6816.

(223) Paschall, A. V.; Yang, D.; Lu, C.; Choi, J. H.; Li, X.; Liu, F.; Figueroa, M.; Oberlies, N. H.; Pearce, C.; Bollag, W. B.; Nayak-Kapoor, A.; Liu, K. *J. Immunol.* **2015**, *195*, 1868-82.

(224) Chen, Y.; Miao, Z.-H.; Zhao, W.-M.; Ding, J. *FEBS Letters* **2005**, *579*, 3683-3690.

(225) Zhang, Y. X.; Chen, Y.; Guo, X. N.; Zhang, X. W.; Zhao, W. M.; Zhong, L.; Zhou, J.; Xi, Y.; Lin, L. P.; Ding, J. *Anti-Cancer Drugs* **2005**, *16*, 515-524.

(226) Figueroa, M.; Graf, T. N.; Ayers, S.; Adcock, A. F.; Kroll, D. J.; Yang, J.; Swanson, S. M.; Munoz-Acuna, U.; Carcache de Blanco, E. J.; Agrawal, R.; Wani, M. C.; Darveaux, B. A.; Pearce, C. J.; Oberlies, N. H. *J. Antibiot.* **2012**, *65*, 559-64.

(227) Maslen, S. L.; Goubet, F.; Adam, A.; Dupree, P.; Stephens, E. *Carbohydr. Res.* **2007**, *342*, 724-735.

(228) Schmidt, G. *Chem. Eur. J.* **2012**, *18*, 8180-8189.

(229) Li, Z.; Wang, Y.; Ouyang, H.; Lu, Y.; Qiu, Y.; Feng, Y.; Jiang, H.; Zhou, X.; Yang, S. *J. Chromatogr. B Analyt. Technol. Biomed. Life Sci.* **2015**, *988*, 45-52.

(230) Egan, J. M.; Kaur, A.; Raja, H. A.; Kellogg, J. J.; Oberlies, N. H.; Cech, N. B. *Phytochem. Lett.* **2016**, *17*, 219-225.

(231) Bode, H. B.; Bethe, B.; Hofs, R.; Zeeck, A. *ChemBioChem* **2002**, *3*, 619-27.

(232) Abreu, L. M.; Moreira, G. M.; Ferreira, D.; Rodrigues-Filho, E.; Pfenning, L. H. *Fungal Biol.* **2014**, *118*, 1004-12.

(233) Raja, H. A.; Kaur, A.; El-Elimat, T.; Figueroa, M.; Kumar, R.; Deep, G.; Agarwal, R.; Faeth, S. H.; Cech, N. B.; Oberlies, N. H. *Mycology* **2015**, *6*, 8-27.

(234) Raja, H. A.; Baker, T. R.; Little, J. G.; Oberlies, N. H. *Food Chem.* **2017**, *214*, 383-92.

(235) Raja, H.; Schoch, C. L.; Hustad, V.; Shearer, C.; Miller, A. *MycoKeys* **2011**, *1*, 63.

(236) Schroers, H. J. *Stud. Mycol.* **2002**, *2001*, 1-211.